



Universität Hamburg  
DER FORSCHUNG | DER LEHRE | DER BILDUNG

**A seismic approach to classify carbonate contourite drifts around  
active isolated carbonate platforms (Bahamas, Maldives)  
and its significance for the reconstruction of paleo-currents**

**DISSERTATION**

zur Erlangung des Doktorgrades der Naturwissenschaften  
an der Fakultät für Mathematik, Informatik und Naturwissenschaften  
Fachbereich Geowissenschaften  
der Universität Hamburg

vorgelegt von

Lars Marco Paulat

aus Bad Oldesloe, Deutschland

Hamburg  
2019

Als Dissertation angenommen am Fachbereich Geowissenschaften

Gutachter:

Dr. Thomas Lüdmann

Prof. Dr. Christian Betzler

Tag des Vollzugs der Promotion:

03.07.2019

Vorsitzender des Fachpromotionsausschusses  
Geowissenschaften:

Prof. Dr. Dirk Gajewski

Dekan der Fakultät MIN:

Prof. Dr. Heinrich Graener

*Für Elisa*

## Abstract

The interaction between bottom currents, platform-derived particles, and the bathymetric framework of isolated carbonate platforms can result in complex current-controlled depositional patterns, which are not entirely understood. The continuous supply and usually local deposition of carbonate particles around platforms, combined with the natural variations in the hydrodynamic regime at various depths, contribute significantly to the heterogeneity of carbonate contourite drifts. This thesis sheds light on the interplay between bottom currents and isolated carbonate platforms in two representative study areas. Moreover, this study presents a classification of carbonate contourite (sediment) drifts related to the architecture and sediment distribution of carbonate platforms based on seismic datasets, as well as the identification of the main driving mechanisms and depositional architecture. Two realms of isolated carbonate platforms were studied, which are located in the Bahamian and Maldivian archipelagos. Both are influenced by major ocean current systems, which were investigated to understand their effects on the depositional patterns. The study areas were targeted by geophysical methods during two scientific cruises, which produced dense grids of high-resolution seismic datasets, allowing new insights to be gained into the sedimentary dynamics of both archipelagos. To achieve the main objectives seismic and hydroacoustic datasets around isolated carbonate platforms were compiled and analyzed, combined with lithostratigraphic and chronological borehole data from multiple sites of the IODP expedition 359 and the ODP Site 1006. (Re-)Interpretation of multichannel seismic cross sections, subordinated echosounder sub-bottom profiling and bathymetric data as well as former inventory data revealed the history of oceanographic processes resulting in various geomorphologies of contourite drifts. The seismic data emphasize the diversity of the sedimentation pattern developed under the influence of long-term bottom current activity.

Both archipelagos are occupied by sheeted, mounded, and platform-edge drifts, with their associated drift-related features, which are produced by several different mechanisms. These mechanisms include variable current velocities, off-bank transport and subsidence, as well as erosion and redeposition of carbonate particles by contour currents. Buried and unburied contourite drifts and moats indicate that sedimentation has been controlled by bottom currents since the Middle Miocene in the investigated areas. The changes in the depositional patterns can be partly related to major oceanographic current system, thus recording significant developments in the global climate system. In areas influenced by high-fluctuating currents, an interplay occurs between erosional and depositional processes, resulting in complex seismic facies patterns with variable contourite drift migration, as well as variations in slopal morphology and moat geometry. Moreover, major aggrading contourite drift bodies may accumulate in areas with lower current variability.

The first survey targeted the Santaren Channel, where the interplay of the Florida Current and the Antilles Current propels the two main contour currents which flow in opposite directions. The eastern part of the Santaren Channel is dominated by a strong contour current that flows northwards and merges with the Florida Current at the conjunction of the Santaren Channel and the Florida Channel. The center of the Santaren Channel is occupied by an elongated channel-related contourite drift, the Santaren Drift. In addition, a joined together current flows along the eastern margin of the Cay Sal Bank. A paleoceanographic reconstruction spanning the last 12 Myrs was carried out for the Santaren Channel, which allowed a detailed insight into the four major growth phases of the contourite drift and to infer its sedimentation rates. The results showed that the evolution of the depositional patterns of the Santaren Drift that are closely linked to the development of the Gulf Stream, and its shape and geometry record the local to global oceanographic, climatic and tectonic events. The data document that the signature of a bottom current flow initiated about 12.3 Ma in the Santaren Channel, as indicated by the first occurrence of sheeted contourite drifts and moat development in the northern part of the Santaren Channel. Narrowing and steepening of moat flanks, as well as the pronounced upslope migration of the moat, reflect a sustained current acceleration of the bottom currents until 5.5 Ma, associated with a transformation into elongated mounded channel-related contourite drifts. Between 5.5 Ma and 3.1 Ma, bottom current intensity reached its maximum, which was probably caused by the final closure of the Central American Seaway. The last 3.1 Myr were characterized by a marked increase in volume throughflow reaching a maximum during the past 900 kyr. The importance of moats and associated contourite drifts for paleoceanographic reconstruction is reflected by the sensitivity of geomorphological differences due to current variations in the hydrodynamic regime. Contourite drift growth was driven by the combined sources of export from the shallow-water carbonate factory and by pelagic rain. The Middle Miocene sheeted contourite drift of the inner Santaren Channel is characterized by low accumulation rates, which contrasts with the rapid increase of accumulation rates during the Early Pliocene. However, the contourite drift buildup was disturbed by minor erosional phases with narrow moats in the Late Pliocene due to increasing bottom-current velocities forced by strengthening Atlantic Ocean ventilation. Subsequently, the Early Pleistocene was dominated by increased periplatform sedimentation and margin progradation, which was facilitated by a reduction in along-slope current flow speed and a concurrent widening and flattening of the moats. The channel-related contourite drift in the Santaren Channel represent an exclusive archive of the Bahamian currents system due to its long-lasting sediment accumulation. Going back to the Middle Miocene, the Santaren Drift provides evidence for the possible initiation of the Gulf Stream and its long-term variability. Moreover, this thesis highlights the significant control of oceanic gateways on the regional oceanographic processes.

The second study area is from the Maldivian archipelago in the Indian Ocean, where the atolls encompass an elongated inter-atoll basin, which is dominated by the monsoon-induced ocean current system. The results highlight the strong overprint of bottom currents on the stratigraphic architecture of isolated carbonate platforms. In addition, the data document how the current

regime of the monsoonal climate shaped the Maldivian archipelago. A stacked record of ten stratigraphic sequences of carbonate contourite drifts indicates that the basin infill was successively accumulated under the influence of variable, but persistent bottom currents, resulting in a carbonate contourite depositional system in the investigated inter-atoll basin, which reflects the paleo-current regime changes. Inter-atoll channels opened up in the process of partial platform drowning during the Middle Miocene and subsequently the basin was rapidly filled by carbonate delta drift sediments under the influence of strong bottom currents. Moreover, as topographic obstacles of a smaller scale, such as drowned patch reefs or carbonate mounds, are known to interact with bottom currents, these added more variability to the already vigorous flow dynamics, leading to the development of scours and small-scale patch drifts.

Overall, this study highlights the interplay of bottom current activity and bathymetric features on different scales and their role in shaping carbonate contourite drifts and carbonate contourite depositional systems using various examples. The results of this thesis help to develop a conceptual model for carbonate contourite drifts by determining their geometry and the mechanisms involved for drift development and related features on two isolated carbonate platforms. In addition, the paleoceanographic history of the influence of bottom currents in both areas is advanced and it is clearly shown that contour currents are an undervalued depositional mechanism around isolated carbonate platforms. The influence of interactive processes on the depositional patterns in these settings allows a classification system to be developed for carbonate contourite drifts around isolated carbonate platforms. The classification of contourite drifts is a significant step in understanding the role of bottom currents for shaping the depositional patterns of isolated carbonate platforms, while the decryption of the geometry and current-related features of contourite drifts provides a valuable geological linkage for revealing paleoceanographic information.

## Kurzfassung

Die Interaktion von Bodenströmungen mit biogenen Komponenten des marinen Karbonatsystems und mit den vorherrschenden topographischen Gegebenheiten von isolierten Karbonatplattformen können zu einem überaus komplexen strömungskontrollierten Ablagerungsmuster führen, das noch nicht vollständig verstanden ist. Die beständige Produktion und Ablagerung von karbonatischen Komponenten im Bereich der Plattformen in Verbindung mit den fortwährenden natürlichen Änderungen des hydrodynamischen Milieus in unterschiedlichen Tiefen lassen heterogene karbonatische Konturit-Drifts entstehen.

Diese Arbeit trägt dazu bei, das Zusammenspiel zwischen Bodenströmungen und isolierten Karbonatplattformen in zwei repräsentativen Gebieten besser zu verstehen. Darüber hinaus präsentiert diese Studie eine Klassifikation von karbonatischen Konturit-Drifts (Sediment-Drifts) hinsichtlich der Architektur und Sedimentverteilung basierend auf seismischen Datensätzen. Es werden zudem die dahinterstehenden Prozesse sowie die Sedimentarchitektur innerhalb der Konturit-Drifts untersucht. Zwei Arbeitsgebiete wurden untersucht, die Teile der Inselgruppen der Bahamas und der Malediven umfassen. Sie liegen im Einflussbereich von wichtigen Strömungssystemen der Weltmeere, die untersucht wurden um den Effekt auf das Ablagerungsmuster zu verstehen. Die Forschungsgebiete wurden mit geophysikalischen Methoden beprobt, welches ein dichtes Netz von hochauflösenden seismischen Daten erschuf, das neue Einsichten der Sedimentdynamik beider Archipele erlaubt. Die seismischen und hydroakustischen Datensätze von zwei wissenschaftlichen Forschungsfahrten sind, unter Anwendung lithostratigraphischer und chronologischer Daten von Bohrungen der IODP-Expedition 359 und des ODP-Bohrloches 1006, zusammengefügt und analysiert worden. Eine (Neu-) Interpretation von seismischen Mehrkanal-Profilen und Sediment-Echolot-, so wie bathymetrischen Daten enthüllten die Geschichte der ozeanographischen Prozesse, die zu den verschiedenartigen Geomorphologien der Konturit-Drifts beitragen. Die seismischen Daten betonen die Diversität der Sedimentationsmuster, die sich unter dem Einfluss der langanhaltenden Bodenströmungen entwickelten.

Beide Inselgruppen zeigen sogenannte „sheeted“, „mounded“ und „platform-edge“ Drifts, sowie assoziierte Merkmale, die durch unterschiedliche Mechanismen erzeugt werden. Hierzu zählen variable Strömungsgeschwindigkeiten, unterschiedliche Transportwege der karbonatischen Partikel und die Subsidenz, so wie Erosion und erneute Ablagerung der Partikel durch Kontur-Strömungen. Versunkene und unverschüttete Konturit-Drifts und deren Strömungskanäle weisen darauf hin, dass die Sedimentation in den untersuchten Gebieten seit dem Mittleren Miozän durch Bodenströmungen kontrolliert wurde. Zudem kann die Veränderung im Ablagerungsmuster teilweise wichtigen Strömungsänderungen in den Ozeanen zugeordnet werden, die eine wichtige Komponente im globalen Klimasystem darstellen. In variablen strömungsbeeinflussten Gebieten werden unter einem Wechselspiel von Erosions- und Ablagerungs-Prozessen komplexe Muster der seismischen Fazies erzeugt, wie zum Beispiel dynamische Migration der Konturit-Drifts und

Variationen der Hang- und Strömungskanal-Geometrie. Des Weiteren können mächtige Konturit-Drift-Körper in Gebieten mit niedriger Strömungsvariabilität akkumulieren.

Die erste Erkundungsfahrt untersuchte den Santaren Kanal, wo das Zusammenspiel von Florida Strömung und der Antillen Strömung die beiden entgegen gerichteten Kontur-Strömungen antreibt. Der östliche Teil des Santaren Kanals ist dominiert von einer starken Kontur-Strömung, die nordwärts fließt und sich mit der Florida-Strömung am Kreuzungspunkt des Santaren Kanals und des Florida Kanals vereinigt. Das Zentrum des Santaren Kanals ist charakterisiert durch den entlang des Kanals getreckten Santaren Drift. Zusätzlich fließt eine entgegengesetzte Strömung an der östlichen Plattformkante der Cay Sal Bank entlang. Für den Santaren Kanal wurde eine paläoozeanographische Rekonstruktion über die letzten 12 Mio. J. geschaffen. Diese erlaubt eine detaillierte Sicht auf die vier großen Wachstumsphasen des Konturit-Drifts, sowie ein Rückschluss auf seine Sedimentationsraten. Das Ergebnis zeigt, dass die Entwicklung des sedimentären Ablagerungsmusters des Santaren Drifts mit der Entwicklung des Golf Stroms eng verknüpft ist und dessen Ausformung und Geometrie lokale und globale ozeanographische, klimatische und tektonische Ereignisse dokumentiert. Die Daten zeigen, dass die ersten nachweisbaren Anzeichen eines Boden-Strömungsflusses vor 12,3 Mio. J. auftraten. Dies ist belegt durch die Ablagerung von Schichtdrifts und der Entwicklung eines Strömungskanals im nördlichen Teil des Santaren Kanals. Die Verengung und Versteilung der Flanken des Strömungskanals, sowie die ausgeprägte hangwärtige Migration des Strömungskanals reflektieren die anhaltende Beschleunigung der Boden-Strömung bis vor 5,5 Mio. Jahren. Die folgende Änderung im Strömungsregime wurde begleitet von einer Transformation des Konturit-Drifts zu einem „mounded“ Drifttyp. Zwischen 5,5 und 3,1 Mio. J. erreichte die Bodenströmungs-Intensität das Maximum, welche wahrscheinlich von der endgültigen Schließung der Zentral-Amerikanischen Meeresstraße verursacht wurde. Die letzten 3,1 Mio. J. sind charakterisiert durch einen markanten Anstieg im Volumendurchfluss, der in den letzten 900.000 Jahren sein Maximum erreicht hat. Die Strömungskanäle und die angrenzenden Konturit-Drifts sind für eine paläoozeanographische Rekonstruktion von großem Wert. Dies ist bedingt durch die Sensitivität der geomorphologischen Veränderung des Konturit-Drifts im Zuge der Veränderung von Strömungen im hydrodynamischen Regime. Die Akkumulation des Konturit-Drifts wird gesteuert von den Einträgen des Exports der Flachwasser-Karbonatproduktion kombiniert mit pelagischen Überresten. Der geschichtete Konturit-Drift des zentralen Santaren Kanals ist charakterisiert durch niedrige Akkumulationsraten im Mittleren Miozän und verzeichnet einen starken Anstieg der Sedimentationsraten während des Frühen Pliozäns. Das Wachstum des Konturit-Drifts wurde unterbrochen von kleineren Erosionsphasen im Späten Pliozän, angezeigt durch schmale Strömungskanäle, die durch ansteigende Bodenströmungsgeschwindigkeiten entstanden, bedingt durch die verstärkte Ventilation des Atlantischen Ozeans. Das Frühe Pleistozän wurde dominiert durch eine höhere Sedimentationsrate im vorgelagerten Bereich des Plattformhangs und einer Progradation der Plattformkante, die einher geht mit einer Reduktion der Strömungsgeschwindigkeit entlang des Hanges und der gleichzeitigen Verbreiterung und Abflachung der Strömungskanäle. Die langanhaltende

Sedimentakkumulation der Konturit-Drifts im Santaren Kanal repräsentiert ein einzigartiges Archiv des Strömungs-Systems der Bahamas. Der Santaren Drift beinhaltet Beweise für das mögliche Einsetzen des Golf Stroms im Mittleren Miozän und seiner Langzeit-Variabilität. Darüber hinaus unterstreicht diese Arbeit die signifikante Kontrolle von Meerestrassen auf das regionale hydrodynamische Regime.

Das zweite Arbeitsgebiet liegt im Archipel der Malediven im Indischen Ozean, wo die Atolle ein nach Nord-Süd ausgerichtetes Becken umschließen, welches von dem Monsun-induzierten Meeresströmungssystem dominiert wird. Die Ergebnisse betonen den starken Einfluss von Bodenströmungen auf das stratigraphische Gebilde von isolierten Karbonatplattformen. Zusätzlich dokumentieren die Daten wie das Strömungsregime des Monsun-Klimas das Archipel der Malediven formen. Eine Abfolge von zehn stratigraphischen Sequenzen von karbonatischen Konturit-Drifts dokumentiert, dass die Beckenfüllung sukzessive unter dem Einfluss sich ändernder, aber beständiger Bodenströmungen stattfand, die im Aufbau eines karbonatischen Konturit Ablagerungssystems in dem untersuchten Becken mündete, das die Änderungen des Paläoströmungs-Regime reflektiert. Im Prozess des partiellen Ertrinkens während des Mittleren Miozäns öffneten sich Kanäle zwischen den Atollen und das Becken füllte sich zügig mit karbonatischen Delta Drift Sedimenten, die unter dem Einfluss von starken Bodenströmungen abgelagert wurden. Des Weiteren sind kleinskalige topographische Hindernisse, wie ertrunkene Fleckenriffe oder biogene Karbonat-Hügel, bekannt dafür mit Bodenströmungen zu interagieren und zusätzliche Variabilität in die bereits lebhaftige Strömungsdynamik bringen, die dann zur Auskolkung und Entwicklung von kleinskaligen Driftkörpern führt.

Insgesamt erweitert diese Arbeit das Wissen um das Zusammenspiel von der Bodenströmungs-Aktivität und bathymetrischen Beschaffenheiten unterschiedlicher Größe und belegt ihre Rolle bei der Modellierung karbonatischer Konturit-Drifts und karbonatischen Konturit-Ablagerungssystemen durch mehrere Beispiele. Die Ergebnisse dieser Studie helfen durch Bestimmung der Geometrie und Mechanismen der Konturit-Drift-Entwicklung und ihrer zugehörigen Merkmale ein konzeptionelles Modell von karbonatischen Konturit-Drifts zu entwickeln. Zusätzlich ist die paläoozeanographische Vorgeschichte des Einflusses von Bodenströmungen in beiden Arbeitsgebieten erweitert worden und es wurde deutlich gezeigt, dass Kontur-Strömungen ein unterschätzter Ablagerungsmechanismus an isolierten Karbonatplattformen ist. Der Einfluss der interaktiven Prozesse auf das Ablagerungsmuster in dieser Umgebung ermöglicht die Entwicklung einer Klassifikation von karbonatischen Konturit-Drifts im Bereich von isolierten Karbonatplattformen. Die Klassifikation von karbonatischen Konturit-Drifts ist ein wichtiger Schritt, um die Rolle von Bodenströmungen bei der Ausgestaltung der Ablagerungsmuster der isolierten Karbonatplattformen zu verstehen, während die Entschlüsselung der Geometrie und der strömungsbedingten Merkmale von Konturit-Drifts ein wertvolles geologisches Mittel beinhaltet um paläoozeanographische Informationen zu enthüllen.

# Table of Contents

<b>Abstract</b> .....	<b>I</b>
<b>Kurzfassung</b> .....	<b>IV</b>
List of Figures .....	X
List of Tables .....	XI
List of Abbreviations .....	XII
<b>1 Introduction</b> .....	<b>1</b>
1.1 Motivation .....	1
1.2 Research objectives and structure of this thesis.....	6
<b>2 Geologic Background and Oceanographic Setting</b> .....	<b>9</b>
2.1 Contourite drifts .....	9
2.1.1 Impact of bottom currents .....	9
2.1.2 Depositional and erosional features .....	9
2.2 Warm-water isolated carbonate platforms.....	11
2.2.1 Facies of isolated carbonate platforms .....	12
2.2.2 Physical properties of carbonates and its implications for seismic measurements	13
2.3 Bahamas.....	15
2.3.1 Geologic evolution.....	15
2.3.2 Oceanographic background .....	17
2.4 Maldives.....	18
2.4.1 Geologic evolution.....	18
2.4.2 Oceanographic background .....	19
<b>3 Data and Methods</b> .....	<b>22</b>
3.1 Theory of marine seismic reflection .....	25
3.1.1 Seismic interpretation .....	26
3.2 Multichannel seismic reflection data acquisition and processing .....	29
3.2.1 The seismic source .....	29
3.2.2 The seismic receiver .....	30
3.2.3 The data storage.....	30
3.2.4 The data processing.....	31
3.3 Sub-bottom profiler - Parasound .....	37
3.4 Multibeam echosounder .....	37
3.5 Well data .....	38

3.5.1 Chronostratigraphic framework - Maldives.....	38
3.5.2 Chronostratigraphic framework - Bahamas.....	39
<b>4 Results .....</b>	<b>41</b>
4.1 General overview about the bathymetric framework of the study areas (Maldives, Bahamas) .....	41
4.1.1 Maldives.....	41
4.1.2 Bahamas .....	42
4.2 Seismic Facies .....	43
4.2.1 Seismic Facies 1 (SF-1) – carbonate platform .....	43
4.2.2 Seismic Facies 2 (SF-2) – periplatform deposits.....	43
4.2.3 Seismic Facies 3 (SF-3) – periplatform mass transport deposits.....	43
4.2.4 Seismic Facies 4 (SF-4) – contourite drift.....	43
4.2.5 Seismic Facies 5 (SF-5) – sediment waves .....	44
4.2.6 Seismic Facies 6 (SF-6) – mass transport deposits .....	44
4.2.7 Seismic facies 7 (SF-7) – (hemi-)pelagic ooze.....	45
4.3 Maldives, Indian Ocean.....	46
4.3.1 Depositional features and geometries .....	46
4.3.2 Kardiva Channel system.....	46
4.3.3 The Inner Sea .....	56
4.3.4 Drowned atolls .....	61
4.3.5 Intra-Atoll area .....	66
4.4 Bahamas, Santaren Channel.....	67
4.4.1 Depositional features and geometries .....	67
4.4.2 Detailed description of the MCS data.....	67
<b>5 Discussion .....</b>	<b>73</b>
5.1 Revealing the Carbonate Contourite Drifts .....	73
5.1.1 Maldivian contourite drifts .....	73
5.1.2 Bahamian contourite drifts.....	79
5.2 Concept and classification of carbonate contourite drifts .....	81
5.2.1 Drowned Platform Drifts.....	82
5.2.2 Contour Channel Drift.....	82
5.2.3 Slope-related Drifts .....	83
5.2.4 Slope-to-Basin Drifts.....	84
5.2.5 Basin Drifts .....	85
5.2.6 Contourite Depositional System (CDS) .....	86
5.2.7 Patch Drifts.....	86
5.3 Examples of Carbonate Contourite Drifts in the sedimentary record .....	88
5.4 Reconstruction of paleo-currents affecting the Santaren Drift (Bahamas) and its significance for the global current pattern .....	92
5.4.1 Factors controlling contourite architecture.....	92

---

5.4.2 Reading the contourite drift architecture.....	93
5.4.3 Oceanographic events expressed in the contourite drift accumulation rates .....	98
<b>6 Conclusions.....</b>	<b>101</b>
<b>7 Publication.....</b>	<b>104</b>
<b>8 References .....</b>	<b>104</b>

## List of Figures

<b>Figure 1.1:</b> Locations of the study areas and an overview of the large deep and surface ocean currents and the simplified Monsoon system.....	3
<b>Figure 1.2:</b> A: Regional map of the Bahamian realm showing the location of the study area.....	5
<b>Figure 1.3:</b> A: Map of the Maldivian archipelago, indicating main wind and ocean current direction, the location of seismic profile grid of the acquired MCS and sub-bottom profiler datasets, and the position of the NMA-1 and ARI-1 drillholes.....	7
<b>Figure 2.1:</b> Sketches of plan views and cross-sections of sediment drift types and inferred bottom-current paths.....	10
<b>Figure 2.2:</b> Main characteristics of areal and linear, large-scale contourite erosional features.....	11
<b>Figure 2.3:</b> Depositional settings of isolated carbonate platforms.....	12
<b>Figure 2.4:</b> Industrial seismic profile of MCS data across the central Santaren Channel connected with the schematic platform growth of the Great Bahama Bank and the topography of Cay Sal Bank.....	16
<b>Figure 2.5:</b> Schematic cross section through the Maldives carbonate platform system with projected location of industry wells ARI-1 and NMA-1 as well as the locations of IODP sites.....	19
<b>Figure 2.6:</b> Seismic line across the Maldives Inner Sea with line drawing showing the platform sequence boundaries (PS) and the drift sequence boundaries (DS).....	20
<b>Figure 3.1:</b> A: Map of the MCS profiles that were acquired during M74 and SO236 cruises.....	24
<b>Figure 3.2:</b> Example of reflection termination patterns.....	26
<b>Figure 3.3:</b> Terminology to define and describe seismic reflections, reflection configuration, and seismic facies resulting in interpretation of geological features.....	27
<b>Figure 3.4:</b> General overview of the multichannel reflection seismic system and the data flow used during research cruises SO236 and M95.....	30
<b>Figure 3.5:</b> General overview of the seismic processing steps applied to the SO236 MCS data.....	31
<b>Figure 3.6:</b> Section of a seismic profile p38(SO236), showing shot, midpoints, and CMP-bin positions...	32
<b>Figure 3.7:</b> Semblance velocity-analysis plot and the points of picked velocities for the RMS velocity calculation.....	34
<b>Figure 3.8:</b> Screenshot of an interpolated 2D velocity field window of the processing software.....	34
<b>Figure 3.9:</b> Comparison of the raw data stack (A) and the stacked and migrated data (B) after post processing.....	36
<b>Figure 3.10:</b> Lithostratigraphic summary of ODP Site 1006A.....	40
<b>Figure 4.1:</b> A: Sketch map displaying the morphological features of the MA and an overview about the locations of the shown seismic and hydroacoustic profiles.....	41
<b>Figure 4.2:</b> Properties of the seismic facies SF-1 to SF-7 that are identified in the study areas.....	44
<b>Figure 4.3:</b> A: Raw data of the north-south oriented cross-section of two compiled SO236 MCS profiles, p18 and p19, across the NKC.....	47
<b>Figure 4.4:</b> A: Seismic image of a segment of profile p19 (SO236).....	48
<b>Figure 4.5:</b> A: Uninterpreted MCS data of profile p23(SO236).....	49
<b>Figure 4.6:</b> A: Uninterpreted MCS data of profile p44(SO236).....	52
<b>Figure 4.7:</b> A: Raw MCS data of profile p36(SO236).....	53
<b>Figure 4.8:</b> Seabed slope angle map of the surveyed western and eastern oceanward parts of the KC.....	55
<b>Figure 4.9:</b> A: Uninterpreted MCS data of profile p65(M74).....	56
<b>Figure 4.10:</b> A: Uninterpreted MCS data of segments of profiles p24a(M74), p62(M74), p24b(m74), and p63(M74).....	59
<b>Figure 4.11:</b> A: Segment of MCS data of profile p16(SO236) and p16-1(SO236).....	60
<b>Figure 4.12:</b> 3D-view on the bathymetry of the north-eastern entrance of the Kardiva Channel.....	62
<b>Figure 4.13:</b> A: Segment of uninterpreted Parasound data of profile P50(SO236).....	63
<b>Figure 4.14:</b> A: Segment of raw MCS data of profile p10(M74) across the Fuad Bank.....	64

<b>Figure 4.15:</b> A: Segment of shallow-water single-channel seismic data of profile p44(2011).....	66
<b>Figure 4.16:</b> Bathymetric map of the surveyed area during M95 cruise. ....	67
<b>Figure 4.17:</b> A: Uninterpreted seismic data of profile p17(M95) representing a northern transect across the Santaren Channel.....	68
<b>Figure 4.18:</b> A: Uninterpreted seismic data of profile p27(M95) displaying a central transect across the Santaren Channel.....	69
<b>Figure 4.19:</b> A: Uninterpreted seismic data of profile p8(M95) representing a southern transect across the Santaren Channel. The detailed location can be found on the maps. ....	70
<b>Figure 4.20:</b> A-F: Thickness maps of sediment deposition within the SC and adjacent areas over time since the Middle Miocene.....	72
<b>Figure 5.1:</b> A-D: Thickness map of compiled sequences in milliseconds of TWT.....	75
<b>Figure 5.2:</b> Paleo-Surface map of DS5 of the western branch of the NKC.....	77
<b>Figure 5.3:</b> A: Map showing the locations of classified carbonate contourite drifts of the north-western Bahamian archipelago.....	79
<b>Figure 5.4:</b> Overview of various carbonate contourite drift types (plan views and/or cross-sections) that are revealed by seismic datasets of isolated carbonate platforms.....	84
<b>Figure 5.5:</b> Compilation sketch of different contourite drift types and related features around isolated carbonate platforms. ....	87
<b>Figure 5.6:</b> Seismic lines of the Pre-Site-survey and locations of ODP Leg 194 sites. ....	90
<b>Figure 5.7:</b> Geomorphology of the Bassas da India Atoll. ....	91
<b>Figure 5.8:</b> Moat geometries and sedimentary processes according to the modifications of the sea floor morphology and variations of the bottom-current velocity modified after Faugères and Stow (2008).....	93
<b>Figure 5.9:</b> Santaren Drift facts are compared with major events affecting Atlantic Ocean current circulation and global climate.....	96

## List of Tables

<b>Table 1:</b> General information about the scientific cruises, the seismic acquisition systems, and survey settings.....	22
<b>Table 2:</b> Coring Summary of ODP and IODP Sites in the working areas. ....	38
<b>Table 3:</b> Depths and ages of sequence boundaries at sites cored during IODP Expedition 359.....	39

---

## List of Abbreviations

ADCP	Acoustic Doppler current profiler
AMOC	Atlantic Meridional Overturning Circulation
BA	Bahamian archipelago
CAS	Central American Seaway
CCD	Carbonate Contourite Drift
CDS	Contourite Depositional System
CMP	Common Mid-Point
CSB	Cay Sal Bank (Bahamas)
DMO	Dip moveout
DSDP	Deep Sea Drilling Project
FB	Fuad Bank (Maldives)
GA	Goidhoo Atoll (Maldives)
GBB	Great Bahama Bank (Bahamas)
GBBD	Great Bahama Bank Drift
GPS	Global Positioning System
IODP	Integrated Ocean Discovery Program
IS	Inner Sea (Maldives)
KC	Kardiva Channel (Maldives)
LBBD	Little Bahama Bank Drift
MA	Maldivian archipelago
mbsf	meters below sea floor
MCS	Multi-channel seismic
NKC	Northern branch of the Kardiva Channel (Maldives)
NMO	Normal moveout
OBC	Old Bahama Channel
ODP	Ocean Drilling Program
PSU	Practical Salinity Unit
KC	Kardiva Channel (Maldives)
RV	Research Vessel
S/N	Signal-to-noise
SC	Santaren Channel (Bahamas)
SD	Santaren Drift (Bahamas)
SF	Seismic Facies
SKC	Southern branch of the Kardiva Channel (Maldives)
SMA	South Mallhosmadulu Atoll (Maldives)
TWT	Two-way travel time
VE	Vertical exaggeration

# 1 Introduction

## 1.1 Motivation

The world is changing. Every day and night natural forces reshape the face of the earth on different time scales. From short time events of earthquakes and abrupt rock-, land-, and mudslides on the land and turbidites, slumps and slides in the ocean over medium-time events of changing riverbeds and migrating dunes to long-time events of rise and fall of mountain ranges due to plate tectonics, volcanic activity and erosion, and growing of carbonate platforms and building of contourite drifts by bottom currents in the ocean. At last, the face of the earth is formed by processes of relocating solids by transport in a gaseous, liquid and solid medium, often a mixture of it, propelled by gravity, sun energy and heat flows inside the earth mantle.

Contourite drifts also referred to as sediment drifts are part of this complex system. Sediment drifts are dynamic subaerial sediment bodies at the sea bottom, which are formed by fall out of solid material of a persistent bottom-current flow at the sea floor. The impact of bottom current activity was first identified and verified by photographs of current ripples and lineations and current measurements at the seafloor in abyssal water depth by Heezen *et al.* (1966). Contourite drifts are defined as sedimentary bodies formed by along-slope contour currents of and may be interbedded with other sediment types (Rebesco *et al.*, 2014). Contourite drifts have been discovered and documented during the past 55 years, many of them consisting of siliciclastic components (Wold, 1994; Rebesco *et al.*, 2014; Vadorpe *et al.*, 2014; Pérez *et al.*, 2015). The contourite research was promoted and widened during the last two decades, enhanced by advanced technological possibilities with use of high-resolution 2D/3D seismic-reflection profiling, multibeam, ADCP (Acoustic Doppler current profiler), ROVs (remotely operated vehicles), and AUVs (autonomous underwater vehicles) in connection with detailed sedimentological datasets and geochemical and/or geophysical examination of international oceanic drilling programs (DSDP/ODP/IODP) and various ship-based expeditions. The progress in research of contourites and drifts resulted in scientific books and specific papers about contourites concerning classifications of contourite drifts (Faugères *et al.*, 1999; Rebesco *et al.*, 2014; Esentia *et al.*, 2018), a description of the contourite depositional system (Hernández-Molina *et al.*, 2003, 2008a), and a bedforms-current velocity matrix (Stow *et al.*, 2009). Contourite drift's morphology and its sedimentary record serve as repositories for a wide range of paleoceanographic information by storing the changes of the ambient current regime, for example, the variability of ocean circulation patterns, current velocities, basin interconnectivity, sea-level variations, climatic proxies and tectonic processes (Knutz, 2008; Rebesco *et al.*, 2014; Betzler *et al.*, 2018). An overview of seismic characteristics of contourite drifts has been given by different authors (Faugères *et al.*, 1999; Anselmetti *et al.*, 2000; Stow and Faugères, 2008; Nielsen *et al.*, 2008; Lüdmann *et al.*, 2013, 2018). Many studies

investigate the bottom current activity and their sedimentological footprint (Hübscher *et al.*, 2010; Hernández-Molina *et al.*, 2014a; Rebesco *et al.*, 2014). The contourite drift sediments consist mostly of reworked periplatform ooze, that is, a mixture of particles derived from the shallow-water platform interior and pelagic organisms (Betzler *et al.*, 2009, 2013a, 2013b, 2014a; Lüdmann *et al.*, 2013, 2018; Tournadour *et al.*, 2015; Chabaud *et al.*, 2016). The thickness of contourite drifts can increase up to hundreds of meters and depends on the continuity of the bottom currents and the availability of suspended sediments. The size, shape and composition of contourite drifts depend on variable multiple factors, for example, the current position within the topographic framework, the sediment supply, the directivity and velocity diversification of the bottom current (Esentia *et al.*, 2018).

While extensive research has been presented in primarily siliciclastic settings connected with sedimentation processes around continental margin or in deep ocean basins (Wold, 1994; Rebesco *et al.*, 2014; Vandorpe *et al.*, 2014; Pérez *et al.*, 2015) with a good understanding of their flow processes (Faugères *et al.*, 1993; Rebesco, 2005; Faugères and Stow, 2008; Rebesco *et al.*, 2014). Contourite drifts have been described mainly in the North and South Atlantic basins but exists in all oceanic basins and are associated with deep, intermediate and shallow water masses (Rebesco *et al.*, 2014). Modern and ancient carbonate platforms (for example, the Maldives, and the Marion Plateau) were bathed in ocean currents and carbonate contourite drifts were formed at their flanks (Lüdmann *et al.*, 2013; Betzler *et al.*, 2014a; Isern *et al.*, 2004.). The sedimentation concerning drift accumulation on tropical isolated carbonate platforms with their complex interaction of platform/atoll growth, steered by changing climate and sea-level cycles, subsidence processes, biogenic sediment flux and current activity remain poorly studied. Several studies give a glimpse at the appearance and importance of sediment drifts at warm-water carbonate platform systems (Anselmetti *et al.*, 2000; Betzler *et al.*, 2009, 2013a, b, 2014a; Lüdmann *et al.*, 2013, 2016, 2018; Tournadour *et al.*, 2015; Chabaud *et al.*, 2016).

The targeted warm-water isolated carbonate platform systems of the Bahamian archipelago (BA) and Maldivian archipelago (MA) are bathed in the water masses of the global ocean current system (Fig. 1.1) and, thus, represent interesting sites for paleoceanographic studies. Several authors have investigated the addressed archipelagoes and have found evidences for bottom current activity. Contourite drifts, witnesses of these currents and their interaction with sedimentation processes have been the subjects of research around the BA over the last decades (Neumann and Ball, 1970; Mullins *et al.*, 1980; Betzler *et al.*, 1999, 2014a; Bergman, 2005; Anselmetti *et al.*, 2000; Tournadour *et al.*, 2015; Chabaud *et al.*, 2016; Wunsch *et al.*, 2017, 2018). The Caribbean is a key area in the path of the Atlantic Ocean conveyor belt that transports heat, salt, and moisture via surface ocean currents into the North Atlantic Ocean. Plate tectonic changes modulating such an ocean current system in oceanic gateway areas have a significant impact on climate at regional and larger scales (Berggren, 1982; Livermore *et al.*, 2007; Sijp *et al.*, 2014; Scher *et al.*, 2015). The main ocean currents affecting the study area are the northward-flowing Caribbean Current, the Loop Current, and the Florida Current, which is a significant part of the Gulf Stream (Fig. 1.2A). The strength and

shape of the Caribbean currents are variable over time, affected by the tectonic and climate evolution, and related to the Atlantic Ocean current pattern pushed by the global ocean conveyor belt (Haug and Tiedemann, 1998).

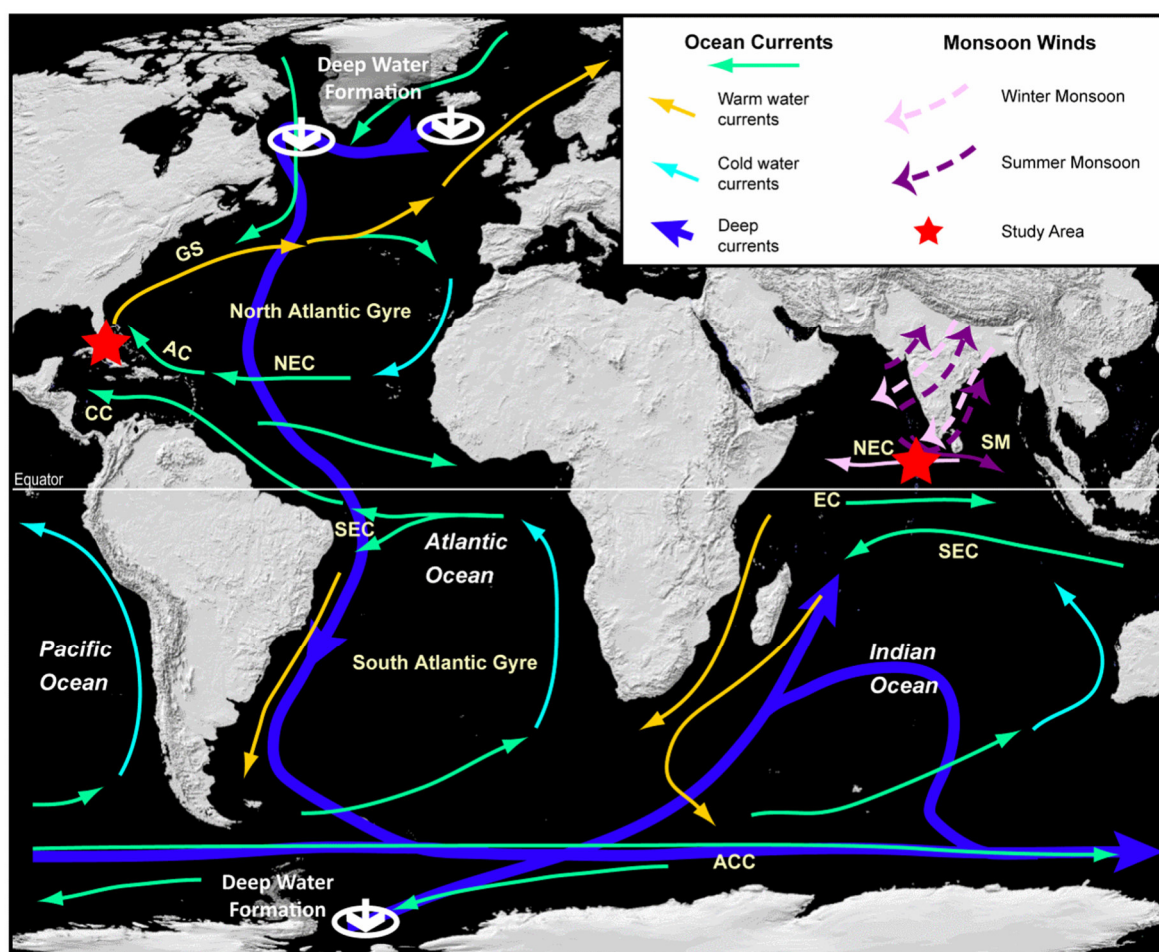


**Figure 1.1:** Locations of the study areas and an overview of the large deep and surface ocean currents and the simplified Monsoon system. AC=Antilles Current, ACC=Antarctic Counter Current, CC=Caribbean Current, EC=Equatorial Current, GS=Gulf Stream, NEC=North Equatorial Current, SEC=South Equatorial Current, SM=Summer Monsoon Current.

The shallowing and closure of major gateways, such as the Central American Seaway (CAS), cut off the equatorial exchange of water masses between the Pacific and Atlantic oceans, with implications for climate, oceanography and biota (Haug and Tiedemann, 1998; Haug *et al.*, 2001; Lear *et al.*, 2003; Jain and Collins, 2006; Schneider and Schmittner, 2006; Steph *et al.*, 2006; Lunt *et al.*, 2008; Haywood *et al.*, 2009; Karas *et al.*, 2017). Both, the new geochronology data that portend a closure of the CAS in Middle Miocene times (Montes *et al.*, 2015) and the significance of the CAS closure are still matter of debate in the scientific community (Bell *et al.*, 2015a; O’Dea *et al.*, 2016). In any case, the gradual closing of the Isthmus of Panama influenced major oceanic current flows, which played an important role in the reorganization of the ocean currents in the Atlantic Ocean realm (Haug and Tiedemann, 1998; Haug *et al.*, 2001; Lear *et al.*, 2003; Schneider and Schmittner, 2006; Karas *et al.*, 2017). The Bahamian carbonate platforms occupy a key region affected by the interplay

of different ocean surface and bottom currents of surface and intermediate water masses, (Lüdmann *et al.*, 2016) associated with the upper limb of the Atlantic conveyor belt (Anselmetti *et al.*, 2000). The variability of these current patterns can be traced back through time, because the sediment load of the currents form contourite drifts, recording the current variability.

The Maldivian carbonate platforms occupy a region affected by the interplay of different ocean surface and bottom currents as well. The impact of bottom currents in the Maldivian archipelago (MA) have been described by Betzler *et al.* (2013a, 2018) and Lüdmann *et al.* (2013). Further researches reveal that the bottom current activity and the reposition of transported material are the main reason for sedimentation processes in the inter-atoll basins (Lüdmann *et al.*, 2013, 2018). Additionally, climate changes modulating the ocean current system have a significant impact on the shape and geometry of Maldivian carbonate platforms (Betzler *et al.*, 2009). Therefore, ancient contourite drifts comprise the essential information of the action of paleo-ocean currents of different scales and allow an attempt for reconstruction of paleo-ocean currents linked to climate variables. This study aims at the decoding of these valuable archives.

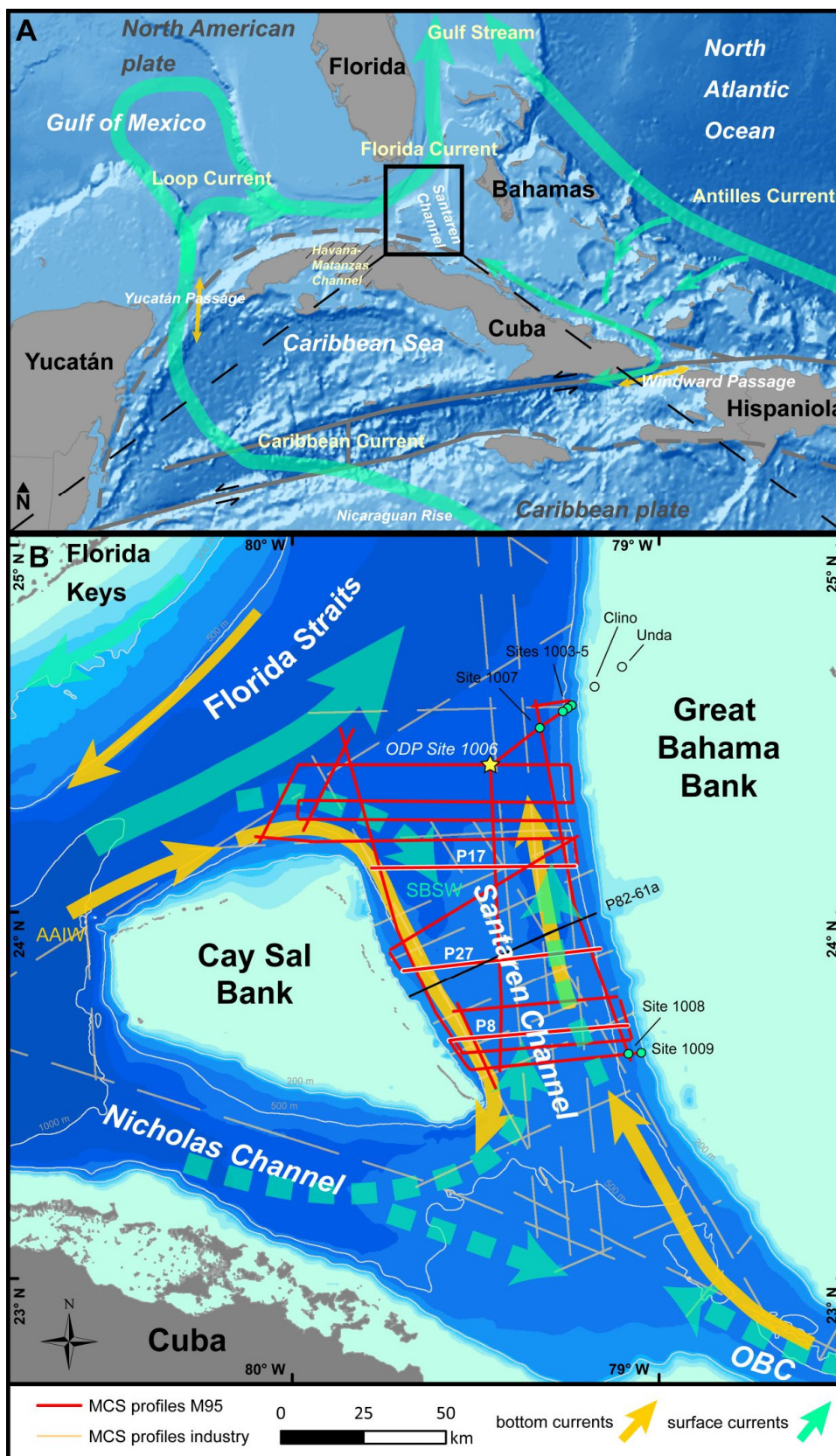


**Figure 1.2:** A: Regional map of the Bahamian realm showing the location of the study area with important ocean currents (green), deep water exchange passages (orange), active (solid dark gray) and inactive (striped dark gray) tectonic plate boundaries. B: Detailed map of the study area displaying the grid of the multichannel seismic (MCS) lines of M95 cruise (solid red lines) and industrial data (striped beige lines) in the Santaren Channel. Main modern current flow pathways of stable surface-to-sub-surface currents (solid green), seasonal variable surface currents (striped green), and (near-)bottom currents (orange) are represented by arrows. AAIW=Antarctic Intermediate Water, CP=Caribbean Plate, OBC=Old Bahama Channel, SBSW=South Bahamian Surface Water.

## 1.2 Research objectives and structure of this thesis

This thesis thematises the interaction between isolated carbonate platform settings and bottom current activity in two diverse areas. The unique location of the MA within the sphere of influence of the Indian monsoon system with its seasonally reversal wind and ocean current system (Fig. 1.1) and its depositional processes of platform-derived material and the changing platform geometry overtime bear the potential to form variety shapes of contourite drifts. The MA, a double chain of several carbonate platforms seated upon a former drowned platform, is dissected by inter-atoll channels. These inter-atoll channels are pathways for water masses, which have a significant impact on the depositional process on the platform-derived material. The second study area contains the Santaren Channel (SC) between the Great Bahama Bank (GBB) and the Cay Sal Bank (CSB) of the BA (Fig 1.2), whose ambient ocean currents are strongly related to the Gulf Stream system (Figs. 1.1 and 1.2A). Therefore, the Bahamian and Maldivian archipelagos appear to be good locations for study the variety of contourite drifts in a complex hydrodynamic setting around isolated carbonate platforms.

The objectives of the study are the identification, classification and characterization of contourite drifts that are associated to warm-water isolated platform systems and to describe their significance for the reconstruction of bottom current activity since the Miocene.

To achieve this aim a partial mapping and a detailed analysis of sediment drifts around isolated carbonate platforms and their adjacent basins since the Miocene are provided. It documents details of bottom current activity by describing the development of different carbonate contourite drifts in the BA and MA. The two working areas represent carbonate settings that are remarkably influenced by important ocean currents of the Gulf Stream system and the wind-driven Monsoon system (Fig. 1.1). Seismic data are used to reveal the seismic facies and external depositional geometry of the contourite drift bodies. In consequence the identification of a variety of bottom current influenced deposits and its spatial and temporal evolution in these systems from the past to nowadays is ensured. This thesis provides the determination of different contourite drift types in the area of the Kardiva Channel (KC) and the Inner Sea (IS) in the MA (Fig. 1.3) and the SC in the BA (Fig. 1.2B). The results will help to understand sedimentological interpretation in the geological record in further detailed studies.

Comparison to recent and ancient examples from other studies will be implemented and discussed. Subordinately, a description of their depositional system and its geomorphology and an attempt for reconstruction of pathways of interacting paleo-ocean currents will be given. By studying the shape and geometry of contourite drifts and its associated moats, as a consequence of bottom current activity, the reconstruction of bottom current activity through time and its impact on the environment of oceanographic events bridging from the local to global scale on the earth's system is placed at the disposal.

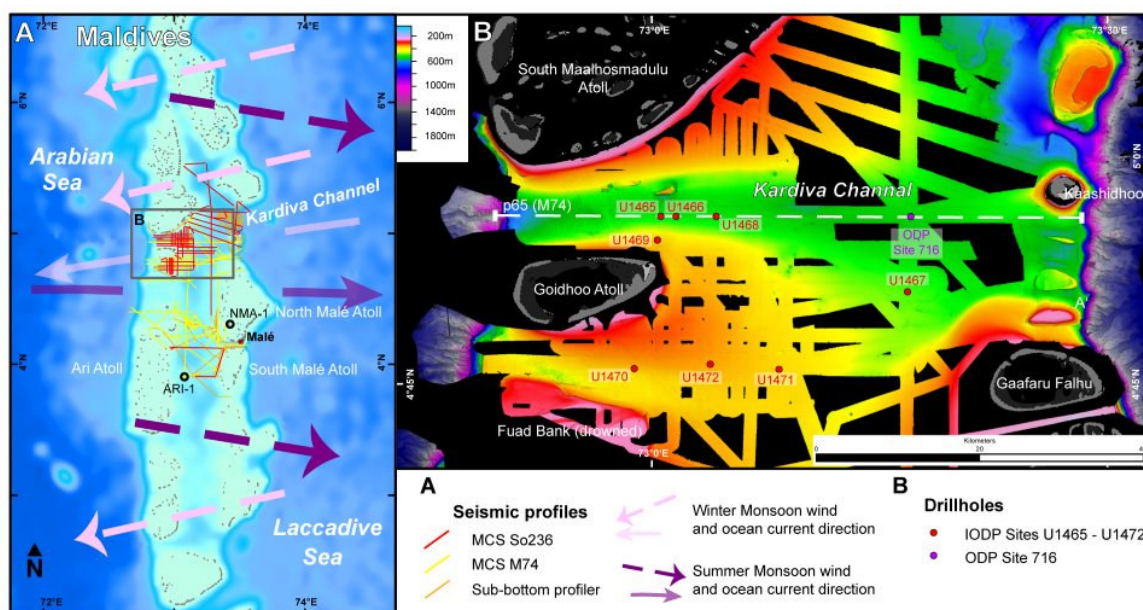


**Figure 1.3:** **A:** Map of the Maldivian archipelago, indicating main wind and ocean current direction, the location of seismic profile grid of the acquired MCS and sub-bottom profiler datasets, and the position of the NMA-1 and ARI-1 drillholes. **B:** Sketch of the atolls and bathymetric data of the Kardiva Channel, which divides the Northern from the Central atolls of the Maldives. Positions of ODP/IODP drillholes and the seismic line p65(M74) are indicated. Black areas indicate areas of data gaps.

Overall, this study uses a combination of 2D seismic surveys integrated with well data in order to: (1) characterize the architecture of the contourite drifts around carbonate platforms; (2) reconstruct the paleoceanographical evolution of the contourite drifts; and (3) identify the main controls on the contourite drift initiation, growth and demise.

With the purpose of achieving the aforementioned objectives, imaging and drillhole-based geophysical measurements as well as sedimentological properties of sediment drifts are regarded. Acquired multichannel seismic will be interpreted, supported by multibeam and sediment echosounder datasets. In addition, sedimentological analysis of IODP drill cores and sea bottom surface samples of marine expeditions are implemented. The drillhole core and well-log information will be used to correlate the mapped seismic sequences and facies with the sedimentological facies. Surface maps are created and seismic facies analysis is performed. The results are analyzed with regard to the influence of bottom current activity of this specific depositional system.

A special focus is put on the ocean current activity in the ocean gateway key area of the Florida Current, which propelled the modern Gulf Stream in the Atlantic Ocean. The high-resolution seismic profiles are correlated with ODP Leg 166 Site 1006 to place ages on the main contourite drift stages and to track drift sedimentation phases across the SC. Using the variable depositional geometries within the contourite drift body and the shapes of the moats and the lower slopes of the adjacent carbonate platforms, the impact of accelerated water masses in this channel and its correlation with the change of the platform and slope geometry is presented. This detailed analysis provides a geological linkage of the data, in context, to global Caribbean high-impact paleoceanographic

events concerning the Gulf Stream system, the North Atlantic subtropical gyre (which is part of the buoyancy-driven Atlantic Meridional Overturning Circulation {AMOC}), and the closure of the CAS, as well as their effects on bottom-current flow processes in the SC. The issue results in the manuscript 'Neogene palaeoceanographic changes recorded in a carbonate contourite drift (Santaren Channel, Bahamas)' by Paulat *et al.* (2018) published in the scientific journal 'Sedimentology'. Finally, an approach for a systematic classification and description of carbonate contourite drifts is given.

This study should shine a light on specific following questions:

- Are there different types of carbonate contourite drifts around warm-water isolated carbonate platforms?
- What are the factors for controlling the shape and geometry of these contourite drift types?
- What is the potential of carbonate contourite drifts to reconstruct bottom current activity?
- It is possible to establish a classification for contourite drifts for isolated carbonate platforms depositional systems?

This work is structured as follows:

- 1) Introduction
- 2) A geological and oceanographic overview of isolated carbonate platforms and especially the Bahamian and Maldivian archipelagos.
- 3) A specific overview and description about the acquisition and processing methods, as the results of this study are mainly based on multichannel seismic data.
- 4) The main results of chapter 4 are divided into two main parts, each for the examined region of the Bahamian and Maldivian archipelago. After a general overview and a description of the seismic facies in chapter 4.2, chapter 4.3 presents the main current-related features of the Kardiva Channel of the Maldivian archipelago. Chapter 4.4 highlights the drift features identified at the Bahamian archipelago.
- 5) The discussion will answer the previous list of questions concerning carbonate contourite drifts and will discuss the interaction of bottom current activity and the formation of carbonate contourite drifts on isolated platform systems in the past.
- 6) Conclusion

## 2 Geologic Background and Oceanographic Setting

### 2.1 Contourite drifts

#### 2.1.1 Impact of bottom currents

Large bottom current systems are associated with the thermohaline circulation or wind-driven circulation (Stow *et al.*, 2008). Many processes, for example, internal waves, tides, benthic storms, barotropic waves, and dynamic instabilities that are varying the velocity and direction, trigger the bottom current (Rebesco *et al.*, 2008, 2014). Persistent bottom currents lead to features from winnowing the fine-grained sediments up to large-scale erosion and deposition (Rebesco *et al.*, 2014). In fine-grained drifts of calcareous mud and ooze, sediment can accumulate under bottom-current velocities of 5 to 20 cm/s (Stow *et al.*, 2009), while bottom-current speed (> 30 cm/s) are generally related to structures like erosive moats and contourite channels, which cut into the seafloor at the drift's margin.

In this study the term “bottom currents” is defined as a long-persistent water-mass flow that has the capability to interact with the seafloor by erosion, re-suspending, and transporting, as well as controlling the deposition by (re-)sedimentation of the transported solid material. On geological time scales these bottom currents generate large sedimentary bodies and/or erosional features (Hernández-Molina *et al.*, 2008a, b; Rebesco *et al.*, 2014). The term for these sediment bodies has not been well defined yet. Contourites are defined as sedimentary bodies affected by along-slope bottom currents and may be interbedded with other sediment types after Rebesco *et al.* (2014) or as sediments deposited or substantially reworked by the persistent action of bottom (contour) currents (Stow *et al.*, 2002a; Stow and Faugères, 2008; Rebesco *et al.*, 2014). Types of thick, extensive sedimentary accumulations are referred to as drifts or contourite drifts (Rebesco *et al.*, 2008; Hernández-Molina *et al.*, 2016). Most of the contourite drifts are typically deposited below about 300 m water depth (Stow *et al.*, 2008). However, contourite drifts exist from the shallow water to the abyssal floor (Faugères and Stow, 2008) and show a great variety in size, from small patch drifts (*ca* 10 km<sup>2</sup>) to basinal sheeted drifts (> 1,000,000 km<sup>2</sup>; Faugères and Stow, 2008). The sedimentological composition ranges from very fine-grained to coarse-grained deposits of siliciclastic, bioclastic, volcanoclastic and chemogenic components (Stow *et al.*, 2008).

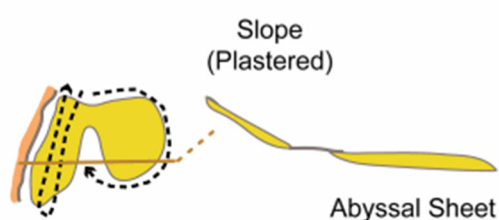
#### 2.1.2 Depositional and erosional features

Contourite drifts can be easily recognized when they have an along-slope, elongated mounded shape, and an adjacent concave moat (Rebesco *et al.*, 2014). Different sediment drift types are postulated by several authors (Rebesco and Stow, 2001, Stow *et al.*, 2002a, Rebesco, 2005, Stow and Faugères, 2008, Esentia *et al.*, 2018). Considering the published material, the drifts are grouped in (1) sheeted drifts, (2) mounded elongated drifts, which are subdivided in plastered, separated, and detached drifts, (3) channel-related drifts, (4) patch drifts, and (5) confined drifts, (6) fault-

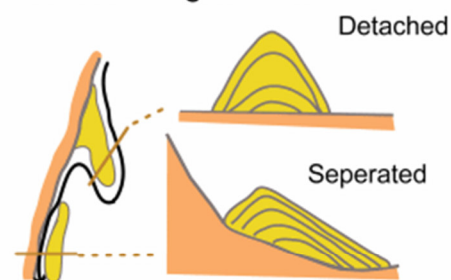
controlled drifts, (7) infill drifts, (8) downwelling drifts (Fig. 2.1), and mixed drifts, where along- and downslope currents shape the drift or in combination with other depositional processes in the building of the drift body (Faugères and Stow, 2008; Esentia *et al.*, 2018). The most recent compilation of contourite drift types and the derived current paths are published by Esentia *et al.* (2018) (Fig. 2.1). The postulated classification shows endmember in specific geological and hydrological contexts, but gradations between the types are abundant. All contourite drifts are

## Principal Drift Types

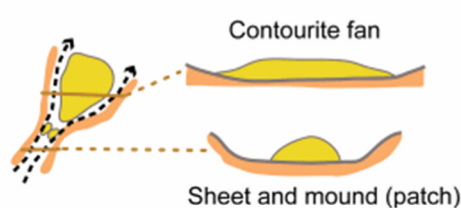
### Sheeted Drifts



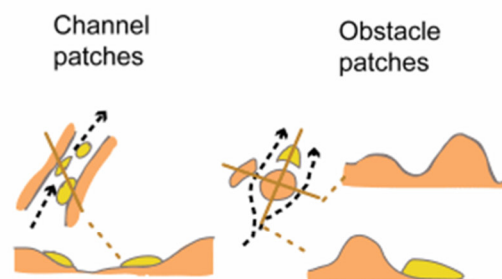
### Mounded Elongate Drifts



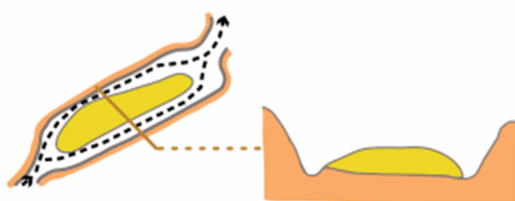
### Channel-Related Drifts



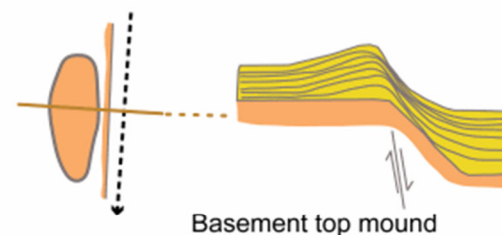
### Patch Drifts



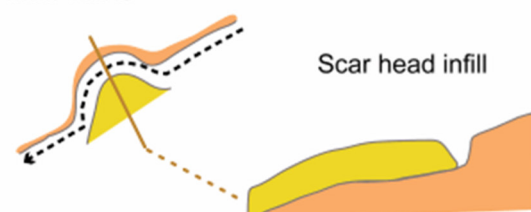
### Confined Drifts



### Fault-Controlled Drifts



### Infill Drifts



### Downwelling Drifts

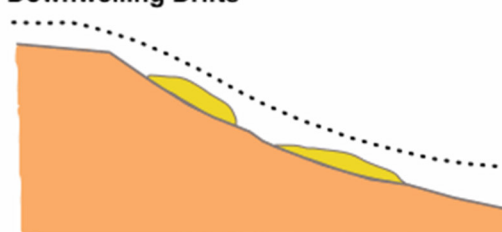


**Figure 2.1:** Sketches of plan views and cross-sections of sediment drift types and inferred bottom-current paths. Adapted from Esentia *et al.* (2018). Modified from work by Rebesco *et al.* (2014), and by Faugères and Stow (2008). The original classification was published in Rebesco and Stow (2001) and Stow *et al.* (2002a).

characterized by a variable degree of mounding and somewhat evident elongation (Rebesco *et al.*, 2014).

The bottom current activity results in several depositional, erosional features and bedforms concerning the contourite depositional system. Erosional features of large-scale erosions are divided in areal and linear features (Rebesco *et al.*, 2014). Areal erosional features are subdivided in terraces and abraded surfaces. Linear erosional features are subdivided by Hernández-Molina *et al.* (2008b) and García *et al.* (2009) in contourite channels, moats and marginal valleys (Fig. 2.2). Contourite channels cut into the basinal surface by the action of bottom currents. Moats are along-slope channels generated by non-deposition and local erosion below the bottom current axis (Rebesco *et al.*, 2014).

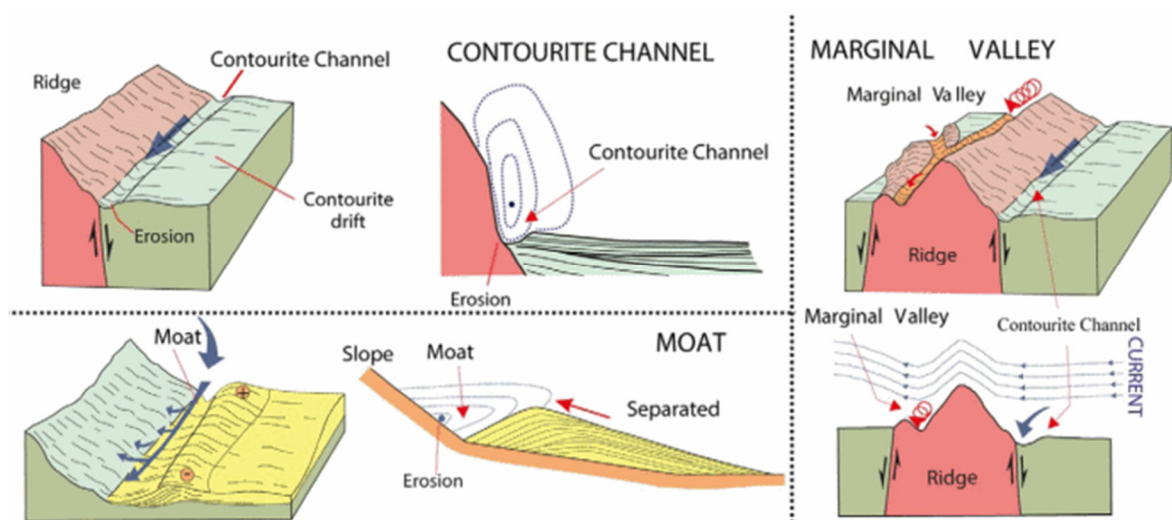


**Figure 2.2:** Main characteristics of areal and linear, large-scale contourite erosional features. Adapted from work by Rebesco *et al.* (2014), modified from work by Hernández-Molina *et al.* (2008) and by García *et al.* (2009).

## 2.2 Warm-water isolated carbonate platforms

Warm-water isolated carbonate platforms are areas of shallow-water carbonate deposition surrounded by deeper water on all sides (Schlager, 2005; Moore and Wade, 2013). They are characterized by steep platform margins and a (windward) platform rim protecting the platform interior against erosive ocean waves and currents. The platform rim consists of barrier reefs, barrier islands, and/or (early lithified) carbonate sand shoals (Schlager, 2005). The reefs of the platform rim are a high production zone for carbonate material, which is shed into the lagoon or down the slope. Under best growth conditions the backreef apron progrades into the lagoon and the rim and slope simultaneously prograde seawards (Schlager, 2005). The inner lagoonal area filled with sediments redistributed by reduced wave and current activity and/or in-situ produced sediments. The growth of patch reefs is abundant on the platform. Additionally, examples for modern platforms are the GBB in the Atlantic Ocean, atolls of the MA in the Indian Ocean and the Eniwetok Atoll in the western Pacific Ocean. The shape of (isolated) carbonate platforms and its

stratal geometries are steered by the lasting evolution through time of the interacting mechanisms of the tectonic setting, eustatic sea-level cycles, differential subsidence, the hydraulic regime and energy, and the type and amount of sediment being produced by the biota (Pomar, 2001; Williams *et al.*, 2011). The sediment is primarily provided by carbonate producing organisms, by growing carbonate shells, and reefal frameworks, as well as anorganic precipitation. The diverse-grained carbonate particles may be transported off-bank by tidal, wind-driven, and cascading density currents in the tropical realm (Eberli and Betzler, 2019).

### 2.2.1 Facies of isolated carbonate platforms

The grain size generally fines up down the slope towards the basin due to gravitative sorting of the platform debris. However, contour currents can be an important factor for sedimentation patterns on carbonate platform slopes (Betzler *et al.* 2013a, 2016b; Wunsch *et al.*, 2017). The facies of the isolated carbonate platform system is subdivided by following depositional settings from the lagoon to the basin after Wilson (1975) (Fig. 2.3):

#### 1) Basin

The setting is dominated by a mixture of pelagic and platform-derived material forming fine-grained carbonate oozes and muds.

#### 2) Deep shelf

This setting is not realized at isolated carbonate platforms due to the absence of continental crust.

#### 3) Toe-of-slope apron

The sea floor inclines with angles  $> 1.5^\circ$  basinwards. Mostly fine grained carbonate material mudstone units. Carbonate turbidites and large-scale, low relief channel are abundant.

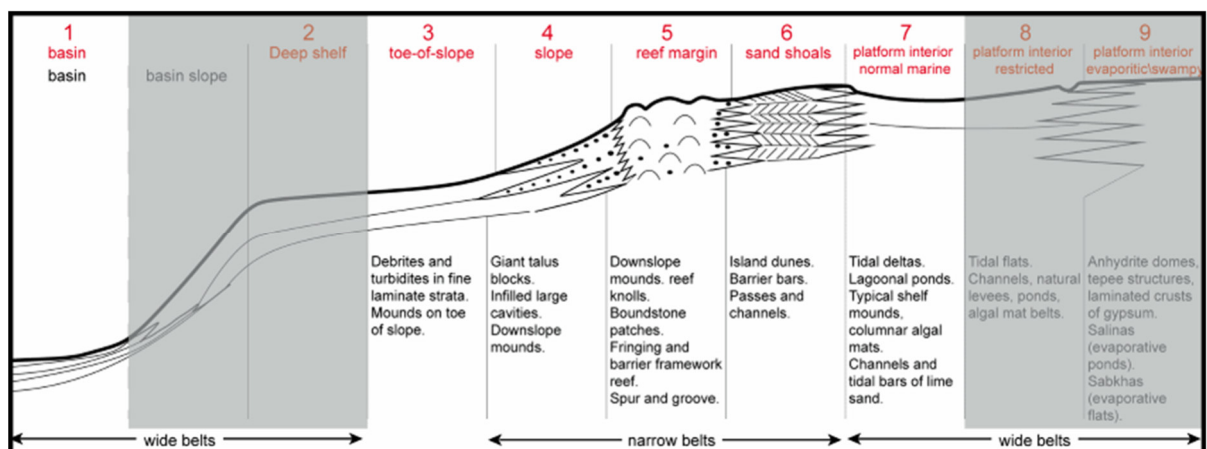


**Figure 2.3:** Depositional settings of isolated carbonate platforms, modified after Wilson (1975) and Schlager (2005). Uncommon settings for isolated carbonate platforms are greyed out.

#### 4) Slope

The sea floor inclines with angles  $> 5^\circ$  to near-vertical angles at platform walls. The slope sediment composition is fed by the reef debris, pelagic material and reworked material of the platform interior. The fore reef sediments are composed of relocated reef wall and crest debris and *in situ* produced material. The grain composition is mixed from silt to boulder-size and thin bedded and classified as mud- to wackestone after Dunham (1962). Blocks broken off the reef wall/crest, coarse-grained carbonate turbidites, and channel fills are common.

#### 5) Reef margin

Wave-resistant line of reefs and/or skeletal sands of pure carbonate material with a wide range of grain size characterizes the reef margin. The reefs are characterized by the consolidation of corals' framework in shallow water and by the greatest diversity of biological facies elements. Patch, fringing and barrier reefs are common. The space between the corals' framework is filled by carbonate detritus, bioeroded elements, and bound by abiotic cement. The reefs circumvallate the platform interior and can be interrupted by inter-reef channels or areas of carbonate shoals. The massive structural framework of the reefs is hardened by *in situ* cementation processes. The carbonate framework resists the wave and tidal energy of the ocean and stabilizes the reef wall. Storm events can cause erosion on the reef and, combined with bio erosion, fill the spaces between the corals with unconsolidated carbonate sand, silt and mud. The platform margin have the highest accumulation rate of carbonate material and faunal diversity compared to the other depositional settings. The reef complex distributes carbonate material in both directions, towards the platform interior and towards the slope and basin area by water, tidal and wind energy.

#### 6) Sand shoals

They are elongated grainstone bodies formed by tidal and current activity in the back reef area. Inter-reef channels can interrupt them.

#### 7) Platform interior/lagoon

The platform interior is shielded from the open ocean by shallow sea, barrier islands, barrier reefs and carbonate sand shoals. The setting is dominated by muds, muddy sands or sands. Grain size distribution depends on winnowing by waves and tidal current activity, as well as local sediment production. The back reef can be configured with patch reefs interveined by skeletal debris relocated from the reef crest.

### 2.2.2 Physical properties of carbonates and its implications for seismic measurements

At the time of deposition carbonate sediments often show very high porosity values between 40 to 60% (Bennett *et al.*, 1990). The porosity values are changed by diagenetic alterations of the

mineralogy, pore types cementation, compaction, dissolution and dolomitization processes (Eberli *et al.*, 2003). These alterations affect elastic properties of the carbonate rocks and results in a wide range of compressional- ( $v_p$ ) and shear-wave ( $v_s$ ) velocities. The compressional-wave velocity varies from 1700 to 6600 m/s, the shear wave velocity ranges from 600 to 3500 m/s (Eberli *et al.*, 2003). Generally, the two most important factors for a significant velocity increase are (1) a decreasing pore volume, whereby the fusing of grains by cementation is the most important factor for an increase in velocity, and (2) frame-forming pore types such as moldic and intraframe porosity. Portions of clay significantly decrease the compressional-wave velocity (Eberli *et al.*, 2003).

## 2.3 Bahamas

### 2.3.1 Geologic evolution

The Bahamian carbonate platforms developed on the extended crust of the North American plate (Mullins and Lynts, 1977). The collision of the northern arc of the Caribbean Plate and the passive margin of North America in the Eocene strongly affected the basement of the BA (Pindell and Kennan, 2009; Mann, 1999). The collision reactivated Jurassic rift faults and caused the breakup of the archipelago and opened seaways between the platforms (Eberli, 1991; Masafarro and Eberli, 1999). The collision phase with the buildup of the Cuban orogen terminated during the Eocene (Cruz-Orosa *et al.*, 2012). Following this collision, the region was transformed from a passive-margin into a foreland basin tectonic setting (Masafarro and Eberli, 1999). With the opening of the Cayman Trough and the shift of the Caribbean plate boundary to the northern edge of the Cayman Trough, the Florida Bahamas region again is in a passive margin setting (Masafarro and Eberli, 1999), although some shortening continued throughout the Neogene (Masafarro *et al.*, 1999). The southern portion of the SC, including CSB is part of the Cuban fold and thrust belt that also extends into the Nicholas Channel and the Old Bahama Channel (OBC) that lies between GBB and Cuba (Fig. 1.2).

The north-south trending SC separates two large isolated carbonate platforms, the GBB and the smaller CSB (Figs. 1.2 and 2.4). The SC opens into the Florida Straits north of CSB and the southern end is bordered by the northwest-southeast trending Nicolas Channel and the OBC. Many authors consider the Florida Straits as a deep open-ocean channel that has been affected by ocean currents since the Paleogene or Late Cretaceous (Mullins and Neumann, 1979; Ball *et al.*, 1985; Denny *et al.*, 1994; Hine, 2013). The morphology of the SC is related to the slope geometry of the two adjacent banks that have steep platform edges and upper slopes with decreasing angles with depth (Wunsch *et al.*, 2017). The SC has a sill depth of *ca* 530 m and a mean width of *ca* 65 km. The SC and its carbonate dominated sedimentation processes are affected by a complex interplay between along-slope bottom currents and density cascading processes off the platform margins (Wilson and Roberts, 1995; Betzler *et al.*, 2014a; Wunsch *et al.*, 2017). In the BA carbonate contourite drifts and current-related features (for example, furrows and sediment waves) are abundant in the seaways and consist mostly of periplatform ooze, that is, a mixture of particles derived from the shallow-water platform interior and pelagic organisms (Betzler *et al.*, 2009, 2013a, b, 2014a; Lüdmann *et al.*, 2013, 2016; Tournadour *et al.*, 2015; Chabaud *et al.*, 2016, Mulder *et al.*, 2019). The Santaren Drift (SD) started to form in the SC during the Middle Miocene (Eberli *et al.*, 1997; Anselmetti *et al.*, 2000; Bergman, 2005). The Sediments of the SD consist of a matrix of nannofossil ooze and minor amounts of micrite with variable amounts of admixed silt and clay. The major allochem is very fine to coarse sand-sized planktonic foraminifers (Eberli *et al.*, 1997). The planktonic foraminiferal associations are a mixture of *in situ* produced and reworked components that have drifted hundreds of kilometers (Lidz and McNeill, 1995). The input of terrigenous clastic sediment is low, and transported by currents from Cuba and Hispaniola (Eberli *et al.*, 1997) and windblown dust

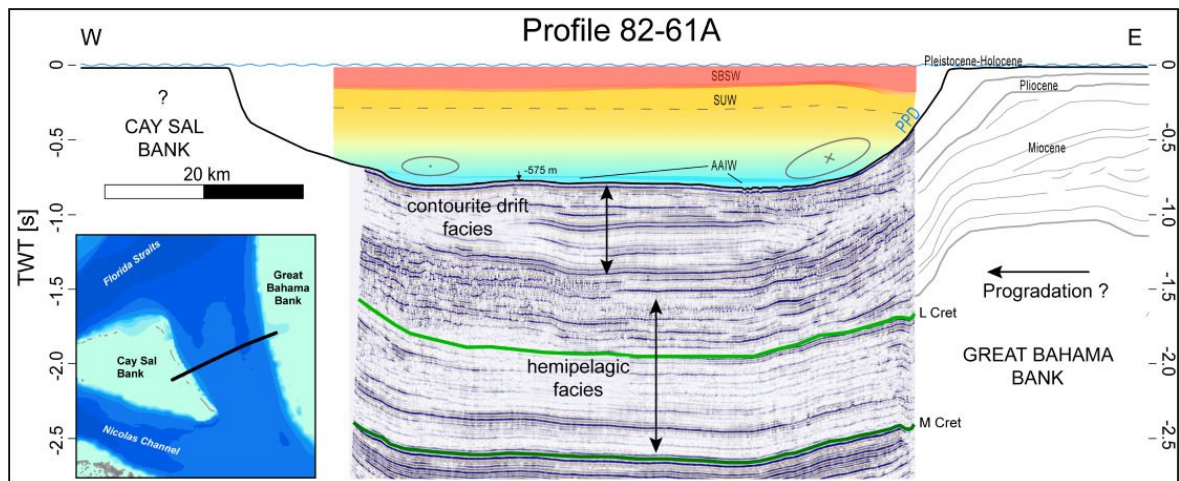


**Figure 2.4:** Industrial seismic profile of MCS data across the central Santaren Channel connected with the schematic platform growth of the Great Bahama Bank (Eberli *et al.*, 1997) and the topography of Cay Sal Bank (see Fig. 1.2B for location). Interpretation from Bergman (2005). Position of periplatform drift (PPD) is adopted from Betzler *et al.* (2014a). Water masses are adopted from Lüdmann *et al.* (2016). SBSW=South Bahama Surface Water, SUW=Subtropical Underwater, AAIW=Antarctic Intermediate Water.

(Westphal *et al.*, 2010). Carbonate contents are generally higher than 80 wt.%, while quartz components make up 0.5 to 1.5 wt.% (Eberli *et al.*, 1997). Acid-insoluble residues are mostly clayey components with a mean content of 12 wt.% (Eberli *et al.*, 1997). In the downhole physical measurements, the sonic and density logs reveal a smooth profile, resulting in small impedance contrasts (Eberli *et al.*, 1997; Kroon *et al.*, 2000), which is a typical feature of homogeneous drift sedimentation. Small impedance contrast and a lower amplitude variation, as in the more variable slope deposits, characterizes the drift deposit of the SD, the lateral homogeneity of the layers results in an extremely coherent seismic reflection pattern (Anselmetti *et al.*, 2000). The sediment drift facies interfingers with prograding carbonate bank deposits in the Florida Straits (Eberli *et al.*, 1997; Kroon *et al.*, 2000) that consist of turbidite, slump, and debris flow bodies (Eberli *et al.*, 1997, 2004; Betzler *et al.*, 1999; Anselmetti *et al.*, 2000).

Several additional contourite drifts are located around the BA: The northeastern slope of the CSB is characterized by the Cay Sal Drift (Bergman, 2005). The Pourtales Drift had been formed from the Middle Miocene to Late Pliocene (Bergman, 2005). It is located along the western margin of the Florida Channel and covers an area of > 24,000 km<sup>2</sup> with a length of > 400 km and a width of *ca* 60 km (Bergman, 2005). The accumulation thickness can reach about 1000 m. The surface of the contourite drift is covered by submarine sand dunes of varying shape and plastered with ripples (Correa *et al.*, 2012). The sediment composition of taken samples consist of coarse sand of mostly planktonic foraminifera and pteropods (Correa *et al.*, 2012). The Great Bahama Bank Drift (GBBD) has a maximum length of *ca* 85 km and a width of 60 km (Mullins *et al.*, 1980). The contourite drift has primarily prograded northwards with secondary growth to the east probably by easterly directed spin-offs from the Florida Current (Mullins *et al.*, 1980). The sedimentary composition consists mostly of moderately to poorly sorted sand-size fractions of carbonate particles of pelagic and bank-derived origin (Mullins *et al.*, 1980). The Little Bahama Bank Drift (LBBDD) reaches from 40 m water depth to 900 m water depth and consists of a periplatform sediment wedge in front of

the northwestern edge of the LBB (Chabaud *et al.*, 2016; Mulder *et al.*, 2019). The LBB extends over 60 km in width and 100 km in length and has prograded to the north (Mullins *et al.*, 1980). The sedimentary composition is characterized by periplatform oozes, which amount of pelagic components increases towards the distal part of the slope (Chabaud *et al.*, 2016). The total carbonate composition are aligned to a wackestone after the carbonate rock classification of Dunham (1962) with coarse bank-derived particles of organisms and clasts as well as fine-grained components, mostly aragonite needles (Chabaud *et al.*, 2016). The composition results in a bi-gradational grain size distribution due to changes in current velocity (Mulder *et al.*, 2019).

### 2.3.2 Oceanographic background

The Florida Straits and the SC are bathed in currents related to the strong Florida Current system. The main components of this system are waters proceeding from the North and South Equatorial Current. A water mass mixture of Antarctic Intermediate Water and the uppermost parts of North Atlantic Deep Water runs through the Windward Passage (Fig. 1.2A) and the Anegada-Jungfern Passage into the Caribbean Basin (Gröger *et al.*, 2003). The South Equatorial Current has lower salinity values due to the inflow of the Orinoco and Amazon Rivers, which, together with the Subtropical Underwater, enter the Caribbean Sea through channels between the Greater and the Lesser Antilles (Steph *et al.*, 2006; Johns *et al.*, 2002), flowing northwest through the Yucatán Channel. In the Gulf of Mexico, the currents form the Loop Current, which flows, deflected to the east, through the Florida Straits into the North Atlantic Ocean (Lynch-Stieglitz *et al.*, 1999).

Due to the complex behavior of the water masses and their interaction with land masses and wind pressure, the Florida Current forms highly variable cyclonic eddies that enter the SC and Nicholas Channel (Kourafalou and Kang, 2012). Three water masses are identified by Lüdmann *et al.* (2016) in the water column of the SC. Salinity increases and temperature decrease from the South Bahama Surface Water (25.5 °C, salinity 36.1 PSU) from the surface towards the salinity maximum of the Subtropical Under Water (STUW, 23 °C, salinity 36.8 PSU) at *ca* 180 m depth (Fig. 2.4). Further down, temperature and salinity declines to the bottom to 9.4°C and 35.1 PSU representing the Antarctic Intermediate Water at *ca* 600 m water depth. Current measurements show a northward-flowing contour current at the east side of the SC and a weaker countercurrent at the margin of the CSB (Leaman *et al.*, 1995; Lüdmann *et al.*, 2016). Approximately less than  $2 \times 10^3 \text{ m}^3/\text{s}$  of inflow enters the Florida Straits via the SC, fed by the OBC, with a strong subsurface current and at maximum speed at 300 m water depth (Rousset and Beal, 2014). The inflow of the subsurface water masses of the North Atlantic Central Water (Talley *et al.*, 2011) through the OBC is propelled by the thermohaline subtropical gyre and wind-driven currents (Johns *et al.*, 2002). Ocean currents line the platform flanks and do not enter the platform interior, where the water circulation follows the prevailing wind regime of easterly winds (Bergman *et al.*, 2010).

## 2.4 Maldives

The Maldivian archipelago is the dominant isolated carbonate platform system within the Indian Ocean and is located in the tropical central equatorial Indian Ocean southwest of India (Fig. 1.1). The double rowed atoll chains characterize the Maldives and divide the Arabian Sea from the Laccadive Sea and enclose the bank-internal hemipelagic basin, called the 'Inner Sea' (IS), with water depths down to 550 m and more in deep water channels (Fig. 1.3B). The recent Maldivian archipelago consists of about 1200 small atolls forming discontinuous rims of 22 ring-shaped and elongated varying-sized reef complexes with lagoonal areas (Aubert and Droxler, 1996) with inner-atoll water depths of up to 50 to 60 m (Betzler *et al.*, 2015a). The main islands, which have a maximum height of 5 m, are located between the *Equator* and latitude 8°N. The water depth varies from the surface at the atolls to 550 m water depths in the channels down to more than 2000 m at the toe of the platform wall at the deep sea basin. The topographic features of the MA intersects all major deep and bottom-water masses in the Indian Ocean and thus they have an impact on the exchange of the water masses between eastern and western bathyal zones of the Maldives.

### 2.4.1 Geologic evolution

The north-south-oriented double chain of atolls is based on an isolated carbonate mega platform with up to 3 km thick coverage of shallow-water carbonates and periplatform ooze (Duncan and Hargraves, 1990; Aubert and Droxler, 1992, 1996; Purdy and Bertram 1993), which accumulated since the Eocene, placed above the central and largest part of the 3000 km long volcanic Laccadive-Chagos ridge (Purdy and Bertram, 1993). The Laccadive-Chagos ridge developed as part of a Hot-Spot-volcanism track during the lower Paleogene (Duncan and Hargraves, 1990), which comprises a connection between Deccan Traps basalts onto the Indian subcontinent and the island of Réunion, east of Madagascar. The ODP Leg 115 recovered basaltic material of the Hot-Spot-track at the areas of the Laccadives, Maldives, Chagos-archipelago, Mascarene Plateau and the islands of Mauritius and Réunion. The following researches show, that the dated ages got younger from north to south (Duncan and Hargreaves, 1990). The volcanic ridge system complex of the Maldives is interveined by faults and graben structures, which are generated in the main phase of volcanic activity (Aubert and Droxler, 1996, Purdy and Bertram, 1993). The top-lying basalts of the basement have an age of 55 Ma. The start of the evolution of carbonate banks were placed at the early Eocene on topographic highs at the outer rim of the volcanic ridge system (Fig. 2.5). The graben-structures were filled by collapsed volcanic material and carbonate sediments (Belopolsky and Droxler, 2004). The formed paleo-platforms show aggradation with backstepping of the inner platform rim during the Oligocene (Belopolsky and Droxler, 2003), that results in an areal extension of the paleo-IS. During the early Miocene, the carbonate production system at the outer rim along the ridge formed

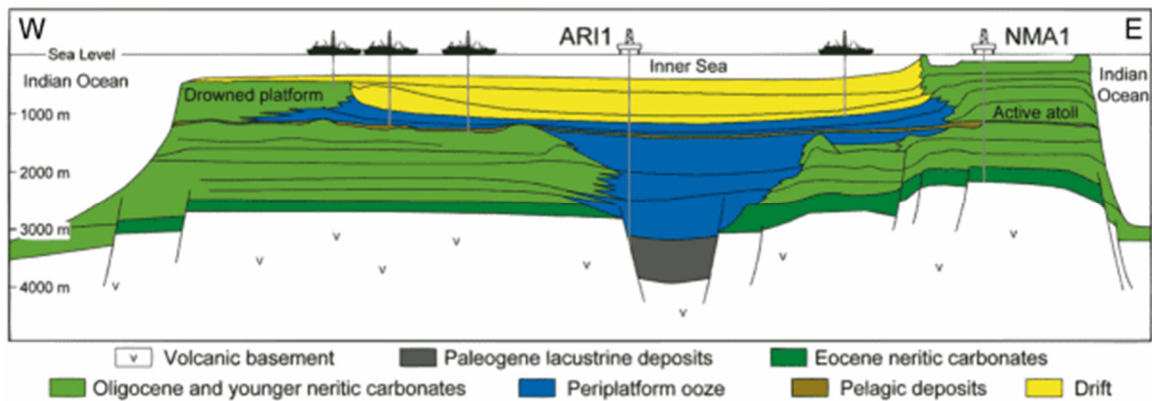


**Figure 2.5:** Schematic cross section through the Maldives carbonate platform system with projected location of industry wells ARI-1 and NMA-1 as well as the locations of IODP sites. The contourite drift facies encompass all current-controlled features and sediments (sheeted drifts, drift fans, and submarine dunes) of the Maldives carbonate platform after Betzler *et al.* (2018).

two north-south oriented lines of platforms that protects the originated IS from the open ocean (Aubert and Droxler, 1996). The western platform line prograded towards the aforementioned inter-platform basin and resulted in the modern shape of the IS during the Miocene (Aubert and Droxler, 1996). Coincident with onset of the monsoon system the IS was filled with carbonate sediment drifts (Lüdmann *et al.*, 2013; Betzler *et al.*, 2016a) and the platform rim was interveined with new established inter-atoll channels due to partial drowning (Betzler *et al.*, 2009). The MA is subjected to an unknown rate of subsidence by cooling of the basement and isostatic levelling of variable sedimentary load and compaction. The ridge and established carbonate platform rise almost 2000 m above the surrounding seafloor. Purdy and Bertram (1993) proposed a subsidence rate of *ca* 7 cm/ka for the Miocene, recent researches determine a rate of 15 cm/ka during the last 135,000 years by analyzing a drill core, which is obtained onto the Rasdhoo-Atoll (Gischler *et al.*, 2008).

The reef complexes are relicts of a drowned mega platform (Figs. 2.5 and 2.6). Coincident with the partial drowning of the mega platform, the drift sedimentation starts to fill the basin of the Inner Sea at the end of the Middle Miocene (Lüdmann *et al.*, 2013, Betzler *et al.*, 2009, 2017). Submerged banks show elongated geometries formed by currents (Betzler *et al.*, 2013a) The margin of the Maldives facing the open ocean is enthroned on steep walls, which drop down to deep lower bathyal water depths. The walls facing the Inner Sea reach down to water depths of a few hundred metres with rapidly declining dip gradients (Fürstenau *et al.*, 2010). The paleo-IS enclosed by the Miocene mega platform provide accommodation space and is filled with periplatform ooze and drifted and reworked calcareous periplatform material by bottom current activity (Betzler *et al.*, 2013b, Lüdmann *et al.*, 2013, 2018). Betzler *et al.* (2009) demonstrate that slope and bank geometry of the MA has been shaped by currents and the monsoon since the Miocene.

#### 2.4.2 Oceanographic background

The Maldives are affected by the equatorial (tropical) climate dominated by the monsoon wind system (Kotttek *et al.*, 2006; Storz and Gischler, 2011). The main force for propelling the ocean

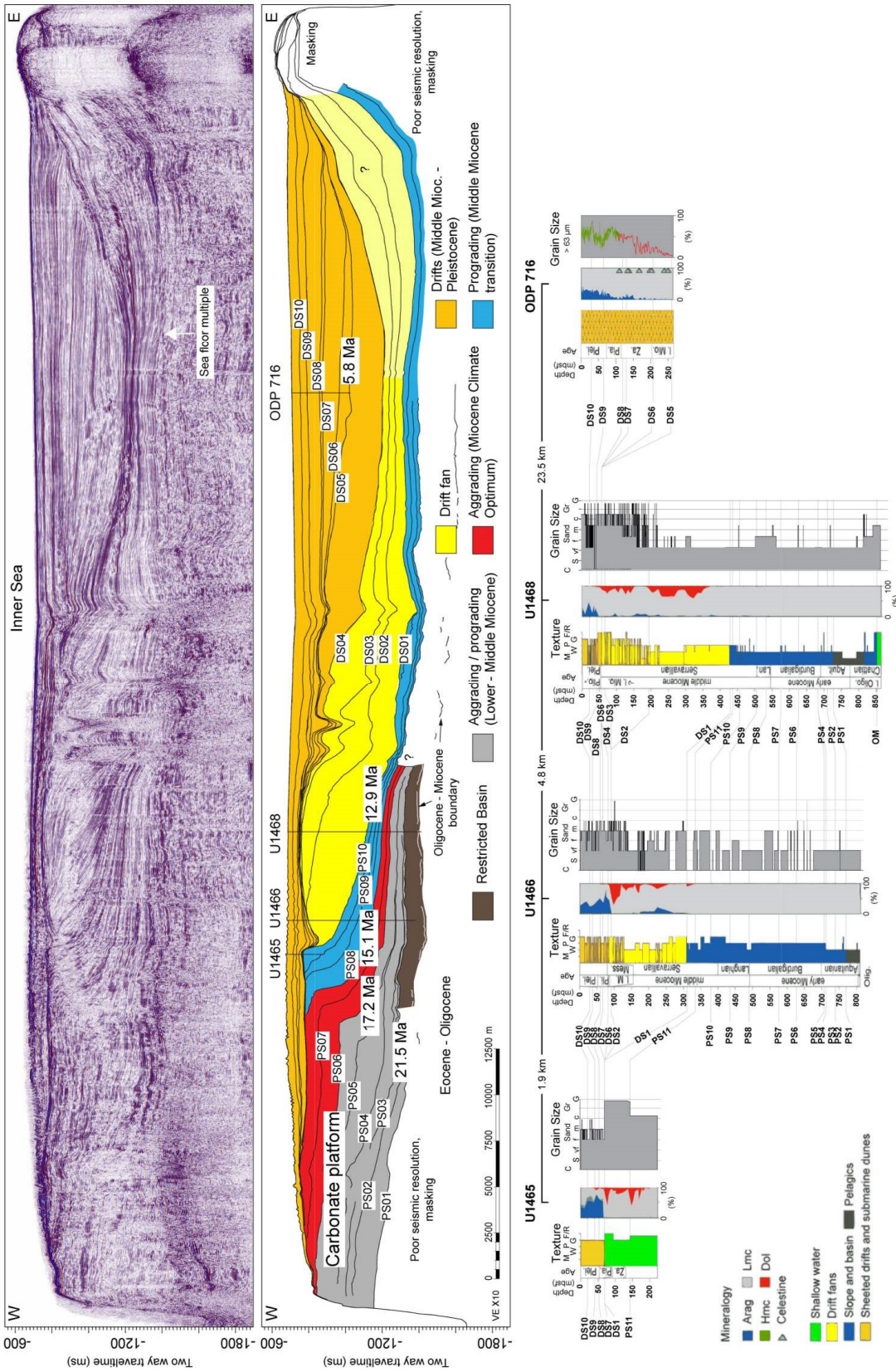


**Figure 2.6:** Seismic line across the Maldives Inner Sea (for location see Fig. 1.3) with line drawing showing the platform sequence boundaries (PS) and the drift sequence boundaries (DS). Three carbonate platform growth packages are differentiated: a lower to middle Miocene aggrading to prograding package, a dominantly aggrading middle Miocene package followed by a Middle Miocene prograding package. Seismic interpretation adapted from Betzler *et al.* (2016a, 2018) and Lüdmann *et al.* (2018). Ages of selected horizons are given. Sequence stratigraphic correlation of IODP and ODP Sites across the Kardiva Channel in the Maldives (see Fig. 1.3 for locations) are adapted from Betzler *et al.* (2017, 2018) and Duncan *et al.* (1990). After Dunham classification of carbonate rocks (1962): M=mudstone, W=wackestone, P=packstone, G=grainstone, and R=floatstone/rudstone. OM=Oligocene-Miocene boundary. Carbonate mineralogy of (I)ODP Sites: blue: aragonite, green: high Mg calcite, gray: low Mg calcite, red: dolomite.

currents at the northern Indian Ocean is the Indian monsoon system (Shankar *et al.*, 2002; Tomczak and Godfrey, 2003). The monsoonal system generates seasonal reversing ocean currents in the MA driven by southwestern winds from April to November and northeastern winds from December to March. Consequently, the MA is bathed in monsoon induced currents, namely the Southwest Monsoon Current and the Winter Monsoon Current (Schott and McCreary, 2001). The number of inter-atoll channels correlates with the influence of the monsoon and decreases in southern direction (Gischler *et al.*, 2013). Vigorously flowing and seasonally reversing ocean currents affect the study area of the KC with its adjacent atolls (Betzler *et al.*, 2009, 2013a, 2016b, Lüdmann *et al.*, 2013, 2018). Open ocean currents reached the archipelago interior via inter-atoll channels and resulted in the deposition of ten mega-drift sequences in the IS (Lüdmann *et al.*, 2013, 2018; Fig. 2.6). Monsoon induced surface and bottom currents have been the most important factor for periplatform depositional system at the MA resulting in contourite drift bodies surrounding the atolls in the IS (Betzler *et al.*, 2009, 2013a, b, 2016a, b; Lüdmann *et al.*, 2013, 2018). The monsoon propelled ocean currents can reach velocities up to 2 m/s within the modern atolls' passages and the currents reach water depths of more than 200 m (Tomczak and Godfrey, 2003). Further research in the area has discovered details of the current activity by forming smaller carbonate contourite drift bodies at the eastern entrance of the KC (Lopez *et al.*, 2011).

### 3 Data and Methods

This thesis brings several geophysical datasets and drill core records from the Miocene, Pliocene, and Pleistocene together. A wide range of datasets of geophysical tools, for example, multichannel seismic, multibeam and sub-bottom profiler, i.e. Parasound, datasets are used in this thesis. This chapter comprises descriptions of the theoretical principles, the methods of data acquisition, as well as the necessary processing procedures to convert the raw data into interpretable data. The main part of the presented multichannel seismic data were acquired during two scientific cruises. The first dataset were acquired by the research vessel (RV) Meteor in April 2013 (M95 by Betzler *et al.*, 2014b) and the second dataset during RV Sonne cruise SO236 (Betzler *et al.*, 2015b) in August 2014. The RV Meteor cruise targeted the BA and the RV Sonne, in preparation for Expedition 359 of the IODP, sailed in inter-atoll channels and across the IS in Maldivian waters. Additional hydroacoustic data were acquired by ship-based parametric sub-bottom echosounder and multibeam devices parallel to the seismic profiling. Previous collected datasets of scientific and industrial surveys were integrated in the database to enhance the quality of the seismic grids (Table 1).

**Table 1:** General information about the scientific cruises, the seismic acquisition systems, and survey settings.

Survey	So236 (2014)	Hope Cruiser (2011)	M74 (2007)	M95 (2013)	RV Lone Star (1994)	Geophysical Service Inc.
Area	Maldives	Maldives	Maldives	Bahamas	Bahamas	Bahamas
Source	1 + 1 GI-Gun	1 Boomer plate (300 J)	2 GI-Guns	1 + 1 GI- Gun	1 GI-Gun	1 Airgun
Volume (litre)	3.2l	-	4.9 l	3.2l	2.2 l	33 l
Pressure (bar)	150 - 180	-	-	150 - 180	150	-
Spatial Shot Interval (m)	12.5 - 16.7	0.533-1.2 s	25	12.5	-	-
Source Depth (m)	2	-	2.5	2.5	2	-
Receiver Depth (m)	2	-	4	2.5 - 4	3 - 4	-
Streamer Length (m)	600	-	600	600	600	3200
No. Of Channels	144	24	144 / 24	144	24	96
Record time (s)	4	0.2 s	3.5	3	2.5	7
Dominant Frequency Bandwidth (Hz)	20 - 200	-	100 - 120	20 - 200	100-200	40-55
Sampling rate (ms)	1	-	1	1	-	-
CMP Interval (m)	16.7	< 2	12.5	18.75 /6.25	12.5	12.5
Acquired MCS profiles	62	-	43	27	-	-
Total MCS profile length (km)	1715	-	about 1460	1393	1200	-
Acquired SBP/SBE Profiles	163	45	75	148	-	-
Total profile length (km)	4247	331.5	about 3720	3016	-	-

## **Bahamas**

The 27 multichannel seismic (MCS) lines were acquired during RV Meteor cruise M95 CICARB (Current Impact on the Facies and Stratigraphy of Bahamas Carbonate Platform) in April 2013, with a total length of *ca* 1,400 km. The acoustic source was a two-gun array of a 150 in<sup>3</sup> GI gun and a 45 in<sup>3</sup> mini-GI gun (SERCEL, Carquefou, France), 3.2 l in total, operated in 2.5 m water depth loaded with 150 to 180 bars. The guns were distance-triggered through a differential Global Positioning System (GPS) navigation with a shot interval of 12.5 m at a survey speed of 5 kn. The reflection seismic investigation was carried out with the use of one 144-channel digital streamer with an active length of 600m (HYDROSCIENCE TECHNOLOGIES, Inc., Mineral Wells, TX, USA). The position of the streamer was controlled and stabilized by four compass birds at an operation depth of 2.5-4.0 m. The seismic data were recorded at a sample rate of 1 ms for 3 s. The data were band-pass filtered and cut to a 20-200 Hz main frequency spectra. To eliminate multiple signals within the water column, a predictive deconvolution of pre-stack data were applied. Further, the data were corrected for normal and dip moveout, post-stack migrated, and stacked with a bin-size distance of 6.25 m, resulting in an average CDP fold of 66. An automatic gain control and other processing steps were applied with a ProMAX 2D (HALLIBURTON-LANDMARK, Houston, TX, USA) software package. The processed data were loaded into Petrel E&P (SCHLUMBERGER N.V., Curaçao, Netherland) software for visualization and interpretation. Additionally, MCS lines are combined with lower-resolution industrial survey data acquired by GEOPHYSICAL SERVICE INC. (Calgary, Canada) to enhance the seismic grid (Table 1).

## **Maldives**

Data of the RV Sonne cruise SO236 in April 2014 comprises geophysical and sedimentological operations in the area of the IS and the KC. Multichannel seismic as well as sub-bottom profiler (Parasound) and multibeam systems were used to study the channel geometry and sedimentary structures in relation to the geologic history of the area. 62 MCS profiles with a total length of 1,715 km cover the KC as well as the IS (Fig. 3.1A) and crosses the location of ODP leg 115 Site 716 (4°55'59.9"N, 73°16'59.9"E). As pre-site survey for IODP Expedition 359 (November 2016), the seismic profile crosses the drill hole sites of the surveyed IODP leg 359 U1465-U1472. The new seismic profiles were jointly interpreted with available seismic data from former surveys of RV Meteor cruise M74 in 2007 and a shallow-water survey of the temporary RV Hope Cruiser resulting in a MCS network of more than 3100 km in the waters of the Maldives (Fig. 3.1A and B).

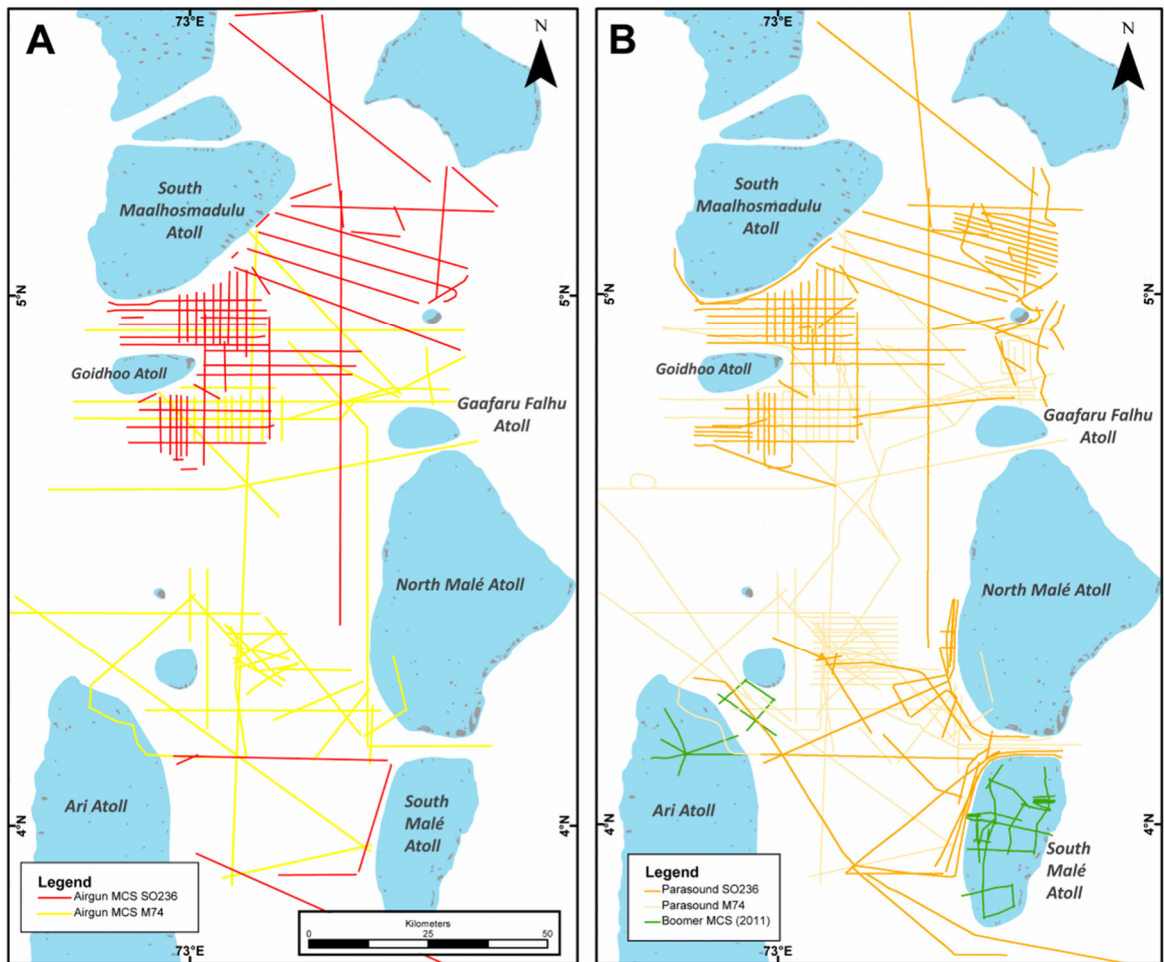


**Figure 3.1:** **A:** Map of the MCS profiles that were acquired during M74 (yellow) and SO236 (red) cruises. **B:** Map of the Parasound echosounder profiles that were acquired during M74 (light orange) and SO236 (orange) cruises. Green lines display the profiles of the RV Hope Cruiser survey in 2011.

### 3.1 Theory of marine seismic reflection

Marine seismic reflection is a geophysical tool of acquiring subsurface data and to image the earth's response to seismic waves. Seismic waves are differentiated in primary compressional waves (P-waves) and secondary shear waves (S-waves). The latter mentioned are unable to propagate and liquids and are negligible in marine environments due to the low energy level of converted waves at the seafloor. The P-wave velocity  $v_p$  depends on the porosity, the lithology, the pressure, the water and gas saturation, the cementation of the solid material, and also the geological bedding is one of several factors, which affect the response (Sheriff, 1977). The P-wave velocity travelling through an isotropic material is defined by:

Eq. 1

$$v_p = \sqrt{\frac{K + \frac{4}{3}\mu}{\rho}}$$

Where  $K$  is the modulus of incompressibility,  $\mu$  the shear modulus, and  $\rho$  the density of the sounded material. The P-wave velocity in the water column is defined by the temperature, pressure and the salinity and is about 1500 m/s. An acoustic signal is emitted by an acoustic source and propagate spherical through the water column into the underlying geological layers. The acoustic signal reflects on different layers with a specific amplitude due to the acoustic impedance contrast, which is defined as quotient of the product of the density and the acoustic velocity of the bottom layer, divided by the product of density and velocity of the upper layer under perpendicular propagation angles. The reflection coefficient  $R$  is related to the acoustic impedance contrasts of both interacting layers:

Eq. 2

$$R_{12} = \frac{\rho_2 v_2 - \rho_1 v_1}{\rho_2 v_2 + \rho_1 v_1}$$

Where  $v$  is the compressional wave velocity and  $\rho$  the density of the upper (1) and lower part (2) of two geological layers. The non-reflected energy of the seismic wave is transmitted and travelled further down through different geologic layers. The energy of the seismic wave decreases with increasing depth due to reflection, attenuation and absorption of the wave energy and the spherical divergence. The vertical and horizontal resolution of the seismic wave depends both on the frequency  $f$  of the seismic wave. The horizontal resolution is defined by the first Fresnel zone, which depends on the depth and the frequency  $f$ . The vertical resolution to differentiate geologic layers is given by a quarter of the wave length  $\lambda$ . Smaller wave lengths differences tend to interfere in a constructive way and prevent the differentiation.

The reflected waves travel back to the ocean's surface and will be recorded by a hydrophone or arrays of hydrophones. A reflected waves can be re-reflected within a geologic layer or between

the sea surface and the seafloor. The amplitude of re-reflected waves correlates with the impedance contrast. The re-reflected waves, secondary reflections or multiples interfere with the useful signal of primary reflections and increases the amount of noise. The identification and attenuation of the multiple signal is an important step during the seismic processing (see chapter 3.2.4).

### 3.1.1 Seismic interpretation

The procedures for interpreting stratigraphy from seismic image involve three principle stages: (1) seismic sequence analysis, (2) seismic facies analysis, and (3) interpretation of depositional environments and lithofacies (Vail, 1987). Seismic sequence analysis involves identification of major reflection packages that can be delineated by recognizing surfaces of discontinuity defining the seismic units. Discontinuities may thus be recognized by interpreting systematic patterns and reflection terminations along the discontinuity surfaces. These reflection terminations are grouped in upper boundaries and lower boundaries (Fig. 3.2). The latter consists of 'onlap' and 'downlap' termed terminations, 'toplap' and (erosional or structural) truncation represent the upper boundary (Mitchum *et al.*, 1977a). A concordance shows no termination reflection against upper and lower boundaries but can be take part as a boundary (Fig. 3.2).

Seismic facies unit analysis takes the interpretation process one step beyond seismic sequence analysis by examining sequences due to smaller reflection units that may be the seismic response to lithofacies. Seismic facies are packages of reflections with a set of internal seismic characteristics differing from adjacent facies (sub-)units. The recognition and mapping of seismic facies units and seismic facies analysis are called seismic stratigraphy after the groundwork of Mitchum *et al.* (1977b). The set includes reflection geometry, continuity, and amplitude and can be extended by internal velocity (Mitchum *et al.*, 1977b). The reflection continuity represents stable physical properties along the reflectors and stable calm conditions of the main energy in the depositional environment. The amplitude strength depends of the reflection coefficient  $R$  (see Eq. 2) and is associated with the change in density. Lateral changes in amplitude strength indicate lateral energetic changes of the depositional environment at the same time interval. High amplitude

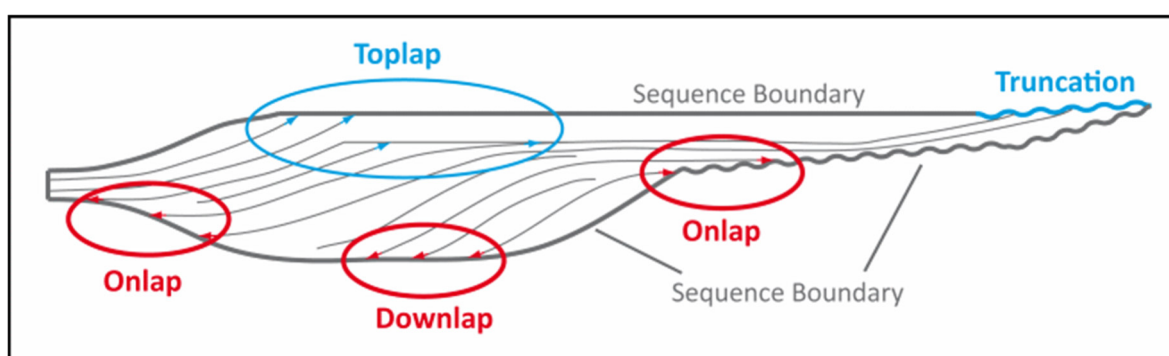


**Figure 3.2:** Example of reflection termination patterns. The upper sequence boundary is defined by toplap terminations and truncations. The lower sequence boundary is defined by onlap and downlap terminations.

reflections and variations in the internal reflections strength can point out large temporary changes in current strength or sediment supply (Nielsen *et al.*, 2008; Müller-Michaelis *et al.*, 2013), while acoustically transparent sediments may indicate towards stable moderate flow velocities (Gruetzner and Uenzelmann-Neben, 2016).

The frequency is defined as the time interval between two stacked over one another reflections and is associated to the bed thickness and the presence of fluids (Mitchum *et al.*, 1977b). The internal velocity gives an estimation of the lithology and/or porosity. The internal reflection configuration consist of a wide range from simple forms of planar dipped and subparallel patterns with wavy or curved character over divergent and chaotic patterns to modified reflection configurations, for example hummocky, lenticular, disrupted, and contorted forms as well as reflection-free patterns (Fig. 3.3). More complex reflection configuration patterns are prograding clinoforms, which are distinguished in sigmoid, oblique, complex, shingled, and hummocky (Mitchum *et al.*, 1977b; Fig. 3.3). A key for understanding the geological processes behind the seismic image for an interpreter is the three-dimensional shape. The external three-dimensional forms are distinguished in sheeted forms, forms with convergent boundaries, for instance, wedges and lenses, and depressions, like trough and elongated troughs (Fig. 3.3). The external form are

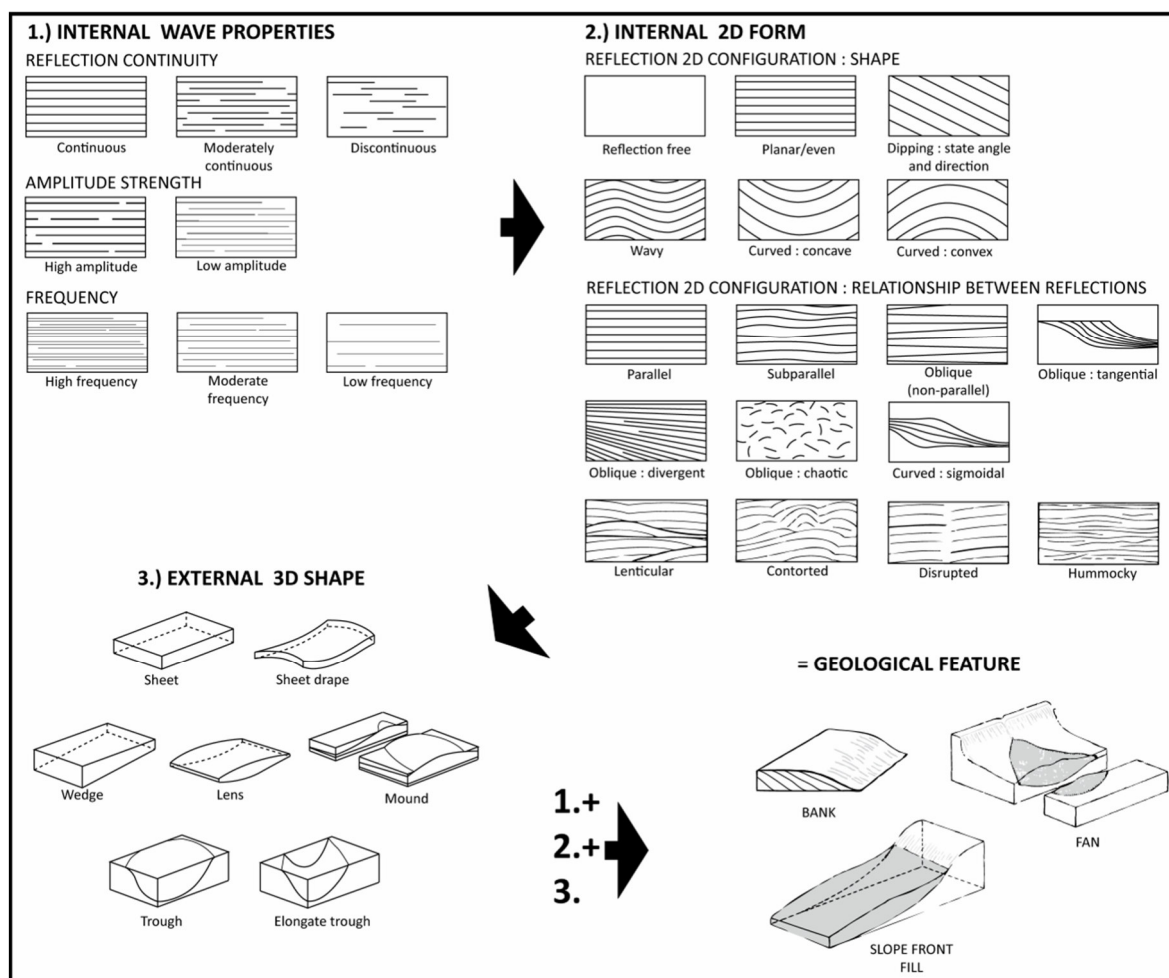


**Figure 3.3:** Terminology to define and describe seismic reflections, reflection configuration, and seismic facies resulting in interpretation of geological features. Compiled and modified from Campbell (1967), Mitchum *et al.* (1977b), Sangree and Widmier (1977), and Allen (1982).

associated to superior geological processes and can be divided into subtypes by their internal reflection pattern. The mounded forms are common for contourite deposits (Faugères *et al.*, 1999). The result of the seismic stratigraphy analysis is associated with a specific depositional environment and geology of the subsurface as well as chronostratigraphic information by tracking sequence boundaries. The seismic interpretation can be correlated with additional data of sedimentological samples and physical drill cores methods to refine the geological model.

#### 3.1.1.1 Seismic interpretation of contourite drifts

Seismic-reflection profiling and multibeam echosounders reveal the internal seismic character and geometry as well as the surface characteristics and the large-scale morphology. An overview of seismic characteristics has been given by different authors (Faugères *et al.*, 1999; Stow and Faugères, 2008; Nielsen *et al.*, 2008). An elongate-mounded contourite drift shows continuous semi-parallel (aggradation) to less continuous, oblique to sigmoidal (progradation) reflections and local slightly erosive structures beneath the (paleo-)current / channel axis (Faugères *et al.*, 1999). The internal seismic character is dominated by a uniform pattern of low to moderate amplitude reflections with continuous or discontinuous and chaotic reflections (Faugères *et al.*, 1999; Nielsen *et al.*, 2008). The external mounded shape of contourite drifts is supported with downlap terminated reflections onto the basal surface.

## 3.2 Multichannel seismic reflection data acquisition and processing

The acquisition of 2D seismic reflection data is briefly described in the first two sections (see section 3.2.1 and 3.2.2). The last two sections address the seismic data storage format (see section 3.2.3) and the 2D seismic data processing (see section 3.2.4). The multichannel seismic dataset of cruise M95, the Parasound and the multibeam datasets had already been processed before this thesis started by the sedimentology and stratigraphy working group of the Institute for Geology (University of Hamburg). The overall configuration of the MCS survey equipment were similar on both cruises of M95 and SO236 (Table 1). The GPS data, bird data and source-receiver geometry were linked together with the internal software program *FogCurve*. The dataset processing of cruise SO236 was realized by *SeisSpace* and *ProMAX* Seismic Processing Software. In particular, the processing of the seismic data using the *ProMAX* software is explained in detail with chosen modules and parameters of the processes. The MCS survey speed was 5 to 5.5 kn for MCS surveys and 6 to 7 kn for hydroacoustic-only surveys.

### 3.2.1 The seismic source

Air is stored in two chambers inside the gun under pressure to create an acoustic signal by deaeration. The generator chamber fires first and releases the accrued air into the water to create a bubble. The blast produces the primary pulse and the bubble starts to expand. Just before the bubble reaches its maximum size and going to collapse with oscillating movements owing to the water pressure, the injector chamber releases the stored air into the bubble. The violent collapse is prevented by the release of additional air of the injector chamber into the bubble and stabilizes the bubble by an increase of the internal pressure. This procedure reduces the oscillation of the bubble and its unwanted resulting secondary pressure pulse. The stabilizing of the generated bubble generates a clean acoustic signature for the emitted sound wave.

An array of two compressed air propelled distance-triggered GI-Guns (Generator/Injector) were used for generating the seismic signal. The array consists of a standard GI gun (SERCEL, Carquefou, France) and a mini-GI gun with a total Volume of 3.2 l (150 cu in + 45 cu in), loaded with 150 bar (15 MPa) or 180 bar (18 MPa). The mini-GI gun emits a signal of higher frequency than the standard GI gun to get a better resolution about the upper sediment structures. The gun-array were towed behind the vessel. The navigation data were provided by a heading GPS system (HEMISPHERE V101, Scottsdale, AZ, USA) for synchronizing the gun-array for a shooting interval of 12.5 m and 16.7 m at a vessel speed of 5 kn. A general overview of the system setting is given in Figure 3.4.

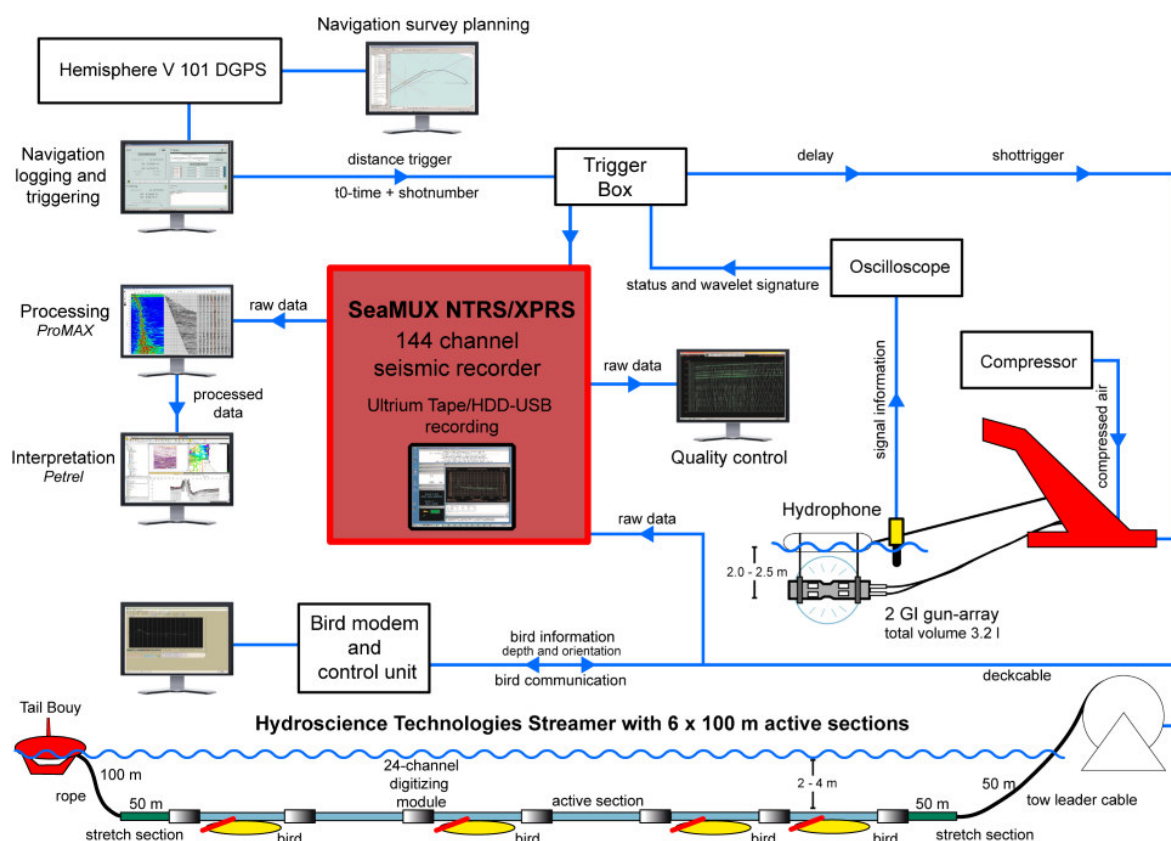


**Figure 3.4:** General overview of the multichannel reflection seismic system and the data flow used during research cruises S0236 and M95.

### 3.2.2 The seismic receiver

The receiver system was an oil filled 144-channel digital streamer with an active hydrophone array length of 600 m (HYDROSCIENCE TECHNOLOGIES, Inc., Mineral Wells, TX, USA). Series of hydrophones are grouped to channelize the signal for each digital channel in increase the signal quality. The streamer was depth controlled by four navigator birds (GEOSPACE TECHNOLOGIES, Houston, TX, USA) at 2 to 2.5 m water depth (Fig. 3.4). The datalink between the navigation computer and the bird are realized by an electromagnetic coil in the streamer system. The datalink is used to control the rudder of the birds and to receive information about the heading of the integrated magnetic compass and the water depth of the integrated pressure sensor. The data was sampled with a rate of 1 ms and a record length of 3 s and digital stored.

### 3.2.3 The data storage

The runtime of the emitted source signal and its reflections are recorded in milliseconds (ms) of their two-way travel time (TWT). Therefore, depth and thickness of seismic profiles and thickness maps are expressed in ms of TWT. The obtained information can be imaged in seismic pictures and/or stored in standard file formats like the open standard SEG-Y file format which is developed

by the Society of Exploration Geophysicists (last version: Hagelund and Levin, 2017). Each shot number and the received signal trace of each channel are stored in a single SEG-Y file.

### 3.2.4 The data processing

Processing of the obtained seismic data (raw data) are necessary to get rid of multiple reflections, coherent and random noise, and geometric effects of the ray path to get a clear image of the subsurface structures for geologic interpretation. Seismic traces show an amplitude decrease with time by divergence, absorption, scattering and transmission losses (Hatton *et al.*, 1986). The seismic data processing is a profound step to get the best possible structural subsurface image for interpretation by eliminating multiple reflections, enhancing weak reflections of the deep subsurface, and increase the signal to noise ratio (S/N). Very detailed analytical procedures

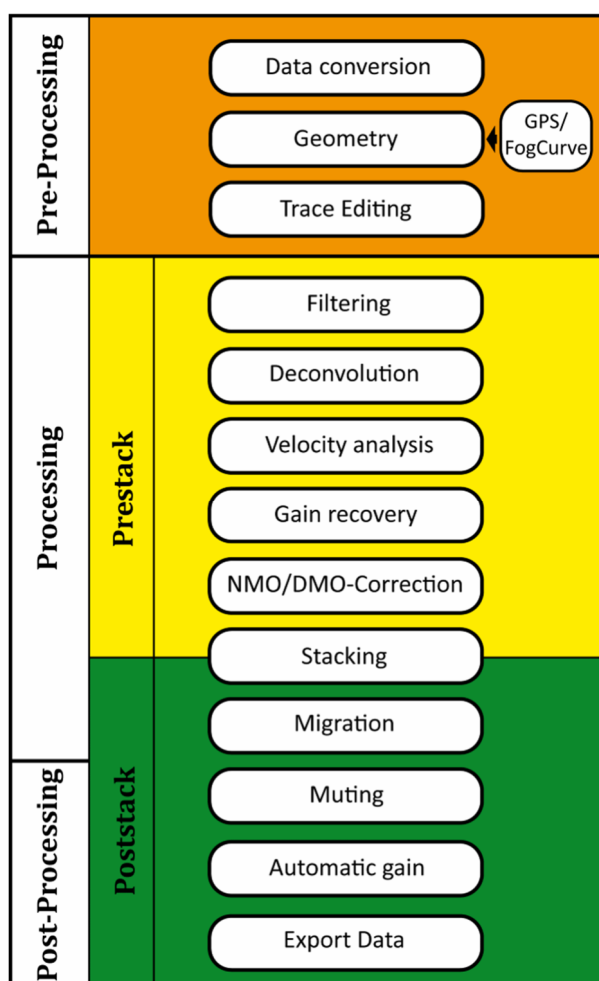


**Figure 3.5:** General overview of the seismic processing steps applied to the S0236 MCS data.

involving numerous steps are best described in Yilmaz (1987) and Hatton *et al.* (1986) with only a general overview given in this chapter (Fig. 3.5). The used software packages to execute these processing steps were the *SeisSpace* processing system (HALLIBURTON-LANDMARK, Houston, TX, USA) with the *ProMAX 2D* processing software (HALLIBURTON-LANDMARK, Houston TX, USA). Both are industry standard software for seismic data processing. The main processing steps that applied to the multichannel seismic data of the S0236 survey with those software are:

#### 3.2.4.1 Import seismic data

The *SeaMux NTRS/XPRS* (HYDROSCIENCE TECHNOLOGIES, Inc., Mineral Wells, TX, USA) has recorded the data for each shot on hard disk drives. The data are imported and converted into an internal *ProMax* data format to be capable of processing tasks.

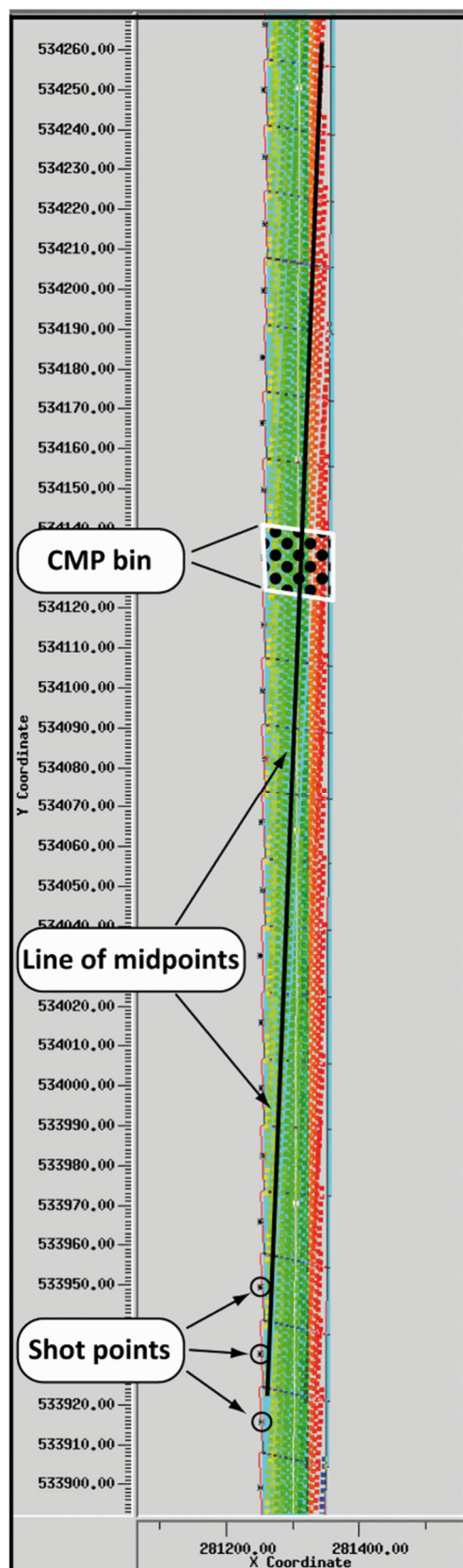


**Figure 3.6:** Section of a seismic profile p38(SO236), showing shot, midpoints, and CMP-bin positions. Each point represents a mid-point between the source and receiver.

### 3.2.4.2 Geometry Processing

The obtained seismic data are recorded by a multichannel streamer and hence single traces have to be gathered to their common midpoint (CMP) positions of various source and receiver positions. The CMP represents a single georeferenced point where multiple signals of different source-receiver positions of the moving ship join together, under the assumption of horizontal layered structures. The GPS navigation data and the ship-referenced system layout of the streamer, including the heading data of the birds, the source, and the GPS antenna position are merged with the program *FogCurve* to calculate UTM-coordinates of the source and each hydrophone position depending on the timestamps of the GPS and MCS datasets. The next processing step loads the position of the source and each hydrophone for every shot in the profile and creates a chain of CMP-bins, which have a length interval of 16.7 m and a specific width to cover the CMPs across the ship track due to deviation of the streamer system by the moving sea surface and currents (Fig. 3.6). The lateral resolution of the seismic data is defined with the along-track bin sizes. The coordinates for source and receiver locations are stored in the trace header and associated to specific CMP-bins. Coordinates are calculated for the center of the CMPs bins. Each source-receiver pair which midpoint is located in a CMP-bin are grouped together in a CMP gather. The number of midpoints located in one bin determine the CMP fold. The fold tapers off at the ends of each profile (Yilmaz, 1987). The binning process is a crucial step for balancing the lateral resolution versus increased S/N.

### 3.2.4.3 Trace Editing

This process is used to remove data of broken hydrophones and to get rid of spikey and noisy traces, dead traces, and monofrequency traces. Some traces have to be adjusted by static corrections due to random

trigger errors, which delayed or early triggered the signal a 3 to 25 ms range. All traces are corrected for -135 ms due to a delay in the source trigger system, mechanical delay of the guns, and the response time of the storage system.

#### 3.2.4.4 Trace Filter

The stored data encompass the useful signal and noisy signals of the swell and the ship's engine, for example. This process isolates the main frequency spectrum of the received useful signal with an Ormsby bandpass filter with a low pass threshold of 25 Hz and a high pass threshold of 200 Hz with tapers at 20 Hz and 220 Hz to eliminate low and high frequency noise. Additionally an  $f,k$ -filter is applied to eliminate unreal strong dipping amplitudes in the  $f,k$  shot gather resulting in a better S/N ratio and seismic resolution as well as the 'Spike and Noise Burst Edit' process to remove over-modulated amplitudes.

#### 3.2.4.5 Deconvolution

This process detects and suppresses recurring signal amplitude patterns and eliminate the multiple echoes. The used 'Targeted Predictive Decon' is designed for optimum multiple attenuation by targeting successive multiple wavelets individually. This processing step tries to predict the initiation of a multiple by its strong periodically occurrence. The process prerequisite a handpicked water-sediment layer for designing the derivation of the deconvolution operation window to get an optimal result.

#### 3.2.4.6 Semblance Velocity Analysis

Nonzero-offset CMP gather yields velocity information about the subsurface (Yilmaz, 1987). By passing through several geologic layers with different elastic (anisotropic) properties the TWTs varies additional to varying source-receiver offsets. These varies can be used to determine velocities of different layers. The semblance velocity analysis shows a spectra of stacked signal semblance of velocity and TWT (Fig. 3.7). The spectra field can be compared with stacked supergather of a specified number of CMPs. Areas of maximum semblance can be picked, stored and used as recalculated root-mean square (RMS) velocities in a 2D velocity model (Fig. 3.8) for the normal moveout (NMO) correction.

#### 3.2.4.7 True Amplitude Recovery

The 'True Amplitude Recovery' process applies a time and space variant gain function to traces to compensate for loss of amplitude due to wavefront spreading of the spherical divergence and attenuation by travelling through the water column and subsurface. The amplitude weakens with increasing TWTs due to reflection depth and increasing source-receiver offsets.

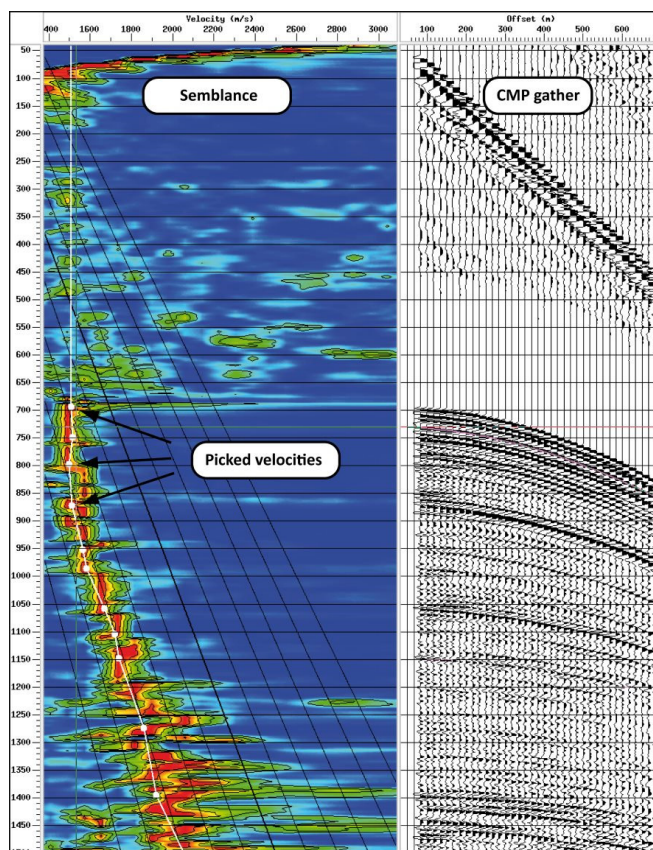


**Figure 3.7:** Semblance velocity-analysis plot and the points of picked velocities (white dots) for the RMS velocity calculation. The colours illustrating areas of non-congruence (blue) to maximum-congruence (red) of stacked CMP traces. The right part showing traces of one or more CMPs sorted by the source-receiver offset.

The ‘Surface Consistent Amplitudes’ sub-process estimates and adjusts the relative amplitude contributions of sources, receivers, offset bins, CMPs and channels, on a statistically surface consistent basis. The amplitude of any trace is a combination of a number of factors. These include the strength of the shot, the response and coupling of the receivers, the performance of the amplifier channel, the offset of the traces, the density and velocity contrasts of the reflecting horizons, and other more ambiguous factors, such as ambient noise. While it is difficult to separate these effects on a single trace, they can be estimated statistically from many traces. For example, the traces of a particularly weak shot will tend to show lower than normal amplitudes. One or more channels may differ in response from the average. Typically CMP, Offset Bin and Channel are not surface consistent domains.

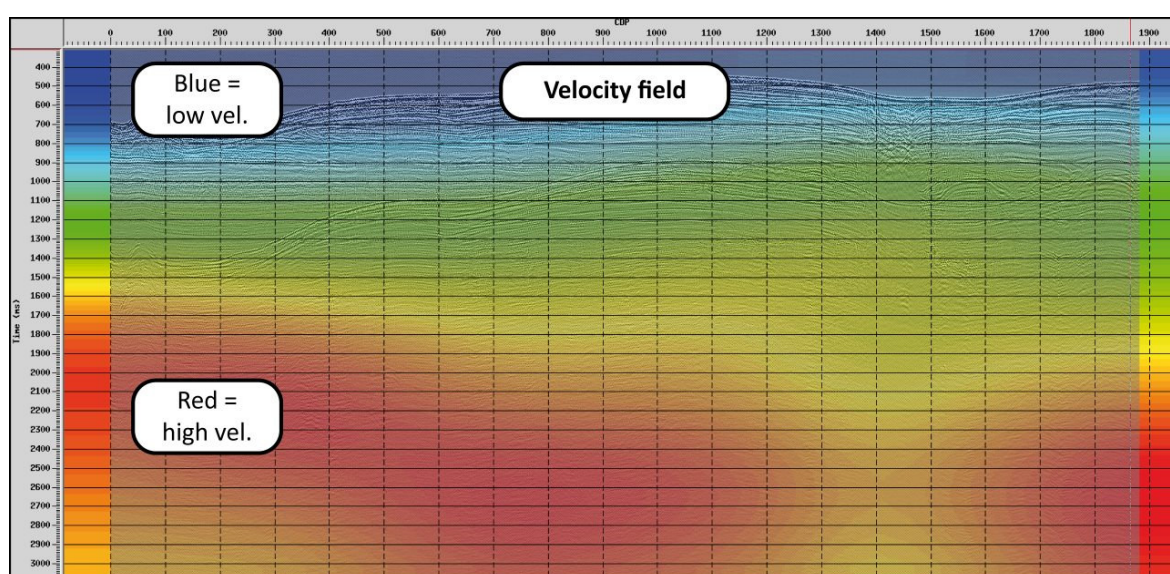


**Figure 3.8:** Screenshot of an interpolated 2D velocity field window of the processing software, which is underlied by the stacked seismic data of profile p38(S0236). The velocity field is assigned to a colour palette that shows cold colours (bluish) for low velocities and warm colours (orange/red) for high velocities.

#### 3.2.4.8 Normal/Dip Moveout Correction

The NMO correction is necessary to compensate the increasing TWT with increasing source-receiver-offsets of the CMP gathers for the stacking process. The NMO correction works accurate for horizontal layers. Dipped layers strongly modify the ray-tracing by changing the reflection angles at the layers' interface. The dip moveout (DMO) process handles ray traces that are reflected by dipping reflectors and correct their position for nonzero-offset data. The dipping of the reflections is calculated by contiguous CMP positions of the previous NMO correction. The largest correction is set for shallow large dip events and decreases with dip angle and increasing velocities (Yilmaz, 1987).

#### 3.2.4.9 Final Stack

Reducing S/N ratio of the seismic CMP gather by stacking ensembles of traces of the CMP-bin to a single zero-offset CMP-trace.

#### 3.2.4.10 Migration

The migration process is executed on the stacked data to increase lateral resolution by collapsing diffractions and to move dipping and angularity events between two or more reflections from the CMP position to their true subsurface position (Sheriff, 1980; Yilmaz, 1987). The velocity field for the calculation based upon the interval velocities of the IODP Leg 359 (Betzler *et al.*, 2017).

#### 3.2.4.11 Post-Processing

The wavelets of the leftover area of the water column are muted to highlight the geological relevant area of the seafloor and below. An 'Automatic Gain Control' process is applied carefully to enhance the amplitude of weak late reflections due to spherical wave front spreading. This process is handled with caution to preserve the characteristic amplitude of the reflections. It is the final step in the processing procedure of the seismic data resulting in good quality data (Fig. 3.9)

#### 3.2.4.12 Export Seismic Data

After (post-) processing procedures the seismic data converted into the common used SEG-Y file format and ready for loading into the *Petrel E&P* (SCHLUMBERGER N.V., Curaçao, Netherland) software package for visualization and interpretation, together with sub-bottom and hydroacoustic data.

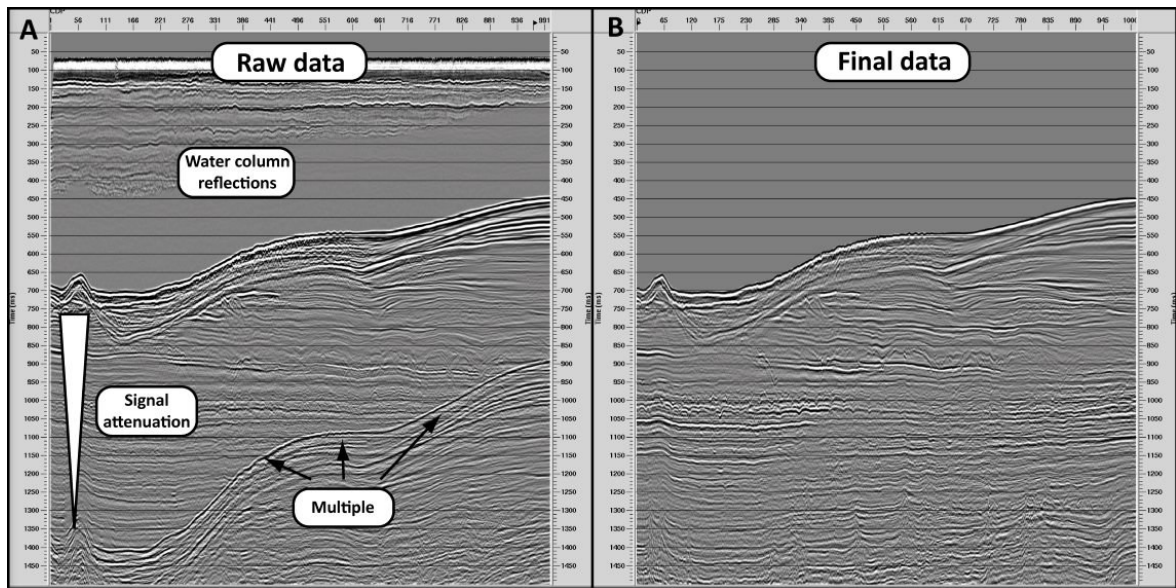


**Figure 3.9:** Comparison of the raw data stack (A) and the stacked and migrated data (B) after post processing. The compared sections show a part of profile p38 (S0236).

### 3.3 Sub-bottom profiler - Parasound

The used hull mounted echosounder device *PARASOUND P70* (ATLAS HYDROGRAPHICS, Bremen, Deutschland) operates with help of the parametric effect (Westervelt, 1963) to create a useful signal for high-resolution sediment profiling of the upper subsurface. The Parasound system is described by Grant and Schreiber (1990) and Spieß (1993). Two simultaneously emitted frequencies (18 kHz and 22 kHz) interfere in a constructive way and generate a lower frequency signal in the upper water column resulting in a narrow beam cone of  $4^\circ$  resulting in a foot print of *ca* 7% of water depth. The constructed signal has a frequency of 4 kHz and is able to penetrate the seafloor up to 200 m under good conditions. The penetration depth depends on grain size, gas load and lithology. The sub-bottom profiler can be operated in 10 to 10,000 m water depth and has a resolution of 15 cm under optimal survey conditions. The processing were accomplished by the hydroacoustic working group of cruise M95 and SO236 (see M95 and SO236 cruise reports; Betzler *et al.*, 2014b, 2015b), respectively. The Parasound data provide high resolution images of the upper subsurface structures and its seismic facies.

### 3.4 Multibeam echosounder

Multibeam data were acquired with the hull-mounted systems *EM120/EM122* (KONGSBERG MARITIME, Kongsberg, Norway) to map the along-track bathymetry of the cruises and its stations. The system works with a wavelet frequency spectrum of 11.25 to 12.60 kHz. The radiated beams were stabilized by a ship-internal gyroscope for yaw, pitch and roll motions. The angular sector coverage for the swath was set to  $120^\circ$  to  $140^\circ$ . The processing of the multibeam datasets were accomplished by the hydroacoustic working group of cruise M95 and SO236 (see M95 and SO236 cruise reports; Betzler *et al.*, 2014b, 2015b), respectively.

### 3.5 Well data

Well data will provide important sedimentological and geophysical aspects to identify and/or define contourite drift facies and to correlate these properties as well as (bio-)stratigraphic ages with the depositional units of contourite drifts. Several holes were drilled in the targeted areas of the BA and the MA (Table 2). The gathered data are used to determine the ages of the sediment, to distinguish carbonate facies and to correlate physical properties with seismic sequences and boundaries. Drillcore data include downhole log data with several tools as well as lithological, chronological and physical properties data from the (I)ODP sites. The observed time interval comprises from the late Miocene through the Pleistocene according to the available sedimentary records of both study areas. The correlation between the true vertical depth of the wells and the seismic two-way travel time are enabled by checkshots and vertical sound velocity measurements.

**Table 2:** Coring Summary of ODP and IODP Sites in the working areas of the Bahamian and Maldivian archipelagos.

Core	Site 1006 A-D	Site 716 A-B	Site U1465 A-C	Site U1466 A-B	Site U1467 A-E	Site U1468 A-B	Site U1469 A-B	Site U1470 A-B	Site U1471 A-E	Site U1471 A-E
Working Area	BA	MA	MA	MA	MA	MA	MA	MA	MA	MA
Longitude	79°27.541' W	73°17.01' E	73°0.6786'E	73°1.6785'E	73°17.0200'E	73°4.2780'E	73°0.410'E	72°59.0324'E	73°08.9825'E	73°04.0111'E
Latitude	24°23.989'N	4°56.00'N	4°55.9873'N	4°55.9880'N	4°51.0139'N	4°55.9832'N	4°54.4143'N	4°45.9828'N	4°45.9825'N	4°46.2653'N
Water depth (m)	657.9	533.3	515.0	518.1	498.4	532.5	438.0	399.7	419.4	379.3
Maximum depth (mbsf)	717.3	264.4	233.2	809.7	714	874.7	161.1	343.7	1003.7	251.9
Total core length (m)	908.0	521.5	410.2	821.9	1184.99	873.7	190.5	364.8	1335.0	251.9
Total core recovered (m)	835.81	529.8	87.38	332.33	1061.72	458.7	4.86	147.13	771.19	233.75
Core recovery (%)	92.0	101.6	21.3	40.4	89.6	52.5	2.6	40.3	57.8	92.8

#### 3.5.1 Chronostratigraphic framework - Maldives

The used MA well dataset is composed of information from nine wells, which provide and refine depths and ages for seismic horizon correlation of the basin sediments since the late Miocene. Sedimentological data from different ODP (716) and IODP (U1465-U1472) Sites are combined with the multi-channel reflection seismic data. Site 716 delivered sediments from the late Miocene through Pleistocene age. The chronostratigraphic groundwork based on two drillcores, NMA-1 and ARI-1, supported by seismic surveys (Purdy and Bertram, 1993; Aubert and Droxler, 1996; Fig 1.3A). The IODP record of expedition 359 provides information about the current activity in the MA by correlating the monsoon activity with the accumulation of contourite drift deposits (Betzler et al, 2017). The stratigraphic model of the KC was refined by the results of the IODP Expedition 359. Sites U1465, U1466, U1468, and U1469 are situated in the northern KC, whereas U1470 to U1472 are drilled through the sediments of the southern KC and U1467 is located in the IS (Fig. 1.3B). The drillhole record were partial correlated with eleven seismic platform sequences and its boundaries (PS01 to PS11; Table 3) of lower and middle Miocene platform strata of Betzler *et al.* (2013a; Fig. 2.6). Additionally, since the upper middle Miocene large-scale drift bodies filled the paleo-IS from west to east (Lüdmann *et al.*, 2013; Fig. 2.6). The deposition history led to additional definition of ten seismic sequences (ds1 to ds10) and sequence boundaries (DS1 to DS10; Fig 2.6), which are recognized in the seismic data and are the basis for age determination of the contourite depositional history in the MA (Table 3). The mapped sequence boundaries of Lüdmann *et al.* (2013)

were integrated in the full extension of the existent dataset and time/depth corrected by using the velocity data acquired during IODP Expedition 359. The age correlation based on the boreholes U1465 to U1472. The biostratigraphic ages were published and revised in Betzler *et al.* (2018).

**Table 3:** Depths and ages of sequence boundaries at sites cored during IODP Expedition 359 after Betzler *et al.* (2018). Depths of correlated sequences are added for ODP Site 716.

	Site U1465		Site U1466		Site U1467		Site U1468		Site U1469		Site U1470		Site U1471		Site U1472		ODP Site 716	
	(Ma)	(mbsf)	(Ma)	(mbsf)														
DS10	1.45	29	1.5	28	1.5	52.5	22.5		25		1.55	31	1.4	53	1.35	33.5		36
DS9	2.15	40.5	2	38	2.1	78	43		38		2.3	49	2.1	90	2.15	54		66
DS8	2.85	52.5	3.6	60	3.9	157.5			64.5		3.65	78	4	166	4	100		119
DS7		70	4.1	65	4.2	181.5			77.5		4.35	93	4.6	198	5.3	135		131
DS6			5.6	81	5.5	295.5			93			135	5.5	242.5	6.6	168		207
DS5					5.8	337			107.5				5.8	261.5	6.9	176		261
DS4					8.8	535	55						8.8	471.5	8.8	223		
DS3					10.5	603	65				148.5		10.6	667				
DS2				94	11.7	656.5	11.3	191			198		12	804.5				
DS1			12.7	310	13	711	13	430	141.5		217		12.9	898				
PS11		142	12.85	336			13.1	438			324.5							
PS10			13.1	380			13.2	457										
PS09			14.2	435			14.2	505										
PS08			15.1	490			15.1	535										
PS07			15.6	525			16.1	573										
PS06			17	625			17.5	626										
PS05			18.5	709				662										
PS04			18.6	712				682										
PS03																		
PS02							21.3	710										
PS01			20.1	770			21.8	730										
O/M							25.65	854.7										

### 3.5.2 Chronostratigraphic framework - Bahamas

The sediment composition and the stratigraphy at ODP Site 1006 in the northern SC was documented in a number of studies (Eberli *et al.*, 1997; Kroon *et al.*, 2000; Wright and Kroon, 2000; Rendle and Reijmer, 2002). Site 1006 is situated at the northern end of the SC, adjacent to the Florida Straits (Fig. 1.2) in a water depth of 657.9 m. The SD and the slope of the GBB are penetrated by four drillholes of the ODP Site 1006(A to D) of Leg 166. The longest core of Site 1006A penetrated 717.3 m through the sedimentary body and recovered 90.2 % core material (Table 2).

The seismic data of the BA are correlated with the seismic sequence boundaries of Eberli *et al.* (1997) of the Bahamas Transect along seven drilled cores of ODP Leg 166 (Fig. 1.2B). Their sequence stratigraphic architecture based on termination geometries and erosional truncation which are best observed at the buried eastern flank of the GBB (Eberli *et al.*, 1997). The chronostratigraphic significance of the boundaries has been demonstrated by Eberli *et al.* (2002). The stratigraphic age model of Site 1006A was published by Eberli *et al.* (1997, 2002), Wright and Kroon (2000), and Kroon *et al.* (2000). These biostratigraphic data were adopted by applying the Gradstein *et al.* (2012) and Wade *et al.* (2011) ages for the different foraminiferal and nannofossil events and republished by Paulat *et al.* (2018; Fig. 3.10). As a consequence of the uncertainty of determination the biostratigraphic events, for example. first occurrence of the planktonic foraminifera *Fohsella*

*robusta* and *Fohsella fohsi*, the age determination remains vague. The Miocene-Pliocene transition is defined at a core depth of 371 meters below seafloor (mbsf) (Kroon *et al.*, 2000).

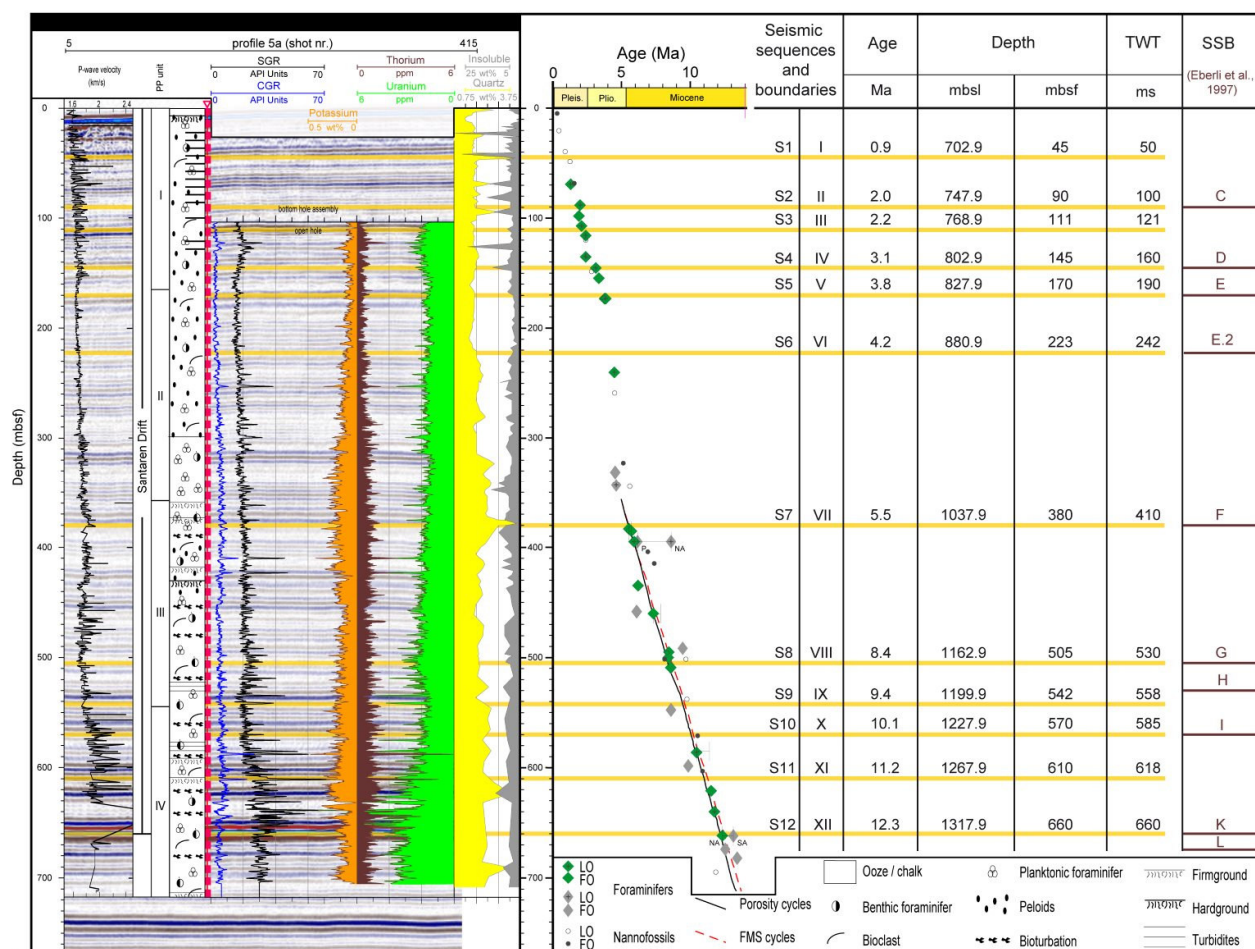


**Figure 3.10:** Lithostratigraphic summary of ODP Site 1006A, tied to a high-resolution seismic image and linked to an age-depth plot of foraminiferal bioevents (used – green diamonds, calibrated – gray diamonds), geophysical properties, and seismic sequence boundaries (SSB) by Eberli *et al.* (1997), updated with the modern ages of Gradstein *et al.* (2012). The content of the ‘insoluble’-fraction consists mainly of clay and negligibly of organic matter (Eberli *et al.*, 1997). PP=Physical properties (Eberli *et al.*, 1997). CGR=computed gamma ray; SGR=standard gamma ray, P=Pacific Ocean, NA=North Atlantic Ocean, SA=South Atlantic Ocean. Adapted from Paulat *et al.* (2018).

## 4 Results

The description of the current related contourite drift deposits of the archipelagoes is referred to four main morphostructural parts: (1) the inter-atoll channels, which connect the surrounding ocean and deeper gateways with the archipelagoes, (2) the basinal areas between the (3) drowned platforms and (4) active carbonate platforms (Fig. 4.1). The available seismic grid of these geological settings are scanned for influences of current activity during the sedimentation process by identifying current-related seismic facies and terminations (see chapter 3.1.1). The main occurrence of current-related structures are identified in the MA and subordinate in the BA.

### 4.1 General overview about the bathymetric framework of the study areas (Maldives, Bahamas)

#### 4.1.1 Maldives

The inter-atoll channels of the main study area (Fig. 4.1A) divide the active and drowned parts of the Miocene paleo-platform with extensions of 1 to 10 km in width and sill water depths between 400 m and 600 m. The channels are mainly east-west oriented. Due to the double-atoll chain morphostructure the channels can be divided in east and west inter-atoll channels that are connected with the IS basin. The KC is the dominant channel system, which is in fact encompassing two inter-atoll channels north and south of the Kaashidhu Atoll at the eastern part of the MA. The western KC is parted by the active Goidhoo Atoll (GA) in a northern branch, between GA and the

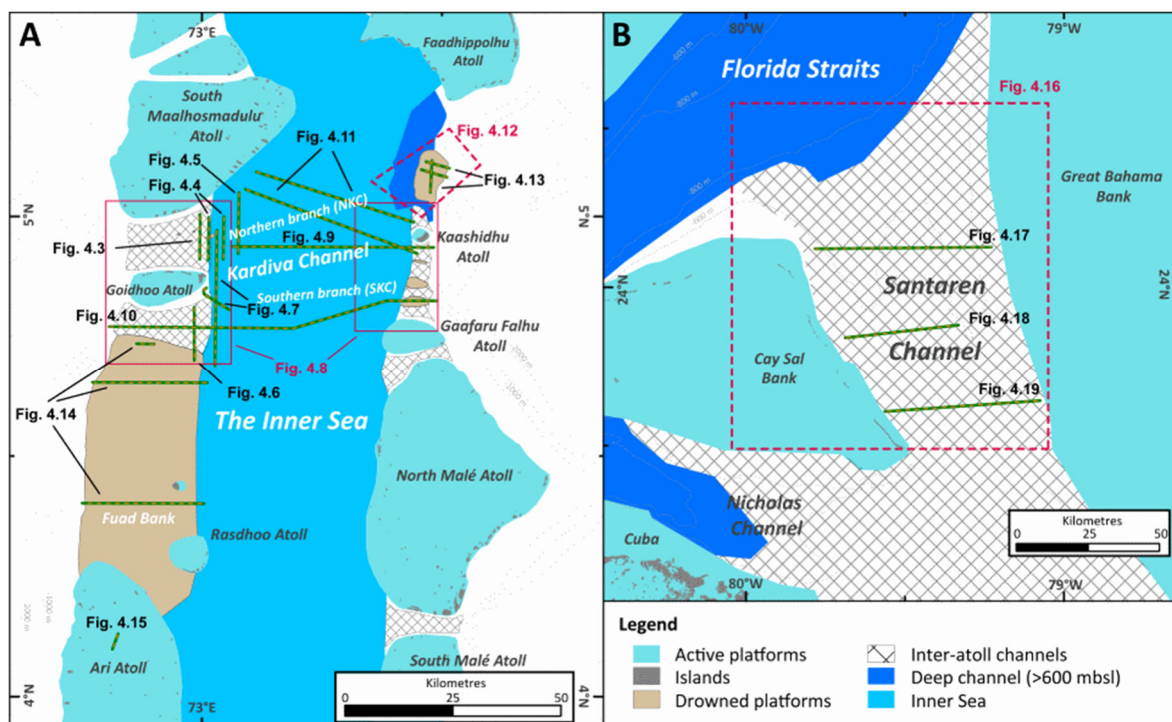


**Figure 4.1:** A: Sketch map displaying the morphological features of the MA and an overview about the locations of the shown seismic and hydroacoustic profiles. B: Sketch map displaying the morphological features of the BA and the location of the shown MCS profiles.

South Maalhosmadulu Atoll (SMA), and a southern branch, between GA and the drowned Fuad Bank (FB, Fig. 4.1).

The bathymetric framework of the northeastern branch is dominated by a drowned platform, which is surrounded by a deep channel between the Kaashidhu and the Faadhippolhu Atoll (Figs. 1.3B and 4.1A). The drowned platform's shape is formed by number of terraces, which are located in water depths between 600 m and 320 m at its top. The surrounding deep channel steps on the MA's structure in a water depth of 850 m at the southern entrance and 1050 m at the northern entrance. In the IS the channel sill depth is 650 m. The northwestern branch or Northern Kardiva Channel (NKC) encompasses the inter-atoll channel between the SMA and the GA (Figs. 1.3B and 4.1A). The northwestern branch has a sill depth of 520 m and the seafloor is occupied by sediment waves with heights up to 15 m. Some smaller drowned atolls are located in the northern channel. The length of the biggest atoll is 2.5 km and 1.2 km in width and its top lies in a water depth of 380 m. The southern branch or Southern Kardiva Channel (SKC) comprises of an inter-atoll channel between the GA and the drowned FB and the eastern channel between the Kaashidhu Atoll and the Gaafaru Falhu Atoll (Fig. 4.1A). The bathymetry of the eastern part of the southern branch is characterized by drowned small elongated platforms, which vary in size from 3.5 to 6.5 km in length and 0.6 to 2.5 km in width. The water depth of their top varies between 540 and 230 m due to the asynchronous date of their drowning events (Figs. 1.3B and 4.1A). The southwestern branch show a slightly WNW-ESE orientation and asymmetric channel axis and shows an average water depth of 470 m next to the framework of the FB. The FB is a drowned platform, which is located in a water depth of 210 to 240 m. The FB is elongated in the north-south direction with a length of *ca* 50 km and a width between 22 km and 32 km (Fig. 4.1A). Its carbonate basement is connected to the Ari Atoll and linked to the active Rasdhoo Atoll. The IS is the north-south elongated *ca* 35 km to 45 km wide basin enclosed by the double chain active and drowned atolls of the MA. Generally, the deepest water depth lies between 540 m in area of the KC and 400 m between the Ari Atoll and the North Malé Atoll. The IS deepens through the NE into a deep channel with a range water depths of about 600 m to 1000 m, that surround a drowned platform at the eastern atoll chain.

#### 4.1.2 Bahamas

The MCS dataset of the BA encompasses the coverage of an inter-atoll channel (Santaren Channel) with a length of *ca* 100 km between GBB and CSB (Figs. 1.2B and 4.1B). The flanks of the channel are characterized by symmetric up-climbing slopes with increasing slope angles. The slope terminates on a steep platform wall on both sides. The seafloor occupied by the Santaren Drift that is the dominant morphological feature in the SC. The northern exit of the SC is connected with the Florida Straits. The water depth is greater than 700 m at the northern conjunction and 65 km of open waters lies between the carbonate platforms. The southern exit is *ca* 47 km wide and terminates in the conjunction with the Nicholas Channel and the Old Bahama Channel with water depths between 500 m and 600 m (Figs. 1.2B and 4.1B).

## 4.2 Seismic Facies

Examination of the acquired 2D multichannel seismic lines and sub-bottom profiler data allowed the differentiation of seven different seismic facies (SF-1 to SF-7; Fig. 4.2) in the working areas of the BA and MA. They are defined by reflection properties of amplitude, continuity, internal and external configuration and terminations. The seismic facies are associated to depositional facies of isolated carbonate platforms (see chapter 2.2.1).

### 4.2.1 Seismic Facies 1 (SF-1) – carbonate platform

SF-1 consists of high amplitude, nearly horizontal reflections at its topmost part. The underlying part is characterized by oblique discontinuous layered to chaotic reflections of moderate to low amplitudes. Masking of the interior reflections are common in the sub-bottom profiler data. SF-1 is associated to carbonate banks and platform interior depositions (see chapter 2.2.1.). The occurrence of SF-1 is common in the dataset (Figs. 4.3, 4.4, 4.6, 4.7, 4.9 to 4.11, and 4.13 to 4.15).

### 4.2.2 Seismic Facies 2 (SF-2) – periplatform deposits

SF-2 consists of semi-continuous medium amplitude dipping reflections. It can form wedges, wavy reflections and additionally downlap terminations are common (Fig. 4.2). The dipping reflections are typical for gravity-steered depositions of platform-derived sediments and, as consequence, the facies are characterized as periplatform sediments. Facies SF-2 is limited to the slopes of carbonate platforms due to the common simultaneous genesis with SF-1. SF-2 is identified in the imaged seismic data (Figs. 4.5 to 4.7, 4.9 to 4.11, and 4.17 to 4.19).

### 4.2.3 Seismic Facies 3 (SF-3) – periplatform mass transport deposits

SF-3 is closely related to SF-2. The low-to-medium amplitude low continuous oblique to chaotic reflections of low frequency. SF-3 is interspersed in the periplatform deposit facies SF-2 or can dominate the slope. Another external expressions of SF-3 are lenticular fills of depressions. The chaotic reflections are typical for gravity-steered mass transport deposits of debris flows and turbidites. Sediments transport by slumps can additionally show shingled patterns in the seismic facies. SF-3 is identified in the MA and BA (Figs. 4.5, 4.7, 4.9 to 4.11, and 4.17 to 4.19)

### 4.2.4 Seismic Facies 4 (SF-4) – contourite drift

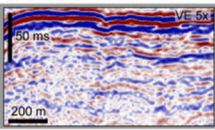
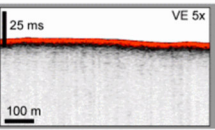
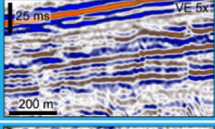
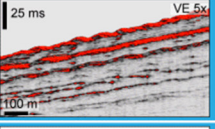
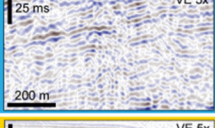
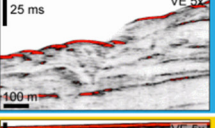
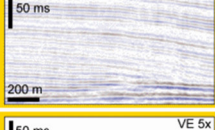
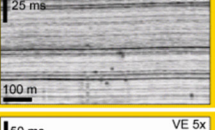
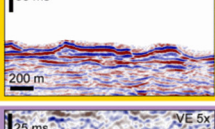
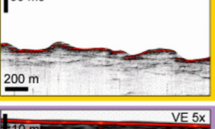
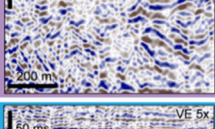
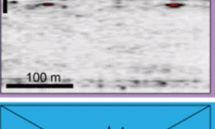
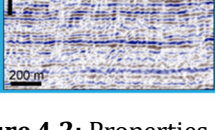
SF-4 forms high continuous (sub-)parallel seismic horizontal to divergent reflectors of low to moderate amplitudes, sigmoidal forms are rare. SF-4 is typical for contourite drift depositional systems. The dominance of these highly continuous, parallel reflectors is significant all over the seismic dataset (Figs. 4.3 to 4.7, 4.9 to 4.11, 4.13 to 4.15, and 4.17 to 4.19). It is associated with the mounded and elongated sediment bodies in the BA and the sigmoidal and prograding basinfill of the IS at the MA as well.

#### 4.2.5 Seismic Facies 5 (SF-5) – sediment waves

SF-5 shows wavy semi-continuous to discontinuous reflections of moderate amplitudes. The occurrence of horizontal and dipped layered and stacked generations of SF-5 is typical for sediments that are reworked by persistent current activity contemporaneous with input of sedimentary material. SF-5 can be neighbored with SF-4 due to its similar formation process. The occurrence of sediment waves and sediment wave fields are common at the inter-atoll channel of the MA (Figs. 4.3, 4.5 to 4.11, and 4.14).

#### 4.2.6 Seismic Facies 6 (SF-6) – mass transport deposits

SF-6 shows low-to-medium amplitude discontinuous layered to chaotic reflections and associated to mass transport deposits that are not linked to periplatform deposits. The seismic facies is similar to SF-3, but it is increased in extension and thickness. SF-6 shows sharp vertical contacts and is able to penetrate and overprint the aforementioned seismic facies. Masking effects are common in sub-bottom profiler data due to its mixing process. Examples of SF-6 are found in the MA and BA (Figs. 4.4, 4.13, 4.14, and 4.17 to 4.19)

Seismic Facies		Internal Configuration	External Configuration	Depositional Interpretation
Multichannel Seismic	Sub-bottom Profiler			
SF1 		low freq., high amp. to medium amp. of the topmost reflection, discontinuous to chaotic low amp. reflections, masking possible	layered with irregular relief, steep margins abundant	Carbonate bank/ platform interior
SF2 		medium freq., medium amp., semicontinuous prograding, dipping, slightly wavy reflections	wedge-shaped	Periplatform sediments
SF3 		low freq., low to medium amp., low continuous layered to chaotic dipping reflections	wedge-shaped and lenticular fills	Periplatform mass transport: slumps, debris flows and turbidites
SF4 		high freq., low to medium amp., high continuous (sub-) parallel/divergent reflections, sigmoidal forms possible	sheeted to mounded and elongated, progradation possible	Sediment drift (sheeted, mounded, mixed, e.g.)
SF5 		med. freq., medium amp., wavy semi-continuous to discontinuous subparallel reflections	wavy (elongated)	Sediment waves (stacked)
SF6 		low to medium amp., chaotic to discontinuous layered reflections, masking common	Mass transport complexes	wedge-shaped and lenticular fills
SF7 		med. freq., low to medium amp., (semi-)continuous parallel reflections, interspersed with slightly undulating reflections, horizontal layered.	sheeted	Basinal hemipelagic or pelagic ooze

**Figure 4.2:** Properties of the seismic facies SF-1 to SF-7 that are identified in the study areas. amp.=amplitude; med. freq.=medium frequency; VE=vertical exaggeration.

#### **4.2.7 Seismic facies 7 (SF-7) – (hemi-)pelagic ooze**

SF-7 is characterized by low-to-medium amplitude (semi-)continuous reflections of low frequency. The external configuration show layered geometries and is associated with hemipelagic or pelagic ooze (Figs. 2.4, 4.9, and 4.10). Sub-bottom data are not available due to its occurrence in greater depths, only.

### 4.3 Maldives, Indian Ocean

The MCS, Parasound, and multibeam data reveal a variety of depositional geometries reshaped by recent and ancient bottom current activity in the study area. The main drift bodies are connected to the inter-atoll channels, which allowed the open ocean water masses to enter the IS and cross the MA (Figs. 1.3B and 4.1A). The interpretation of the MCS datasets based on the groundwork for seismic interpretation is presented in section 3.1.1. The seismic reflection profiles are carefully examined for seismic stratigraphic features and reflection geometries to detect current related depositional environments. An overview of the mapped seismic sequences and their ages is given in Table 3 for the Maldives.

#### 4.3.1 Depositional features and geometries

The depositional system at the MA is divided in four major geological settings covered by seismic profiles, hydroacoustic data and partly groundtruthed by IODP drillcores. In order to present the seismic profiles the morphological settings are the (1) inter-atoll channels, (2) the IS and (3) drowned carbonate platforms, and (4) active carbonate platforms (Fig. 4.1A).

#### 4.3.2 Kardiva Channel system

##### 4.3.2.1 Northern western branch of the Kardiva Channel (NKC)

The analysis of the seismic images of the east-west oriented NKC, south of the South Maalhosmadulu Atoll, reveals that drift sedimentation patterns in the channel varied over time (Fig. 4.3). The combined cross-section profile of the profiles p18 (SO236) and p19 (SO236) shows three different seismic facies (SF-1, SF-4, and SF-5) in the channel. The basement consists of mostly horizontal parallel semi-continuous reflections with moderate/strong amplitudes of SF1 and represent the drowned Miocene paleo-platform. The irregular topmost relief consists of an erosion surface at the channel center, where the horizontal layered platform reflections are truncated. The base of the trough has a width of 2500 m and lies 32 to 40 m under of the undisturbed level of DS1, assuming an average velocity of 1600 m/s for the topmost unconsolidated calcareous drift sediments similar to the recovered sediments of the Sites U1462 to U1465 (Betzler *et al.*, 2017). Two small pinnacle structures are neighbored adjacent to an inclining truncation surface in northern direction. The overlying sediments in the channel center are characterized by discontinuous wavy medium amplitude reflections of SF-5 and represent stacked generations of sediment waves. It allows the differentiation of the sequences ds7 to ds10 above the erosion surface on top of the drowned paleo-platform. The northern top-lying sediments show a seismic pattern of a progradational unit of SF-4 with sigmoidal reflections that terminates with downlap onto the underlying strata (Fig. 4.3)

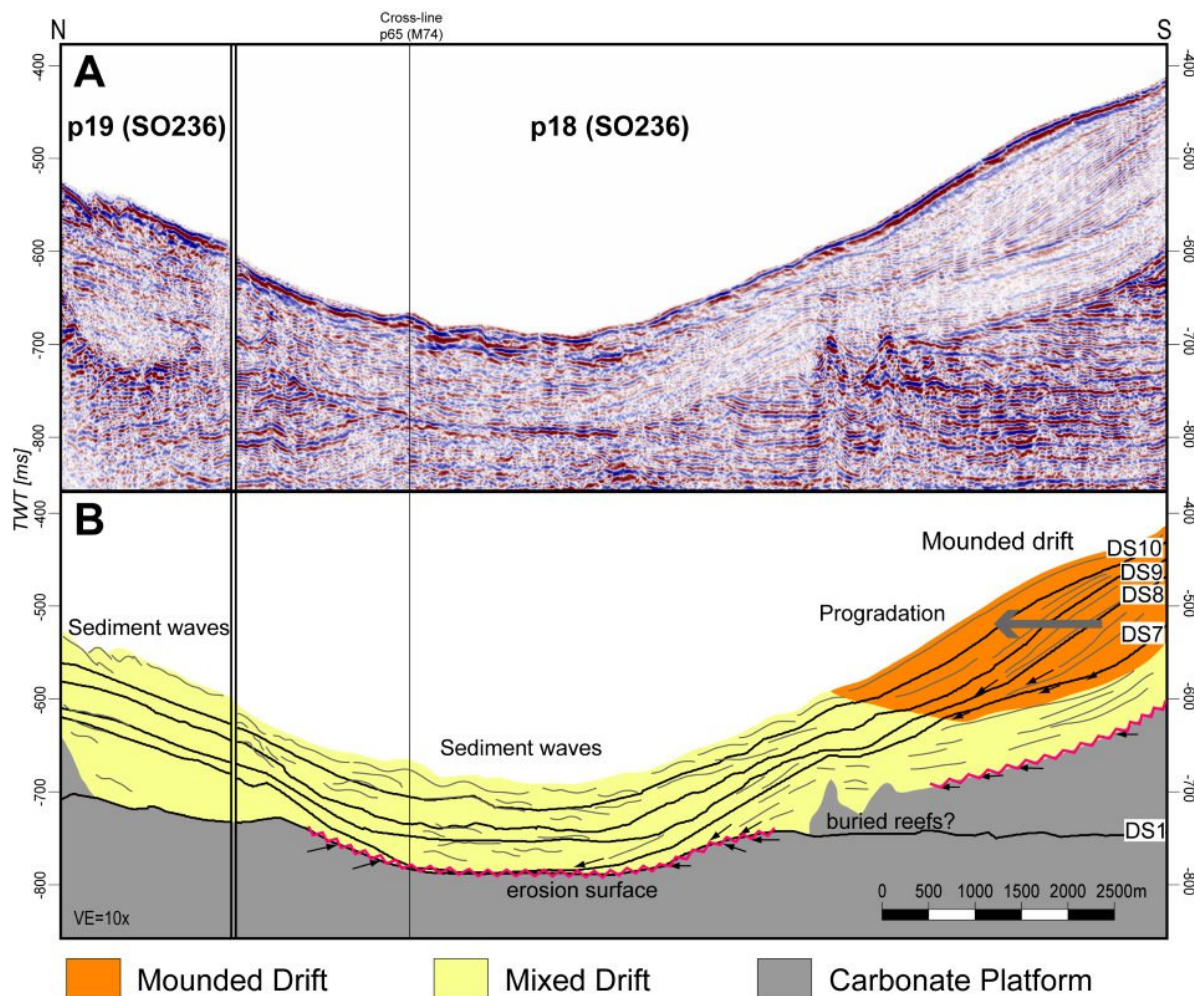


**Figure 4.3:** **A:** Raw data of the north-south oriented cross-section of two compiled SO236 MCS profiles (see Fig. 4.1A for location), p18 and p19, across the NKC. **B:** Seismic facies interpretation assigned to seismic data. VE=Vertical exaggeration.

Another example of current-related sedimentation is revealed in segments of profile p19 (SO236) and p21 (SO236) (Fig. 4.4A to E). A bathymetric high with steep walls, up to 180 m high, is located in the northwestern channel of the KC between the SMA and the GA. The structure's extension at the base is *ca* 2500 m in east-west and *ca* 1500 m in north-south direction, respectively (Fig. 4.4E). It has an overall elongated pinnacle shape. The seismic image of a segment of profile p19 (SO236) shows a strong amplitude assigned to SF-1 at its top and the signal is not able to penetrate its deeper parts (Fig. 4.4A). The seismic image shows aggrading scour complexes interposed with slumps identified by its chaotic seismic facies SF-6. The topmost boundary of the drowned middle Miocene paleo-platform is represented by a strong amplitude reflector with an irregular erosion surface, which cut the horizontal layered reflections of SF-1 of the aforementioned carbonate platform on both sides of the pinnacle structure (Fig. 4.4A and C). The overlying strata thickens towards north and south perpendicular to the channel axis (Fig. 4.4A). The northern sediment accumulation adjacent the SMA shows an aggrading and slightly prograding pattern with downlap terminations of the medium continuous, low to medium amplitude reflections onto the buried carbonate platform during ds3 (Late Miocene). The overlying sediments show an aggrading and

prograding pattern that terminates with a steeper angle than the previous generation on the aforementioned truncation during ds4 (very Late Miocene). The bathymetric map shows that scours around the carbonate mounds are common (Fig. 4.4E). The seismic configuration of the overlying sediments of ds7 to ds10 comprises of down dipping low-to-medium amplitude reflectors intersected by layers of chaotic reflections of slumps that filled the scour area neighboring the carbonate mound. The top of the southern scour is localized on a deeper level than the northern scour with a water depth of 565 m. The distal part of the seafloor towards upslope is covered by sediment waves under condition of increasing slope angles.

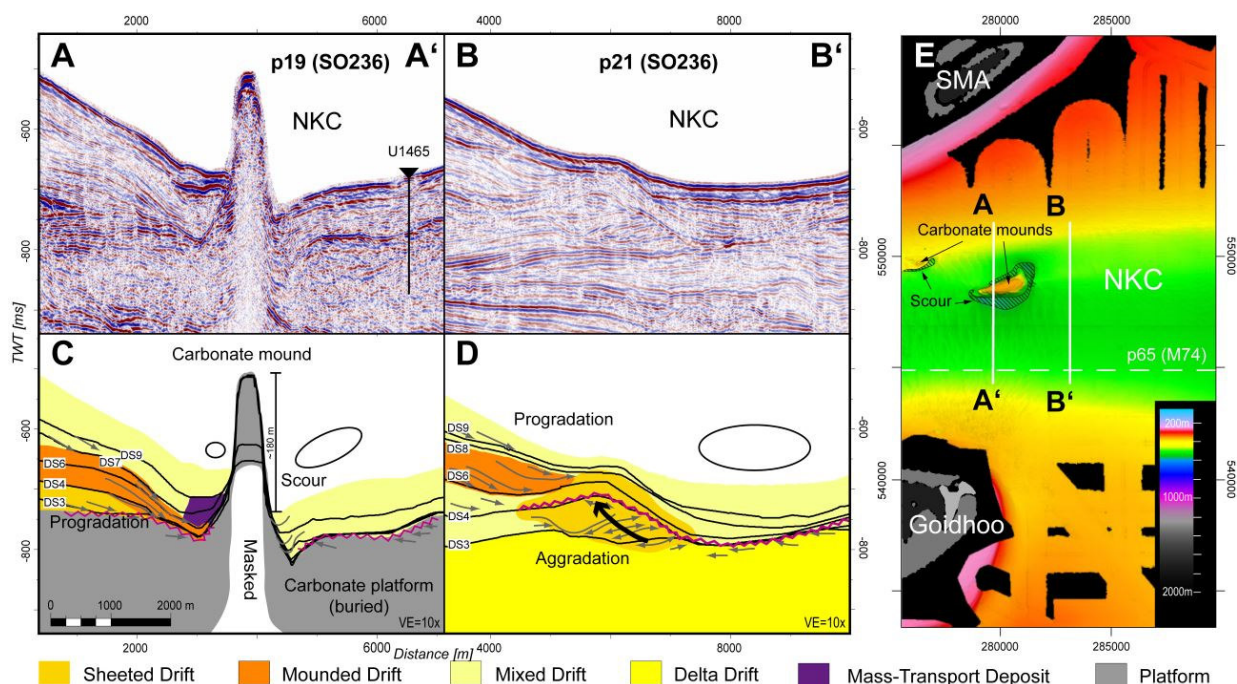


**Figure 4.4:** **A:** Seismic image of a segment (see Fig. 4.1A for location) of profile p19 (SO236). IODP Site U1465 position and drill depth are shown. **B:** Seismic image of a segment of profile p21 (SO236). **C:** Seismic facies interpretation of profile p19 (SO236). **D:** Seismic facies interpretation of profile p21 (SO236). **E:** Bathymetric conditions around the shown MCS profiles. Coordinates are based on the WGS1984 UTM 43 grid. VE=Vertical exaggeration.

A cross-section segment of profile p21 (SO236), located 3.5 km eastwards, shows a high variable sedimentation pattern (Fig. 4.4B and D). The basement with its (semi-)continuous moderate/low amplitude reflections below the sequence boundary DS3 is identified as delta drift deposits (see Fig. 2.6). The geometry of the main erosion surface can be identified by tracking the truncated seismic reflections. sediments accumulated next to the main channel axis during ds3 (Late Miocene). The accumulation is recognized by aggrading concave-up semi-continuous reflections that show downlap termination northwards (Fig. 4.4D). The accumulation of sediments is interrupted by a truncation at the channel contemporaneous with boundary DS4. The overlying sediments show nearly horizontal reflections at the channel center.

The basinward cross-section of the NKC shows that the complex sedimentation pattern and the varying current flow since the Miocene (Fig. 4.5A to D). The profile p23-SO236 of the western NKC shows the basement of the channel formed by proximal slope sediments of the drowned Miocene paleo-platform and the overlying sedimentation structure of the channel with its features. The lower part defined by ds1 to ds3 are characterized by the delta drift in front of the basinward channel exit. The seismic facies SF-4 shows high continuous medium amplitude reflections

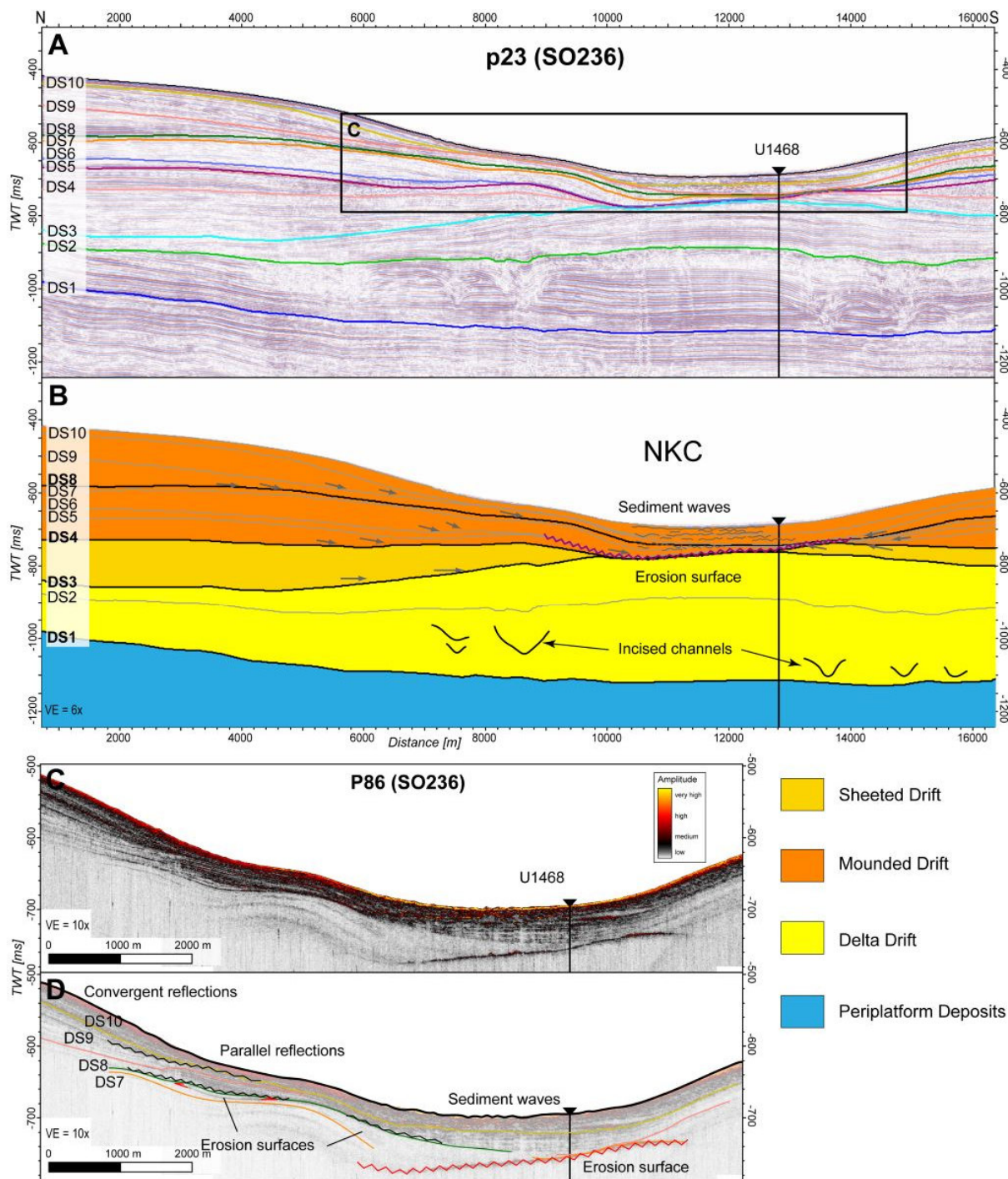


**Figure 4.5:** **A:** Uninterpreted MCS data (see Fig. 4.1A for location) of profile p23(SO236). IODP Site U1468 position is marked. **B:** Seismic facies interpretation of profile p23(SO236). **C:** Raw data segment of Parasound profile P86(SO236). **D:** Seismic facies interpretation of Parasound profile P86(SO236) segment. VE=Vertical exaggeration.

interrupted by mainly east-west oriented channels of the delta drift. Based on data of IODP Site U1468 (Fig. 2.6), the sediments overlying the delta drift consist of very fine to coarse carbonate sands with pack- and grainstone texture following the Dunham classification (Dunham, 1962). The upper termination of the delta drift is defined by an erosion surface, which cut its mounded external shape. The deepest part of the erosion surface is situated 2.4 km south of drillhole U1468 at 780 ms TWT approximately 81 mbsf (Fig. 4.5A and B). A change in the location of the deposition center takes place during ds3 at the channel exit. The mounded relief of the drift fan is onlapped by south-warding reflection terminations at the lower northern part of ds3. This part is characterized by (semi-)continuous to discontinuous reflections of medium amplitude. With ongoing sedimentation the reflection terminations turns from onlap to downlap terminations during ds03 at the delta drift's slope and formed a mounded structure. The southern part is characterized by another erosion surface as upper boundary, which cuts the up dipping reflections. During ds04 the northern part shows continuous medium amplitude reflections that terminate with downlap onto boundary DS04 beside the channel center. The sequence ds05 is subject to low sedimentation rates along the channel axis. The deposition rate strongly increased at the northern channel flank during ds06 with a progradation of the downlap termination towards the channel center. The internal reflections are oblique with low amplitudes at the northern end of profile p23-So236 and turn to moderately continuous subparallel reflections that terminate with downlaps onto DS06 (Fig. 4.5B). The deposition rate are low during ds07, hints for erosion are lacked. The reflection patterns of ds08 at the northern area show a southwards convergent geometry with continuous low to medium amplitude reflections with downlap terminations. The Parasound data display low amplitude reflections that are cut by a minor erosion surface that is part of DS08 (Fig. 4.5C and D). DS08 terminates on the unconformity that capped the delta drift fan at the central channel. The upper boundary of ds8 (DS09) is identified in 43 m mbsf in core U1468. Sequence ds09 is characterized in p23(SO236) by southward convergent continuous reflections of low to moderate amplitudes, which results in a southward prograding sediment body (Fig. 4.5B).

The Parasound image shows the detailed sediment geometry of the channel fill and the adjacent channel slope (Fig. 4.5C). The unconformity is imaged as a slightly dipping moderate continuous moderate amplitude reflection. The data depict the erosion surface as a continuous medium amplitude reflection in a depth between 36 mbsf (730 ms TWT) and the unconformity's lowest point in a depth of 78 mbsf (776 ms TWT). Overlying sediments can be differentiated in four seismic configuration patterns (Fig. 4.5B). The first pattern is characterized by continuous concave-up weak amplitude to reflection-free configuration. The termination at the central unconformity is masked. A further erosion surface cuts the reflections of ds7 and ds8, demonstrated by toplap terminations at a secondary depression north of the channel. The channel center shows semi-continuous horizontal parallel moderate amplitude reflections, which shift to wavy discontinuous high amplitude reflections upwards, at the location of drillhole U1468. The seismic pattern represents stacked generations of sediment waves in the channel. The northward channel slope is

characterized by dipped high-continuous weak to moderate amplitude reflections of SF-4 during ds9 and ds10, which show downlap terminations onto the underlying unconformity.

#### 4.3.2.2 South western branch of the Kardiva Channel (SKC)

The part of the KC shown in profile p44(SO236), south of the GA, is generally characterized by two seismic units, the basement and the channel fill. The basement reflection pattern shows subparallel semi-continuous medium to strong amplitude reflections and is assigned to SF-1 (Fig. 4.6A and B). The reflections are cut by an unconformity or ends in an area of masked reflections. The outer rims of the shown segment are characterized by a topmost high amplitude reflection. SF-1 encompasses the trackable sequences ds1 to ds9. The channel fill is generally characterized by southward dipping oblique reflections. First minor channel fills are identified during ds2. During ds3 to ds6 the reflections consist of moderately continuous pattern with low amplitudes. During that time the flanks of the channel retreat and the channel widens from 3 km to more than 8 km. The reflection terminates with onlap onto the northern upclining basement and with downlap onto the southward basement. A change from downlap to onlap of the southern reflection terminations are identified during ds6 (Late Miocene to Early Pliocene). The reflection pattern of the northern part of the channel infill shows low amplitudes and wavy to transparent reflections (Fig. 4.6A to C). The sequence ds8 is characterized by continuous moderate amplitude reflections across the channel, which results in sediment package of uniform thickness. Younger sequences of ds9 and ds10 show a discontinuous to chaotic reflection pattern at the northern channel and a thickening of the sediments. A detail view into Parasound data of the aforementioned reflection pattern shows the transition of the semi-continuous low amplitude reflections into a chaotic reflection pattern at the northern end of the channel (Fig. 4.6C). The seafloor is characterized by sediment waves with wave heights of up to 3 m (Fig. 4.6C).

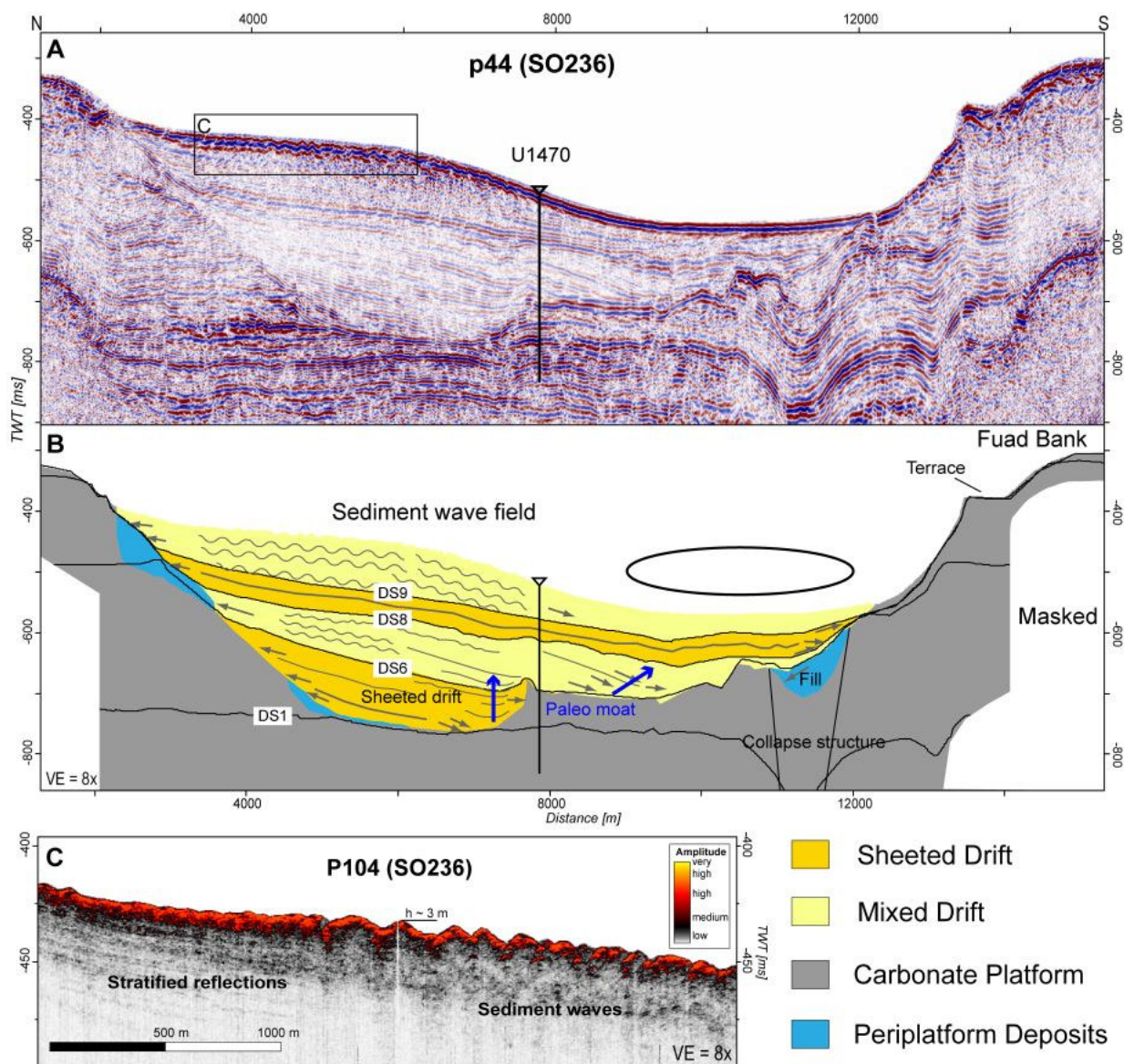


**Figure 4.6:** **A:** Uninterpreted MCS data (see Fig. 4.1A for location) of profile p44(SO236). **B:** Interpreted MCS data of profile p44(SO236). The blue arrows indicate the direction of the moat migration. **C:** Detailed Parasound data of the topmost part of the channel fill showing the area of seismic facies transition from stratified depositions into sediment waves. VE=Vertical exaggeration.

Additional seismic data between the northwestern and southwestern branch of the KC show the stratal reflection pattern behind the GA towards the IS (Fig. 4.7A to E). The seismic image of profile p36(SO236) reveals the evolution of an atoll slope (Fig. 4.7A and B). The identified seismic facies encompasses SF-1 to SF-5. The northwestern part is dominated by SF-1 and represents a drowned part of the GA. The reflections below DS1 are assigned to SF-2 and represents periplatform sediments of the atoll with decreasing thickness towards the IS. The reflection patterns between DS1 and DS3 show a shifting of the deposition center off the platform with erosion and relocation of the deposited sediments. The overlying sediments show a distinct change of the depositional geometry above the sequence boundary DS3. The reflection pattern shifts from dipped to parallel horizontal layered reflections and the terminations onlaps the underlying strata of ds3. Under

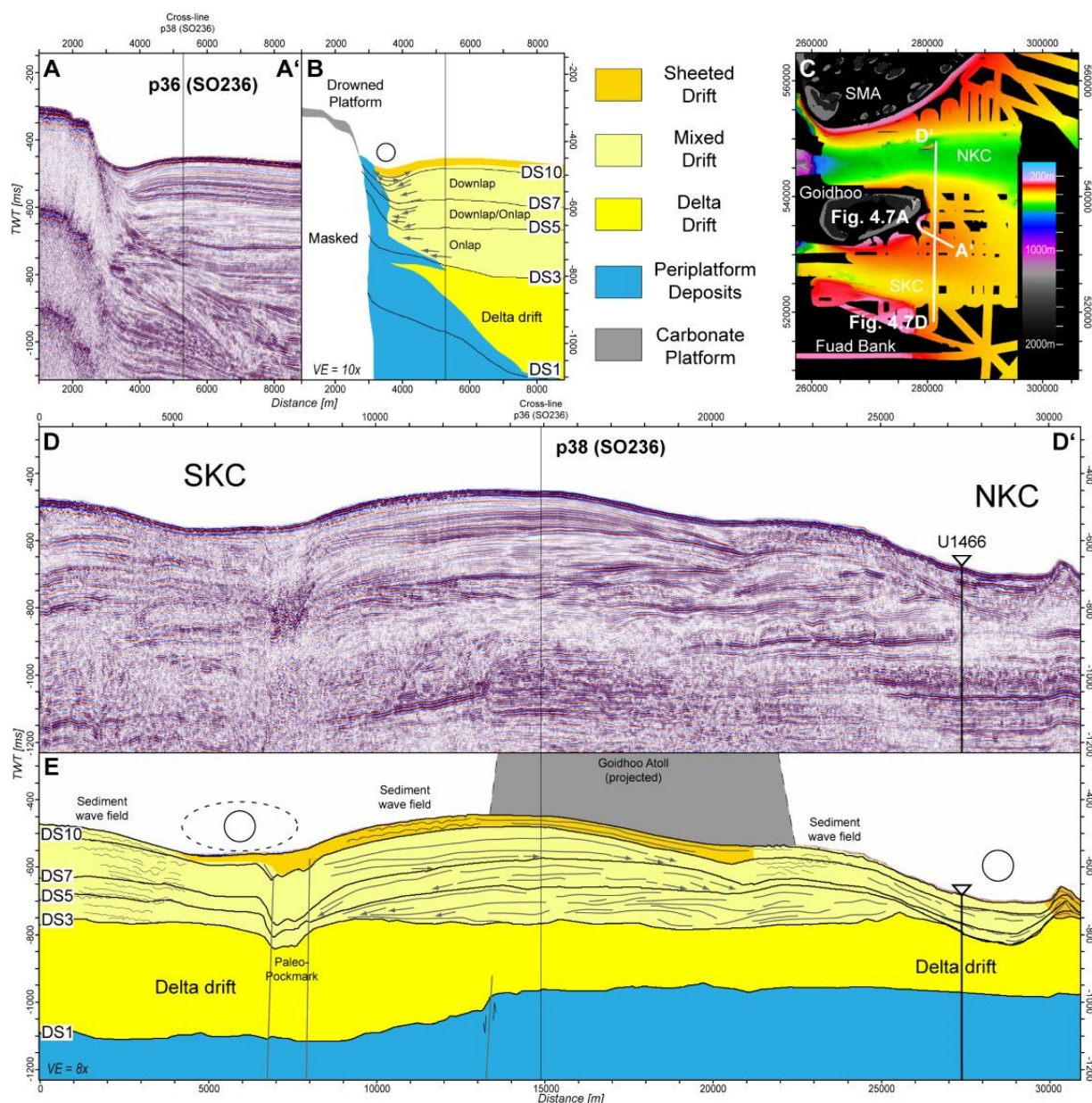


**Figure 4.7:** **A:** Raw MCS data (see Fig. 4.1A for location) of profile p36(SO236). **B:** Seismic facies interpretation of profile p36(SO236). **C:** Map of the bathymetric framework of profile p36 and p38. Coordinates in meters are based on the WGS1984 UTM 43 grid. **D:** Raw MCS data of profile p38(SO236). IODP Site U1466 is marked. **E:** Seismic facies interpretation of profile p38(SO236). VE=Vertical exaggeration.

steady aggradational conditions, the terminations show alternating onlaps and downlaps that result in a moat at the toe-of-slope of the partly drowned GA. Between DS7 and DS10 the seismic image shows stacked reflections with downlap terminations, which increase the moat's steepness. From DS10 to nowadays the moat got flattened and the downlap reflection geometry disappeared. The Profile p38(SO236) crossing p36(SO236) shows the sedimentation pattern behind the GA, between the inter-atoll channels (Fig. 4.7D). Deposits of the delta drift dominate the drift sequences ds1 and ds2 (Fig. 4.7E). The central area in front of the GA is characterized by a hummocky reflection pattern during ds3 and ds4, whereas the southern part is dominated by downlap terminating reflections nearby the SKC. During ds5 and ds6 the internal configuration changes into a subparallel semi-

continuous mounded pattern with downlap termination onto the underlying strata. The depo-center is relocated 3 km southwards and the extension decreased. The growth is characterized by prograding reflections towards northern and southern direction supported by advancing downlap terminations. During ds7 and ds9 the reflection pattern is initiated north of the SKC by onlapping the underlying strata. Under stacking conditions the reflections progress northwards and the terminations turn from onlap into downlap that resulted into a mounded geometry. The progression is interrupted by a depression. The northward neighbored reflection pattern consists of sediment wave facies SF-5 and occupy the slope of the NKC. During ds10 the general reflection pattern changes again into a parallel reflection pattern of SF-4 and both transitional areas towards the channels are occupied by SF-5.

#### 4.3.2.3 Sediment Waves

The seismic and bathymetric image show recent current activity in form of sediment waves at the western oceanwards entrance of the NKC (Figs. 4.3, 4.5, 4.6, and 4.8). The seafloor is characterized by north-south striking submarine dunes due to the bottom current influence in the KC with diffraction of the sediment waves with increased frequency and decreased amplitude in direction of the IS. The seafloor of the channel is dominated by sediment waves with wave heights of 5 to 15 m and wavelengths of 450 to 600 m with decreasing wave heights towards the Inner Sea.

The nowadays seafloor is partly occupied by differential geometries of sediment waves at both sides of the KC (Fig. 4.8). The northwestern channel is dominated by transverse dunes of various wavelengths of 200 to 600 m and heights of 3 to 15 m along the channel axis. A field of shorter sediment waves, which have wavelengths of 200 to 300 m, is embedded into a field of sediment waves that have wavelengths of 400 to 600 m. The geometry of these shorter waves is even, with dip angles up to 25°, whereas mostly of the longer sediment waves are asymmetric (Fig. 4.8). The asymmetric waves have a westwards directed low angle stoss side and a steep leeward side with dip angles up to 17°. The northeastern lower slope of the GA is occupied by a field of asymmetric barchanoid transverse dunes with wavelength between 200 and 400 m. The wave heights can reach up to 12 m and decrease downslope. The geometry of the dune pattern changed into a diffraction transverse dune pattern with decreased wave heights of 2 to 5 m and wavelength of 150 to 200 m by curving around the corner of the GA (Fig. 4.8). The overall field width decreases from *ca* 4000 m to *ca* 2000m. The wave heights decrease southwards and disappear. The southwestern part show a similar dune pattern along the main channel axis with two different fields of transverse dunes. The first field occupies the channel over a length of *ca* 18 km and a width up to 5 km. The wavelength is between 200 and 400 m and the height is up to 8 m. The sediment waves are asymmetric with a low angle stoss side of 3° to 6° and a steep lee side up to 12°. The second field are embedded into the first with maximum extension of 3 km in east-west direction and 2.5 km in north-south direction. The field shows wavelength of 150 to 200 m, heights up to 15 m, and symmetric dip angle up to 18°. The asymmetric sediment waves get flattened eastwards. The

sediment accumulation south of GA is partly covered by star dunes towards the IS as well as the northeastern area off the FB (Fig. 4.8).

The seafloor of the eastern waterways of the KC around the Kaashidhu Atoll and the area towards the Gaafaru Falhu Atoll are covered with different patterns of sediment waves (Fig. 4.8). The very lower slope of the Kaashidhu Atoll show diffraction sediment waves, which are curved around the atoll with crest lines perpendicular to the main atoll morphology and disappear towards the IS (Fig. 4.8). The wavelength is 250 to 400 m, the wave height is up to 13 m in the southern waterway and up to 3 m in the northern passage, and the crest line has a length up to 2200 m. The southward adjacent area is covered with remnants of drowned atolls and asymmetric sediment waves between them (Fig. 4.8). The sediment waves have a high angle stoss side and a steep lee side, where the seafloor climbs up, and a parabolic geometry. Where the seafloor gets planar, the geometry changes into asymmetry with a low-angle ( $< 8^\circ$ ) stoss side and a steep leeside angle ( $< 15^\circ$ ). The distance from crest to crest is about 250 to 500 m. The sediment waves get flattened and disappear towards the IS. The area behind the southernmost drowned atoll and the northwestern lower slope of the Gaafaru Falhu Atoll (Fig. 4.8) are covered with sediment waves, which show a diffraction pattern around the northwestern edge of the Gaafaru Falhu Atoll. The

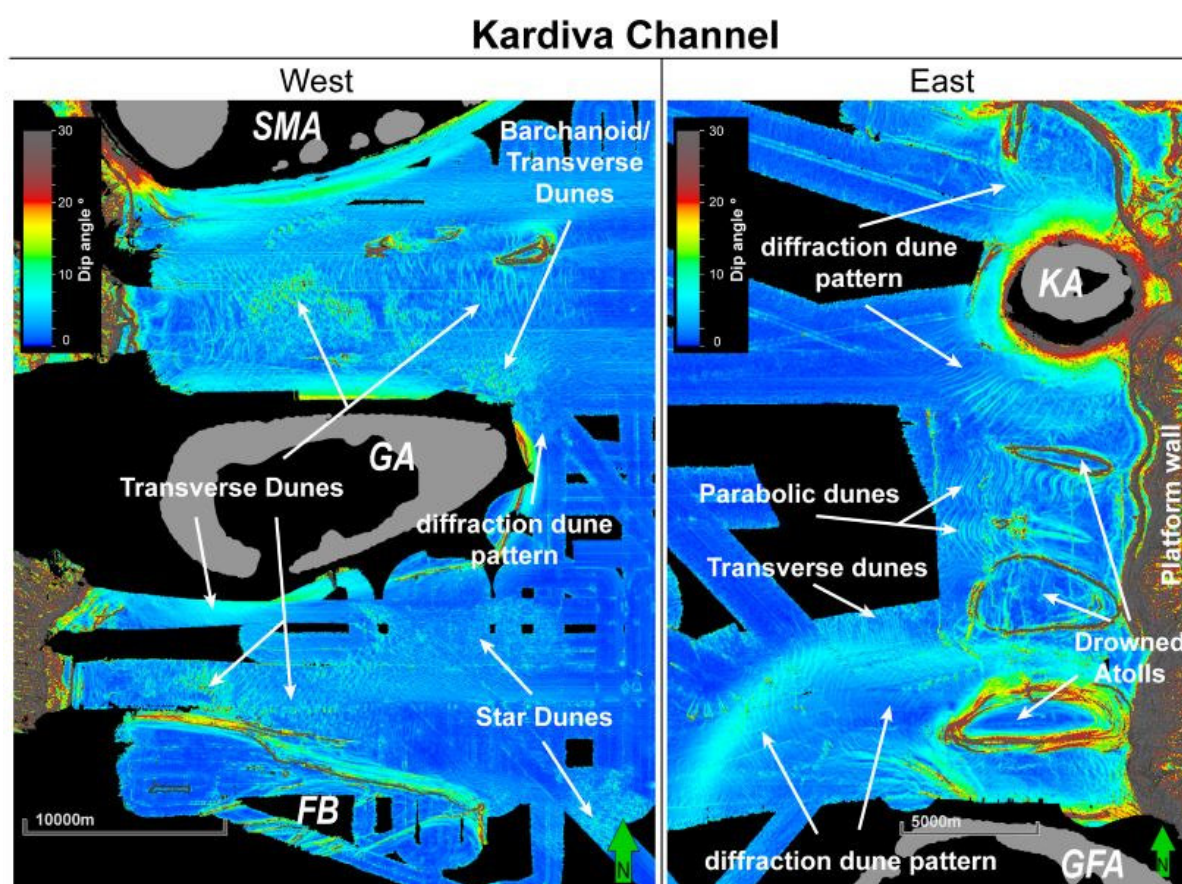


**Figure 4.8:** Seabed slope angle map (see Fig. 4.1A for location) of the surveyed western and eastern oceanward parts of the KC. The occurrence of different types of sediment waves are concentrated in the inter-atoll channels and adjacent areas of the archipelago. No data areas (black gaps) and shallow-water areas/island (gray) are imaged. FB=Fuad Bank; GA=Goidhoo Atoll; GFA=Gaafaru Falhu Atoll; KA=Kaashidhu Atoll; SMA=South Mallhosmadulu Atoll.

wavelengths are between 150 m and 300 m and the wave heights reach 1.5 to 5 m. The waves are situated in a water depth range of 270 to 520 m and disappears southwards.

### 4.3.3 The Inner Sea

The deposition of carbonate material in the basinal area of the KC is described on the basis of two MCS profiles to identify the deposition geometries. The first is the profile p65(M74) (Fig. 4.9), the second is the composite of four sections of M74 profiles, p24a(M74), p62(M74), p24b(M74) and p63(M74), to generate an east-west transect across the MA (Fig. 4.10).

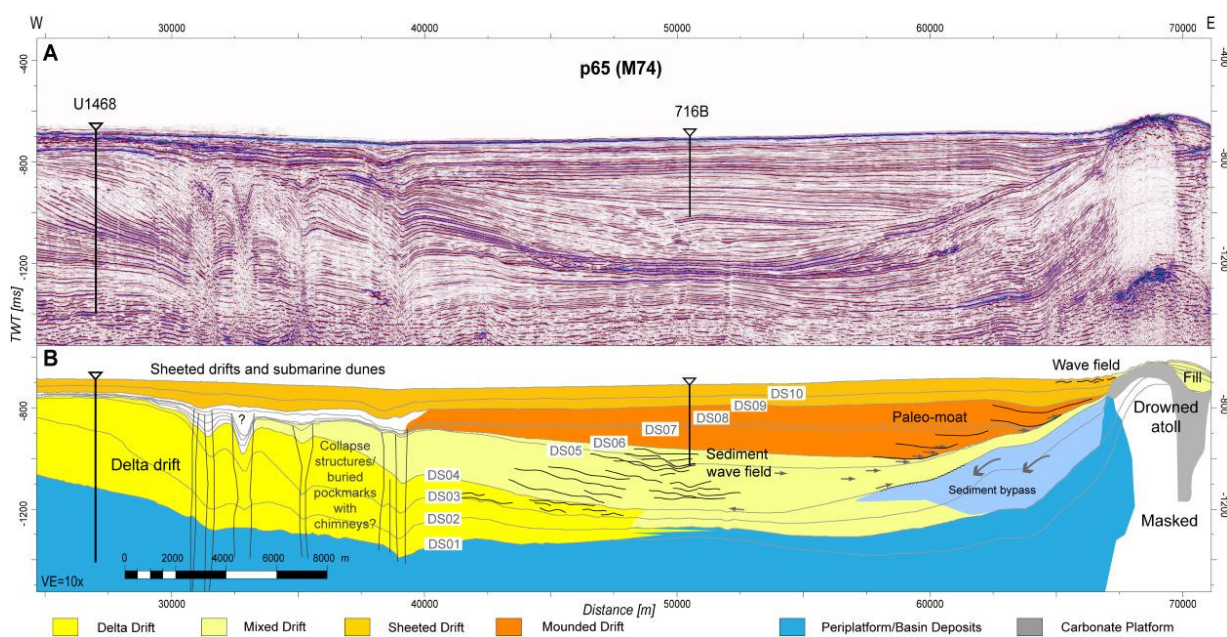


**Figure 4.9:** **A:** Uninterpreted MCS data (see Fig. 4.1A for location) of profile p65(M74). The delta drift and overlying sediments are disturbed by collapse and pockmark structures (disrupted reflections). **B:** Seismic facies interpretation of profile p65(M74). VE=Vertical exaggeration.

The seismic data image of p65(M74) shows the reflection geometry across the IS (Fig. 4.9A). The aggrading and prograding drowned carbonate platform characterizes the western part with its discontinuous strong amplitude reflection pattern and its strong topmost reflection. An eastward prograding pattern of sigmoidal oblique medium amplitude reflections are displayed that continuous into a thin layer of continuous parallel medium amplitude reflections in the central paleo-IS during ds1 to ds3. The sequences ds1 to ds3 are capped by an erosional surface and the lower talus is characterized by reflections of sediment waves. The sequence boundaries are trackable from boundary DS1 to DS10 at the basin. The basin-fill of the IS encompasses the accumulation of the drift fan between the boundaries DS01 and DS04 and the following filling of ds04 to ds10 with varieties in the sedimentation patterns. The eastern part is dominated by SF-1 and part of a drowned atoll (Fig. 4.9A). The eastern depositional patterns adjacent to the atoll structure are dominated by dipped (semi-)continuous moderate to low amplitude reflections during ds1. The middle slope is characterized by horizontal subparallel reflections with an aggrading pattern during ds2. The lower slope shows a prograding pattern during ds3. The depositions center

shifts towards the western central basin during ds4. The drift sequence ds4 is characterized by a transition from convex-up to an oblique-divergent eastward-dipping continuous reflection geometry with moderate amplitudes. The reflections shift from subparallel and wavy forms with a maximum thickness of ds4 at the central paleo-IS to a parallel continuous seismic pattern, which onlaps the inclining slope of the eastern platforms (Fig. 4.9). The reflections on the eastern side show a convergent pattern, which is partially supported by onlap terminations onto the underlying strata of the eastern slope of the ancient eastern platform. The wavy reflections disappear and the deposition is concentrated in the central basin during ds5. The basin-fill succession shows a parallel continuous reflection pattern in the seismic image and a moat system that develops at the eastern side. Between the sequence boundaries DS6 and DS7 the continuous low amplitude reflections show a divergent pattern eastwards that shifts into parallel reflections terminating with onlap onto DS6 and DS5, where DS6 cannot be differentiated. The western part is characterized by an unconformity, which cuts the reflections; whereas the eastern part shows a development of a moat structure during ds05 that climbs up the slope of the eastern platform until ds09 and onlaps the underlying strata. The continuing development of an aggrading and eastwards migrating moat can be observed and tracked during this time (Fig. 4.9). The drift sequences ds7 to ds10 are characterized by a stacked continuous parallel reflection pattern with moderate amplitudes of SF-4. The eastern moat flank geometry shows its steepest shape during ds8, gets flatter during ds9 and disappears during ds10. The last drift sequences ds09 and ds10 are dominated by continuous parallel reflections across the basin of the IS and onlaps the drowned platform, that bordered the western part of the IS (Fig. 4.9).

The southern composited profile shows a similar seismic pattern as the northern profile with some differences at the margins of the drowned platforms (Fig. 4.10). The western side is dominated by an eastward prograding pattern of sigmoidal oblique low-to-moderate amplitude reflections covered by semi-continuous semi-parallel medium amplitude reflections during ds1 to ds3. The drift sequence ds4 is characterized by divergent eastward-dipping semi-continuous reflections with moderate amplitudes. The reflections shift into parallel low-to-medium amplitude reflections and turn from inclining to slightly climbing angles at the central paleo-IS, interrupted by a nearly vertical fault (Fig. 4.10). The reflections on the eastern side form a depression and terminate with onlap onto a minor erosion surface in the eastern slope strata, resulting in a stacking pattern of moat-similar geometries during ds4. The eastern slope is characterized by dipping continuous medium amplitude reflections that turned into semi-continuous reflections at the lower slope during that time. The continuous reflections are interspersed with discontinuous-to-chaotic slightly prograding reflections, which terminate at an erosion surface adjacent to the moat-like feature at the toe-of-slope. The boundaries DS05 and DS06 enclose a thin layer of continuous reflections with a widening moat at the eastern area of the paleo-IS. The reflections of sequence ds6 onlap the western carbonate platform and show a semi-continuous-to-discontinuous pattern of SF-5, which shifts into a semi-continuous subparallel pattern with low amplitudes above the rim of the drowned western platform and the buried delta drift (Fig. 4.10). The central paleo-IS is dominated by continuous

parallel reflections of SF-4, which show a slowly decreasing thickness at the eastern moat position. The reflections, eastward of the moat, show a seismic pattern with semi-to-discontinuous low amplitude reflections interspersed with layers of wavy reflections. The reflection pattern is assigned to SF-4 and SF-5. From ds6 to ds10 the western drowned platform is partly buried by discontinuous or wavy medium amplitude reflections of SF-5. The coverage of relocated sediments onto the drowned platform increases with persistent accumulation during this time period. The reflection pattern is dominated by parallel continuous medium reflections at the central IS during ds6 to ds10. The sequence ds7 shows a very low accumulation thickness overall. The eastern reflection pattern of ds8 shows a westward prograding reflection pattern that narrows and flattens the eastern moat. During ds9 the moat gets levelled and disappears. Adjacent to the drowned eastern atoll a second sediment body with westward prograding reflections is generated (Fig. 4.10). This sedimentary body, with internal sigmoid semi-to-discontinuous medium amplitude reflections, shows a continuous aggradational and progradational growing during ds10. The body is interspersed with discontinuous-to-wavy reflections of SF-5 and the seafloor is dominated by sediment waves.

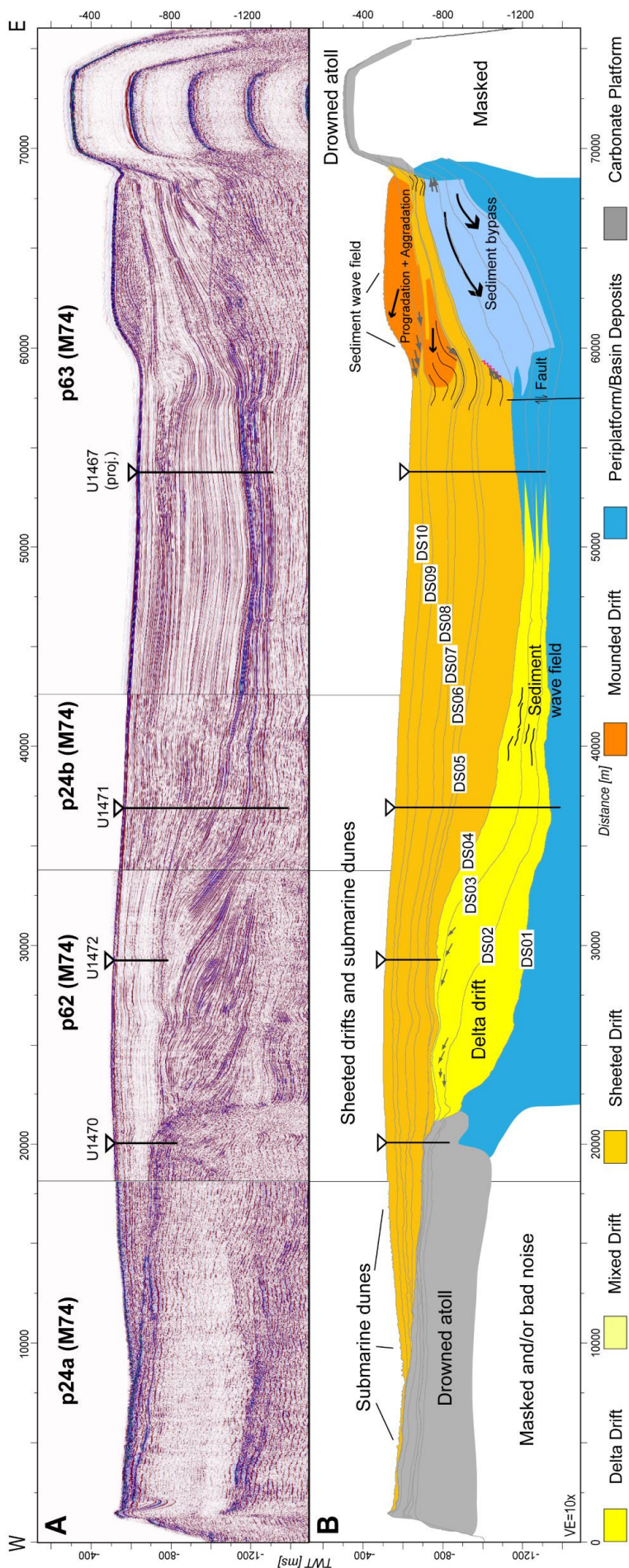


**Figure 4.10:** A: Uninterpreted MCS data of segments (see Fig. 4.1A for location) of profiles p24a(M74), p62(M74), p24b(m74), and p63(M74). B: Seismic facies interpretation of the compiled profile. VE=Vertical exaggeration.

Two seismic images of the northeastern area of the KC, adjacent to the Kaashidu Atoll (Fig. 4.1), show an additional complex fill of sediments (Fig. 4.11A to E). The composited profiles of p16(SO236) and p16-1(SO236) display an atoll structure (SF-1) and slope and basin sediments as the primary composition below DS1 (Fig. 4.11A and B). During ds1 to ds3 the reflection of the slope turns from a steep sigmoid to a flat sigmoid reflection pattern with low-moderate amplitude (semi-)continuous reflections. The seismic pattern is intersected with minor subparallel to wavy reflections of low amplitudes. The general seismic patterns point to sediments, which prograde towards the IS. The main depo-center shifts towards the IS during ds4. The slope is occupied by medium scale sediment waves of SF-5 and the reflections show a divergent pattern towards the basin. The upper part of ds4, adjacent to the platform margin, is characterized by a trough that eroded into the sediments and refilled during ds4. Sediments are bypassed into the basin during ds5. The upper slope is free of newly accumulated sediments and the lower slope shows low accumulation with slightly downlap and onlap terminations. Accumulation of sediments, assigned to SF-4, filled the basin up to the level of the eastern margin of the drowned part of the Kaashidu Atoll during ds6 and ds7 (Fig. 4.11A and B). A short period of mounded contourite drift development are interleaved in the sheeted contourite drifts accumulation shown in profile p16(SO236), which terminates with downlaps onto the underlying strata (Fig. 4.11A and B), whereas the mounded contourite drift development is absent in profile p14(SO236) (Fig. 4.11D and E). The latest drift sequences exhibit an aggradational reflection pattern of SF-4 at the basin and SF-5, which onlaps the slightly inclined platform. High-resolution Parasound data show details of the uppermost sequences of ds9 and ds10 (Fig. 4.11C). The displayed reflections are assigned to SF-1, SF-4 and SF-5. The western part is dominated by SF-4 that pass over eastwards into SF-5 concurrent with a

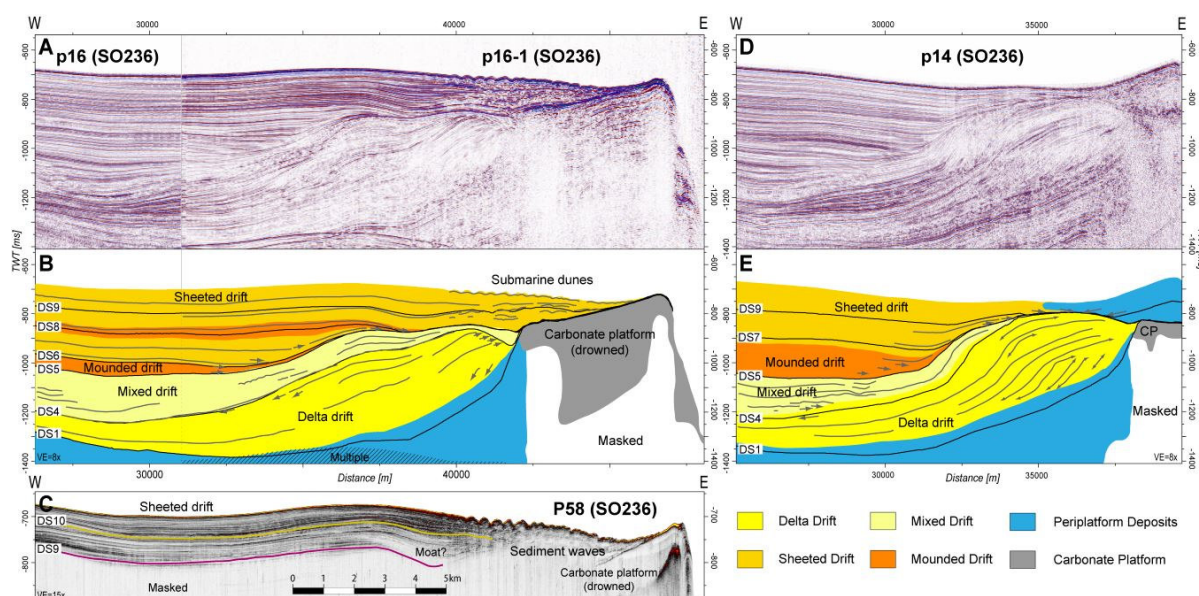


**Figure 4.11:** A: Segment of MCS data (see Fig. 4.1A for location) of profile p16(SO236) and p16-1(SO236). B: Interpreted MCS data of the compiled profile. C: Imaged data of Parasound profile P58(SO236). D: Segment of MCS data of profile p14(SO236). E: Interpreted MCS data of the profile p14(SO236). VE=Vertical exaggeration.

decreased level of reflected energy and thus lower penetration. The sediment wave field extends onto the drowned platform, which outermost margin is kept free of sediments (Fig. 4.11C).

The neighbored profile p14(SO236) shows a similar seismic pattern with a delayed initiation of the sigmoidal prograding reflection pattern during ds1-ds3 (Fig. 4.11D and E). The deposition center shifted from the slope to the basin during ds4. Here, at the toe-of-slope wavy reflections occur. During ds5 the reflections show downlap and onlap terminations that result in a slightly mounded structure, whereas the slope is free of newly accumulated sediments during this time. Downlap terminations peter out and onlap terminations dominate at the lower slope at the end of ds6. Sheeted drift facies SF-4 dominated the basin from this moment on. Contemporaneous, sediments of SF-2 and SF-3 accumulate onto the former platform and terminate with downlaps onto the former sigmoid sediment unit (Fig. 4.11D and E).

#### 4.3.4 Drowned atolls

Drowned platforms are common in the MA, one is located in the eastern NKC in a water depth of > 315 m (Figs. 4.1 and Fig. 4.12). Its overall shape is oval with the long axis orientated NNE-SSW reaching 11.6 km in length and 6.6 km in width. Its western steep slope declines *ca* 2000 m to the deep Mid-Indian basin. The northern and southern slopes are bordered by deep troughs, which are connecting the Inner Sea with the Mid-Indian basin. The western slope is bound to a moat adjacent to the Inner Sea contourite drift system. The drowned atoll geometry has been dominated by a series of step-like terraces since the Miocene except the steep eastern slope (Fig. 4.12). The uppermost terrace of the carbonate bank has an extension of 5.2 km in length and 2.2 km in width. Three WNW-ESE cross-sections of hydro-acoustic Parasound profiles of the topmost part reveal the seismic facies of three dominating types (Fig. 4.13A to G). The first seismic facies is characterized by a strong amplitude continuous reflector with no further internal reflections, assigned to SF-1. The topmost part of the carbonate bank shows a flat relief with steep walls bordering the carbonate bank (Fig. 4.13A to D). The western wall is grounded on a trough followed by an irregular relief and terminated by a steep slope towards a subjacent terrace. The irregular relief is covered by a mounded shaped unit of SF-4 that terminates with downlap eastward. The internal seismic facies consists of divergent low-to-medium continuous amplitude reflectors approaching the eastward rim. The seismic unit covers an area of up to 2.5 km in width and *ca* 6 km in length with a maximum height of *ca* 25m (32 ms TWT) on the step-like terrace (Fig. 4.12). The side towards the topmost carbonate bank is characterized by a circum-confined moat system with angles around 15° up sediment body. Some depressions on the irregular relief are filled with slumps characterized by a chaotic to transparent internal reflection pattern of SF-6. The mounded relief smooths out towards the northern part of the terrace (Fig. 4.13F and G).

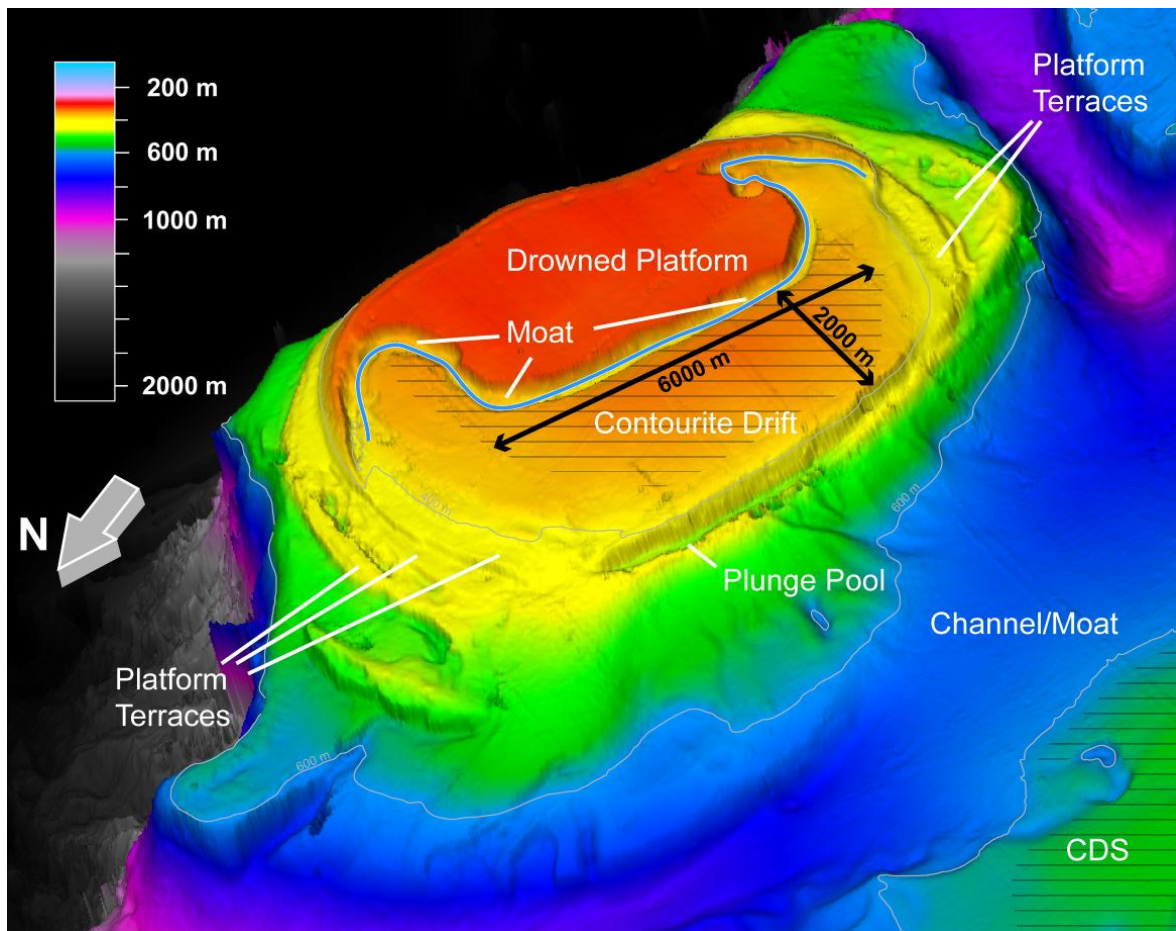


**Figure 4.12:** 3D-view on the bathymetry of the north-eastern entrance of the Kardiva Channel (see Fig. 4.1A for location). The blueish line indicates the pathway of the moat adjacent of the topmost platform. Successive and parallel platform terrace morphologies are typical for backstepped margins. CDS=Contourite Depositional System.

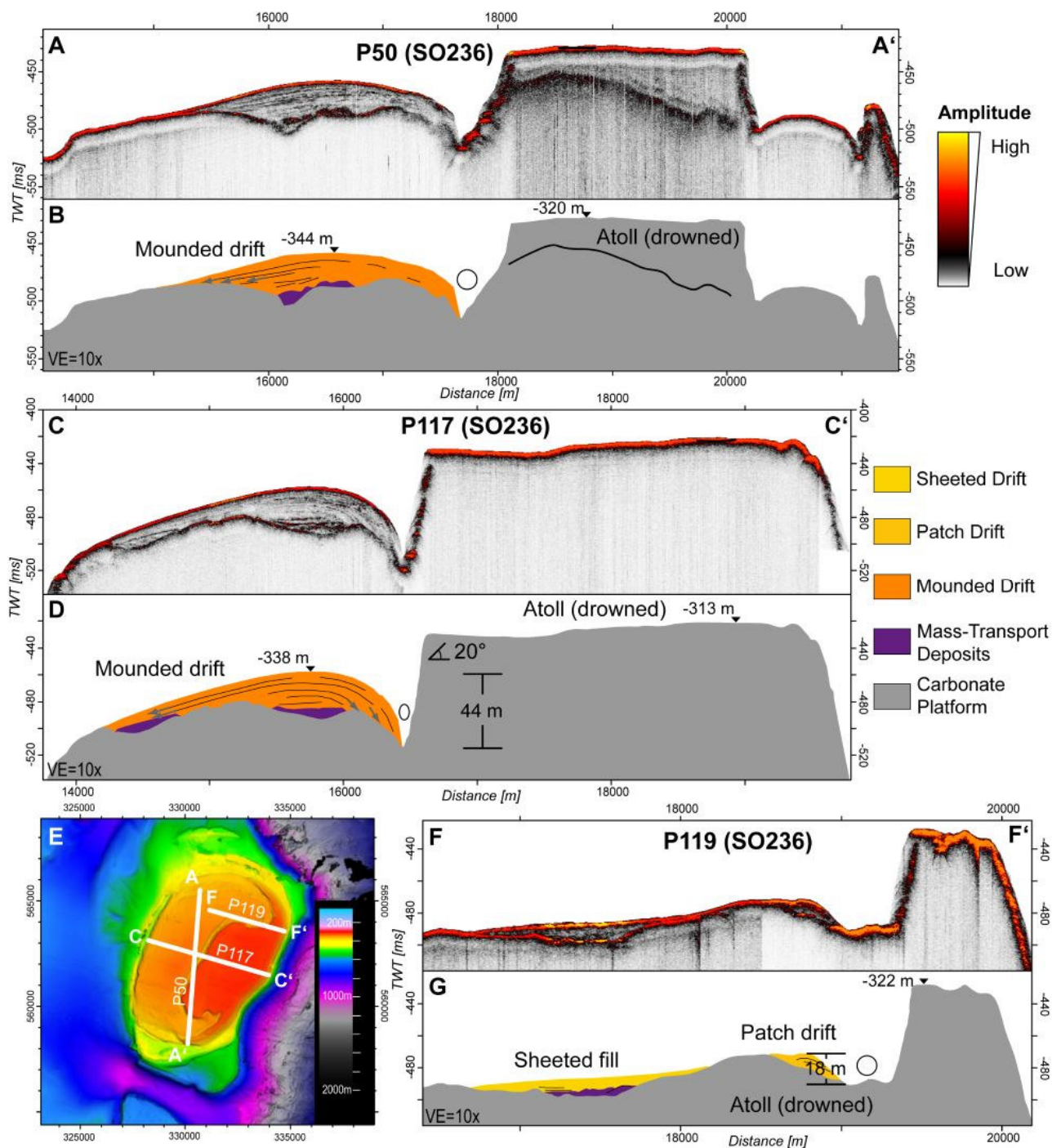


**Figure 4.13:** **A:** Segment of uninterpreted Parasound data (see Fig. 4.1A for location) of profile P50(SO236). **B:** Seismic facies interpretation of profile P50(SO236). **C:** Segment of uninterpreted Parasound data of profile P117(SO236). **D:** Seismic facies interpretation of profile P117(SO236). **E:** Map of the bathymetric framework around the shown profiles. Coordinates in meters are based on the WGS1984 UTM 43 grid. **F:** Segment of uninterpreted Parasound data of profile P119(SO236). **G:** Seismic facies interpretation of profile P119(SO236). VE=Vertical exaggeration.

#### 4.3.4.1 Fuad Bank

The FB is a drowned platform, situated between the North Ari Atoll and the GA (Fig. 4.1A). It lies in a present water depth of 210 to 230 m and has extensions of *ca* 50 km in length and 25 to 30 km in width (Fig. 4.1A). The MCS profiles p10(M74), p22(M74), the Parasound profile P139(SO236), and bathymetric data display cross-sections and the bathymetric framework of the drowned eastern platform of the FB and the sedimentary structure of the 'Inner Sea' (Fig. 4.14A to G). The

bathymetric data reveal a classic platform geometry with reef enthroned on a steep wall and a slightly deeper back reef area. The platform top, with its back reef area and the slightly irregular relief of SF-1 is draped by low-to-medium amplitude parallel (semi-)continuous seismic reflections of SF-4 (Fig. 4.14A to D). The reflections terminate with onlap geometries on the outer rim, which is free of unconsolidated sediments (Fig. 4.14A and B). The thickness of the cover layer is up to 32 m (40 ms TWT). The thickness increases towards the Inner Sea. Their maximum age is about 1.5 Ma (DS10). The low-to-medium amplitude continuous reflections of SF-4 terminate with onlaps onto the drowned topmost surface of the FB. A second MCS profile unveils that the western and eastern barrier reef of the drowned FB is free of unconsolidated sediments (Fig. 4.14C and D). The central lagoonal area with its irregular relief is filled with sediments. The medium amplitude continuous

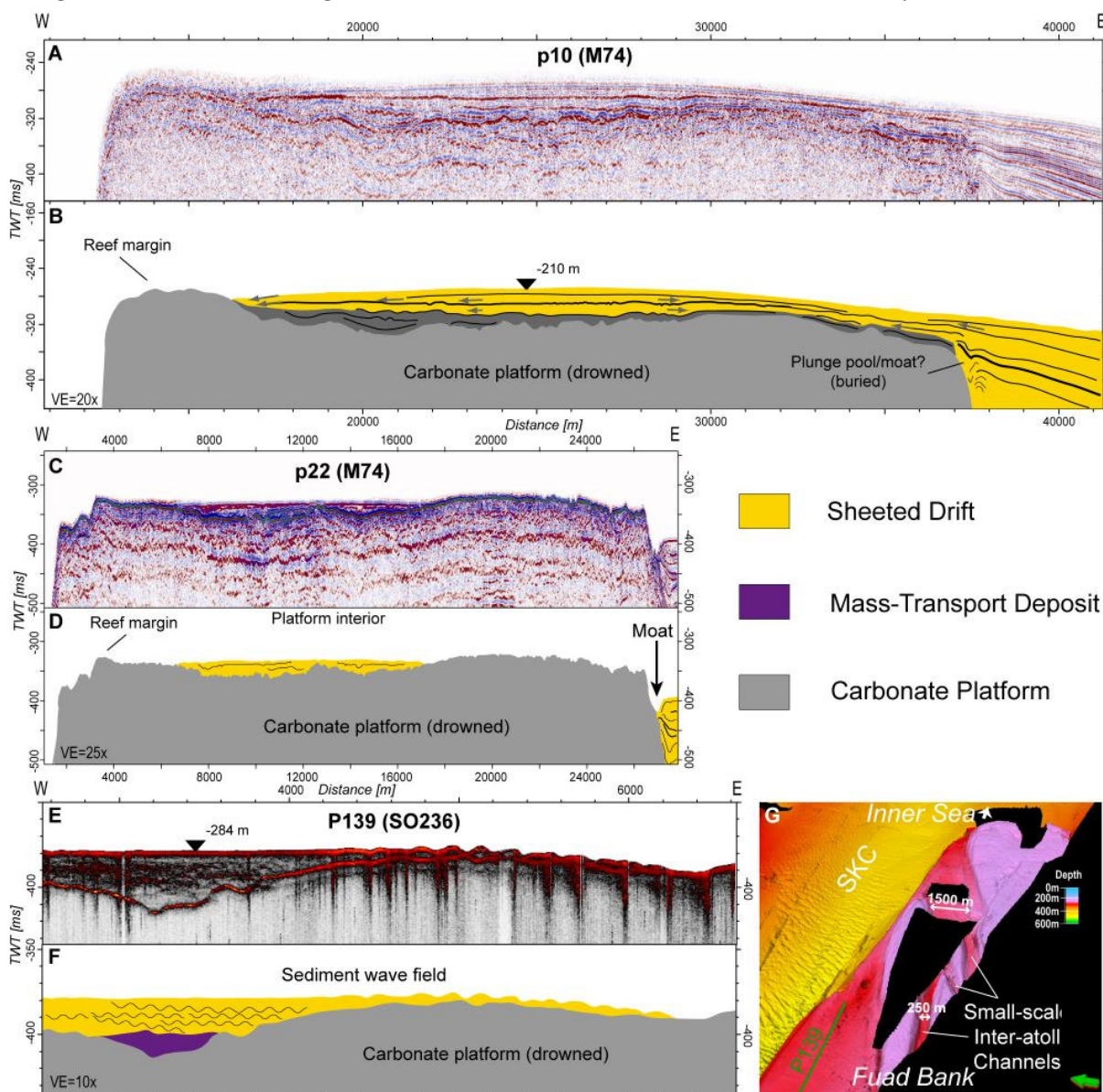


**Figure 4.14:** **A:** Segment of raw MCS data (see Fig. 4.1A for all locations) of profile p10(M74) across the Fuad Bank. **B:** Seismic facies interpretation of profile p10(M74). **C:** Segment of raw MCS data of profile p22(M74) across the Fuad Bank. **D:** Seismic facies interpretation of profile p22(M74). **E:** Segment of raw Parasound data of profile P139(SO236). **F:** Seismic facies interpretation of profile P139(SO236). **G:** 3D-view at the bathymetry along the northern margin of the Fuad Bank. Black areas represent data gaps. VE=Vertical exaggeration.

reflection terminates with onlap against the platform's surface. The sediment layer is up to 20 m thick and extends about 10 km in east-west direction. The reef front is not covered with contourite drift sediments as compared to the southern part. The eastern slope dips down 63 m with an angle of *ca* 9°. A 700 m wide channel strikes along the steep inner platform's slope with a depth 20 to 25 m. It is flanked basinwards by mounded sediment body (Fig. 4.14D). The layered low-to-medium amplitude reflections of this body terminate with downlap onto a hardground in the channel center forming a moat flank. The opposing moat flank is part of the lower platform wall

The Parasound data shows three different seismic facies SF-1, SF-5 and SF-6. The sub-bottom profiler data reveals an irregular relief in the back reef area (Fig. 4.14E). The platform facies SF-1 is characterized by a strong amplitude reflection and no penetration of the seismic signal into the platform interior. The back reef relief is smoothed by overlying unconsolidated sediments, represented by SF-5 and SF-6 that draped the lower parts of the lagoon. The eastern segment of the profile is dominated by sediment wave field with wavelengths of 140 to 270 m and heights of 1 to 3 m. The sediment waves get smoothed westwards, where the back reef area dips and the thickness of the sediment coverage increased. The most northern part of the FB is interveined with former small-scale inter-atoll channels mostly free of unconsolidated sediments with an average depth of 45 m in comparison to the neighbored topmost part of the carbonate banks (Fig. 4.14G). Generally, the drowned part forms a lower-level plateau in a water depth of 280 m adjacent to the topmost level of *ca* 220 m below sea-level.

### 4.3.5 Intra-Atoll area

Seismic data from the shallow-water cruise (2011) on the North Malé Atoll and Ari Atoll reveal several structures with internal horizontal and parallel reflections. The imaged data of profile p44(2011) show two bathymetric highs and the coverage of different sedimentary deposits (Fig. 4.15). The southern sediment wedge with its high continuous low amplitude reflections, assigned to SF-4, terminates with downlap onto the underplayed strata adjacent to the bathymetric high. The flat area between the bathymetric highs is occupied by a body with internal low amplitude parallel semi-continuous reflections. The reflections terminate with downlaps onto the underlying strata, assigned to SF-1. The sediment body has an extension of *ca* 700 m and a height of *ca* 5.5 m above the surrounding surface.

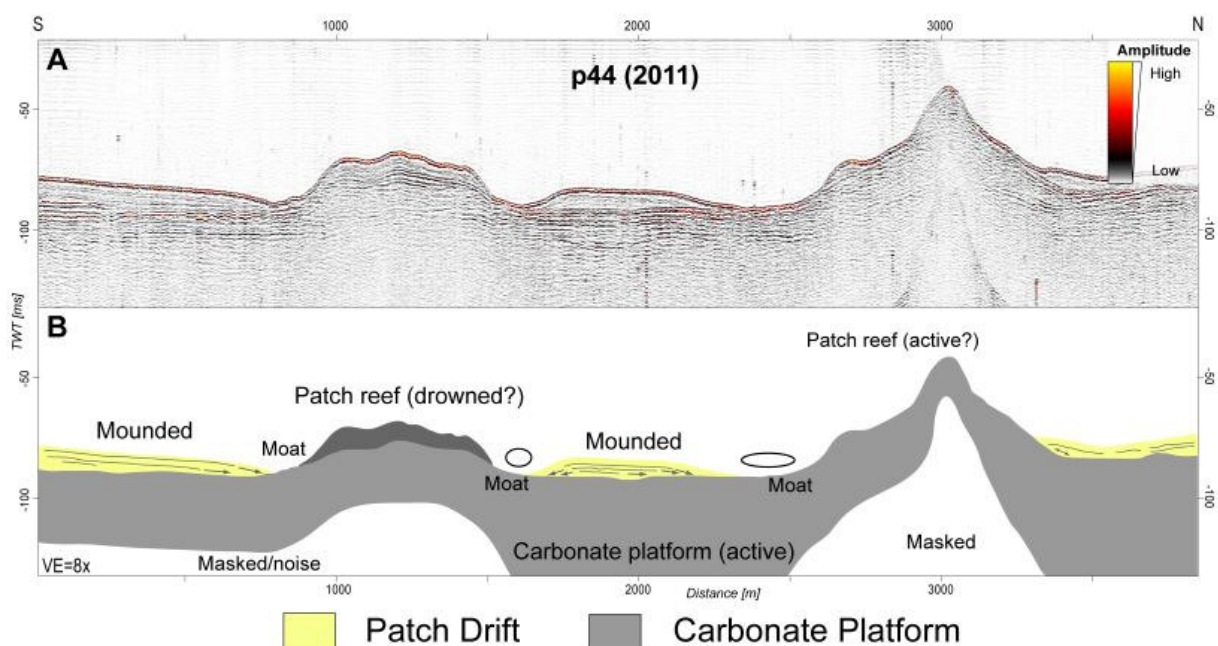


**Figure 4.15:** A: Segment of shallow-water single-channel seismic data (see Fig. 4.1A for location) of profile p44(2011). B: Seismic facies interpretation of profile p44(2011). VE=Vertical exaggeration.

## 4.4 Bahamas, Santaren Channel

### 4.4.1 Depositional features and geometries

The SC represents an inter-atoll channel between the CSB and GBB (Figs. 1.2 and 4.1B). The SD dominates the basinal framework in the SC (Fig. 4.16). Three representative MCS profiles of the investigated region reveal the reflection pattern of the SD (Figs. 4.17 to 4.19).

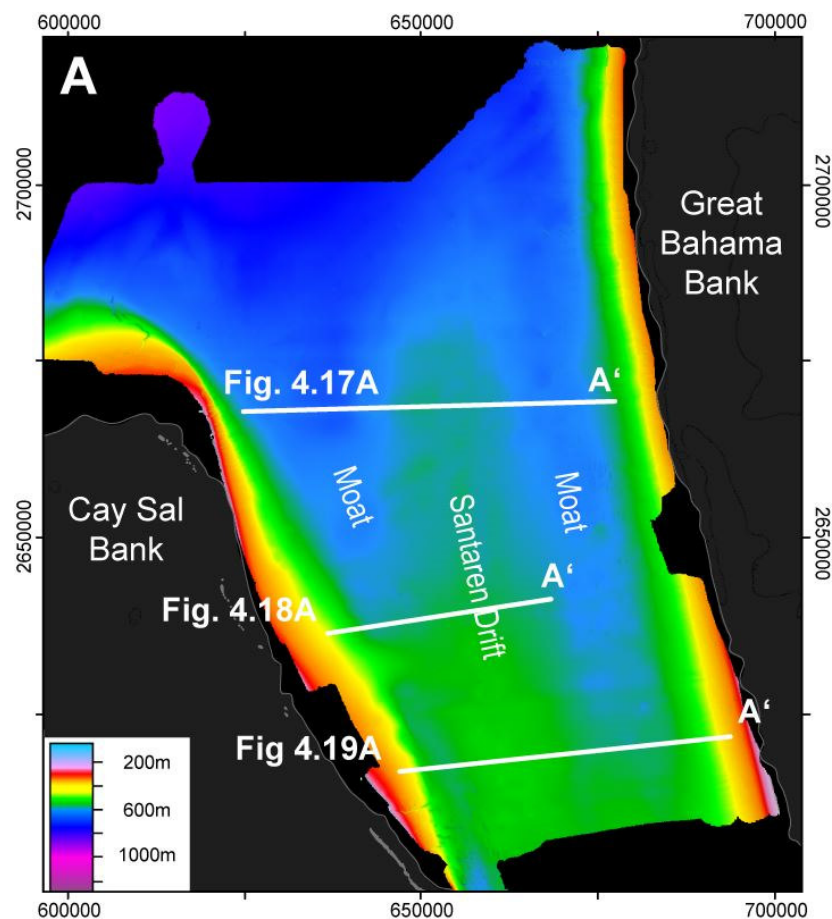


**Figure 4.16:** Bathymetric map of the surveyed area during M95 cruise, inner data gaps are interpolated. The north-south oriented greenish elongated area in the central SC represents the mounded part of the Santaren Drift. No data areas (black), shallow-water areas (dark gray), and islands (gray) are imaged. Coordinates in meter are based on the WGS1984 UTM 17N grid.

### 4.4.2 Detailed description of the MCS data

The description of the seismic sequences are grouped into genetically related depositional units that are characterized by identical geometry and similar superordinate seismic facies pattern (SF1 to SF7; Fig. 4.2). An overview of the seismic sequences (S1 to S12) and their boundaries (I to XII) as well as the lithological and physical characteristics of ODP Site 1006 are given in Figure 3.10. The oldest sequences S12 to S9 form a unit of relatively thin mainly high-amplitude reflections with highly continuous and parallel configuration with low to medium amplitude (SF4; Figs. 4.17 to 4.19) at the channel center. They show fairly uniform thickness and a predominately aggradational stacking pattern. Erosional features and considerable moat development are missing. Applying the

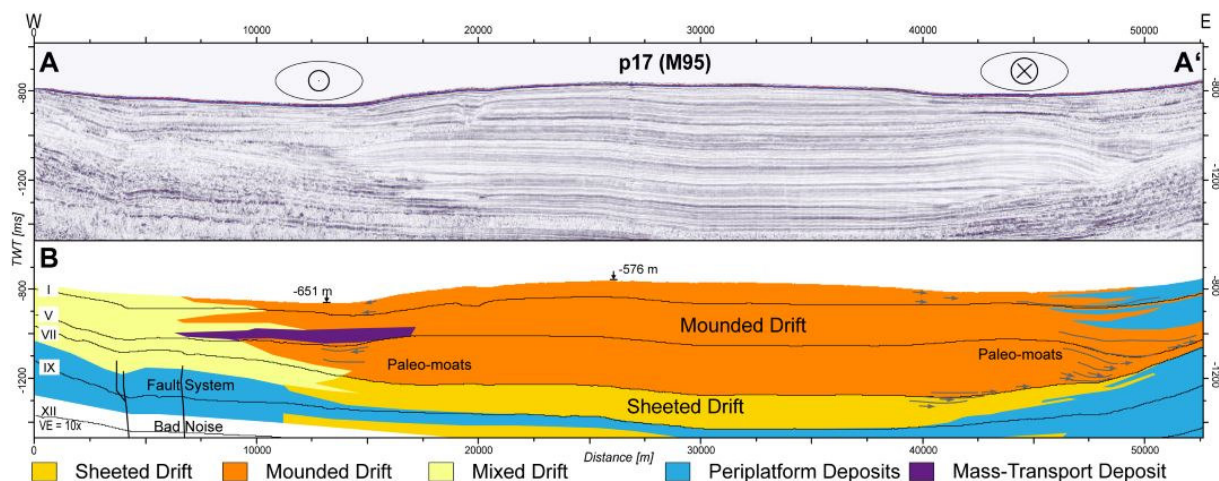


**Figure 4.17: A:** Uninterpreted seismic data of profile p17(M95) representing a northern transect across the Santaren Channel. The detailed location can be found on the maps (Figs. 4.1B and 4.16). **B:** Seismic facies interpretation of profile p17(M95). The first evidences of a current-induced moat are indicated by downlap terminations that are marked with small grey arrows. Warm colours indicates different current-influenced seismic facies. The light yellow color point to current-dominated deposits interspersed with numerous minor mass transport deposits. Major tectonic faults are indicated. White represents the uninterpreted zone with poor-quality data. Modern bottom-current direction is indicated by icons. VE=Vertical exaggeration.

classification of Faugères *et al.* (1999), the sheet-like deposits correspond to sheeted drift bodies. Periplatform deposits are limited to the slopes where they form wedges showing dipping semi-continuous reflections as well as medium-amplitude and frequency, represented by SF2. Facies SF3 has subparallel to chaotic low- to medium-amplitude reflections of low continuity. Like SF2, SF3 occurs at the slopes and is lens- to wedge-shaped. Both seismic facies (SF2 and SF3) appear in sequence S1 to S3 and S8 to S12, respectively (Figs. 4.17 to 4.19). Chaotic to discontinuous-lenticular internal reflections of low-to-medium amplitude are characteristic for the mass-transport facies SF6. It can be found in sequences S1, S5, S7 and S9 to S12.

Starting with S8 at 8.4 Ma and continuing into the present (S1), the geometry of the sequences significantly changed whereby their internal configuration pattern remains generally constant, characterized by parallel, high- amplitude to medium-amplitude reflections of persistent continuity (SF4). This second type of genetically related depositional unit is defined by its mound shape in cross-view with a moat feature at one or both sides (Figs. 4.17 to 4.19). The latter is characterized by erosion or non-deposition or areas of condensed sedimentation (Fig. 4.20). The mounded depositional body, which extends along the SC, matches the criteria of an elongated mounded contourite drift established by Faugères *et al.* (1999). The linear depressions associated with the mounded drifts are moats that were formed by the action of bottom currents. Typical are the convergence of strata from the mounded contourite drift (location of highest accumulation) to the moats (location of lowest accumulation) (Figs. 4.17 to 4.19). During the growth of the mounded drift sequences (S1 to S8), the moats significantly changed in shape and migration direction. All mounded drift sequences (S1 to S8) have moats on the eastern side of the SC off GBB while a western moat off CSB starts to develop first in the north at 5.5 Ma (S7; Fig. 4.17), later in the center at 3.8 Ma (S5; Fig. 4.18) and finally in the south at 3.1 Ma (S4; Fig. 4.19). The eastern moats exhibit

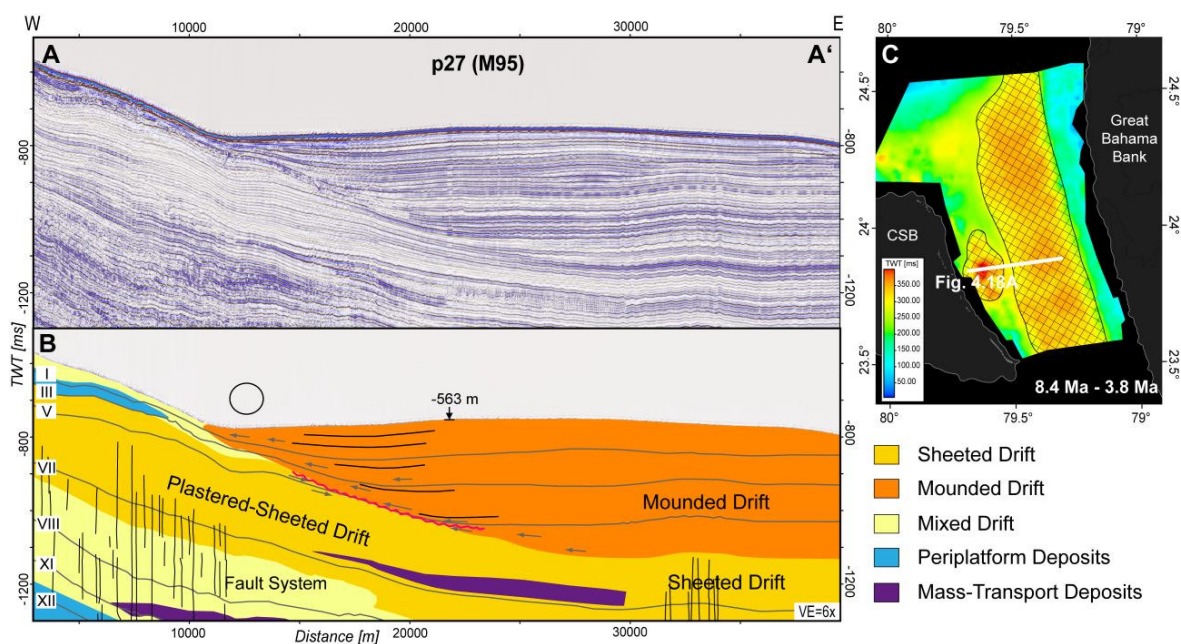


**Figure 4.18:** **A:** Uninterpreted seismic data of profile p27(M95) displaying a central transect across the Santaren Channel. The detailed location can be found on the maps (Figs. 4.1B and 4.16). **B:** Seismic facies interpretation of profile p27(M95). The erosion surface is marked by a red zigzag-line. Mostly vertical faults have been detected at the lower slope of the CSB and in the central basin. The initiation of moat-building structures is indicated by downlap terminations, and other remarkable terminations are marked with small grey arrows. Contourite sediments are lifted to a bulge at the central SC. **C:** Thickness map of accumulated sediments between boundaries VIII (8.4 Ma) and V (3.8 Ma) reveals the separation between the western notch drift and the central elongated contourite drift. VE=Vertical exaggeration.

the following trends: (1) from 8.4 Ma to the end of the Miocene (S8 to middle of S7) the moats are wide and of very low relief; (2) during the Lower Pliocene (5.5 to 3.8 Ma) their relief significantly steepens with coeval shrinking in width, the moat gradually deepens from south to north; (3) from S8 to S5 (5.5 to 3.8 Ma) they migrate eastward, upslope GBB; (4) from S4 to S1 their migration paths move westward towards the SC center and the eastern moat geometry flattens again and widens. In contrast, the western moat off CSB does not exhibit distinct changes in geometry over time; it is generally of low relief but significantly broadens from S4 to S1, analogous to the eastern moat.

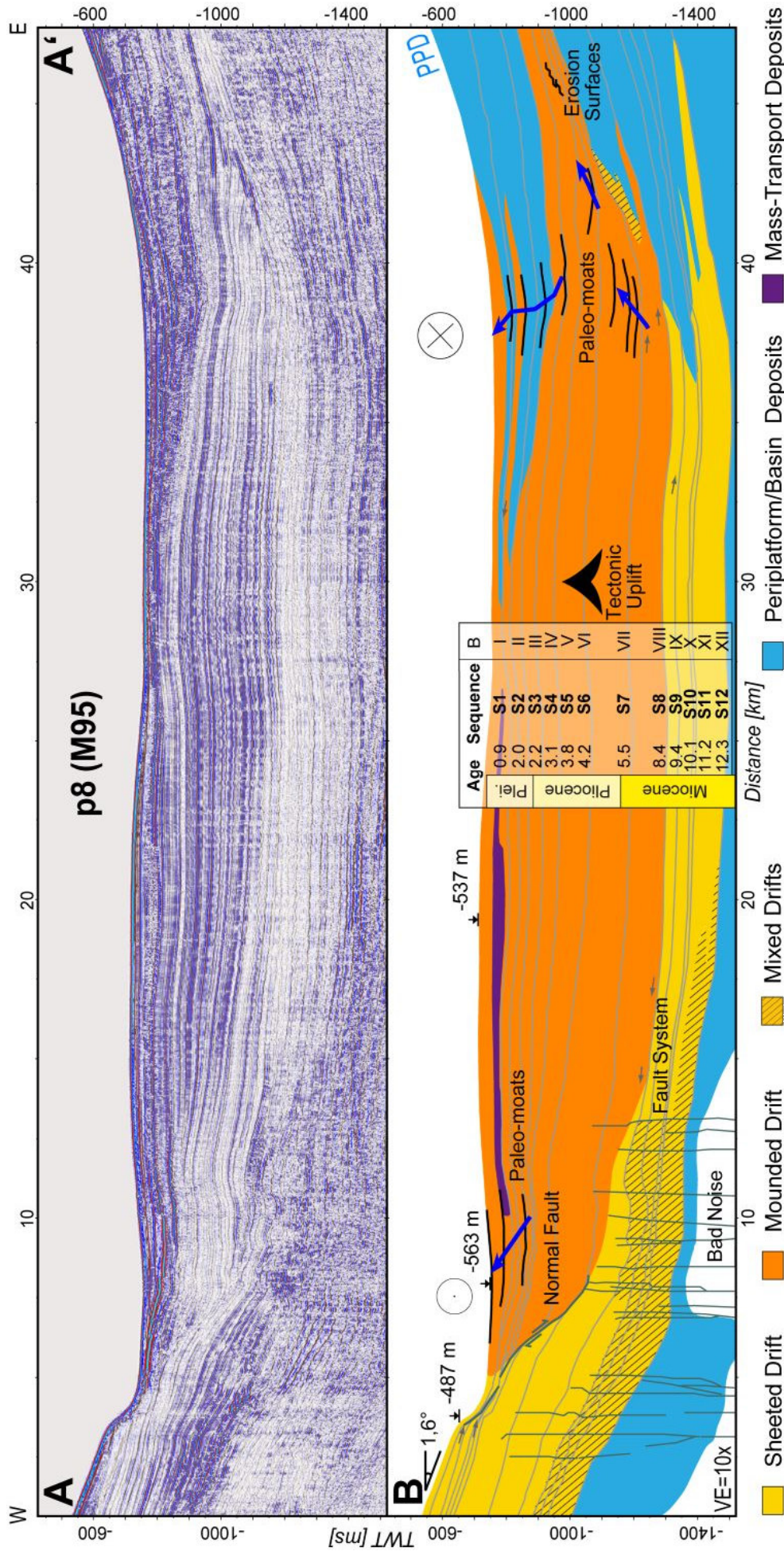


**Figure 4.19:** A: Uninterpreted seismic data of profile p8(M95) representing a southern transect across the Santaren Channel. The detailed location can be found on the maps (Figs. 4.1B and 4.16). B: Seismic facies interpretation of profile p8(M95). Contourite deposits are highly disturbed by deep rooted faults at the western channel. An associated forced normal fault can be traced up to sequence S1 and may have resulted in a significant offset of the sequences S1 to S7, producing a ca 60 m escarpment at the toe of slope of the CSB. Tectonic folding has led to mound-shaped sediments at the central channel. Age is given in million years. B=Boundary; PPD=Periplatform drift after Betzler *et al.* (2014a); VE=Vertical exaggeration.

#### 4.4.2.1 Distribution of the sedimentation pattern

The mapped time-based horizons of the seismic sequence boundaries were converted into true vertical depth in meters by using the interval velocities of ODP Site 1006 to correlate with mapped sequence boundaries (Eberli *et al.*, 1997; Anselmetti *et al.*, 2000). This correlation was used to calculate thickness maps of sediment bodies in the SC according to the data availability of about 7,000 km<sup>2</sup> for the Miocene and Pliocene and 5,500 km<sup>2</sup> for the Pleistocene. The accumulation rates are calculated by drift volume divided by its lateral extension of the contourite drift and varying time intervals.

The analysis of the seismic facies pattern of the contourite drift reveals that drift sedimentation rate varied over time. To document this variability, sequences of similar depositional characteristics are presented in thickness maps (Fig. 4.20). The origin of bottom current activity is constrained by moat development due to condensed sedimentation, which is restricted to the northern region at the junction with the Florida Straits (Fig. 4.20A) with an estimated age of 12.3 Ma (Serravallian). The occurrence of a contourite facies starts with sequence S12, indicated by a package of medium semi-continuous to continuous seismic reflections. A low contourite drift sedimentation accumulation rate of 2.8 to 4.8 cm/ka characterized the Serravallian and the Early to Middle Tortonian (12.3 to 9.4 Ma), with the exception of a small region adjacent to the northern margin of the CSB, where higher sedimentation rates can be differentiated (Fig. 4.20A). The contourite facies started to expand across the channel with an average sedimentation rate of 3.4 cm/ka. During the Late Tortonian and the Messinian (8.4 to 5.5 Ma; S8), the contourite drift continuously expanded with a slightly decreasing sedimentation accumulation rate, at an average of 4.0 cm/ka, concentrating in three NNW-SSE-trending depocenter stripes. One broad depocenter developed in the central SC with a width of *ca* 25 to 35 km and two long stretched depocenters at the platform margins (Fig. 4.20C). The thickest accumulation is found close to the CSB, with dimensions of about 50 km in length, 10 to 15 km in width, and up to 150 m in thickness.

During the Late Pliocene, sedimentation was concentrated in the center of the channel, with increasing accumulation rates going from south to north. Contourite facies expansion and accumulation rates reach their maximum of 5,100 km<sup>2</sup> and 16 cm/ka. Subsequently, during the Middle to Late Pliocene and the Early Pleistocene (3.8 to 2.2 Ma) the rates significantly drop to Upper Miocene values. The deposition focused in the central and eastern part of the SC, with slightly increased drift facies expansion (Fig. 4.20E). During the Early Pleistocene (S3 to S1), drift sedimentation is intercalated with periplatform sedimentation off GBB leading to an accumulation of sediment wedges (Fig. 4.20F). A short period of increased sedimentation is detected in the Pleistocene where rates shortly reached 13.5 cm/ka between 2.2 and 2.0 Ma. Since the Middle Pleistocene bottom currents have formed a more pronounced mounded relief of the SD. Overall

the area occupied by contourite drift sediments varied between 1,500 km<sup>2</sup> in the Middle Miocene and 5,100 km<sup>2</sup> in the Early Pliocene.

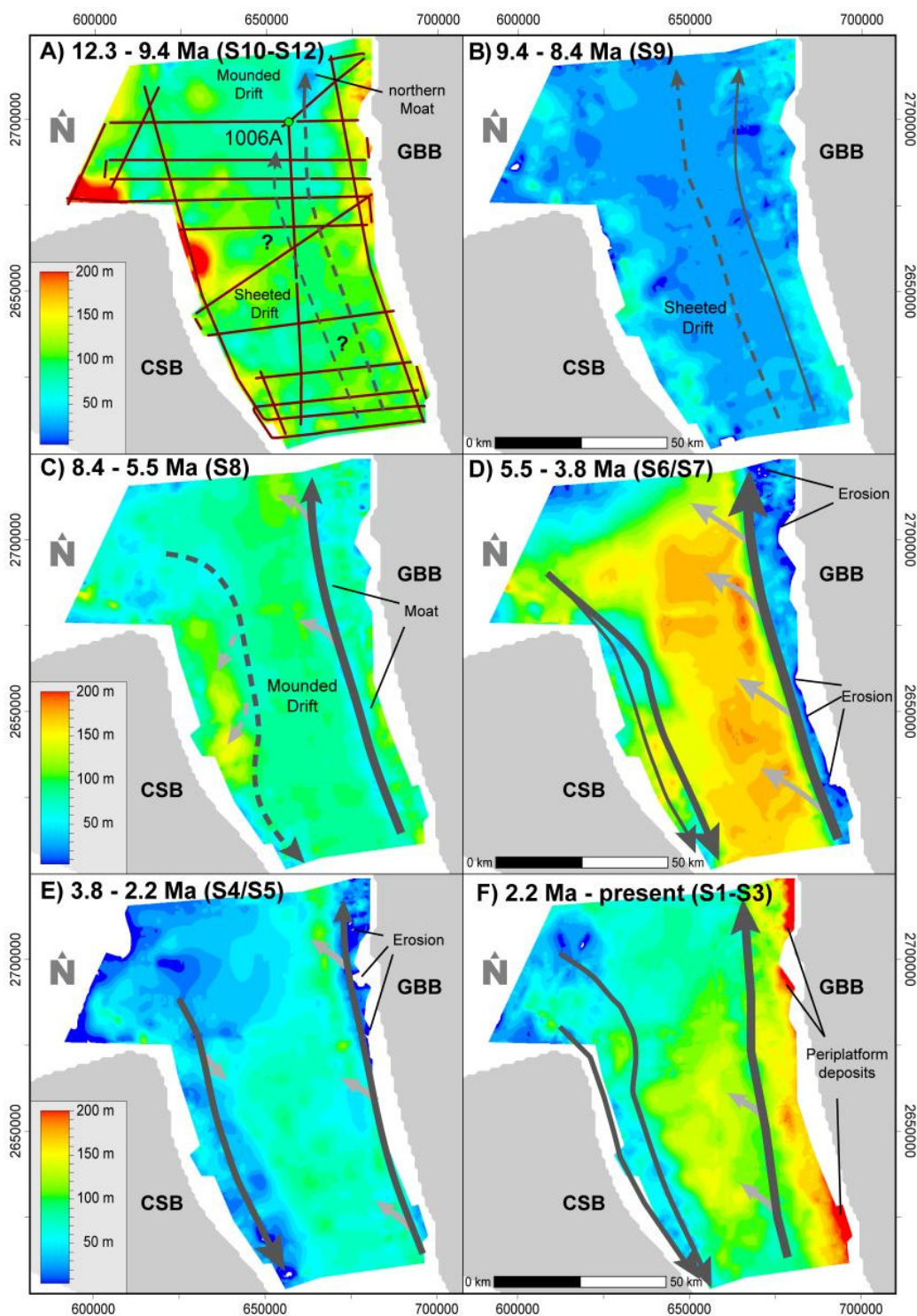


**Figure 4.20: A-F:** Thickness maps of sediment deposition within the SC and adjacent areas over time since the Middle Miocene. Bottom currents are indicated by dark gray arrows. Increased bottom currents are scaled with arrow width. Dominant contourite drift sedimentation within the basin is displayed with light gray arrows. Sediment thickness is displayed in meters. Coordinates in meters are based on the WGS1984 UTM 17N grid.

## 5 Discussion

Based on the results of the seismic reflection data in connection with the seismic facies, Parasound data, and multibeam data allowed the identification of contourite drift deposits as well as drift-related features in the working areas of the MA and BA. The discussion is about the role of the environment of isolated carbonate platforms for the development of different contourite drift types in this setting. This chapter will discuss the paleoceanographic changes of the depositional framework and its implication for reconstructing environmental changes in the past. It is divided into four parts whereby the first two sections deal with the contourite drift deposits of the MA and BA and their genesis. The third section brings similar drift deposits around isolated carbonate platform systems together and they will be characterized and discussed. The last section enlightens the potential of revealing paleoceanographic information by changes of the SD body's shape in the SC.

### 5.1 Revealing the Carbonate Contourite Drifts

Eleven different bodies of bottom-current controlled sedimentation are found within the IS and adjacent channels and the SC. The carbonate contourite drifts (CCD) are discussed in regard to the evolution of the KC since the Late Miocene and different depositional setting and morphostructure of the study areas (Fig. 4.1).

#### 5.1.1 Maldivian contourite drifts

##### 5.1.1.1 Carbonate contourite drift deposition

The western NKC and SKC opened with the drowning of the former Miocene mega platform eventually due to monsoon intensification (Betzler *et al.*, 2009, 2016a). Persistent current flow through these gateways resulted in the accumulation of delta drifts that prograded into the Paleo-IS (Lüdmann *et al.*, 2018). Concurrent with the accumulation of the western delta drifts the eastern KC shows a similar depositional pattern during depositional sequences ds1 to ds3 (Figs. 4.9 to 4.11). Alike in the west, the sediments were bypassed the channel and platform top accumulating at the slope (Figs. 4.9 to 4.11). However, the extension and the volume of deposited material are smaller related to the western delta drifts (Fig. 5.1). The Mid to Late Miocene thickness map of the main (western) delta drift stage, between the boundaries DS1 and DS4, reveals three margin-transverse depocenters at the eastern part of the KC. Their spatial extent is about 190 km<sup>2</sup> in total with widths from 3 km to 8 km and lengths from 8 km to 12 km. The delta drifts are located in front of a series of nowadays drowned atolls, which were active during the Late Miocene. Forced by the onset of the monsoon system at *ca* 12.9 Ma (Betzler *et al.*, 2016a) the eastern banks got under current pressure and let the water masses break through the IS. An interpretation of the few seismic profiles in this area do not support a conclusion of a sea-level controlled bank drowning or erosion triggered by the continual subsidence of the Maldivian basement or eustatic sea-level rise.

Assuming a weaker winter monsoon like today during the Miocene, the easterlies result in a weaker current flow. Together with the smaller extensions of the former eastern platform and a greater amount of drowning are probably responsible for the smaller extension of the eastern delta drifts. The eastern part of profile p65(M74) (Fig. 4.9) show a side section of the delta lobe, which is also imaged in Figure 4.11 south of the Kaashidho Atoll. The lithological characteristics of the eastern delta drifts are most likely analogous to the western ones described in Lüdmann *et al.* (2018) and Reolid *et al.* (2018). Here, the carbonate texture reaches from packstone and grainstone to rudstone after Dunham (1962) in the proximal part. The distal part is dominated by wackestone and packstone textures (Lüdmann *et al.*, 2018). The sedimentological analysis hints to a minimum depositional water depth of 50 to 100 m (Reolid *et al.*, 2018). The accumulation of sediment is not exclusively controlled by current-released components, in-situ produced carbonate material in the photic zone are abundant by the occurrence of coralline algae and green macroalgae (*Halimeda*) in ds2 (Reolid *et al.*, 2018)

Since the Late Miocene, the contourite drift sedimentation has become more variable. The interpretation of the thickness maps and the seismic images reveal the growth of different contourite drift bodies across the IS (Fig. 5.1). Under the influence of the monsoon system and the increased amount of waterways, which connect the IS with the surrounding open ocean, the pathways of currents developed a greater complexity. Along the basinward slope of the western platforms, in front of SMA, GA, and FB, a north-south oriented moat originate by the inflow of water masses through the eastern NKC (Fig. 5.1; Lüdmann *et al.*, 2013). The seismic data indicate that the branches of the western KC between the atolls were free of sediments and the currents delivered the carried sediments directly into the IS. Here, in the current shadow of GA a mounded contourite drift formed between the main channel axis of the SKC and NKC (Fig. 5.1). Attached to GA, the internal reflection of this mounded contourite drift terminate radially with downlap onto the underlying strata. During ds3 and ds5 the drift growth off the GA was probably dominantly steered by eddies that are originated by the current inflow around the atoll as described by Turnewitsch *et al.* (2013). Where shed eddies pass over seafloor areas downstream of an obstacle, here the atoll, the water mass is related to increased current flow speeds and increased variability of current directions, increasing the probability of non-deposition, erosion and/or resuspension of sediment. The variable deposition conditions resulted in multiple generations of small scale reflections with downlap terminations as well as wavy reflections (Fig. 4.7B and E). A similar depositional pattern, including multi-directional sediment waves, are observed by Haberkern *et al.* (2017) downstream of a topographic obstacle at the Galicia Margin. The eastern boundary is absent due to the transition into sheeted contourite drifts, which dominates the central IS and onlap the western slope of the eastern banks.

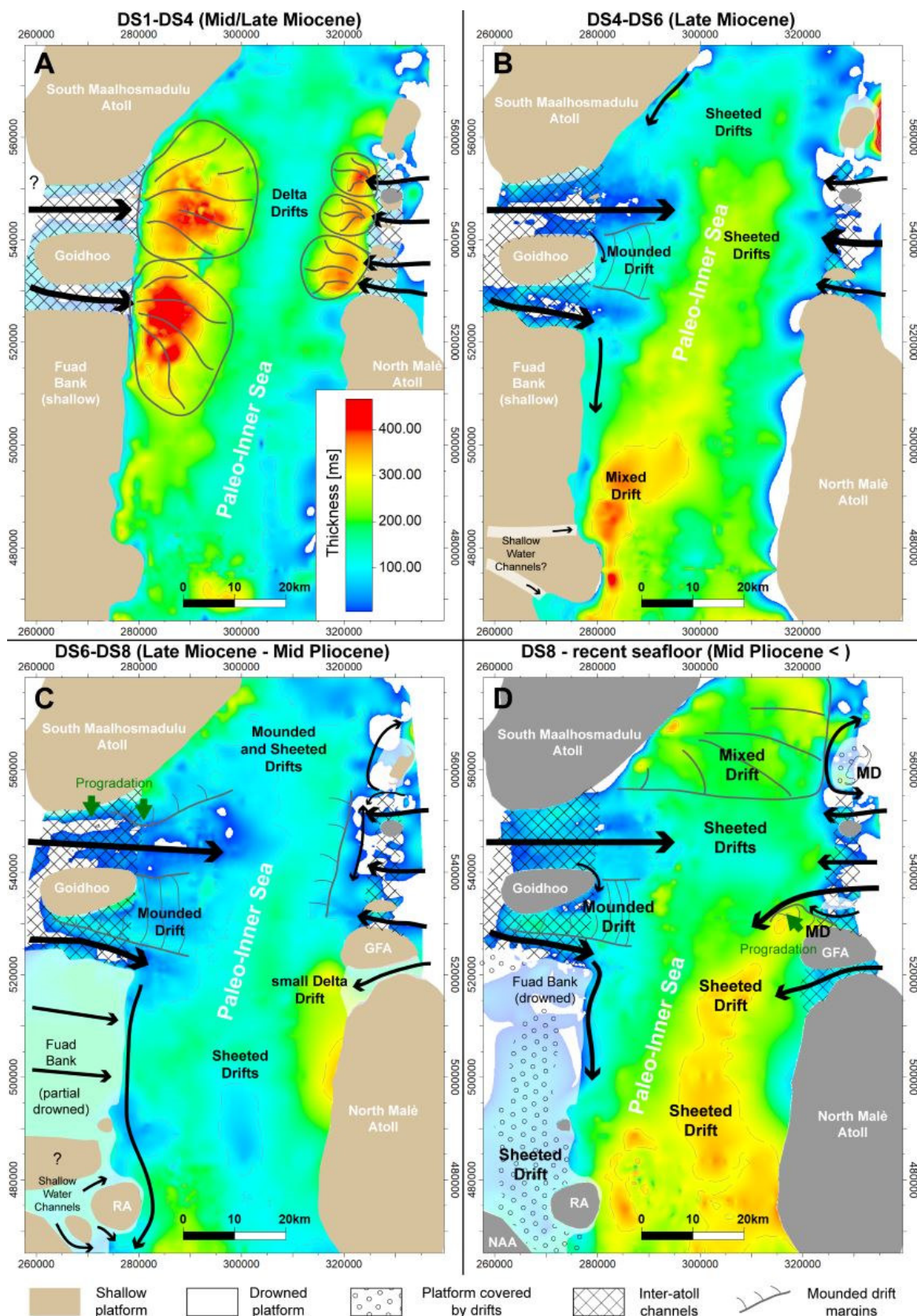


**Figure 5.1: A-D:** Thickness map of compiled sequences in milliseconds of TWT. Black arrows indicates bottom currents propelled by the monsoon activity. GFA=Gaafaru Falhu Atoll, MD=Mounded Drift, NAA=North Ari Atoll, RA=Rasdhoo Atoll.

A patch drift started to form adjacent to the northern delta drift in the western NKC during the Late Miocene (Fig. 5.2). The formation of the patch drift and adjacent scours are owed to a strong refocused bottom current activity that kept the main channel free of unconsolidated sediments and erode the top of the former deposited drift delta (Lüdmann *et al.*, 2018). The patch drift depocenter is located downstream next to the main channel axis behind a small-scale carbonate structure (Fig. 5.2), it represents an obstacle that facilitates the formation of eddies (Turnewitsch *et al.*, 2013). The obstacle reaches *ca* 195 m in height next to the scour, thereby focussing the present bottom current, as evident from the growth of the slightly mounded patch drift. Consequently, in this setting the control of the channel on the orientation and position of the carbonate mound was subdued to bottom current focussing. The depocenter in front of the eastern margin of the southern FB is related to a prograding pattern of an initial delta drift (Fig. 5.1), which is probably fed by shallow water channel system onto the platform. The MA is subdued to an unknown subsidence rate during this time. Data from the NMA-1 core point to a total subsidence of *ca* 1300 m since the Lower Miocene (Purdy and Bertram, 1993). The drowning lefts over relicts of reefs in the western NKC (Fig. 5.2), remnants of a small scale atoll chain southwards off the Kaashidhoo Atoll, and a drowned platform between the Kaashidhoo Atoll and the Faadhippolhu Atoll (Figs. 4.12, 4.13, and 5.1). The latter show different levels of terraces (Figs. 4.12 and 4.13). Generally, the formation of terraces is either steered by partially drowning and back-stepping of the platform or erosional activity by currents.

During the latest Miocene and Early Pliocene (DS6 to DS8) the drowning of the MA continued. As consequences the FB partially drowned as well as an inter-atoll channel opened and separated the Gaafaru Falhu Atoll from the North Malé Atoll. A sigmoidal prograding pattern of the sediments in front of the inter-atoll channel hints to a small-scale delta drift-like sigmoidal pattern, which accumulated during ds7 (Fig. 5.1). The main current channel of the western SKC slightly moved southwards and turned to WSW. With decreasing current velocity at the southern margin of the GA carbonate sediments were allowed to settle down and expanded the mounded contourite drift in the current shadow of the GA southwards (Fig. 4.6). A similar depositional pattern is found at the southern margin of the SMA, where the sediments prograded southwards into the channel (Fig. 5.1). The former moat structure along the eastern margin of the SMA got filled and the accumulation of carbonate sediments formed a mounded contourite drift along the western branch of the NKC. The transition in direction of the IS is characterized by a flatten relief of sheeted contourite drifts. The central IS were dominated by sheeted contourite drifts during this time period. A moat were formed between the Gaafaru Falhu Atoll and the drowned atoll north of the Kaashidhoo Atoll along the eastern margin of the IS, that is related to an increased inflow of bottom currents through the extended channel network in the MA. The FB is subdued to two drowning phases at least. The first is defined by backstepping of the northern margin contemporaneous with drift sequence boundary DS7 during Early Pliocene (Figs. 4.6 and 4.14). The following development of a shallow channel network between the atolls onto the FB cannot be unveiled in this sparsely

profiled area of the MA and got finally drowned during the second drowning phase during the Late Pliocene (ds8).

Since the Mid Pliocene notable amounts of carbonate sediments have been accumulated in the inter-atoll channels of the western NKC and SKC (Fig. 5.1). By implementing the IODP data of drillhole U1465 (Betzler *et al.*, 2017) the central NKC is covered with a 69.1 m thick layer of poorly lithified bioclastic sediment, dominated by grainstone texture. Intervals of very fine grained packstone are interspersed and rudstone intervals are locally present. The evidence of physical abrasion of some bioclasts and all lithoclasts is existent (Betzler *et al.*, 2017). Together with the occurrence of submarine dunes at the seafloor and the observed seismic reflection pattern SF-5 the sediments are assigned to a channel fill that are impacted by a bottom-current velocity of 0.5 to 1.0 m/s after the bedform-velocity matrix of Stow *et al.* (2009). The mounded contourite drift behind the GA has been continued its growth. A small moat formed along the contours of the GA as well as the northeastern part of the drowned FB. The moat disappeared in southern direction and the FB got covered with sheeted contourite drifts, which extend from the central IS onto the FB north of Rasdhoo Atoll. The northern FB is partly covered by sheeted drifts at the depressional areas of its former lagoon.

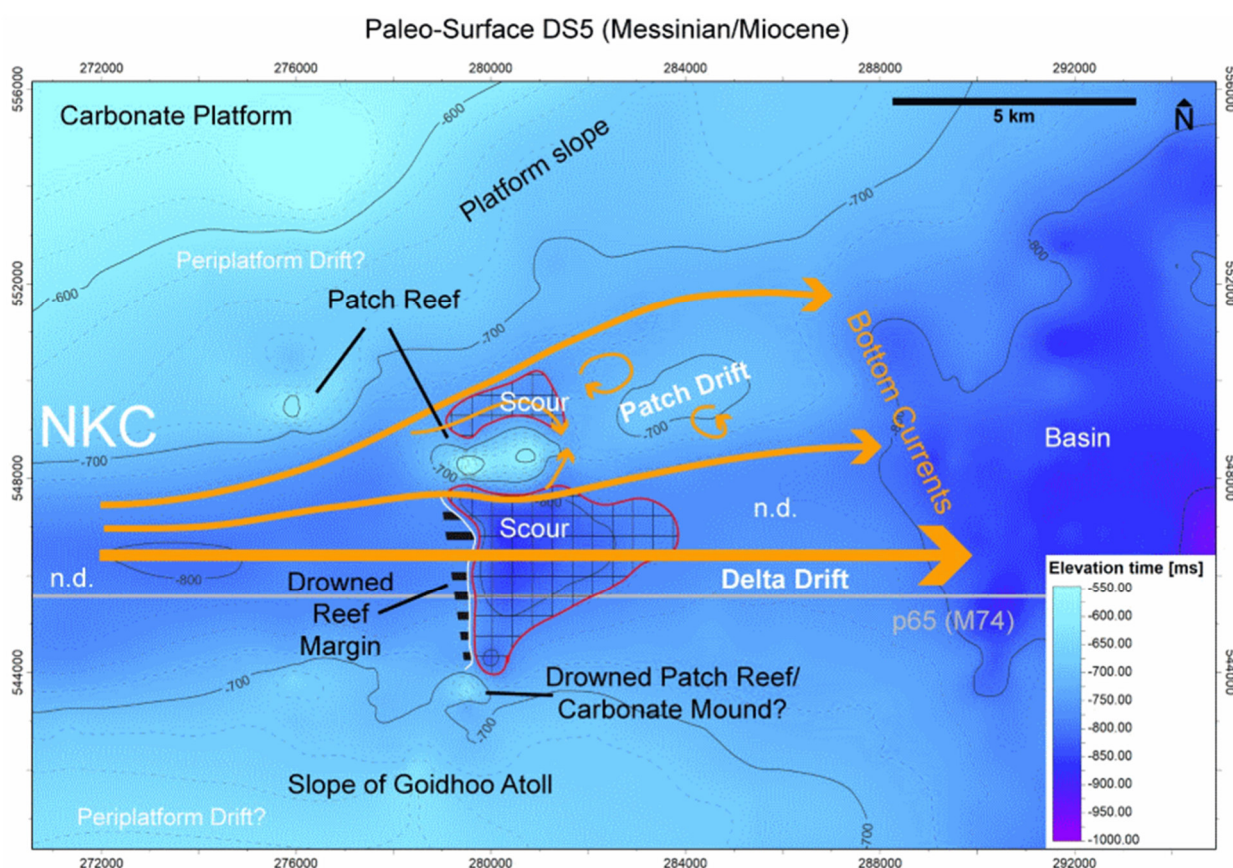


**Figure 5.2:** Paleo-Surface map of DS5 of the western branch of the NKC (see Fig. 5.3B for location). Several patch reefs and bathymetric highs are located in the NKC. The bottom currents are reoriented and accelerated by flowing around the patch reef. The increased current velocity results in development of scours. The area behind the obstacle are dominated by eddies and decelerated waters, where the patch drift is formed by depositional processes. n.d.=non deposition.

The recent bedform features of well-developed sediment wave fields on the seafloor in the western and eastern waterways are the result of different mechanisms. Different definable ocean currents interact with the topography of the MA (Lüdmann *et al.*, 2013). A simple mechanism is the development of subaqueous sand waves by a dominant strong unidirectional bottom-current flow with decreasing wave geometry near the edge of the wave field (Wynn and Stow, 2002), how it is realized in the inter-atoll channels. The observed diffraction pattern of the dunes on the northern basinward slope of GA and Gaafaru Falhu Atoll is probably a result of internal solitary waves. The internal solitary waves have the capability to develop bedforms by erosion, mobilizing and resettlement of sediments (Reeder *et al.*, 2011; Droghei *et al.*, 2016; Thran *et al.*, 2018). Velocity and temperature measurements show the layering of the water masses (Lüdmann *et al.*, 2013), where internal waves can be formed at their boundary. The small scale fields of star dunes (Fig. 4.8) are a result of eddy activity downstream due to interaction of the bottom current with obstacles, in the case of the MA carbonate features like patch reefs, similar to the observed multi-directional sediment waves downstream of topographic obstacles at the Galicia Margin (Haberker *et al.*, 2017). Furthermore, computational models demonstrate the strong influence of bottom currents and kinetic energy of eddies as well on the formation of contourite features (Thran *et al.*, 2018).

#### 5.1.1.2 Depositional model of the Kardiva Channel and adjacent areas of the Inner Sea

The evolution of the northern IS can be generally subdivided into three main stages since the Miocene. The first stage during the Middle Miocene is expressed by a pro- and aggrading platform growth of the western elongated mega platform with parallel discontinuous high amplitude reflections (Betzler *et al.*, 2016a). The platforms shed the produced material into the Inner Sea and formed slopes of periplatform deposits, which thinned towards the Inner Sea. The second stage is dominated by sigmoid clinoforms of the sediment filling the 'empty bucket' structure of the Inner Sea from west and the east by delta drifts (Lüdmann *et al.*, 2013, 2018). The accumulation of sediments in front of the western and the eastern platforms are fed by the opening inter-atoll channels. The basinward clinoform's geometry of the delta drifts is disturbed by collapse and pockmark-like structures, which are commonly spread across the IS (Betzler *et al.*, 2013). A seismostratigraphic correlation between the IODP sequences ages and the paleo-platform margins point to an increased subsidence rate since the Late Miocene (DS4 <). The expansion of the accommodation space and the extension of the inter-atoll channel facilitate the development of additional drift bodies due to increased complexity of the bottom current pattern. The basinward termination of the clinoform complex shows an aggrading pattern of sediment waves during the end of the second stage (Figs. 5.1 and 4.10). The top of the western contourite apron are eroded hinted by toplap terminations of the underlying sequences. These erosion surfaces define the start of the third stage. The transition into the third stage get together with the smoothing of the wavy reflections at the delta drift's toe-of-slope into parallel continuous reflections with low-to-medium amplitude in the seismic image. The accumulation of carbonate sediments increased in the current shadow of the basinward slopes of the newly established separated carbonate banks adjacent to

the east-west oriented channel axis during the Late Miocene. Drift accumulation, adjacent to the SMA and GA, leads to an external mound shape geometry with general low-to-medium amplitude reflectors which ends with downlap termination towards the KC channel axis. This geometry dominates the recent sedimentation pattern.

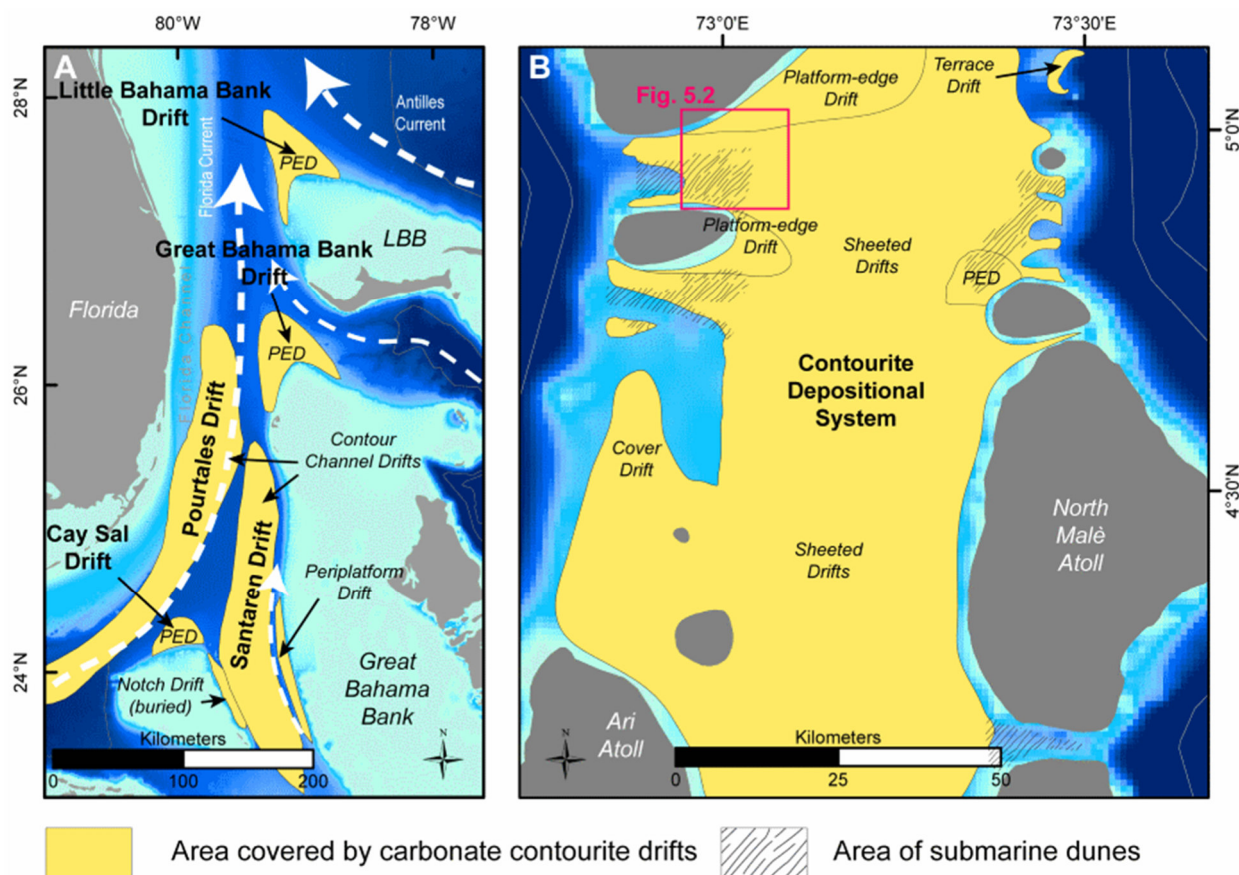


**Figure 5.3:** **A:** Map showing the locations of classified carbonate contourite drifts of the north-western Bahamian archipelago. The extension of the contourite drifts based on drawings of Bergman (2005). Little Bahama Drift's extension based on data of Principaud *et al.* (2018), Betzler *et al.* (2014) for the Periplatform Drift and own data for the buried drift **B:** Map showing the area that is covered by carbonate contourite drifts and current-related features of submarine dunes.

### 5.1.2 Bahamian contourite drifts

The seismic data of the SC reveal different contourite drift bodies, which had formed simultaneously during the Pliocene. After the establishing of sheeted contourite drifts in the Late Miocene two depocenters are formed by the activity of bottom currents. The first contourite drift is the north-south oriented mounded SD that covers the central part along the SC (Bergman, 2005), which has accumulated since the Middle Miocene. In the central and southern SC the seismic sequences exhibit a distinct up-doming which has affected the strata (Figs. 4.18 and 4.19). The bulge-shaped structure is dissected by closely spaced vertical faults of minor offset resulting in stacked wavy reflections indicating a vertical fault system by fluid velocity effects (Figs. 4.18 and 4.19). The second drift is attached to the eastern slope of the CSB probably accumulated in an embayment of the CSB during the Late Miocene. The embayment protects the sediment from the

main current channel and creates a low-energy environment, where the notch drift accumulates. Carbonate contourite drifts of different types are common in the deeper channels (> 150 m) of the BA (Fig. 5.3). The Pourtales Drift is related to the development of the Florida Current (Bergman, 2005). The GBBD and the LBBD and the northern part of the SD are formed by converging currents of the Florida Current and additional inflows from the (south-)east through the BA and the northern Antilles Current (Mulder *et al.*, 2019; Fig. 5.3A). The northeastern slope of the CSB is characterized by the Cay Sal Drift (Fig. 5.3A).

## 5.2 Concept and classification of carbonate contourite drifts

The occurrence of carbonate contourite drifts, proven by the aforementioned examples, has a need of classification and maybe simplification to enhance the recognition of further carbonate contourite drifts (CCDs) in seismic surveys or fossil carbonate contourite drifts exposed on land related to isolated carbonate platforms. The formation of CCDs are associated with additional processes of downslope and pelagic processes (Esentia *et al.*, 2018). The difference between siliciclastic contourite drifts and CCDs around isolated platform systems is the persistent availability of biogenic particles that are produced on the shallow platform carbonate factory. Especially the travelling distance between the origin where the sediment was created and where it was deposited, distinguishes siliciclastic from CCDs. Carbonate particles are usually deposited close to the source where they were originate, while siliciclastic components may travel hundreds of kilometers down river systems into the ocean before deposition. The locally deposition and supply contributes significantly to the heterogeneity of CCDs. The scale of carbonate contourite drifts of isolated platforms system ranges from 0.1 km<sup>2</sup> to > 10<sup>5</sup>. Additionally the drifts can be combined in carbonate contourite depositional systems (CDS), which fill a large part of the IS of the Maldives. The herein presented CCD occupy areas from the shallow water setting of platform lagoons to basinal areas between platforms of < 1000 m water depths.

Six fundamental types of CCDs could be defined, according to their depositional setting of isolated carbonate platforms. The CCDs are assigned to (drowned) platforms, inter-atoll channels, platform slopes, slope-to-basin areas, inter-atoll basins and to a general type of patch drifts that is related to obstacles from lagoonal areas down to basinal areas (Fig. 5.4). These various types are formed by different environmental impacts: the regime of the bottom-current flow, the bathymetric framework, and the sediment supply, which are mostly a mixture of platform originated and pelagic carbonate material. The lateral and vertical transition can be continuous between the drift types as well as an abrupt change is possible. The basin-related drifts and patch drifts, which are formed downcurrent behind smaller obstacles (such as carbonate mounds), are related to classical drift types, which are already recognized in siliciclastic systems (Rebesco *et al.*, 2014). Changing environmental conditions overtime can lead to a CDS by accumulation of a stacked pattern of different types of CCDs.

The depositional pattern of the channel- and basin-related drifts is subdued to processes that are persisting over time periods of 10<sup>6</sup> to 10<sup>7</sup> yrs and have an impact on areas of 1 to 10<sup>3</sup> km<sup>2</sup> in a water depth of 10<sup>2</sup> to 10<sup>3</sup> m, whereas inner-atoll CCDs are closely related to the evolution of the lagoons and subjected to variations of the sea-level (for example, glacial-interglacial cycles). These relative small-scale 0.01 to 10 km<sup>2</sup> contourite drifts are deposited onto the platforms in a water depth of 10 to 10<sup>2</sup> m. Their accommodation space is restricted by the sea-level and the platform's topography.

## 5.2.1 Drowned Platform Drifts

### 5.2.1.1 Terrace Drift

The terrace drift is associated to drowned platform terraces (Figs. 4.12 and 4.13). The accumulation of a terrace drift prerequisite a water depth below the sea surface level of the glacial maxima for establishing. The accumulated drift consists primarily of pelagic carbonate components due to the distance to active platforms. The pelagic settling are dominated by fine-grained sediments, which consists of pteropods, nanofossils and planktonic foraminifera in carbonate settings (Flügel, 2004). The wall base of the uppermost platform level stays free of unconsolidated sediments due to a current along the contour of the platform edge. The formation process of carbonate terraces are variable and can be associated to sea-level variations, especially phases of accelerated sea-level rise (Fürstenau *et al.*, 2010), and/or subsidence (Szabo and Moore, 1986). During the phases of high subsidence and rising sea-level some atolls cannot keep up in the well-lighted high production zone and the reef steps back and/or get starved and drowned. The drowned platforms provide new sedimentation room for current delivered pelagic particles, where the topmost reefal structure protects lower terraces from the current flow (Fig. 5.4).

### 5.2.1.2 Cover Drift

The cover drift refers to drowned platforms which lagoonal areas are filled and draped by drift sediments (Fig. 4.14). The internal reflections are horizontal layered and partly acoustically transparent, which indicates deposition by current action under a tabular flow with very low flow speeds. The elevated margins can stay free off sediments due to the action of bottom currents. By increased supply of carbonate material or/and decreasing strength of bottom flow activity the margin get covered and overlapped with slope- or basin-related drifts. The transition to basinal sheeted drifts are completed if the drowned platform get fully covered by obscuring of the former platform margin topography. The cover drift hints to a stable and simple current regime of a tabular and broad current.

## 5.2.2 Contour Channel Drift

The contour channel drift is assigned to broad inter-atoll channels, for example, the Santaren Channel (Figs. 4.17 to 4.19), where unidirectional and later bidirectional contour currents form the contour channel drift body (Bergman, 2005; Lüdmann *et al.*, 2016; Paulat *et al.*, 2018). The deposition geometry follows the slope of the adjacent platforms, where the moat is formed. The moat can show erosive or non-depositional to low-depositional features, this depends on the current speed and directivity of the current flow (Wunsch *et al.*, 2018; Paulat *et al.*, 2018).

### 5.2.3 Slope-related Drifts

#### 5.2.3.1 Periplatform Drift

Betzler *et al.* (2014) introduced the term 'periplatform drift' where ocean currents influenced strongly the sedimentation pattern of carbonate slopes. The periplatform drift primarily describe rather a strong impact on the carbonate slope depositional processes than a vast redistribution of carbonate sediments. The periplatform drift refers to a 'mixed drift' in siliciclastic systems, a term that general refers to the interaction of alongslope and downslope flow processes (Faugères and Stow, 2008; Esentia *et al.*, 2018). The term 'periplatform drift' is used to highlight the carbonate origin of the shed material, which consists of platform-derived material (Betzler *et al.*, 2014; Wunsch *et al.*, 2017). Prerequisites for the occurrence of periplatform drifts are (1) a strong alongslope current that influences the slope on a wide depth range and (2) a transport process to supply vast amount of calcareous sediments of the nearby shallow-water platform down the slope. The process is realized on the leeward GBB by the prevalent westward wind direction that propels the water masses on the platform westwards (Bergman *et al.*, 2010) and density cascading by density enriched waters of the inner-platform waters (Wilson and Roberts, 1995). The process is interrupted by sea-level lowstands when the platform is subaerial (Wunsch *et al.*, 2017). The periplatform drift can be occupied by further current-related features like cyclic steps, furrows and gravity steered features of scarps, gullies and large slope failures (Betzler *et al.*, 2014; Principaud *et al.*, 2016, Wunsch *et al.*, 2017). Chabaud *et al.* (2016) noted, that it could be difficult investigate the impact of currents on ancient (buried) periplatform slopes by seismic tools.

#### 5.2.3.2 Notch Drift

Notch drifts are related to bathymetric embayments of the platform geometry and a strong unidirectional main current flow and branching off flows. The contourite body thins out where the embayment of the platform terminates. A sediment-laden current release the carbonate particles due to the decreased current velocity. The detailed depositional processes remains speculative due to lack of seismic lines off CSB, where a plastered drift is revealed thought to be a part of a notch drift (Fig. 4.18). Similar notch drifts are recognized in the Great Australian Bight, where in-situ produced carbonate particles accumulates under the influence of a bottom current on the Australian shelf embayment (Anderskov *et al.*, 2010). The shelf slope is occupied by sediment waves that are developed by density cascading along the isobaths (Anderskov *et al.*, 2010). This phenomenon cannot be identified at the notch drift of CSB, where the prevalent wind direction of the Northeast Trade Winds ensure the (south-)eastern movement of the brine enriched water masses off the CSB and GBB (Kourafalou and Kang, 2012).

## 5.2.4 Slope-to-Basin Drifts

### 5.2.4.1 Platform-edge Drift

Platform-edge drifts are found in both investigated areas (Fig. 5.3A and B). They are developed downcurrent behind carbonate platforms by a straight uni-directional current or by two converging currents (Figs. 5.4 and 5.5). The term is established by Eberli and Betzler (2019). The uni-directional type are recognized as a 'mounded patch drift' southeast of Goidhoo Atoll by Betzler *et al.* (2013b). The classical term was used due to the recognition of the phenomenon of a drift behind an obstacle in the pathway of a current, here the GA. The sedimentary composition of the drift are not exclusively released by the sediment-laden current but also the active platform contribute huge amounts of carbonate particles for drift building. The type of converging currents are established in the BA northwest of the GBB and the LBB, where the drift is affected by the confluence of the north-flowing Florida Current and the northwestern flowing Antilles Current (Chabaud *et al.*, 2016). The Platform-edge drift of the GBB is formed by the Florida Current as well and currents, which are enters the inter-atoll channel system between the GBB and the LBB.

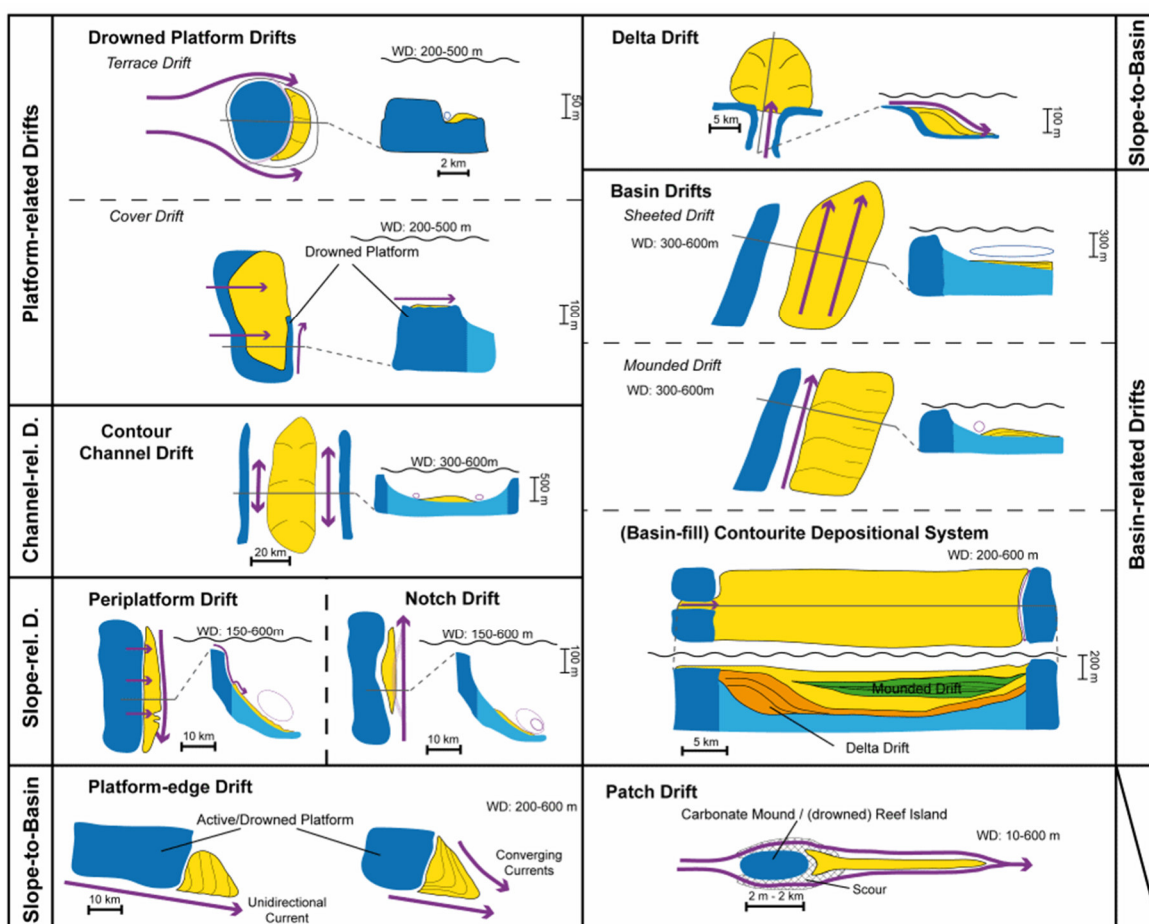


**Figure 5.4:** Overview of various carbonate contourite drift types (plan views and/or cross-sections) that are revealed by seismic datasets of isolated carbonate platforms. Different colours represent platform facies (dark blue), slope and basin facies (light blue), and drift facies (yellow) and for further subdivision (orange and green). The arrows indicate the dominant bottom current direction.

#### 5.2.4.2 Delta Drift

Lüdmann et al. (2018) give the description of two delta drifts in the Maldives. The discovering of smaller buried delta drifts in the eastern IS (Figs. 4.11 to 4.13, 5.1A and C) point to a more common occurrence of these types at isolated platform systems. The delta drift is related to inter-atoll channels and a basinward water flow that transport huge volume of planktonic microfossil assemblages as well as calcareous components, derived from the adjacent atolls, into the basin. By entering the basin the water depth expands and the water masses decelerate, which ensue an increased fallout of the carried components. The facies vary from coarse-grained, off the platform, to fine-grained in the distal areas of the delta drift (Lüdmann *et al.*, 2018; Fig. 2.6). The delta drift exhibits a sigmoidal geometry that results in a progradation pattern of clinoforms (Lüdmann *et al.*, 2018). The sediment lacks bedding and lamination structures due to intense bioturbation and shows grain size varies from coarse sand to fine carbonate debris (Lüdmann *et al.*, 2018). The carbonate facies ranges from fine-grained packstone and wackestone to locally coarser grainstone and rudstone (Reolid and Betzler, 2018; Reolid *et al.*, 2018). Several minor features are related to its formation: (1) the lower part of the prograding clinoforms can show cyclic steps, (2) the lobe of the delta drift can be intersected by minor radial-patterned channels, and (3) the apex can show structures of excavation related to the adjacent cemented drowned platform margin (Lüdmann *et al.*, 2018). The described prograding complexes by Belopolsky and Droxler (2004) yield the potential to be delta drifts similar to the newly discovered ones in the northern MA.

### 5.2.5 Basin Drifts

#### 5.2.5.1 Sheeted Drift

The sheeted drifts can occupy the basinal areas between carbonate platforms (Figs. 4.9 to 4.11, and 4.17 to 4.19). The boundary, if existent, show onlap or very-low-angle downlap terminations. The occurrence and formation of sheeted drifts point towards deposition under a simple and tabular, broad and regionally stable bottom-current flow regime (Stow et al., 2002a; Hernandez-Molina *et al.*, 2008a), as well as giant eddy circulation (Esentia *et al.*, 2018). The overall geometry is steered by a consistent sedimentation rate throughout the area. The sediment consists of light grey to brownish planktonic foraminifer-rich, fine- to medium-grained packstone to wackestone (Betzler *et al.*, 2017). Local variations are common, grainstone facies occur in the sheeted drifts at Site U1468 in the MA (Reolid and Betzler, 2018). Whereas the initial sheeted drifts in the BA consists of silt- to fine sand-sized planktonic and benthic foraminifera with occasional occurrences of firm grounds (Eberli *et al.*, 1997). Overall bioturbation is pervasive (Eberli *et al.*, 1997, Betzler *et al.*, 2017) and thus results in homogenized facies (Reolid and Betzler, 2018).

#### 5.2.5.2 Mounded Drift

The mounded drift has a center of deposition and decreases in thickness towards the margins (Fig. 5.4). The depo-center is located, where the sediment-laden bottom-current flow decreases

under a certain threshold, which allowed the settling of the transported components. Typical termination forms are downlaps with steeper angles towards the current flow axis. The force of slope-parallel bottom currents mostly elongates the overall geometry. The moat the mounded drift can be of erosive or non-erosive character right up to minor amounts deposition of coarser grained material. The contourite drift is formed by helicoidal current flows along the toe-of-slope (Hernández-Molina *et al.*, 2008b). The sediment consists of silt- to fine sand-sized planktonic and minor benthic foraminifera (Eberli *et al.*, 1997). The spatial-varying grain size distribution across the contourite drift is existent. Seafloor sampling across SD shows a fining in grain size basinwards off the moat channel (Wunsch *et al.*, 2017).

### 5.2.6 Contourite Depositional System (CDS)

The CDS is a term for the lateral and temporal variability and connectivity of processes associated with contourite systems (Rebesco *et al.*, 2014). It regards to an association of various contourite drift types and their related erosional features that have been formed by relatively long-persistent action (several millions of years) of bottom currents (Stow *et al.*, 2002a; Rebesco, 2005; Hernández-Molina *et al.*, 2008b; Esentia *et al.*, 2018). The term CDS contains vertical and spatial variation in time of the dominating bottom-current flows (Hernández-Molina *et al.*, 2016) and delivery mechanisms for the calcareous components, which results in stacks or interleaving of different contourite drift types on different scales. The presented data of the basin-fill of the paleo-IS fulfil the certain criteria of the CDS. The basin-fill sediments of the IS contains different bodies of drift types, for example, delta drifts, mounded drifts, and sheeted drifts (Figs. 4.9 and 4.10). Therefore, varieties of oceanographic processes are responsible for deposition of these contourite drift types.

### 5.2.7 Patch Drifts

Patch drifts occupy a wide range of water depth, as well as accumulation rates. The occurrence are associated with obstacles in the direction of the current flow. These obstacles can be pinnacle reefs on the platform interior (Fig. 4.15) as well as carbonate mounds or drowned patch reefs in intra-atoll channels (Fig. 4.4) and basinal areas. Patch drifts encompass varies of geometries and can be precursor of larger scale contourite drifts (Esentia *et al.*, 2018) Scours beside or around the obstacle are common due to locally current acceleration and redirection of the flow. Moats are common in the lagoon on the platforms around islands (Kench *et al.*, 2005). Their development are steered by seasonal beach changes, where uncemented deposits can be reworked by monsoon-induced currents above a cemented paleoreef surface (Kench *et al.*, 2005; Kench and Brander, 2006).



**Figure 5.5:** Compilation sketch of different contourite drift types and related features around isolated carbonate platforms.

### 5.3 Examples of Carbonate Contourite Drifts in the sedimentary record

Some examples of fossil CCDs are known and an incomplete compilation were presented in Hüneke and Stow (2008). The highlighted contourite drifts encompasses the Ordovician Jiuxi Drift in China (Duan *et al.*, 1993), parts of the Paleogene Lefkara Formation of Cyprus, the Neogene Misaki Formation in Japan, Devonian current-reworked deposits of Gondwana and Laurussia (Hüneke, 2006, 2007), and the Late Cretaceous–Palaeocene Chalk Group in the Danish Basin (Surlyk and Lykke-Andersen, 2007, Esmerode *et al.*, 2007). Their sedimentary composition is dominated by pelagic biogenic particles, but with noticeable amounts of siliciclastic (Lefkara Formation) and volcanoclastic (Misaki Formation) components.

The Chalk Group show a high CaCO<sub>3</sub> content due to its structure made of coccolith biomicrite. Its genesis and composition differs from the CCDs around isolated carbonate platforms with high amount of clayey grain sizes of *ca* 90% to 95% (Surlyk and Lykke-Andersen, 2007). However they show a series of contourite-related features such as moats, sediment wave fields, and elongate mounded and sheeted contourite drifts (Surlyk and Lykke-Andersen, 2007, Esmerode *et al.*, 2007, Hüneke and Stow, 2008) and their depositional depth of 300 to 800 m fits to depositional depth of slope- and basin-related CCDs of isolated platforms and its geomorphology is similar to a mounded drift (Fig. 5.4). The threshold for mobilizing coccolith ooze is thought to be lower with 8 to 20 cm/s for non-deposition and erosion (Surlyk and Lykke-Andersen, 2007) than for modern platform drifts with coarser grain sizes, where most of the structures observed were probably formed under current speeds in the range of 10 to 15 cm/s.

The identified elongate mounded Jiuxi Drift extend over 120 km along the lower paleocontinental margin of the middle Yangtze Terrane, southern China, (Duan *et al.*, 1993) fits to the herein presented drift type of a basin-related mounded drift (Fig. 5.4). It is located on a mid to base-of-slope of a continental setting, which margin is occupied by carbonate platforms (Duan *et al.*, 1993). The lithological composition differs from the contourite drifts of isolated platforms. The composition is more variable with five identified facies and dominant grain size ranges from sand to mud with an average sedimentation rate up to 3.5 cm/ka (Duan *et al.*, 1993). Fining and coarsening upward sequences can be identified in intervals between 10 cm and 200 cm due to varying bottom current velocities (Duan *et al.*, 1993). The intense bioturbation through the drift body and the deposition depth of 350 to 450 m (Duan *et al.*, 1993) fits the characteristics identified for mounded drifts of the MA and BA. The Pingliang contourite drift is located along the western slope of the Ordos Platform during the Middle Ordovician (Luo *et al.*, 2002). The contourite drift has a length of 70 km and is associated to a gateway between two deep-water basins and water depth > 1000 m. The accumulation rate were low with up to 1.5 cm/ka (Luo *et al.*, 2002).

The upper parts of the Lefkara Formation and its current-reworked sediment facies are associated to a carbonate slope-apron system, which are affected by alongslope currents and turbidites (Stow *et al.*, 2002b). Low sedimentation rates of < 1 cm/ka are described, due to the sparsely documented overall geomorphology, this type cannot be associated to a carbonate contourite drift.

The Cretaceous Talme Yafe Formation is located at the northwest continental margin of the Arabian Craton. It consists of carbonate biochemical components that originated on the shelf and skeletal fragments derived from the rudistid reefs on the platforms (Bein and Weiler, 1976). It is thought that the contourite drift is generated by along-shore currents (Bein and Weiler, 1976) or by converging current of the lee-side of a platform (Mullins *et al.*, 1980). The thickness and drift geometry could be also assigned to a delta drift if a feeder channel were present perpendicular to the coastline, where a sediment-laden current can enter the basin. By decelerating the sediment shed off the current and form a delta drift.

A research cruise targeted the Marion Plateau, offshore from northeastern Australia (Isern *et al.*, 2002). The seismic lines reveal that the depositional environment has been affected by bottom currents since the Late Miocene (Eberli *et al.*, 2010). Contourite drift bodies are identified due to mounded seismic units, which terminate with downlaps onto the underlying strata. Furthermore erosional features, for example, moats, truncated reflections, are imaged in the seismic data (Fig. 5.6). The moat is located in front of the drowned carbonate platform of the Northern Marion Plateau. The basement of the moat is stabilized by current-swept phosphatic hardgrounds (Glenn and Kronen, 1993). Reduced sedimentation on carbonate contourite drifts leads to early marine cementation and hardened surfaces (Eberli and Betzler, 2019). The sediments of the drift consist of undolomitized silt-size to medium-grained packstones with widely varying mud content and less common fine- to medium-grained grainstones (Ehrenberg *et al.*, 2006). The existent drift bodies can be assigned to drift types of a mounded basin drift, sheeted drift and a cover drift overlying the North Marion Platform (Fig. 5.6).

Drift features on drowned platform terraces are revealed in the bathymetric dataset of steep isolated carbonate platforms in the southern Mozambique Channel (Courgeon *et al.*, 2016). The terrace development of the Bassas da India Atoll is a result of a major backstepping phase (Courgeon *et al.*, 2016), which provide the accommodation space for the formation of terrace drifts and probably periplatform drifts (Fig. 5.7). The bottom currents form asymmetric sediment waves that point to the presumable prevalent southwestern directivity of the bottom current activity (Fig. 5.7).

## Contourite Depositional System, Marion Plateau, Australia

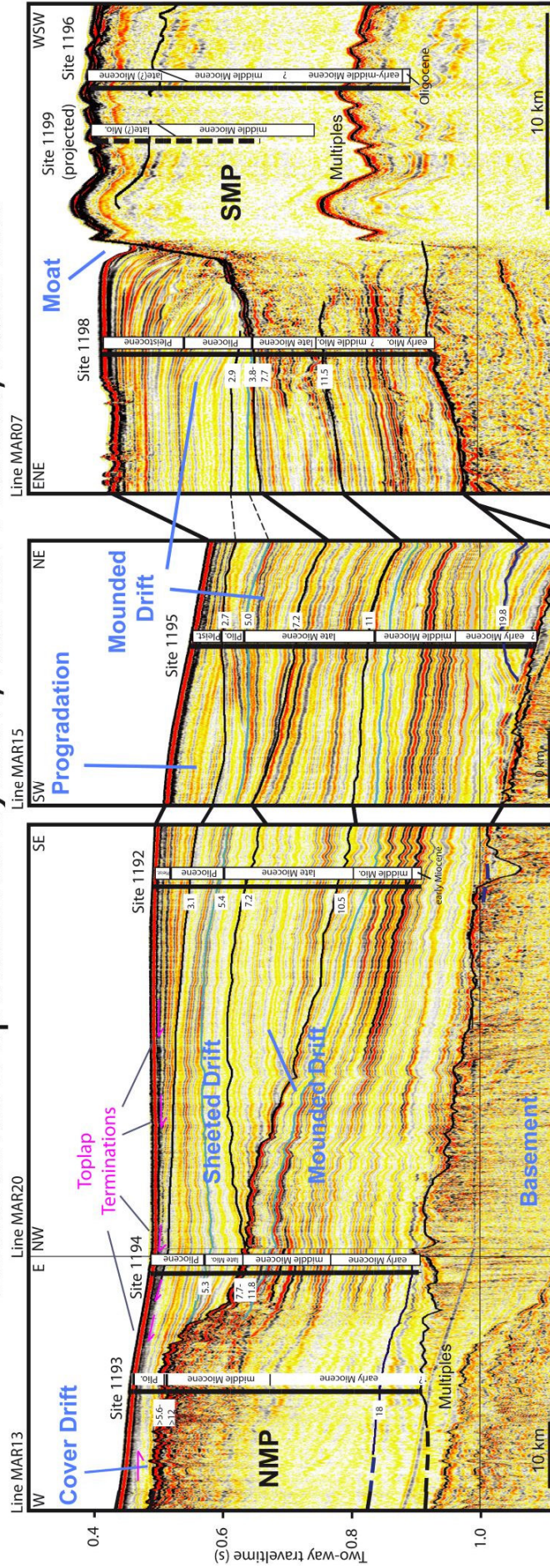


**Figure 5.6:** Seismic lines of the Pre-Site-survey and locations of ODP Leg 194 sites. Carbonate contourite drift types and features are marked. The various drift types has been formed a contourite depositional system since the Miocene. Ages are based on shipboard models. Black lines separate the seismic units. The figure is adapted and modified from Isern *et al.* (2002).

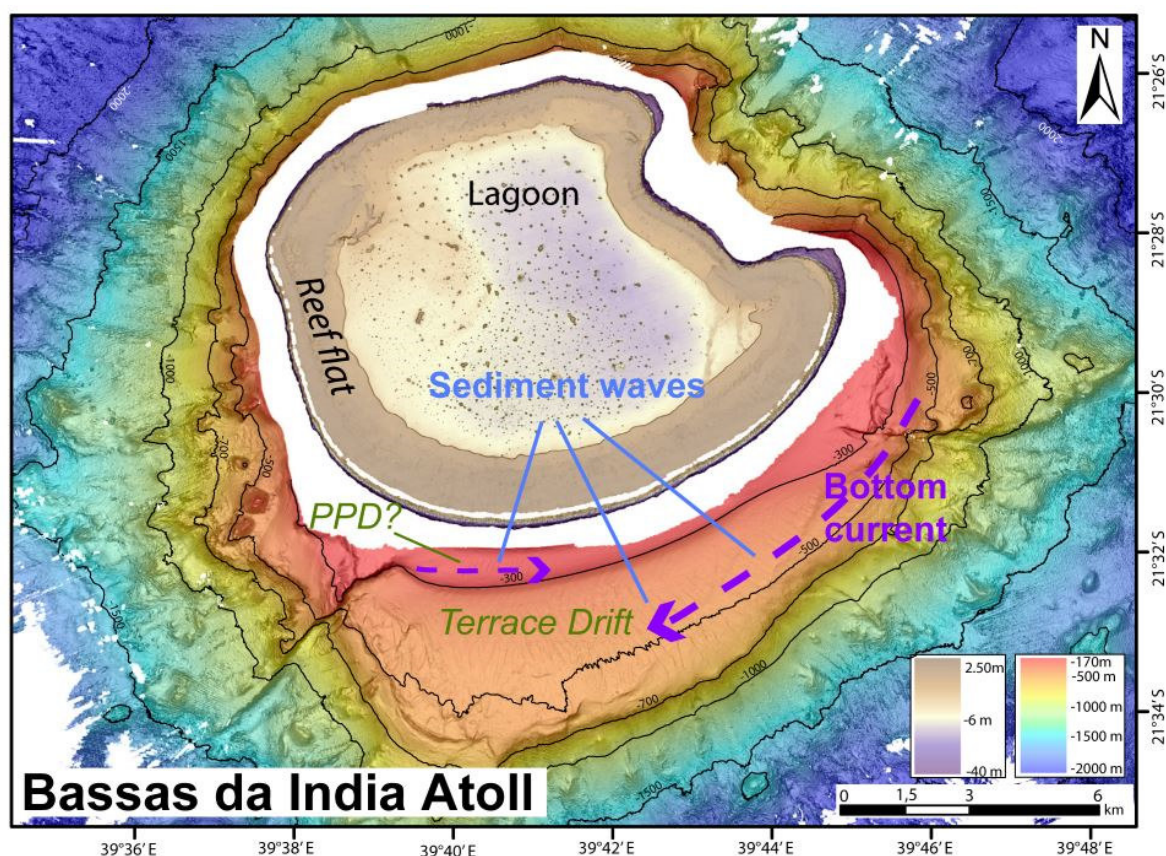


**Figure 5.7:** Geomorphology of the Bassas da India Atoll (modified from Courgeon *et al.*, 2016). The terrace and parts of the slope are occupied by sediment waves that indicates strong bottom current influence at a depth between 200 and 500 m in the Mozambique Channel. White areas show bathymetric data gaps. PPD=periplatform drift.

Latest research reveal CCD deposits in Italy (Eberli *et al.*, 2019; Slooman *et al.*, 2019). Calcareous bioclastic wedges of the Orfento Formation in the Montagna della Maiella were interpreted as a carbonate delta drift, which accumulated during the Upper Cretaceous (Campanian-Maastrichtian) (Eberli *et al.*, 2019). The sedimentary texture consists of grainstone and rudstone in general, but it also show varieties from wackestone to float-rudstones (Eberli *et al.*, 2019). The grainstones generally are moderately bioturbated and the depositional environment is associated to a water depth of tens to a couple of hundred meters (Eberli *et al.*, 2019). Shallow water clinofomed carbonate wedges were developed during the Lower Pleistocene in front of Favignana Island (Italy) in a shallow-marine channel between two topographic highs (Slooman *et al.*, 2019). Their facies are assigned to short lasting (hours to days) subcritical and supercritical turbidity current events, where the carbonate particles deposited in shallow waters in water depths up to 50 m on a cool-water carbonate ramp (Slooman *et al.*, 2019). The development of the carbonate wedges is related to storm-induced currents and tsunamis (Slooman *et al.*, 2019) and do not fit into the classification for long-term accumulated CCDs.

## 5.4 Reconstruction of paleo-currents affecting the Santaren Drift (Bahamas) and its significance for the global current pattern

Utilizing a seismic grid dissecting the contourite drift, the spatial and temporal evolution of the SD can be reconstructed. Using the variable depositional geometries within the contourite drift body and the shape of the moats and lower slopes of the adjacent carbonate platforms, the impact of accelerated water masses in this channel in the past and its correlation with changing platform and slope geometry is revealed.

### 5.4.1 Factors controlling contourite architecture

The architecture of contour channel drifts is mainly controlled by the bathymetric-topographic framework, the current volume, velocity structure, rheology, stratification, the amount and type of sediment available, and the temporal continuity of bottom current processes (Thran *et al.*, 2018; Cossu *et al.*, 2015; Peakall *et al.*, 2011; Faugères *et al.*, 1999). The current direction is steered by the pressure gradient and influenced by the Coriolis force, which vary over time and latitude (Cossu *et al.*, 2015; Peakall *et al.*, 2011). The long-term change in the aforementioned factors are preserved in the SD architecture. The velocity field of bottom currents define the width of the moats and the steepness of its flanks, whereas the volume of the contourite drift is a consequence primarily of the sediment flux. Although the Bahamian region has experience complex diastrophism, the study area is considered to have been relatively stable during the post-orogenic phase of the Cuban Orogen (Cruz-Orosa *et al.*, 2012), with minor modifications concerning anticlinal structures (Kula, 2014; Masferro *et al.*, 1999) and the preserved tectonic features of deep rooted faults at the slope of CSB and the slightly uplifting processes with bulged-shape reflections associated with vertical faults affecting the SD. The deep-rooted fault system interleaved the north-south trending lower slope of the CSB, which steepens in southern direction, increasing from  $0.6^\circ$  at the northwestern SC (Fig. 4.17) to  $1.6^\circ$  at the southwestern SC (Fig. 4.19). The upper and lower terminations of the bulge dissecting vertical faults are defined by decreasing offsets within the contourite sediments, and the faults can be traced for 150 to 200 m in the vertical direction (Fig. 4.18), comprising sequence S12 to S7 and placing them in the Lower Pliocene (4.2 Ma). Their close standing alignment are typical for polygonal faults (Gay *et al.*, 2004). The tectonic overprint is probably responsible for the diachronic occurrence of the western moat.

During contourite drift accumulation, the bottom current pattern in the SC is proposed to be comparable with the present day situation, as described by Lüdmann *et al.* (2016), with a northward flow off GBB and a southward flow off CSB. Within this context, the geometry of the moats created by the bottom current reflects changes in flow intensity and volume. Smaller moats with higher relief may express stronger and more focused currents and vice versa. After Faugères and Stow

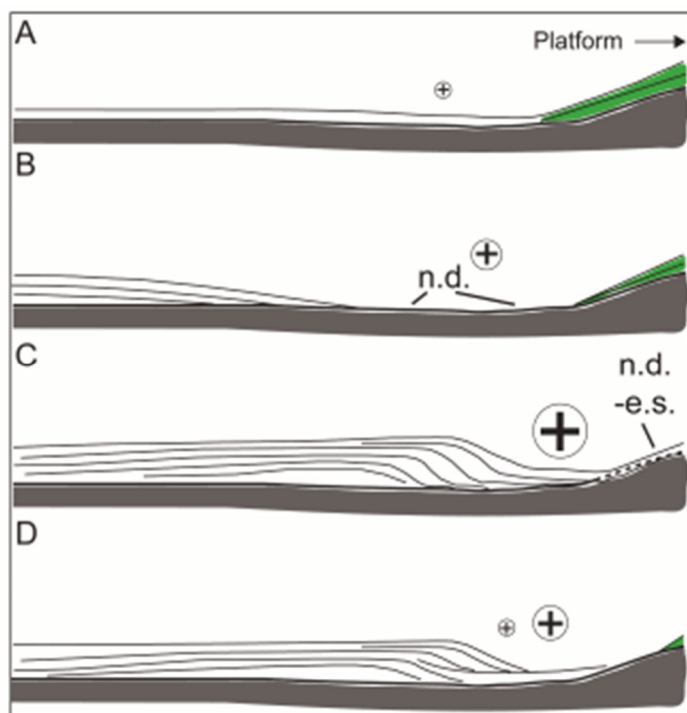


**Figure 5.8:** Moat geometries and sedimentary processes according to the modifications of the sea floor morphology and variations of the bottom-current velocity modified after Faugères and Stow (2008). **A:** Low-velocity current; drift sediments are draped onto the former sea floor. The impact of the adjacent carbonate platforms is expressed by occurrence of periplatform deposits (green). **B:** Medium to high current velocity; deposition with slightly downlapping reflectors resulting in a low mounded relief of the contourite drift (n.d.=non-deposition). **C:** High current velocity concentrated in the channel. Mounded relief is developed, and the moat migrates upslope. Deposits of periplatform sediments are prevented (n.d., non-deposition; e.s., erosion surface). **D:** Alternating current velocities results in onlapping and downlapping contourite drift deposits.

(2008) low-velocity current results in draping deposits (Fig. 5.8A), medium to high current velocity results in deposition with gently downlapping reflectors and an infancy mounded-drift relief (Fig. 5.8B). High velocity currents are concentrated at the moat with a well-developed mounded contourite drift relief and oblique to sigmoid deposits (Fig. 5.8C). If the current velocity is fluctuating, the moat is filled by alternating downlapping and onlapping deposits (Fig. 5.8D). Additionally, broader moats indicate an increased flow cross-section or meandering flows. In general, a stronger current is subjected to an increasing Coriolis force that deflects a northward flowing water mass to the right in the northern hemisphere (Talley *et al.*, 2011). Sediment accumulation rates within the contourite drifts are thought to be mainly driven by carbonate production in the SC water column and on the adjacent platforms, as the siliciclastic content of the sediments is negligible (see chapter 2.3).

#### 5.4.2 Reading the contourite drift architecture

Today's contourite drift sedimentation in the SC is the result of water mass flow triggered by the Gulf Stream system as part of North Atlantic circulation (Lüdmann *et al.*, 2016). By using the contourite drift architecture and depositional stages, the hydrodynamic regime in the SC and the adjacent Florida Current is divided into four evolutionary phases, tracking back its action to its origin in the Middle Miocene and discriminating the initiation and significant changes in current flow intensity in the context of major global oceanic events.

#### 5.4.2.1 Phase 1: Initiation of bottom-current flow (Serravallian to Tortonian)

The start of relocation of sediments by bottom current activity within the SC in the form of contourite drifts is indicated by packages of continuous reflections overlying hemipelagic sediments (Fig. 4.17). These first indications of moat building by bottom current action seen in the data are limited to the northern exit of the SC (Fig. 4.20A). Seismic profiles in the south show neither moat development nor current-deposit-related terminations in seismic reflections, and they are highly influenced by tectonic activity in the southern SC off CSB that disguises current-related features from the Late Miocene (Fig. 4.19). Sediment supply from the bank-tops was generally high, with a local depocenter at the northeastern CSB (Fig. 4.20A). Uranium content and P-wave velocity as well as potassium and thorium decrease from the bottom to the top of the sheeted contourite drift sequences S12 to S9 (Fig. 3.10). Both, organic matter and siliciclastic clay diminish probably as a consequence of an ongoing intensification of the bottom current during the time interval, coeval with lowered uranium, potassium and thorium contents of the deposited material.

The onset of contourite drift sedimentation at *ca* 12.3 Ma, deduced from the first appearance of a moat channel at the northern conjunction to the Florida Straits and sheeted contourite drifts in the central SC (Fig. 4.20A), that corresponds with the initiation and/or intensification of the Loop Current flow about 12 to 15 Ma (Mullins *et al.*, 1988) probably forced by multiple triggers including (Fig. 5.9): (1) the late Middle Miocene climate transition; (2) the opening of ocean gateways in the Antilles (Pindell and Kennen, 2009); (3) the foundering of the Northern Nicaragua Rise megabank (Mutti *et al.* 2005); and (4) the beginning closure of the CAS (Coates and Stallard, 2013). Another important factor that influenced the Loop Current flow was the stabilization of the East Antarctic Ice Sheet (Verducci *et al.*, 2007), which facilitated the modern Antarctic Circumpolar Current (Livermore *et al.*, 2007), and a modern Atlantic Ocean current system. Additionally, the overflow of Northern Component Water at the Greenland-Scotland Ridge during the Middle Miocene (12 Ma) was an important event that changed the interoceanic current system (Poore *et al.*, 2006) and initiated the contourite drift accumulation at the North Atlantic (Knutz, 2008).

Evidences in the SD of a Late Miocene uplift of the Greater Antilles islands Cuba and Hispaniola (de Zoeten and Mann, 1991, Iturralde-Vinent and MacPhee, 1999, Mann, 1999) are probably provided by gamma ray logs from ODP borehole 1006A. The logs show slightly increasing potassium and thorium values, which indicate mostly terrestrial origin components in this carbonate setting (Fig. 3.10). Source of the terrestrial components which are transported via the OBC into the SC are most likely the Greater Antilles. The OBC trough flow must have been significantly enhanced owing to the Greater Antilles uplift and the closing of the deep water Havana-Matanzas Channel (Iturralde-Vinent *et al.*, 1996; Iturralde-Vinent and MacPhee, 1999; Matos-Maraví *et al.* 2014) (Figs. 1.2A and 5.9). The closing restricted water exchange between the Caribbean basin and the Gulf of Mexico, promoted the path along the Antilles for the Caribbean current system until the Northern Nicaraguan Rise had drowned.

Another key event was the beginning closure of the CAS (Coates and Stallard, 2013) that successively reduced the water mass exchange between the Pacific and Atlantic oceans. Consequently, ocean currents had to reorganize their path through the Caribbean Basin and were deflected to the north. There exist different timing scenarios for this event including the assumption of Montes *et al.* (2015) of a Middle Miocene (13 to 15 Ma) complete CAS closure. The resulting total blocking of the Atlantic water outflow should have contributed to an enhancement of the water volume and possibly also its velocity in the Loop Current significantly altering the hydrodynamic regime in the Bahamian waterways. This scenario is not supported by the study's data, which lacks any abrupt change in sedimentation pattern during this time interval. The interpretation of the current dataset favors a successive shallowing of the seaway that first hinders the deep water circulation and finally cuts off the surface water exchange between both oceans. A rough estimation of the former sill depth of the CAS reached values shallower than 850 m. Based on the current study's seismic data the paleo-depth in the SC at 12.3 Ma was *ca* 850 m. Under the assumption that contourite drift sedimentation in the SC was among other factors mainly triggered by CAS shallowing, then at 12.3 Ma the swell started to hinder the exchange of intermediate water above 850 m. This water mass was then instead pushed through the Bahamian realm and accounted for the onset and ongoing contourite drift sedimentation.

#### 5.4.2.2 Phase 2: From sheeted to mounded contourite drifts (Tortonian to Messinian)

First sporadic downlap terminations within the seismic data are found in S9 that indicate bottom-current induced moat structures (Fig. 4.18). This hints to a northward directed sporadic focused bottom current along the 'toe of slope' of the GBB (Fig. 4.20B) with weak to medium velocities (Fig. 5.8A and B). First evidence of a stronger impact by stable current activity in the entire SC are found for the Late Miocene (S8, 8.4 to 5.5 Ma). Seismic profiles illustrate the formation of downlapping terminations on underlying layers and the basinward thickening of sediment layers, which reflects the effect of bottom currents forcing the creation of a moat system at the 'toe of slope' of the GBB (Figs. 4.17 to 4.19). Here, it formed a wide depression with a flat relief created by a northward current which indicates a still relatively low bottom current intensity (Fig. 5.8A and B) along the entire channel. A distinct change in bottom current dynamics at the end of phase 2 is reflected by the upslope migration of the moats as the result of an increasing intensification of bottom-current velocity and stronger current deflection by the Coriolis force, which induced a positive lateral velocity gradient towards the slope.

In the southern SC (Figs. 4.19) the transition of hemipelagic to sheeted drift facies becomes indistinct and is not definable during that time interval. The process to pile up a local depocenter of current reworked sediments off CSB is assigned to the development of a notch drift (Figs. 4.18

and 4.20C). Overall this phase is characterized by a gradual transition from sheeted to elongated mounded drift geometry flanked by a broad shallow-relief moat off the GBB that points to a steady strengthening of the current flow of the northward flowing water mass (Fig. 5.9). The main driver is assumed to be the gradual CAS shallowing that gradually restricted the water mass exchange between the Atlantic and Pacific oceans and enhanced the Loop Current intensity.

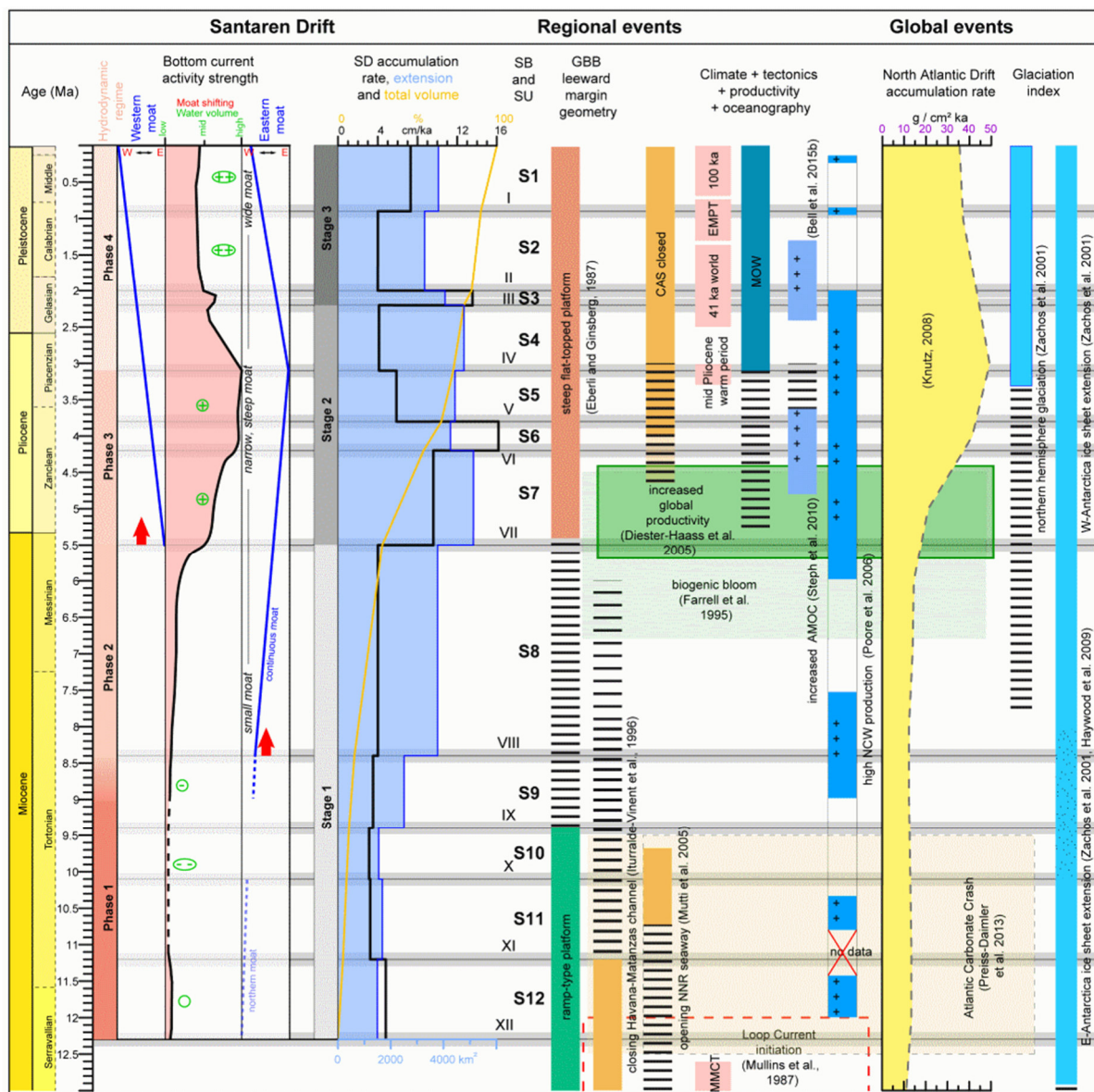


**Figure 5.9:** Santaren Drift facts are compared with major events affecting Atlantic Ocean current circulation and global climate. ++ in columns indicate activity peaks. EMPT, Early Middle Pleistocene transition; MMCT, Middle Miocene climate transition; MOW, Mediterranean Outflow Water; SB, Sequence boundary; SU, Sequence.

### 5.4.2.3 Phase 3: Contourite drift growth (Messinian to Piacenzian)

Phase 3 is marked by a significant increase in current strength in the SC expressed by two major changes in moat architecture (Fig. 5.9). Firstly, the moat in the northern SC off GBB suddenly narrowed with steep flanks at 5.5 Ma (Fig. 4.17). However, to the south its relief flattens which is related to a northward flow acceleration within the conduit (Figs. 4.18 and 4.19). Additionally, the

eastern moat started to migrate 3 to 7 km eastwards supported by the stronger Coriolis force caused by an increase in current speed (Figs. 4.17 to 4.19). Secondly, at about 5.4 Ma, a moat structure appears for the first time in the western part of the SC attributed to the onset of a counter-current off CSB (Figs. 4.17 and 4.20C). It is a distributary of the Florida Current that probably starts to enter the SC from the north, when the Florida Current speed reached a certain threshold. This current intensified through time indicated by a steady upslope migration of the moat (deflection to the west) and a temporal southward progradation of moat initiation from north to south at 5.4 and 3.8 Ma, respectively (Figs. 4.18 and 4.19).

The beginning of phase 3 at 5.5 Ma, the Miocene-Pliocene boundary, marks also a turning point in SD accumulation rates and extension of the contourite drift that significantly increased (Fig. 5.9). It is coincident with a peak of quartz content in ODP core 1006A by drifted material (VII, Fig. 3.10). This rapid contourite drift growing phase lasted 2.4 Ma and comprises drift sequences S7 to S4 (Fig. 5.9). Contemporaneously, the periplatform sediments significantly retreated at the eastern margin of the GBB in S7 to S4 (Figs. 4.17 to 4.19). In addition, the stronger bottom-current velocity along the GBB margin prevented slope sedimentation in the Early Pliocene and forced the sediment to deposit more towards the basin, where the bottom-current velocity gradually lowered (Fig. 4.20D). All east-west trending profiles show a drop in sedimentation rate within the eastern moat axis right up to areas of erosion at the GBB slope during that time (Fig. 4.20D and E). The stronger bottom current activity is probably also responsible for a change in slope geometry of GBB reflected by the transition of a ramp-type platform to a steep-margin type documented by Eberli and Ginsburg (1987). In combination with increased sedimentation rates on the GBB slope, hindered sedimentation at the toe of slope by aforementioned bottom currents and aggrading platform conditions the platform flank steepens. Off CSB a giant mass transport deposit was emplaced in sequence S5 and filling the moat depression triggering a moat jump towards the center of the SC; however, did not affect its general westward migration (Fig. 4.17). The western slope sedimentation pattern hints at a stable lateral splitting contour current with multiple arms affecting the sedimentation process (Figs. 4.18 and 4.20D) similar to modern twofold currents at the western SC (Lüdmann *et al.*, 2016).

Phase 3 was probably initiated by the significant increase in Northern Component Water (NCW) overflow at 6 Ma, determined by Poore *et al.* (2006). The strengthening of bottom currents in the North Atlantic Ocean is documented by increased sedimentation rates of the North Atlantic drifts (Knutz, 2008; Fig. 5.9), which indicates ventilation of the North Atlantic Deep Water. The NCW overflow lasted 4 Myr and led to an enhanced water mass exchange between the North and South Atlantic Ocean that intensified the Gulf Stream and increased the inflow in the SC through the Nicholas Channel and/or the OBC as well as through the Florida Straits. At 4.2 Ma, with the deposition of sequence S6, bottom current activity in the SC reached its maximum level for a duration of 1.1 Myr (Fig. 5.9). Its upper time limitation is marked by a distinct reduction in SD accumulation rates (see chapter 4.4.2.1). This scenario fits with the findings of Bartoli *et al.* (2005)

and O'Dea *et al.* (2016) placing the closure of the CAS around 4.5 to 3.0 Myr ago and accordingly earlier at 2.8 Ma.

#### 5.4.2.4 Phase 4: Moat broadening (Piacenzian to Holocene)

From 3.1 Ma to present, the SD is marked by another change in moat architecture, i.e. a relief flattening, coevally occurring at both sides of the SC and expressed by a distinct widening, that reached its maximum in the Pleistocene (Figs. 4.17 to 4.19). A recalibration of the bottom-current flow occurred off GBB associated with a basinward shift of the moat axis and the dominance of periplatform deposits at the toe of slope (Fig. 4.20F). This major event displays a further fundamental rearrangement of the previous hydrodynamic regime of the SC flow. It can be attributed to a distinct increase in through-flow cross-section of the bottom current volume causing a moat widening and a coeval reduction in flow velocity. This process would imply a decrease in Coriolis force reducing its eastward deflection. Two global events could have been responsible for this observation (Fig. 5.9): (1) the effect of the CAS closure which caused a larger volume of water passing through the Caribbean channel network and provoking a strengthening of the AMOC due to the higher saline concentration of northward-flowing water masses via the Gulf Stream, a fact supported by paleoceanographic modeling (Lunt *et al.*, 2008; Steph *et al.*, 2010); and (2) the intensification of the AMOC and thermohaline circulation released by the establishment of Mediterranean Outflow Water that added relatively salty water at intermediate depths (Hernández-Molina *et al.*, 2014a, 2014b) and by the northern hemisphere glaciation (Zachos *et al.*, 2001), which enhance the AMOC by an increase in the wind-driven ocean circulation at the North Atlantic mid-latitudes (Sherriff-Tadano *et al.*, 2018).

However, the data imply that not only a significant change in the hydrodynamics steers the moat migration but an increase in platform export and/or a pronounced channelward progradation of the steep platform edge. This additional volume of periplatform deposits built a sediment wedge and pushed the moat westward (Fig. 4.20E and F) in addition to redeposited material by slope failures which filled the former moats (Wunsch *et al.*, 2018). Winnowing has prevented further westward migration of the slope since the middle Pleistocene (Wunsch *et al.*, 2018) probably by the extension of the volume through flow.

#### 5.4.3 Oceanographic events expressed in the contourite drift accumulation rates

The SD accumulation rates (SDAR) and its extension are not always in agreement with a continuously intensifying Gulf Stream system. Moreover, they are the product of local variations in sediment flux. The SD accumulation can be subdivided into three stages (Fig. 5.9). The first stage during the Miocene is expressed by a steady increase of the sedimentation accumulation rate and contourite drift extension. A second stage from the Pliocene to early Pleistocene corresponds with highest contourite drift extension, followed by a third stage of lower rates and decreasing drift extension.

During the Middle to Upper Miocene (12.3 to 5.5 Ma) accumulation rates were low ( $\leq 5$  cm/ka) and SD extension ( $< 3800$  km<sup>2</sup>) was slowly increasing. Sedimentation rates of sheeted contourite drifts within the SC were low with calculated SDAR of 3.2 to 4.8 cm/ka during the 12.3 to 9.4 Ma interval (Figs. 4.20 and 5.8A). A possible explanation might be a low productivity in the seaways and on neritic carbonate factories, significantly reducing the flux of carbonate particles. Preiss-Daimler *et al.* (2013) showed that it is not a local phenomenon but events of carbonate accumulation lowering affected the entire Atlantic Ocean and adjacent ocean basins. The last drop in carbonate content (carbonate crash event) was dated to 9.5 Ma for the Atlantic Ocean basin (Fig. 5.9).

The Miocene-Pliocene boundary 5.5 Ma marks a turning point and begin of the second stage, where SDAR and extension significantly increased. This process lasted until about 2 Ma and comprises drift sequences S7 to S4 where  $> 50$  % of the total SD volume were accumulated (Fig. 5.9). During this time interval SDAR reached its highest average rate of 16.2 cm/ka and its greatest extension ( $> 5100$  km<sup>2</sup>) which correlates well with a peak in the Early Pliocene North Atlantic paleo-productivity, a period persisting over 900 kyr (Diester-Haass *et al.*, 2005; Fig. 5.9) contemporaneous with a biogenic bloom period in the Pacific Ocean (Farrell *et al.* 1995; Fig. 5.9). For the GBB, Eberli *et al.* (1997) and Reijmer *et al.* (2002) determined a high productivity period on the platform top and increased sediment export onto the leeward slope. The steepened and prograding GBB margin facilitates the sediment flux towards the basin. Additionally, the SDAR increases by redeposited periplatform material by erosional bottom currents affecting the slope. The time interval from 3.8 Ma to the present illustrates that SDAR is not proportional to bottom current strength in the SC. Although bottom current intensity remains high until 3.1 Ma, SDAR decreased from 16.2 cm/ka over 5.9 cm/ka to 4.1 cm/ka (Fig. 5.9). The data support that this trend is related to the CAS closure successively preventing the flow of nutrient-rich sub-surface waters from the Pacific into the Atlantic and diminishing the overall biological activity in the North Atlantic (Jain and Collins, 2006; Schneider and Schmittner, 2006). Another reason for lower SDAR values could be the long-term trend of decreasing silicate-weathering and atmospheric CO<sub>2</sub> that could have reduced the burial rates of calcifying organisms (Suchéras-Marx and Henderiks, 2014).

The observed SDAR reduction of the third stage is continued up to present days and is only shortly interrupted by a high SDAR event of *ca* 13.5 cm/ka at 2.2 Ma spanning *ca* 200 ka (Fig. 5.9; S3). The cause of this short event remains speculative. Variable deep-Atlantic conditions in glacial and interglacials indicate a new Atlantic Ocean circulation regime (Bell *et al.*, 2015b) influencing the SC bottom current regime. The Middle-Pleistocene transition 0.9 Ma to 0.7 Ma, which describes a period of establishing longer glacial/interglacial cycles and higher amplitude in sea-level fluctuations due to the increased influence of the 100 kyr eccentricity in the Earth's orbital cycles. This is coincident with the age of seismic sequence S1 in the SC and Horizon Ple.2 of Principaud *et al.* (2016) at the GBB margin in the Florida Straits, with a slight difference in age, determined at 0.85 Ma. This short-term event of increased bottom current velocity is recorded in the SD by a high amplitude reflection across the channel, peaks in quartz and insoluble contents in ODP core 1006A (Fig. 3.10) and a lateral change of the SD depocenter. Additionally, benthic carbon isotope datasets

show a strong presence of Northern Component Water in the Southern Ocean Water at 0.9 Ma (Poore *et al.*, 2006; Fig. 5.9) and could be related to a short-period, increased exchange of water volume between the North Atlantic and the South Atlantic, whereas other authors see an reduced thermohaline circulation with enhanced stratification and reduced North Atlantic Deep Water production (Diester-Haass *et al.*, 2018). The factors controlling the sedimentation rate of carbonate sediments in the SC are more complex than proposed for classical sea-level-controlled carbonate systems, with high sediment delivery to the basin during sea-level highstands and starved sedimentation during sea-level lowstands (Droxler and Schlager, 1985; Schlager *et al.*, 1994).

## 6 Conclusions

The results of this study contribute to a better understanding of current-induced depositional record at isolated carbonate platforms. It demonstrates that currents may redistribute the sediments at a small- to large-scale and create a variety of contourite features which provide an archive of the prevailing current activity. A combination of 2D seismic (seismic facies) with well-data (sedimentary facies) and bathymetric data (slope angle) have enabled the regional paleoceanographical reconstruction of the hydrodynamic regime around isolated carbonate platforms.

A prerequisite for the accumulation of large contourite drift bodies at isolated carbonate platforms is the persistent supply of biogenic and abiogenic calcareous particles created by the shallow water carbonate factory of the platform. In the framework of this study various carbonate contourite drifts have been identified in the archipelagos of the Bahamas and the Maldives. The drift bodies are related to a wide range of water depths from lagoonal areas (< 40 m) down to inter platform basins (> 400 m). Contourite drifts were found to be common around isolated carbonate platforms, which act as bathymetric obstacles, with ocean currents being accelerated and reoriented. The special topographic framework of isolated carbonate platforms and bottom current activity have resulted in a variety of different contourite drifts, which differs in size and shape. The carbonate contourite drifts can be classified as: (drowned) platform-related drifts (*terrace drifts* and *cover drifts*), channel-related drifts (*contour channel drifts*), slope related drift (*periplatform drifts* and *notch drifts*), slope-to-basin drifts (*platform-edge drifts* and *delta drifts*), basin drifts (*sheeted drifts* and *mounded drifts*), Contourite Depositional Systems, and small-scale *patch drifts*. The prerequisite for the development of carbonate contourite drifts at isolated platform settings is the existence of stable, long-persistent bottom currents. Additionally, extrinsic factors, such as the geometry of the platform, the availability of sediments and the bottom-current shape and strength have a combined impact on the architecture of the contourite drift bodies. Furthermore, the ocean currents are propelled and influenced by different processes, for example, the wind, density-temperature changes, the Coriolis effect, internal waves, and tides.

The case study from the Bahamian archipelago presents the evolution of a carbonate-ooze-dominated contourite drift in the Santaren Channel. It has clearly shown the conformity between the development, through time and space, of the Santaren Drift and oceanographic processes in the Caribbean and Atlantic realms, as well as the synchronous current activity in the Florida Straits. Based on the distribution and internal seismic character of erosional and depositional features, bottom current pathways and intensities could be derived. The analyzed features of the Santaren Drift display bottom current activity and sedimentation rates closely related to important paleoceanographic changes, including the shoaling of the Central American Seaway, the drowning of the Northern Nicaragua Rise megabank, global biogenic blooms and enhanced current activity in the Atlantic Ocean since the Miocene. The results document the complexity of contour channel

drift sedimentation in the Santaren Channel being out of phase with bottom-current flow variations and mainly controlled by local and regional variations in sediment flux.

The results help to facilitate the interpretation of the carbonate sedimentary record due to greater understanding of the various contourite drift types around isolated carbonate platforms. Indeed, the recognition of carbonate contourite drifts in seismic images is made easier by the identification of current-related features. Nevertheless, corresponding depositional systems, similar to those presented here, should be carefully examined for the presence of carbonate contourite drifts. Therefore, understanding of the processes and results of bottom-current flow activity around isolated carbonate platforms has major implications for paleoceanography, sedimentology, paleoclimatology, and hydrocarbon exploration.

Carbonate contourite drift systems and their paleoceanographic history comprise an underestimated field of research. Fluctuations in bottom current activity around modern and ancient isolated carbonate platforms can form carbonate contourite drifts with changing body and associated moat geometries, as well as stratal patterns. Carbonate contourite drifts represent unique archives of intensified and lowered bottom-current strength, as well as the current's dimensions via changes in the geometry and lateral migration of paleo-moats. As such, they could reveal information about paleo-current activity by analyzing the drift's evolution similar to the presented data. The interplay between the hydrodynamic regime and the depositional patterns are not entirely understood. For being applicable, the mechanisms which form the moats and contourite drifts remain to be entirely deciphered. Variations in the bathymetric framework on different scales, from tectonic activity through to sedimentary mass movements and biogenic construction of carbonate mounds and atolls, may cause similar changes in the seismic reflection patterns as variation in the current dynamics. The variability of the interactive mechanisms in the depositional settings and the consequences have yet to be completely encrypted in order to strengthen and verify the conclusions of the paleoceanographic research presented here, but this is a fruitful field to be pursued. Future work would benefit from filling the following gaps:

- a. The compilation of sediment production, transport processes and biotic impact require careful examination in order to clarify the development of carbonate contourite drifts in detail. The preservation of small-scale layering without bioturbation in some outcrops remains a secret to be unlocked.
- b. Regional oceanographic modelling studies would shed light on the interplay between downslope transport of the platform-derived material and the distribution of carbonate particles with different physical properties, as well as current focussing and splitting due to the bathymetric framework.
- c. Greater knowledge of the budgets of sources and sinks and the impact of the great variety of oceanographic processes that induce current activity.
- d. Paleo-ocean circulation models and a better understanding of the development of platform-related channels have the potential to reveal further insights into the recognition of ancient carbonate contourite drifts.

- e. The role of current effects such as eddies, benthic storms and internal waves in the depositional environment are unclear.
- f. Indications of the relative intensities of bottom currents are inferred from a contour channel drift's shape and moat geometries, but further work is required to refine and expand the procedure to other types of carbonate contourite drifts.
- g. Highly fissured fields of carbonate platforms yield the potential for the development of carbonate contourite drifts due to the availability of myriad waterways where currents can interact with the carbonate sediments. Very high-resolution seismic data have to be carefully examined to detect small-scale carbonate contourite drifts.

## 7 Publication

**Paulat, M., Lüdmann, T., Betzler, C., Eberli, G.P.**, 2018. Neogene paleoceanographic changes recorded in a carbonate contourite drift (Santaren Channel, Bahamas). *Sedimentology* 66(4), 1361–1385. DOI: 10.1111/sed.12573

## 8 References

**Allen, J.R.L. (ed.)**, 1982. *Sedimentary structures their character and physical basis volume I*. Developments in Sedimentology 30a, 593 p. Elsevier, Amsterdam.

**Anderkuov, K., Surlyk, F., Huuse, M., Lykke-Andersen, H., Bjerager, M., Tang, C.D.**, 2010. Sediment waves with a biogenic twist in Pleistocene cool water carbonates, Great Australian Bight. *Marine Geology* 278, 122–139. DOI:10.1016/j.margeo.2010.09.009

**Anselmetti, F.S., Eberli, G.P., Ding, Z.-D.**, 2000. From the Great Bahama Bank into the Straits of Florida: A margin architecture controlled by sea-level fluctuations and ocean currents. *GSA Bulletin* 112(6), 829–844.

**Aubert, O., Droxler, A.W.**, 1992. General Cenozoic evolution of the Maldives carbonate system (Equatorial Indian Ocean). *Bulletin du Centre de Recherches Elf Exploration Production Elf Aquitaine* 16, 113–136.

**Aubert, O., Droxler, A.W.**, 1996. Seismic stratigraphy and depositional signatures of the Maldivian carbonate system (Indian Ocean) *Marine Petroleum Geology* 13, 503–536

**Ball, M.M., Martin, R.G., Bock, W.D., Sylwester, R.E., Bowles, R.M., Taylor, D., Coward, E.L., Dodd, J.E., Gilbert, L.**, 1985. Seismic structure and stratigraphy of northern edge of Bahaman-Cuban Collision Zone. *The American Association of Petroleum Geologists Bulletin* 69(8), 1275–1294.

**Bartoli, G., Sarntheim, M., Weinelt, M., Erlenkeuser, H., Garbe-Schonberg, D., Lea, D.W.**, 2005. Final closure of Panama and the onset of northern hemisphere glaciation. *Earth and Planetary Science Letters* 237, 33–44. DOI: 10.1016/j.epsl.2005.06.020

**Bein, A., Weiler, Y.**, 1976. The Cretaceous Talme Yafe Formation: a contour current shaped sedimentary prism of calcareous detritus at the continental margin of the Arabian Craton. *Sedimentology* 23, 511–532.

**Bell, D.B., Jung, S.J.A., Kroon, D., Hodell, D.A., Lourens, L.J., Raymo, M.E.**, 2015a. Atlantic deep-water response to the Early Pliocene shoaling of the central American seaway. *Nature, Scientific Reports* 5, 12252. DOI: 10.1038/srep12252

**Bell, D.B., Jung, S.J.A., Kroon, D.**, 2015b. The Plio-Pleistocene development of Atlantic deep-water circulation and its influence on climate trends. *Quaternary Science Reviews* 123, 265–282.

- Belopolsky, A.V., Droxler, A.W.**, 2003. Imaging Tertiary carbonate system—the Maldives, Indian Ocean: Insights into carbonate sequence interpretation. *The Leading Edge* 22, 646–652. DOI: 10.1190/1.1599690
- Belopolsky, A.V., Droxler, A.W.**, 2004. Seismic expressions of prograding carbonate bank margins: middle Miocene, Maldives, Indian Ocean. In Eberli, G.P., Masferro J.L., Sarg J.F., (eds) *Seismic imaging of carbonate reservoirs and systems*, 267–290.
- Bennett, R.H., Li, H., Lambert, D.N., Fischer, K.M., Walter, D.J.**, 1990. In situ porosity and permeability of selected carbonate sediment: Great Bahama Bank. Part 1: Measurements. *Marine Geotechnology* 9, 1–28.
- Berggren, W.A.**, 1982. Role of Ocean Gateways in Climate Change. In: *Climate in Earth History: Studies in Geophysics*, National Research Council, The National Academies Press, Washington, DC, 118-125. DOI: 10.17226/11798.
- Bergman, K.L.**, 2005. Seismic Analysis of Paleocurrent Feature in the Florida Straits: Insights into the Paleo-Florida current, upstream tectonics, and the Atlantic-Caribbean connection. PhD dissertation, 206 p. University of Miami, FL.
- Bergman, K.L., Westphal, H., Janson, X., Poiriez, A., Eberli, G.P.**, 2010. Controlling Parameters on Facies Geometries of the Bahamas, an Isolated Carbonate Platform Environment. In: Westphal, H., Riegl, B., Eberli, G.P. (eds), *Carbonate Depositional Systems: Assessing Dimensions and Controlling Parameters*, 5–80. Springer Science+Business Media BV, Dordrecht. DOI: 10.1007/978-90-481-9364-6\_2.
- Betzler, C., Reijmer, J.J.G., Bernet, K., Eberli, G.P., Anselmetti, F.S.**, 1999. Sedimentary patterns and geometries of the Bahamian outer carbonate ramp (Miocene±Lower Pliocene, Great Bahama Bank). *Sedimentology* 46, 1127–1143.
- Betzler, C., Hübscher, C., Lindhorst, S., Reijmer, J.J.G., Römer, M., Droxler, A.W., Fürstenau, J., Lüdmann, T.**, 2009. Monsoonal-induced partial carbonate platform drowning (Maldives, Indian Ocean). *Geology* 37, 867–870.
- Betzler, C., Fürstenau, J., Lüdmann, T., Hübscher, C., Lindhorst, S., Paul, A., Reijmer, J.J.G., Droxler, A.**, 2013a. Sea-level and ocean-current control on carbonate-platform growth, Maldives, Indian Ocean. *Basin Research* 25, 172–196.
- Betzler, C., Lüdmann, T., Hübscher, C., Fürstenau, J.**, 2013b. Current and sea-level signals in periplatform ooze (Neogene, Maldives, Indian Ocean). *Sedimentary Geology* 290, 126–137.
- Betzler, C., Lindhorst, S., Eberli, G.P., Lüdmann, T., Mobius, J., Ludwig, J., Schutter, I., Wunsch, M., Reijmer, J.J.G., Hübscher, C.**, 2014a. Periplatform drift: The combined result of contour current and off-bank transport along carbonate platforms. *Geology* 42(10), 871–874.
- Betzler, C., Lindhorst, S., Lüdmann, T., von Borstel, F., Büld, M., Djamlan, E., Eberli, G.P., Eversheim, J., Jentzen, A., Keizer, F., Ludwig, J., Möbius, J., Paulat, M., Reiche, S., Reijmer,**

- J., Reolid, J., Schiebel, L., Schutter, I., Ulferts, L., Winter, S., Wolf, D., Wunsch, M., Rentsch, H., Raeke, A.**, 2014b. CICARB - Cruise No. M95 – March 29 – April 25, 2013 – Kingston (Jamaica) – Pointe à Pitre (Guadeloupe). METEOR-Berichte M95, 36 p. DOI:10.2312/cr\_m95
- Betzler, C., Lindhorst, S., Lüdmann, T., Weiss, B., Wunsch, M., Braga, J.C.**, 2015a. The leaking bucket of a Maldives atoll: Implications for the understanding of carbonate platform drowning. *Marine Geology* 366, 16–33. DOI: 10.1016/j.margeo.2015.04.009
- Betzler, C., Lahajnar, N., Lindhorst, S., Lüdmann, T., Wiesner, M.**, and SO236 scientific party, 2015b. RV Sonne Cruise Report / Fahrtbericht SO-236, Malé to Colombo, 9 to 29 August 2014. RV Sonne Fahrtbericht, 48 p. DOI:10.2312/cr\_so236
- Betzler, C., Eberli, G. P., Kroon, D., Wright, J., Swart, P.K., Nath, B.N., Alvarez-Zarikian, C., Alonso-García, M., Bialik, O.M., Blättler, C.L., Guo, J.A., Haffen, S., Horozal, S., Inoue, M., Jovane, L., Lanci, L., Laya, J.C., Hui Mee, A.L., Lüdmann, T., Nakakuni, M., Niino, K., Petruny, L.M., Pratiwi, S.D., Reijmer, J.J.G., Reolid, J., Slagle, A.L., Sloss, C.R., Su, X., Yao, Z., Young, J.R.**, 2016a. The abrupt onset of the modern South Asian Monsoon winds. *Scientific Reports* 6, 29838. DOI: 10.1038/srep29838
- Betzler, C., Hübscher, C., Lindhorst, S., Lüdmann, T., Reijmer, J.J.G., Braga, J.-C.**, 2016b. Lowstand wedges in carbonate platform slopes (Quaternary, Maldives, Indian Ocean). *The Depositional Record* 2(2) 196–207. DOI: 10.1002/dep2.21
- Betzler, C., Eberli, G.P., Alvarez-Zarikian, C.A.**, and the Expedition 359 Scientists, 2017. Maldives Monsoon and Sea Level. *Proceedings of the International Ocean Discovery Program*, 359. DOI: 10.14379/iodp.proc.359.2017
- Betzler, C., Eberli, G. P., Lüdmann, T., Reolid, J., Kroon, D., Reijmer, J.J.G., Swart, P.K., Wright, J., Young, J.R., Alvarez-Zarikian, C., Alonso-García, M., Bialik, O.M., Blättler, C.L., Guo, J.A., Haffen, S., Horozal, S., Inoue, M., Jovane, L., Lanci, L., Laya, J.C., Hui Mee, A.L., Nakakuni, M., Nath, B.N., Niino, K., Petruny, L.M., Pratiwi, S.D., Slagle, A.L., Sloss, C.R., Su, X., Yao, Z.**, 2018. Refinement of Miocene sea level and monsoon events from the sedimentary archive of the Maldives (Indian Ocean). *Progress in Earth and Planetary Science* 5(5). DOI: 10.1186/s40645-018-0165-x
- Campbell, C.V.**, 1967. Lamina, laminaset, bed and bedset. *Sedimentology* 8, 7–26.
- Chabaud, L., Ducassou, E., Tournadour, E., Mulder, T., Reijmer, J.J.G., Conesa, G., Giraudeau, J., Hanquiez, V., Borgomano, J., Ross, L.**, 2016. Sedimentary processes determining the modern carbonate periplatform drift of Little Bahama Bank. *Marine Geology* 378, 213–229.
- Coates, A.G., Stallard, R.F.**, 2013. How old is the Isthmus of Panama? *Bulletin of Marine Science* 89(4), 801–813. DOI: 10.5343/bms.2012.1076

- Correa, T.B.S., Eberli, G.P., Grasmueck, M., Reed, J.K., Correa, A.M.S.,** 2012. Genesis and morphology of cold-water coral ridges in a unidirectional current regime. *Marine Geology* 326, 14–27. DOI: 10.1016/j.margeo.2012.06.008
- Cossu, R., Wells, M.G., Peakall, J.,** 2015. Latitudinal variations in submarine channel sedimentation patterns: the role of Coriolis forces. *Journal of the Geological Society* 172, 161–174. DOI: 10.1144/jgs2014-043
- Courgeon, S., Jorry, S.J., Camoin, G.F., BouDagher-Fadel, M.K., Jouet, G., Révillon, S., Bachèlery, P., Pelleter, E., Borgomano, J., Poli, E., Droxler A.W.,** 2016. Growth and demise of Cenozoic isolated carbonate platforms: New insights from the Mozambique Channel seamounts (SW Indian Ocean). *Marine Geology* 380, 90–105. DOI:10.1016/j.margeo.2016.07.006
- Cruz-Orosa, I., Sàbat, F., Ramos, E., Vázquez-Taset, Y.M.,** 2012. Synorogenic basins of central Cuba and collision between the Caribbean and North American plates. *International Geology Review*, 54(8), 876–906. DOI: 10.1080/00206814.2011.585031
- De Zoeten, R., Mann, P.,** 1991. Structural Geology and Cenozoic Tectonic History of the Central Cordillera Septentrional, Dominican Republic. In: Mann, P., Draper, G., Lewis, J.F. (eds), *Geologic and Tectonic Development of the North America-Caribbean Plate Boundary in Hispaniola*, Geological Society of America Special Paper 262, 265–280.
- Denny, W., Austin, J.A. and Buffler, R.T.,** 1994. Seismic stratigraphy and geologic history of Mid-Cretaceous through Cenozoic rocks, Southern Straits of Florida. *AAPG Bulletin* 78, 461–487.
- Diester-Haass, L., Billups, K., Emeis, K.C.,** 2005. In search of the late Miocene–early Pliocene “biogenic bloom” in the Atlantic Ocean (Ocean Drilling Program Sites 982, 925, and 1088). *Paleoceanography* 20(4), 1–13. DOI: 10.1029/2005PA001139
- Diester-Haass, L., Billups, K. and Lear, C.,** 2018. Productivity changes across the mid-Pleistocene climate transition. *Earth-Science Reviews* 179, 372–391. DOI: 10.1016/j.earscirev.2018.02.016
- Droghei, R., Falcini, F., Casalbore, D., Martorelli, E., Mosetti, R., Sannino, G., Santoleri, R., Chiocci, F.L.,** 2016. The role of Internal Solitary Waves on deep-water sedimentary processes: the case of up-slope migrating sediment waves off the Messina Strait. *Nature Scientific Reports* 6, 36376. DOI:10.1038/srep36376
- Droxler, A., Schlager, W.,** 1985. Glacial versus interglacial sedimentation rates and turbidite frequency in the Bahamas. *Geology* 13(11), 799–802. DOI: 10.1130/0091-7613(1985)13<799:GVISRA>2.0.CO;2
- Duan, T., Gao, Z., Zeng, Y., Stow, D.,** 1993. A fossil carbonate contourite drift on the Lower Ordovician palaeocontinental margin of the middle Yangtze Terrane, Jiuxi, northern Hunan, southern China. In: Stow, D.A.V., Faugères, J.-C. (eds), *Contourites and Bottom Currents*. *Sedimentary Geology* 82, 271–284.

- Duncan, R.A., Hargraves, R.B.**, 1990.  $^{40}\text{Ar}/^{39}\text{Ar}$  geochronology of basement rocks from the Mascarene Plateau, the Chagos Bank, and the Maldives Ridge. *Proceedings of the Ocean Drilling Program, Scientific Results* 115, 43–51.
- Duncan, R.A., Backman, J., Peterson, L.C., et al.**, 1990. *Proceedings of the Ocean Drilling Program, Scientific Results* 115. Ocean Drilling Program, College Station, TX.
- Dunham, R.J.**, 1962. Classification of Carbonate Rocks according to Depositional Texture. *American Association of Petroleum Geologists* 1, 108–12.
- Eberli, G.P.**, 1991. Growth and demise of isolated carbonate platforms: Bahamian controversies. In: Müller, D. W., McKenzie, J.A. and Weissert, H. (eds) *Controversies in Modern Geology*, 231–248. Academic Press, London.
- Eberli, G.P., Ginsberg, R.N.**, 1987. Segmentation and coalescence of Cenozoic carbonate platforms, northwestern Great Bahama Bank. *Geology* 15, 75–79.
- Eberli, G.P., Betzler, C.**, 2019. Characteristics of modern carbonate contourite drifts. *Sedimentology*, in press. DOI: 10.1111/sed.12584
- Eberli, G.P., Swart, P.K.S., Malone, M., et al.**, 1997. A synopsis of the Bahamas drilling project: Results from two deep core borings drilled on the great Bahama Bank. *Proceedings of the Ocean Drilling Program, Initial Reports, Leg 166*, 850 p. College Station, Texas.
- Eberli, G.P., Anselmetti, F.S., Kroon, D., Sato, T., Wright, J.D.**, 2002. The chronostratigraphic significance of seismic reflections along the Bahamas Transect. *Marine Geology* 185, 1-17.
- Eberli, G.P., Baechle, G.T., Anselmetti, F.S., Incze, M.**, 2003. Factors controlling elastic properties in carbonate sediments and rocks. *The Leading Edge* 22, 654–660.
- Eberli, G.P., Anselmetti, F.S., Betzler, C., Van Konijnenburg, J.-H., Bernoulli, D.**, 2004. Carbonate platform to basin transitions on seismic data and outcrops: Great Bahama bank and the Maiella Platform margin, Italy. In: Eberli, G.P., Massaferro, J.L., Sarg, J.F. (eds), *Seismic Imaging of Carbonate Reservoirs and Systems*. AAPG Memoir 81, 207–250.
- Eberli, G.P., Anselmetti, F.S., Isern, A.R., Delius, H.**, 2010. Timing of changes in sea-level and currents along Miocene platforms on the Marion Plateau, Australia. In: Morgan, W.A., George, A.D., Harris, P.M., Kupecz, J.A., Sarg, J.F. (eds) *Cenozoic Carbonate Systems of Australasia*. SEPM Special Publication 95, 219–242.
- Eberli, G.P., Bernoulli, D., Vecsei, A., Anselmetti, F.S., Mutti, M., Della Porta, G., Lüdmann, T., Grasmueck, M., Sekti, R.**, 2019. A Cretaceous carbonate drift delta in the Montagna della Maiella, Italy. *Sedimentology*, in press. DOI: 10.1111/sed.12590
- Ehrenberg, S.N., Eberli, G.P., Baechle, G.**, 2006. Porosity–permeability relationships in Miocene carbonate platforms and slopes seaward of the Great Barrier Reef, Australia (ODP Leg 194, Marion Plateau). *Sedimentology* 53, 1289–1318. DOI: 10.1111/j.1365-3091.2006.00817.x

- Esentia, I., Stow, D., Smillie, Z.**, 2018. Contourite Drifts and Associated Bedforms. In: Micallef, A., Krastel, S., Savini, A. (eds), *Submarine Geomorphology*, 301–331. Springer Geology, Cham. DOI: 10.1007/978-3-319-57852-1\_16
- Esmerode E.V., Lykke-Andersen, H., Surlyk, F.**, 2007. Ridge and valley systems in the Upper Cretaceous chalk of the Danish Basin: contourites in an epeiric sea. In: Viana, A.R., and Rebesco, M. (eds), *Economic and Palaeoceanographic Significance of Contourite Deposits*, 265–282. Geological Society, London.
- Farrell, J.W., Raffi, I., Janecek, T.R., Murray, D.W., Levitan, M., Dadey, K.A., Emeis, K.-C., Lyle, M., Flores, J. A., Hovan, S.**, 1995. Late Neogene sedimentation patterns in the eastern equatorial Pacific Ocean. *Proceedings of the Ocean Drilling Program, Scientific Results* 138, 717–756.
- Faugères, J.-C., Stow, D.A.V.**, 2008. Contourite drifts: Nature, evolution and controls. In: Rebesco, M., Camerlenghi, A. (eds), *Contourites. Developments in Sedimentology* 60, 259–288. Elsevier, Amsterdam.
- Faugères, J.-C., Mézerais, M.L., Stow, D.A.V.**, 1993. Contourite drift types and their distribution in the North and South Atlantic Ocean basins. *Sedimentary Geology* 82, 189–203. DOI: 10.1016/0037-0738(93)90121-K
- Faugères, J.-C., Stow, D.A.V., Imbert, P., Viana, A.**, 1999. Seismic features diagnostic of contourite drifts. *Marine Geology* 162, 1–38.
- Flügel, E. (ed.)**, 2004. *Microfacies of Carbonate Rocks: Analysis, Interpretation and Application*. First edition, Springer, Berlin-Heidelberg. DOI: 10.1007/978-3-662-08726-8
- Fürstenau, J., Lindhorst, S., Betzler, C., Hübscher, C.**, 2010. Submerged reef terraces of the Maldives (Indian Ocean). *Geo-Marine Letters* 30, 511–515
- García, M., Hernández-Molina, F.J., Llave, E., Stow, D.A.V., León, R., Fernández-Puga, M.C., del Río, V.D., Somoza, L.**, 2009. Contourite erosive features caused by the Mediterranean Outflow Water in the Gulf of Cadiz: Quaternary tectonic and oceanographic implications. *Marine Geology* 257, 24–40. DOI:10.1016/j.margeo.2008.10.009
- Gay, A., Lopez, M., Cochonat, P., Sermondadaz, G.**, 2004. Polygonal faults-furrows system related to early stages of compaction – upper Miocene to recent sediments of the Lower Congo Basin. *Basin Research* 16(1), 101–116. DOI: 10.1111/j.1365-2117.2003.00224.x
- Gischler, E., Hudson, J.H., Pisera, A.**, 2008. Late Quaternary reef growth and sea level in the Maldives (Indian Ocean). *Marine Geology* 250, 104–113.
- Gischler, E., Storz, D., Schmitt, D.**, 2013. Sizes, shapes, and patterns of coral reefs in the Maldives, Indian Ocean: The influence of wind, storms, and precipitation on a major tropical carbonate platform. *Carbonates and Evaporites* 29, 73–8. DOI: 10.1007/s13146-013-0176-z

- Glenn, C.R., Kronen, J.D.**, 1993. Origin and significance of late Pliocene phosphatic hardgrounds on the Queensland Plateau, northeastern Australian margin. *Proceedings of the Ocean Drilling Program, Scientific Results* 133, 525–534.
- Grant, J. A., Schreiber, R.**, 1990. Modern swaths sounding and sub-bottom profiling technology for research applications: The Atlas HYDROSWEEP and PARASOUND systems. *Marine Geophysical Research* 12, 9–19.
- Gradstein, F.M., Ogg, J.G., Schmitz, M.D., Ogg, G.M.**, 2012. *The Geologic Time Scale 2012*, first edition. Elsevier BV, Amsterdam.
- Gröger, M., Henrich, R., Bickert, T.**, 2003. Variability of silt grain size and planktonic foraminiferal preservation in Plio/Pleistocene sediments from the western equatorial Atlantic and Caribbean. *Marine Geology* 201, 307–320.
- Gruetzner, J., Uenzelmann-Neben, G.**, 2016. Contourite drifts as indicators of Cenozoic bottom water intensity in the eastern Agulhas Ridge area, South Atlantic. *Marine Geology* 378, 350–360. DOI:10.1016/j.margeo.2015.12.003
- Haberkern, J., Schwenk, T., Hernández-Molina, F.J., Hanebuth, T.J.J., Spiess, V.**, 2017. Morphology and evolution of contouritic depositional systems steered by the interaction of bottom currents with distinct seafloor topography at the Galicia Margin (NW Spain) In: Haberkern, J., *Contouritic depositional systems influenced by complex seafloor topography*, PhD dissertation, 119 p. Universität Bremen.
- Hagelund, R. and Levin, S.A. (eds)**, 2017. SEG-Y revision 2.0 Data Exchange format. Society of Exploration Geophysicists, 147 p. Tulsa, OK.
- Hatton, L., Worthington, M.H., Makin, J. (eds)**, 1986. *Seismic Data Processing: Theory and Practice*. 177p. Blackwell Science, Oxford.
- Haug, G.H., Tiedemann, R.**, 1998. Effect of the formation of the Isthmus of Panama on Atlantic Ocean thermohaline circulation. *Nature* 393(6686), 673–676.
- Haug, G.H., Tiedemann, R., Zahn, R., Ravelo A.C.**, 2001. Role of Panama uplift on oceanic freshwater balance. *Geology* 29(3), 207–210.
- Haywood, A.M., Smellie, J.L., Ashworth, A.C., Cantrill, D.J., Florindo, F., Hambrey, M.J., Hill, D., Hillenbrand, C.-D., Hunter, S.J., Larter, R.D., Lear, C.H., Passchier, S., van de Wal, R.**, 2009. Middle Miocene to Pliocene History of Antarctica and the Southern Ocean. in: Florindo, F., Siebert, M. (eds), *Developments in Earth & Environmental Sciences* 8, 401–463. Elsevier Science BV, Amsterdam.
- Heezen, B.C., Hollister, C.D., Ruddiman, W.F.**, 1966. Shaping of the continental rise by deep geostrophic contour currents. *Science* 152, 502–508.

- Hernández-Molina, F.J., Llave, E., Somoza, L., Fernández-Puga, M.C., Maestro, A., León, R., Medialdea, T., Barnolas, A., García, M., Díaz-del-Río, V., Fernández Salas, L., Vazquez, J.-T., Lobo, F.J., Dias, J., Rodero, J., Gardner, J., 2003.** Looking for clues to paleoceanographic imprints: a diagnosis of the Gulf of Cadiz Contourite Depositional Systems. *Geology* 31, 19–22. DOI:10.1130/0091-7613(2003)031<0019:LFCTPI>2.0.CO;2
- Hernández-Molina, F.J., Maldonado, A., Stow, D.A.V., 2008a.** Abyssal plain contourites. In: Rebesco, M., Camerlenghi, A. (eds), *Contourites. Developments in Sedimentology*, 60, 345–378. Elsevier, Amsterdam.
- Hernández-Molina, F.J., Stow, D.A.V., Llave, E., 2008b.** Continental slope contourites. In: Rebesco, M., Camerlenghi, A. (eds), *Contourites. Developments in Sedimentology*, 60, 379–408. Elsevier, Amsterdam.
- Hernández-Molina, F. J., Stow, D. A., Alvarez-Zarikian, C. A., Acton, G., Bahr, A., Balestra, B., Ducassou, E., Flood, R., Flores, J. A., Furota, S., Grunert, P., Hodell, D., Jimenez-Espejo, F., Kim, J. K., Krissek, L., Kuroda, J., Li, B., Llave, E., Lofi, J., Lourens, L., Miller, M., Nanayama, F., Nishida, N., Richter, C., Roque, C., Pereira, H., Sanchez Goni, M. F., Sierro, F. J., Singh, A. D., Sloss, C., Takashimizu, Y., Tzanova, A., Voelker, A., Williams, T., Xuan, C., 2014a.** Onset of Mediterranean outflow into the North Atlantic. *Paleoceanography* 34(6189), 1244–1250.
- Hernández-Molina, F.J., Llave, E., Preu, B., Ercilla, G., Fontan, A., Bruno, M., Serra, N., Gomiz, J.J., Brackenridge, R.E., Sierro, F.J., Stow, D.A.V., García, M., Juan, C., Sandoval, N., Arnaiz, A., 2014b.** Contourite processes associated with the Mediterranean Outflow Water after its exit from the Strait of Gibraltar: Global and conceptual implications. *Geology* 42(3), 227–230. DOI: 10.1130/G35083.1
- Hernández-Molina, F.J., Wåhlin, A., Brunoc, M, Ercilla, G., Llave, E., Serra, N., Rosón G., Puig, P., Rebesco, M., Van Rooij, D., Roque D., González-Pola, C., Sánchez, F., Gómez, M., Preun, B., Schwenk, T., Hanebuth, T.J.J., Leal, R.F.S., García-Lafuente, J., Brackenridge, R.E., Juand, C, Stow, D.A.V., Sánchez-González, J.M., 2016.** Oceanographic processes and morphosedimentary products along the Iberian margins: A new multidisciplinary approach. *Marine Geology* 378, 127–156. DOI:
- Hine, A.C., 2013.** *Geologic History of Florida—Major Events That Formed the Sunshine State.* University Press of Florida, 229 p. Gainesville, FL.
- Hübscher, C., Dullo, C., Flögel, S., Titschack, J., Schönfeld, J., 2010.** Contourite drift evolution and related coral growth in the eastern Gulf of Mexico and its gateways. *International Journal of Earth Sciences* 99, 191–206. DOI:10.1007/s00531-010-0558-6
- Hüneke, H., 2006.** Erosion and deposition from bottom currents during the Givetian and Frasnian: response to intensified oceanic circulation between Gondwana and Laurussia. - *Palaeogeography, Palaeoclimatology, Palaeoecology* 234, 146–167.

- Hüneke, H.**, 2007. Pelagic carbonate ooze reworked by bottom currents during Devonian approach of the continents Gondwana and Laurussia. In: Viana, A.R., and Rebesco, M., (eds), *Economic and Palaeoceanographic Significance of Contourite Deposits*, 299–328. Geological Society, London.
- Hüneke H., Stow, D.A.V.**, 2008. Identification of ancient contourites: Problems and palaeoceanographic significance. In: Rebesco, M., Camerlenghi, A. (eds), *Contourites. Developments in Sedimentology* 60, 323–408. Elsevier, Amsterdam.
- Isern, A.R., Anselmetti, F.S., Blum, P. et al.**, 2002. Proceedings of the Ocean Drilling Program, Initial Reports 194. DOI:10.2973/odp.proc.ir.194.2002
- Isern, A.R., Anselmetti, F.S. and Blum, P.**, 2004. A Neogene carbonate platform, slope, and shelf edifice shaped by sea level and ocean currents, Marion Plateau (northeast Australia). In: Eberli, G.P., Masaferrro, J.L., Sarg, J.F. (eds), *Seismic imaging of carbonate reservoirs and systems*. AAPG Memoir 81, 291–307.
- Iturralde-Vinent, M., Hubbell, G., Rojas, R.**, 1996. Catalogue of Cuban fossil Elasmobranchii (Paleocene to Pliocene) and paleogeographic implications of their Lower to Middle Miocene occurrence. *Boletín de la Sociedad Jamaicana de Geología*, 31, 7–21.
- Iturralde-Vinent, M.A., MacPhee, R.D.E.**, 1999. Paleogeography of the Caribbean region: Implications for Cenozoic biogeography. *Bulletin of the American Museum of Natural History*, 238, 95 p.
- Jain, S., Collins, L.S.**, 2006. Trends in Caribbean paleoproductivity related to the Neogene closure of the Central American Seaway. *Marine Micropaleontology* 63, 57–74.
- Johns, W.E., Townsend, T.L., Fratantoni, D.M., Wilson, D.**, 2002. On the Atlantic inflow to the Caribbean Sea. *Deep Sea Research Part I: Oceanographic Research Papers* 49(2), 211–243.
- Karas, C., Nuernberg, D., Bahr, A., Groeneveld, J., Herrle, J.O., Tiedemann, R., deMenocal, P.B.**, 2017. Pliocene oceanic seaways and global climate. *Scientific Reports* 7, 39842. DOI:10.1038/srep39842
- Kench, P.S., Brander, R.W.**, 2006. Response of reef island shorelines to seasonal climate oscillations: South Maalhosmadulu atoll, Maldives. *Journal of geophysical Research* 111, F01001. DOI:10.1029/2005JF000323.
- Kench, P.S., McLean, R.F., Nichol, S.L.**, 2005. New model of reef-island evolution: Maldives, Indian Ocean. *Geology* 33, 145–148; DOI:10.1130/G21066.1
- Knutz, P.C.**, 2008. Palaeoceanographic significance of contourite drifts. In: Rebesco, M., Camerlenghi, M.A. (eds), *Contourites. Developments in Sedimentology* 60, 511–535. Elsevier BV, Amsterdam.

- Kottek, J., Grieser, J., Beck, C., Rudolf, B., Rubel, F.,** 2006. World Map of the Köppen-Geiger climate classification updated. *Meteorologische Zeitschrift* 15, 259–263. DOI:10.1127/0941-2948/2006/0130
- Kourafalou, V. H., Kang H.,** 2012. Florida Current meandering and evolution of cyclonic eddies along the Florida Keys Reef Tract: Are they interconnected? *Journal of Geophysical Research* 117, C05028. DOI:10.1029/2011JC007383.#
- Kroon, D., Williams, T., Pirmez, C., Spezzaferri, S., Sato, T., Wright, J.D.,** 2000. Coupled Early Pliocene – Middle Miocene Bio-Cyclostratigraphy of Site 1006 reveals orbitally induced cyclicity patterns of Great Bahama Bank carbonate production. *Proceedings of the Ocean Drilling Program, Scientific Results* 166, 155–166.
- Kula, D.,** 2014. Neotectonics on the edge of the Cuban fold and thrust belt. Open Access Theses, Paper 498, University of Miami, 118 p. [http://scholarlyrepository.miami.edu/oa\\_theses/498](http://scholarlyrepository.miami.edu/oa_theses/498)
- Leaman, K.D., Vertes, P.S., Atkinson, L.P., Lee, T.N., Hamilton, P., Waddell, E.,** 1995. Transport, potential vorticity, and current/temperature structure across Northwest Providence and Santaren Channels and the Florida Current off Cay Sal Bank. *Journal of Geophysical Research* 100, 8561–8569.
- Lear, C.H., Rosenthal, Y., Wright, J.D.,** 2003. The closing of a seaway: ocean water masses and global climate change. *Earth and Planetary Science Letters* 210(3-4), 425–436. DOI: 10.1016/S0012-821X(03)00164-X
- Lidz, B.H., McNeill, D.F.,** 1995. Reworked Paleogene to early Neogene planktic foraminifera: implications of an intriguing distribution at a late Neogene prograding margin, Bahamas. *Marine Micropaleontology* 25, 221–268.
- Livermore, R., Hillenbrand, C.-D., Meredith, M., Eagles, G.,** 2007. Drake Passage and Cenozoic climate: An open and shut case? *Geochemistry, Geophysics, Geosystems* 8, Q01005. DOI: 10.1029/2005GC001224.
- Lopez, K., Fürstenau, J., Thomas Lüdmann, T., Droxler, A., Betzler C., Reijmer, J.J., Hübscher, C.P., Paul A.A.,** 2011. Nature and Timing of Quaternary Carbonate Sediment Drift, Inner Sea of the Maldives Archipelago. *American Association of Petroleum Geologists, Search and Discovery Article #50485.*
- Lüdmann, T., Kalvelage, C., Betzler, C., Fürstenau, J., Hübscher, C.,** 2013. The Maldives, a giant isolated carbonate platform dominated by bottom currents. *Marine and Petroleum Geology* 43, 326–340. DOI: 10.1016/j.marpetgeo.2013.01.004
- Lüdmann, T., Paulat, M., Betzler, C., Möbius, J., Lindhorst, S., Wunsch, M., Eberli, G.,** 2016. Carbonate mounds and depositional regime in the Santaren Channel, Bahamas: a current-dominated periplatform depositional regime. *Marine Geology* 376, 69–85. DOI: 10.1016/j.margeo.2016.03.013

- Lüdmann, T., Betzler, C., Eberli, G.P., Reolid, J., Reijmer, J.J.G., Sloss, C.R., Bialik, O.M., Alvarez-Zarikian, C.A., Alonso-García, M., Blättler, C.L., Guo, J.A., Haffen, S., Horozal, S., Inoue, M., Jovane, L., Kroon, D., Lanci, L., Laya, J.C., Mee, A.L.H., Nakakuni, M., Nath, B.N., Niino, K., Petruny, L.M., Pratiwi, D.S., Slagle, A.L., Su, X., Swart, P.K., Wright, J.D., Yao, Z., Young, J.R.,** 2018. Carbonate delta drift: A new sediment drift type. *Marine Geology* 401, 98–111. DOI: 10.1016/j.margeo.2018.04.011
- Lunt, D.J., Valdes, P.J., Haywood, A., Rutt, I.C.,** 2008. Closure of the Panama Seaway during the Pliocene: implications for climate and Northern Hemisphere glaciation. *Climate Dynamics* 30, 1–18. DOI: 10.1007/s00382-007-0265-6
- Luo, S., Gao, S., He, Y., Stow, D.A.V.,** 2002. Ordovician carbonate contourite drifts in Hunan and Gansu Provinces, China. In: Stow, D.A.V., Pudsey, C.J., Howe, J.A., Faugères, J.-C., Viana, A.R. (eds), *Deep-Water Contourite Systems: Modern Drifts and Ancient Series, Seismic and Sedimentary Characteristics*, Memoirs 22, 433–442. Geological Society, London.
- Lynch-Stieglitz, J., Curry, W.B., Slowey, N., Schmidt, M.W.,** 1999. The overturning circulation of the glacial Atlantic – A view from the top. In: Abrantes, F., Mix, A.C. (eds), *Reconstructing Ocean History – A windows into the Future*, 33–56. Springer Science+Business Media, New York.
- Mann, P.,** 1999. Caribbean sedimentary basins: Classification and tectonic setting from Jurassic to Present. In: Mann, P. (ed.), *Caribbean Basins, Sedimentary Basins of the World 4*, 3–31. Elsevier Science BV, Amsterdam.
- Masaferro, J.L., Eberli, G.P.,** 1999. Jurassic-Cenozoic structural evolution of the southern Great Bahama Bank. In: Mann, P. (ed.), *Caribbean Basins, Sedimentary Basins of the World 4*, 167–193. Elsevier Science BV, Amsterdam.
- Masaferro, J.L., Poblet, J., Bulnes, M., Eberli, G.P., Dixon, T.H., McClay, K.,** 1999. Palaeogene–Neogene/present day(?) growth folding in the Bahamian foreland of the Cuban fold and thrust belt. *Journal of the Geological Society* 156, 617–631.
- Matos-Maraví, P., Águila, R.N., Pena, C., Miller, J.Y., Sourakov, A., Wahlberg, N.,** 2014. Causes of endemic radiation in the Caribbean: evidence from the historical biogeography and diversification of the butterfly genus *Calisto* (Nymphalidae: Satyrinae: Satyrini). *BioMed Central Evolutionary Biology*, 14, 199. DOI: 10.1186/s12862-014-0199-7
- Mitchum, R.M., Vail, P.R., Thompson, S.,** 1977a. Seismic Stratigraphy and global changes of sea level, part 2: The depositional sequence as a basic unit for stratigraphic analysis. In: Payton, C. (ed.), *Seismic Stratigraphy – applications to hydrocarbon exploration*. AAPG Memoir 26, 53–62. The American Association of Petroleum Geologists, Tulsa, OK.
- Mitchum, R.M., Vail, P.R., Sangree, J.B.,** 1977b. Seismic Stratigraphy and global changes of sea level, part 6: Stratigraphic interpretation of seismic reflection patterns in depositional

- sequences. In: Payton, C. (ed.), *Seismic Stratigraphy – applications to hydrocarbon exploration*. AAPG Memoir 26, 117–133. The American Association of Petroleum Geologists, Tulsa, OK.
- Montes, C., Cardona, A., Jaramillo, C., Pardo, A., Silve, J.C., Valencia, V., Ayala, C., Pérez-Angel, L.C., Rodriguez-Parra, L.A., Ramirez V., Nino, H.**, 2015. Middle Miocene closure of the Central American Seaway. *Science* 348(6231), 226–229.
- Moore, C.H., Wade, W.J.**, 2013. The basic nature of carbonate sediments and sedimentation. In: van Loon, A.J. (ed.), *Carbonate Reservoirs, Porosity and diagenesis in a sequence stratigraphic framework*. *Developments in Sedimentology* 67, 3–21.
- Mulder, T., Ducassou, E., Hanquiez, V., Principaud, M., Fauquemberg, K., Tournadour, E., Chabaud, L., Reijmer, J., Recouvreur, A., Gillet, H., Borgomano, J., Schmitt, A., Moal, P.**, 2019. Contour current imprints and contourite drifts in the Bahamian archipelago. *Sedimentology*, in press. DOI: 10.1111/sed.12587
- Müller-Michaelis, A., Uenzelmann-Neben, G., Stein, R.**, 2013. A revised Early Miocene age for the instigation of the Eirik Drift, offshore southern Greenland: evidence from high-resolution seismic reflection data. *Marine Geology* 340, 1–15. DOI: 10.1016/j.margeo.2013.04.012
- Mullins, H.T., Lynts, G.W.**, 1977. Origin of the northwestern Bahama Platform: Review and reinterpretation. *Geological Society of America Bulletin* 88, 1447–1461. DOI: 10.1130/0016-7606(1977)88<1447:OOTNBP>2.0.CO;2.
- Mullins, H.T., Neumann, A.C.**, 1979. Geology of the Miami Terrace and its paleo-oceanographic implications. *Marine Geology* 30, 205–232.
- Mullins, H.T., Neumann, A.C., Wilber, R.J., Hine, A.C., and Chinburg, S.J.**, 1980. Carbonate sediment drifts in the northern Straits of Florida, *American Association of Petroleum Geologists Bulletin* 64, 1701–1717.
- Mullins, H.T., Gardulski, A.F., Hine, A.C., Melillo, A.J., Wise, S.W.jr., Applegate, J.**, 1988. Three-dimensional sedimentary framework of the carbonate ramp slope of central west Florida: A sequential seismic stratigraphic perspective. *Geological Society of American Bulletin* 100, 514–533.
- Mutti, M., Droxler, A.W., Cunningham, A.D.**, 2005. Evolution of the Northern Nicaragua Rise during the Oligocene–Miocene: Drowning by environmental factors. *Sedimentary Geology* 175, 237–258: DOI: 10.1016/j.sedgeo.2004.12.028
- Neumann, A.C., Ball, M.M.**, 1970. Submersible observations in the Straits of Florida: geology and bottom currents. *Geological Society of America Bulletin* 81, 2861–2874.
- Nielsen, T., Knutz, P.C., Kuijpers, A.**, 2008. Seismic expression of contourite depositional systems. In: Rebesco, M., Camerlenghi, M.A. (eds), *Contourites*, *Developments in Sedimentology* 60, 301–321. Elsevier Science BV, Amsterdam. DOI: 10.1016/S0070-4571(08)00216-1

- O'Dea, A., Lessios, H.A., Coates, A.G., Eytan, R.I., Restrepo-Moreno, S.A., Cione, A.L., Collins, L.S., de Queiroz, A., Farris, D.W., Norris, R.D., Stallard, R.F., Woodburne, M.O., Aguilera, O., Aubry, M.-P., Berggren, W.A., Budd, A.F., Cozzuol, M.A., Coppard, S.E., Duque-Caro, H., Finnegan, S., Gasparini, G.M., Grossman, E.L., Johnson, K.G., Keigwin, L.D., Knowlton, N., E.G., Leonard-Pingel, J.S., Marko, P.B., Pyenson, N.D., Rachello-Dolmen, P.G., Soibelzon, E., Soibelzon, L., Todd, J.A., Vermeij, G.J., Jackson, J.B.C., 2016.** Formation of the Isthmus of Panama. *Science Advances* 2(8), e1600883. DOI: 10.1126/sciadv.1600883
- Paulat, M., Lüdman, T., Betzler, C., Eberli, G.P., 2018.** Neogene paleoceanographic changes recorded in a carbonate contourite drift (Santaren Channel, Bahamas). *Sedimentology* (in press). DOI: 10.1111/sed.12573
- Peakall, J., Kane, I.A., Masson, D.G., Keevil, G., McCaffrey, W., Corney, R., 2011.** Global (latitudinal) variation in submarine channel sinuosity. *Geology* 40(1), 11–14. DOI: 10.1130/G32295.1
- Pérez, L.F., Hernández-Molina, F.J., Esteban, F.D., Tassone, A., Piola, A.R., Maldonado, A., Preu, B., Violante, R.A., Lodolo, E., 2015.** Erosional and depositional contourite features at the transition between the western Scotia Sea and southern South Atlantic Ocean: links with regional water-mass circulation since the Middle Miocene. *Geo-Marine Letters* 35, 271–288, DOI: 10.1007/s00367-015-0406-6.
- Pindell, J., Kennan, L., 2009.** Tectonic evolution of the Gulf of Mexico, Caribbean and northern South America in the mantle reference frame: an update. *Geological Society, Special Publications* 328, 1-55. DOI: 10.1144/SP328.1
- Pomar, L., 2001.** Types of carbonate platforms: a genetic approach. *Basin Research* 13, 313–334.
- Poore, H.R., Samworth, R., White, N.J., Jones, S.M., McCave, I.N., 2006.** Neogene overflow of Northern Component Water at the Greenland-Scotland Ridge. *Geochemistry, Geophysics, Geosystems* 7(6), Q06010. DOI: 10.1029/2005GC001085
- Preiss-Daimler, I.V., Heinrich, R., Bickert, T., 2013.** The final Miocene carbonate crash in the Atlantic: Assessing carbonate accumulation, preservation and production. *Marine Geology* 343, 39-46. DOI:10.1016/j.margeo.2013.06.010
- Principaud, M., Ponte, J.-P., Mulder, T., Gillet, H., Robin, C., Borgomano, J., 2016:** Slope-to-basin stratigraphic evolution of the carbonate northwestern Great Bahama Bank (Bahamas) during the Neogene to Quaternary: interactions between downslope and bottom currents deposits. *Basin Research* 29(6), 699–724. DOI: 10.1111/bre.12195
- Principaud, M., Mulder, T., Hanquiez, V., Ducassou, E., Eberli, G.P., Chabaud, L., Borgomano, J., 2018:** Recent morphology and sedimentary processes along the western slope of Great Bahama Bank (Bahamas). *Sedimentology* 65, 2088–2116. DOI: 10.1111/sed.12458

- Purdy, E.G., Bertram, G.T.**, 1993. Carbonate concepts from the Maldives, Indian Ocean. *American Association of Petroleum Geologists, Studies in Geology* 34, 56.
- Rebesco, M.**, 2005. Contourites. In: Selley, R.C., Cocks, L.R.M. and Plimer, I.R. (eds), *Encyclopedia of Geology*, 513–527. Elsevier, Oxford.
- Rebesco, M., Stow, D.**, 2001. Seismic expression of contourites and related deposits: a preface. *Marine Geophysical Researches* 22, 303-308.
- Rebesco, M., Camerlenghi, A., Van Loon, A.J.**, 2008. Contourite research: A field in full development. In: Rebesco, M., Camerlenghi, M.A. (eds), *Contourites, Developments in Sedimentology* 60, 3–10. Elsevier Science BV, Amsterdam.
- Rebesco, M., Hernández-Molina, F.J., Van Rooij, D., Wåhlin, A.**, 2014. Contourites and associated sediments controlled by deep-water circulation processes: State-of-the-art and future considerations. *Marine Geology* 352, 111–154.
- Reeder, D.B., Ma, B.B., Yang, Y.J.**, 2011. Very large subaqueous sand dunes on the upper continental slope in the South China Sea generated by episodic, shoaling deep-water internal solitary waves. *Marine Geology* 279, 12–18. DOI:10.1016/j.margeo.2010.10.009
- Rendle, R.H., Reijmer, J.J.G.**, 2002. Quaternary slope development of the western, leeward margin of the Great Bahama Bank. *Marine Geology* 185, 143–164.
- Reolid, J., Betzler, C.**, 2018. The ichnology of carbonate drifts. *Sedimentology*, in press. DOI:10.1111/sed.12563
- Reolid, J., Betzler, C., Lüdmann, T.**, 2018. Facies and sedimentology of a carbonate delta drift (Miocene, Maldives). *Sedimentology*, in press. DOI:10.1111/sed.12575
- Reijmer, J.J.G., Betzler, C., Kroon, D., Tiedemann, R., Eberli, G.P.**, 2002. Bahamian carbonate platform development in response to sea-level changes and the closure of the Isthmus of Panama. *International Journal of Earth Sciences* 91, 482–489. DOI: 10.1007/s00531-001-0235-x
- Rousset, C., Beal L. M.**, 2014. Closing the transport budget of the Florida Straits, *Geophysical Research Letters* 41, 2460–2466. DOI: 10.1002/2014GL059498.
- Sangree, J.B., Widmier, J.M.**, 1977. Seismic Stratigraphy and global changes of sea level, part 9: Seismic interpretation of clastic depositional facies. In: Payton, C. (ed.), *Seismic Stratigraphy – applications to hydrocarbon exploration*. AAPG Memoir 26, 165–184. The American Association of Petroleum Geologists, Tulsa, OK.
- Scher, H.D., Whittaker, J.M., Williams, S.E., Latimer, J.C., Kordesch, W.E.C., Delaney, M.L.**, 2015. Onset of Antarctic Circumpolar Current 30 million years ago as Tasmanian Gateway aligned with westerlies. *Nature* 523, 580–583. DOI: 10.1038/nature14598.

- Schlager, W., Reijmer, J.J.G., Droxler, A.**, 1994. Highstand shedding of carbonate platforms. *Journal of Sedimentary Research* 64(3), 270–281.
- Schlager, W. (ed.)**, 2005. Carbonate Sedimentology and Sequence Stratigraphy. SEPM, Concepts in Sedimentology and Paleontology Series 8, Society for Sedimentary Geology (SEPM).
- Schneider, B., Schmittner, A.**, 2006. Simulating the impact of the Panamanian seaway closure on ocean circulation, marine productivity and nutrient cycling. *Earth and Planetary Science Letters* 246, 367–380.
- Schott, F.A., McCreary Jr., J.P.**, 2001. The monsoon circulation of the Indian Ocean. *Progress in Oceanography* 51, 1–123.
- Shankar D., Vinayachandran, P.N., Unnikrishnan. A.S.**, 2002. The monsoon currents in the north Indian Ocean. *Progress in Oceanography* 52, 63–120. DOI: 10.1016/S0079-6611(02)00024-1
- Sheriff, R.E.**, 1977. Limitations on resolution of seismic reflections and geologic detail derivable from them. In: Payton, C. (ed.), *Seismic Stratigraphy – applications to hydrocarbon exploration*. AAPG Memoir 26, 3–14. The American Association of Petroleum Geologists, Tulsa, OK.
- Sheriff, R.E.**, 1980. *Seismic Stratigraphy*. 227 p. International Human Resources Development Corporation, Boston.
- Sherriff-Tadano, S., Abe-Ouchi, A., Yoshimori, M., Oka, A. and Chan W.-L.**, 2018. Influence of glacial ice sheets on the Atlantic meridional overturning circulation through surface wind change. *Climate Dynamic* 50, 2881–2903. DOI: 10.1007/s00382-017-3780-0
- Sijp, W.P., von der Heydt, A.S., Dijkstra, H.A., Flögel, S., Douglas, P.M.J., Bijl, P.K.**, 2014. The role of ocean gateways on cooling climate on long time scales. *Global and Planetary Change* 119, 1–22. DOI: 10.1016/j.gloplacha.2014.04.004.
- Slootman, A., De Boer, P.L., Cartigny, M.J., Samankassou, E., Moscariello, A.**, 2019. Evolution of a carbonate delta generated by gateway-funnelling of episodic currents. *Sedimentology*, in press. DOI:10.1111/sed.12585
- Spieß, V.**, 1993. *Digitale Sedimentechographie - Neue Wege zu einer hochauflösenden Akustostratigraphie*. Reports 35, 199p. Faculty of Geosciences, University of Bremen.
- Steph, S., Tiedemann, R., Prange, M., Groeneveld, J., Nürnberg, D., Reuning, L., Schulz, M., Haug, G.H.**, 2006. Changes in Caribbean surface hydrography during the Pliocene shoaling of the Central American Seaway. *Paleoceanography* 21(4), PA 4221. DOI: 10.1029/2004PA001092
- Steph, S., Tiedemann, R., Prange, M., Groeneveld, J., Schulz, M., Timmermann, A., Nürnberg, D., Rühlemann, C., Saukel, C., Haug, G.H.**, 2010. Early Pliocene increase in thermohaline

overturning: A precondition for the development of the modern equatorial Pacific cold tongue. *Paleoceanography* 25(2), PA2202. DOI: 10.1029/2008PA001645

- Storz, D., Gischler, E.**, 2011. Coral extension rates in the NW Indian Ocean: reconstruction of 20th century Indian monsoon strength and rainfall over India. *Geo Marine Letters* 31. 141–162.
- Stow, D.A.V., Faugères, J.-C.**, 2008. Contourite Facies and the Facies Model. In: Rebesco, M., Camerlenghi, M.A. (eds), *Contourites, Developments in Sedimentology* 60, 223–256. Elsevier Science BV, Amsterdam.
- Stow, D. A. V., Faugères, J.-C., Howe, J. A., Pudsey, C. J., Viana, A. R.**, 2002a. Bottom currents, contourites and deep-sea sediment drifts: current state-of-the-art. In: Stow, D.A.V., Pudsey, C.J., Howe, J.A., Faugères, J.-C., Viana, A.R. (eds), *Deep-Water Contourite Systems: Modern Drifts and Ancient Series, Seismic and Sedimentary Characteristics*, *Memoirs* 22, 7–20. Geological Society, London.
- Stow, D.A.V., Kahler, G., Reeder, M.**, 2002b. Fossil contourites: type example from an Oligocene palaeoslope system, Cyprus. In: Stow, D.A.V., Pudsey, C.J., Howe, J.A., Faugères, J.-C., Viana, A.R. (eds) *Deep-Water Contourite Systems: Modern Drifts and Ancient Series, Seismic and Sedimentary Characteristics*, *Memoirs* 22, 443–455. Geological Society, London.
- Stow, D.A.V., Hunter, S., Wilkinson, D., Hernández-Molina, F.J.**, 2008. The nature of contourite deposition. In: Rebesco, M., Camerlenghi, M.A. (eds), *Contourites, Developments in Sedimentology* 60, 143–156. Elsevier Science BV, Amsterdam.
- Stow, D.A.V., Hernández-Molina, F.J., Llave, E., Sayago-Gil, M., del Río, V.D., Branson, A.**, 2009. Bedform-velocity matrix: The estimation of bottom current velocity from bedform observations. *Geology* 37, 327–330. DOI:10.1130/G25259A.1
- Suchéras-Marx, B., Henderiks, J.**, 2014. Downsizing the pelagic carbonate factory: Impacts of calcareous nannoplankton evolution on carbonate burial over the past 17 million years. *Global and Planetary Change* 123, 97–109. DOI:10.1016/j.gloplacha.2014.10.015
- Surlyk, F., Lykke-Andersen, H.**, 2007. Contourite drifts, moats and channels in the Upper Cretaceous chalk of the Danish Basin. *Sedimentology* 54, 405–422. DOI: 10.1111/j.1365-3091.2006.00842.x
- Szabo, B.J., Moore, J.G.**, 1986. Age of -360-m reef terrace, Hawaii, and the rate of late Pleistocene subsidence of the island. *Geology* 14, 967–968. DOI:10.1130/0091-7613(1986)14<967:AOMRTH>2.0.CO;2
- Talley, L.D., Pickard, G.L., Emery, W.J., Swift, J.H. (eds)**, 2011. *Descriptive Physical Oceanography - An Introduction*, sixth edition, Elsevier Academic Press. DOI:10.1016/B978-0-7506-4552-2.10033-2

- Thran, A.C., Dutkiewicz, A., Spence, P., Müller, R.D.,** 2018. Controls on the global distribution of contourite drifts: Insights from an eddy-resolving ocean model. *Earth and Planetary Science Letters* 489, 228–240. DOI:10.1016/j.epsl.2018.02.044
- Tomczak, M., Godfrey, J.S.,** 2003. *Regional Oceanography: an introduction*. 390 p. Daya Publishing House, Delhi.
- Tournadour, E., Mulder, T., Borgomano, J., Hanquiez, V., Ducassou, E., Gillet, H.,** 2015. Origin and architecture of a Mass Transport Complex on the northwest slope of Little Bahama Bank (Bahamas): Relations between off-bank transport, bottomcurrent sedimentation and submarine landslides. *Sedimentary Geology* 317, 9–26.
- Turnewitsch, R., Falahat, S., Nycander, J., Dale, A., Scott, R.B., Furnival, D.,** 2013. Deep-sea fluid and sediment dynamics—Influence of hill- to seamount-scale seafloor topography. *Earth-Science Reviews* 127, 203–241. DOI:10.1016/j.earscirev.2013.10.005
- Vail, P.R.,** 1987. Seismic stratigraphy interpretation using sequence stratigraphy. Part I: Seismic stratigraphy interpretation procedure. In: A.W. Bally (ed.), *Atlas of Seismic Stratigraphy 1–10*. American Association of Geology, *Studies in Geology* 27.
- Vandorpe, T., Van Rooij, D., de Haas, H.,** 2014. Stratigraphy and paleoceanography of a topography-controlled contourite drift in the Pen Duick area, southern Gulf of Cádiz. *Marine Geology* 349, 136–151.
- Verducci, M., Foresi, L.M., Scott, G.H., Tiepolo, M., Sprovieri, M., Lirer, F.,** 2007: East Antarctic Ice Sheet fluctuations during the Middle Miocene Climatic Transition inferred from faunal and biogeochemical data on planktonic foraminifera (ODP Hole 747A, Kerguelen Plateau). In: Cooper, A.K., Raymond, C.R., et al. (eds), *Antarctica: A Keystone in a Changing World – Online Proceedings of the 10th ISAES*. USGS Open-File Report 2007-1047, Short Research Paper 037, 5 p. DOI: 10.3133/of2007-1047.srp037
- Wade, B.S., Pearson, P.N., Berggren, W.A., Pälike, H.,** 2011. Review and revision of Cenozoic tropical planktonic foraminiferal biostratigraphy and calibration to the geomagnetic polarity and astronomical time scale. *Earth-Science Reviews* 104, 111–142.
- Westervelt, P.J.,** 1963. Parametric Acoustic Array. *Journal of Acoustical Society of America*, 35, 535–537.
- Westphal, H., Riegl, B., Eberli, G.P. (eds),** 2010. *Carbonate Depositional Systems: Assessing Dimensions and Controlling Parameters: The Bahamas, Belize and the Persian/Arabian Gulf*. First edition, Springer Science+Business Media BV.
- Williams, H.D., Burgess, P.M., Wright V.P., Della Porta, G., Granjeon, D.,** 2011. Investigating Carbonate Platform Types: Multiple Controls and a Continuum of Geometries. *Journal of Sedimentary Research* 81(1), 18-37. DOI: 10.2110/jsr.2011.6

- 
- Wilson, J.L.**, 1975. Carbonate Facies in Geologic History. 471 p. Springer-Verlag, New York. DOI: 10.1017/S0016756800041406
- Wilson, P.A., Roberts, H.H.**, 1995. Density Cascading: Off-shelf sediment transport, evidence and implications, Bahama Banks. *Journal of Sedimentary Research* A65, 45–56.
- Wold, C.N.**, 1994. Cenozoic sediment accumulation on drifts in the northern North Atlantic. *Paleoceanography* 9(6), 917–941.
- Wright, J.D., Kroon, D.**, 2000. Planktonic foraminiferal biostratigraphy of leg 166. Proceedings of the Ocean Drilling Program, Scientific Results 166, 3–12.
- Wunsch, M., Betzler, C., Lindhorst, S., Lüdmann, T., Eberli, G.P.**, 2017. Sedimentary dynamics along carbonate slopes (Bahamas archipelago). *Sedimentology* 64(3), 631–657. DOI: 10.1111/sed.12317
- Wunsch, M., Betzler, C., Eberli, G.P., Lindhorst, S., Lüdmann, T., Reijmer, J.J.G.**, 2018. Sedimentary dynamics and high-frequency sequence stratigraphy of the southwestern slope of Great Bahama Bank. *Sedimentary Geology* 363, 96–117. DOI: 10.1016/j.sedgeo.2017.10.013
- Wynn, R.B., Stow, D.A.V.**, 2002. Classification and characterisation of deep-water sediment waves. *Marine Geology* 192, 7–22. DOI: 10.1016/S0025-3227(02)00547-9
- Yilmaz, Ö.**, 1987. Seismic Data Processing. In: Doherty, S.M. (ed.), *Investigations to Geophysics*, 526 p. Tulsa, OK.
- Zachos, J., Pagani, M., Sloan, L., Thomas, E., Billups, K.**, 2001. Trends, Rhythms, and Aberrations in Global Climate 65 Ma to Present. *Science* 292 (5517), 686–693.

